CRANFIELD UNIVERSITY

SCHOOL OF APPLIED SCIENCES

PhD THESIS

Academic Year 2010 - 2013

STEPHANIE CAMPBELL

POLYMER-BASED TREATMENTS TO CONTROL RUNOFF, LEACHATE AND EROSION FROM ENGINEERED SLOPES AT SIMFER MINE, GUINEA, AFRICA.

Supervised by Dr Robert W. Simmons and

Prof Jane Rickson

May 2013

This thesis is submitted in partial fulfilment of the requirements for the degree of doctor of philosophy

ABSTRACT

It is necessary to understand the erodibility and hydrological response of mine-site slope forming materials (SFMs), because of increasing awareness of the environmental impacts of mining. Steep engineered slopes in high intensity rainfall environments present a serious erosion risk. Temporary surface stabilisers, such as polyacrylamides (PAMs) and polyvinylacrylic latex (PVALs) are potentially cost effective erosion control solutions. In this study PAM and PVAL efficacy to reduce runoff, leachate and erosion was assessed at two application rates, with and without gypsum on SFMs from an iron ore mine in Guinea (West Africa). NSPASS (near-surface photogrammetry assessment of slope forming materials' surface roughness) is a novel method that integrates digital image capture and GIS. It is shown to detect and quantify surface micro-relief changes of 2-3 mm, not visible to the naked eye.

As expected, soil and non-soil SFMs were significantly different in terms of their physical and chemical properties. Phase I of the study investigated the erodibility of ten SFMs, including soil, ore and waste-rock. The results indicate that the hydrological response to rainfall of most SFMs is to generate leachate. Weathered phyllite (PHY-WEA) is the most erodible SFM by both runoff and leachate. Multiple regression analysis demonstrated that magnetic susceptibility, mineralogy and dry aggregate distribution; parameters not commonly assessed in erosion studies, are important in explaining SFM erodibility and hydrological response.

Phase II evaluated critically the effectiveness of three commercially available polymer solutions (two PAMs and one PVAL) at reducing runoff, leachate and erosion from four of the most erodible SFMs identified in Phase I. The results indicate that some PAM and PVAL treatments significantly reduce runoff, leachate and erosion. Polymer efficacy is highly dependent on the physical and chemical properties of the SFM, as well as the mechanism of polymer to SFM adsorption. Increasing the application rate of select treatments lowered leachate volumes, runoff and leachate total sediment loads. Contrary to previous studies, gypsum amendments did not significantly improve polymer efficiency.

This research has added to our understanding of the erodibility and hydrological response of soil and non-soil SFMs. This is the first study to evaluate critically the efficacy of PVALs in controlling erosion from mine-site SFMs. Future studies should continue to optimise NSPASS performance in monitoring changes in surface micro-relief.

Keywords: - Slope forming materials (SFMs), erodibility, hydrological response, polymer-based treatments (PBTs), polyacrylamide (PAM), polyvinylacrylic latex (PVAL)

ACKNOWLEDGMENTS

Most importantly I would like to thank my supervisors Rob Simmons and Jane Rickson for passing on their scientific knowledge and experience. I have learnt so much about soils, land management and erosion over the past three years from you both; it is almost hard to believe how I started this journey. I have been very lucky that both of my supervisors have been completely hands on; reading everything I send their way, always there for advice and supporting me throughout my time at Cranfield University. Your passion and enthusiasm for soil conservation is inspiring, so please keep doing what you are doing.

Thank you to all the technical staff from Buildings 54 and 244. I would like to especially thank Rob Read and Richard Andrews for being supportive and giving advice whilst conducting my experimental work. I would like to thank Toby Waine and Daniel Simms for their time and expertise in helping me to make NSPASS happen. Also to Pat Bellamy, thank you for always being on hand to help me brain storm.

I would like to thank Rio Tinto Iron Ore Atlantic for funding my research, and to all those at Rio Tinto, particularly Lucas Kitchen for increasing my understanding about iron ore mining and supporting me in my work.

Working at Cranfield I have met many people in particular Jo Niziolomski and Alissa Cotton have become friends that I have been able to share my PhD experience with. Thanks also to my non-PhD friends for your motivating chats and your well needed down time company.

I have some fantastic family, and I have enjoyed my visits home to North Wales as you have all helped to remind me of what is important. Thank you to Debbie for always being supportive. To my great parents Angela and Martin, I am always thankful for your love, support, encouragement and giving me the freedom to make my own decisions in life. I am also very grateful you have made me feel that I will always have a home in Wales to return to if needed.

To Kevin, you have been on this journey from the start, and despite the days feeling stressed, thank you for listening, taking an interest in my research and being there for me.

Finally, I would like to dedicate this thesis to the memory of my beautiful little sister Sadie. You are in my thoughts every day, and I hope that you are proud.

TABLE OF CONTENTS

LIST OF FIGURES

LIST OF TABLES

LIST OF ABBREVIATIONS

AD_{amc}	Air dry antecedent moisture conditions
$Aggregates^{NS}$	Non-soil aggregates
$Aggregates^{S}$	Soil aggregates
ALL	Alluvisol
ANOVA	Analysis of variance
Bmax	Cameras maximum parallax
CEC	Cation exchange capacity
CE90	Circular error of 90%
COMB-WEA	A 50:50 combined blend of two NEW-WEA samples
D_{50}	Median raindrop diameter
DAD	Dry aggregate distribution
DC90	Soilfloc® DC90
DEM	Digital elevation model
DSD	Drop size distribution
EC	Electrical conductivity
FC_{amc}	Field capacity antecedent moisture conditions
FER	Ferralitic soil
GIS	Geographic information system
HGF	Friable Geothitic Haematite
HRS	Haul Road Sample
KE	Kinetic energy
LE90	Linear error of 90%
LITH	Lithosol
MRA	Multiple regression analysis
MS	Magnetic susceptibility
NEW-WEA	Weathered mineralisation
NSDP	Near surface digital photogrammetry
NSPASS	Near surface photogrammetry assessment of slope forming material surface roughness
PAM	Polyacrylamide
PBT	Polymer based treatment
PHV	Very weak weathered phyllite
PHY-WEA	Weathered phyllite
PSD	Particle size distribution
PVA	Polyvinylacetate
PVAL	Polyvinylacrylic latex
RD	Rubbly Drift
SA	Surface area
SFM	Slope forming material

SR	Surface roughness
SRE	A soil rejuvenated by erosion
SS6	Siltstop® APS 605
SS7	Siltstop® APS 705
TIFF	Tagged image file format
TRN	Transitional material
TSC	Total sediment concentration
TSL	Total sediment load

Chapter 1. Introduction

1.1 Introduction and project outline

Rio Tinto is one of the world's largest mining companies (Rio Tinto, 2010). In 2003, Rio Tinto signed a mining convention with the Guinean Government to develop an iron ore mining concession at Simfer Mine, located at the Simandou mountain range in Guinea, West Africa. Currently the mine development is in the exploration and mine planning phase, and mining operations are intended to start in 2015, when Rio Tinto plan to mine 40 Mt yr^{-1} (Rio Tinto, 2010).

There are two common types of mining excavation, Surface Mining and Sub-Surface Mining (Hartman et al., 2002). Strip Mining will be the surface approach adopted to remove Iron ore from Simandou. More specifically Rio Tinto will be applying what is referred to as *'Mountain Top Removal'*, to obtain the iron ore. Mining will produce a range of slope forming materials (SFMs) including iron ore, soil and waste-rock, which will be moved to waste-rock piles and ore stockpiles on site (Lucas Kitchen, personal communication, 26th November 2010). Mining operations create a continuously changing landscape as the mine's operations expand. Rio Tinto currently use a range of erosion control options at the Simfer site, including check dams, hydro-seeding, vetiver planting and geotextiles, but realise these will not be sufficient to control erosion and runoff from waste-rock dumps and ore stockpiles once mining commences.

Rainfall-induced erosion is considered a serious risk on sites with mountainous topography and where there is a lack of vegetation cover and intense tropical rainfall during operations (Hustrulid et al., 2000; Brotons et al., 2010). High erosion rates and runoff volumes can disrupt mining operations, making haul roads impassable and impacting on sensitive aquatic ecosystems. Managing this can become very expensive (Schwab et al, 1981; Brotons et al., 2010). Therefore, understanding and quantifying the hydrological response and erodibility of the different SFMs excavated during mining is important for sediment and water management planning; where decisions about how and where to locate SFMs during the life of the mine will be made.

Across Africa soil erosion is a serious environmental and social problem (Lal, 1988; Wild, 1995). Published data in relation to the erodibility of West African soils are sparse as compared to Europe (Rejman et al, 1998; Siegrist et al., 1998), USA (Giley et al., 1977; Young and Mutchler, 1977; Mutchler and Carter, 1983), Canada (Bryan, 2000), and Australia (Loch and Rosewell, 1992; Loch,

1994; Loch et al., 1998; Williams, 2001). To date there are no known research papers about soil erodibility in African Guinea, or specifically on mined SFMs in this region. This study enhances our scientific understanding of the physical and chemical characteristics of West African soils, as well as waste-rock and iron ore SFMs.

Research since the 1980s has demonstrated the effectiveness of polyacrylamides (PAMs) in controlling soil erosion in an agricultural context, but little research has been undertaken in the mining or construction sectors. There is no research on the efficiency of Polyvinylacrylic latex (PVAL) to control erosion from soils, iron ore or associated waste-rock SFMs. Mined landscapes are dynamic and temporary surface stabilisers such as PAMS and PVALs, which control erosion at source, are considered cost effective erosion control solutions that can be applied over large areas (Green and Stott, 2001; Nwankwo, 2001; Vacher et al., 2003; Sojka et al., 2007).

This research critically evaluates the effectiveness of selected commercially available Polymer Based Treatments (PBTs) at reducing runoff and erosion on the most erodible SFMs from Simfer mine. PBT efficacy is evaluated using three products namely Siltstop® APS 705 powder (PAM), Siltstop® APS 605 emulsion (PAM) and Soilfloc® DC90 liquid (PVAL), at two application rates, with and without the addition of gypsum. Using a near-surface photogrammetry and integrated GIS-based technique (NSPASS) developed specifically for this project; the results give a better understanding of the mechanisms involved in PBT efficacy. These findings will be relevant to the wider mineral and metals mining sector, where at present PBTs are not widely used, but have the potential to reduce the costs of erosion control, significantly reduce erosion and runoff volumes, and improve on-site and off-site water quality by reducing the transport of contaminants. This thesis is structured into six chapters, as outlined in Figure 1.1

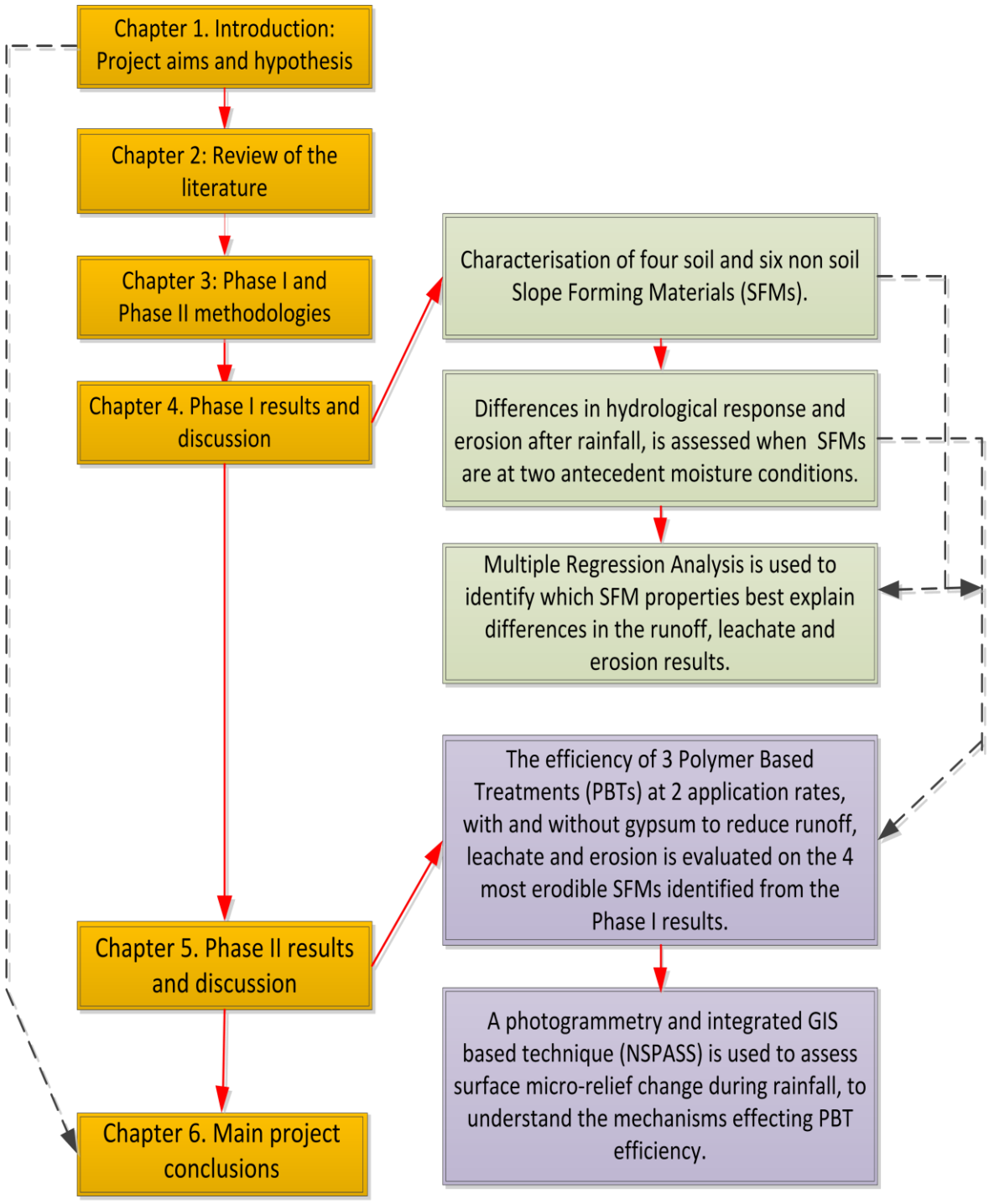

Figure 1.1. Thesis structure showing linkages between chapters

1.2 Research Aims

The aim of this project is to test whether polymer based treatments (PBTs) will reduce runoff, leachate and erosion from selected slope forming materials (SFMs) derived from Simfer iron ore mine Guinea. This overall aim was deconstructed into the following Phase I and Phase II objectives.

Phase I objectives

1. To characterise ten SFMs derived from Simfer Mine in-terms of factors affecting their erodibility and hydrological response.

2. To quantify and critically evaluate key indicators of the erodibility and hydrological response of the selected SFMs, namely runoff volume, runoff total sediment load (TSL), leachate volume and leachate TSL at field capacity and air dry antecedent moisture conditions.

3. Identify physical and chemical properties of the SFMs which affect their erodibility and hydrological response, as a pre-requisite to explaining the efficacy of the PBTs tested in Phase II.

4. Identify four SFMs to take forward into Phase II, based on their erodibility and hydrological response to rainfall.

Phase II objectives

1. Critically evaluate three commercially available PBT products, namely two PAMs and one PVAL to reduce runoff, leachate and erosion, on four selected SFMs.

2. Develop an integrated near surface photogrammetry-GIS method that can quantify change in surface micro-relief, and enhance our understanding of why some PBTs are more effective than others.

1.3 Hypothesis

The overarching project hypothesis is that PBTs will reduce runoff, leachate and erosion from SFMs derived from Simfer mine-site. To address this hypothesis, the following sub-hypotheses were formulated.

Phase I sub-hypotheses

1. Significant differences will be observed between the physical and chemical properties of the soil and non-soil SFMs.

2. Different SFMs will have different hydrological responses in terms of:
    a) runoff volume and associated TSL, and
    b) leachate volume and associated TSL.

3. Antecedent moisture conditions (i.e. air dry v. field capacity) will affect the erodibility and hydrological responses of the SFMs.

4. Erodibility and hydrological responses of SFMs can be explained by their physical and chemical properties.

Phase II sub-hypotheses

1. PBTs will have a significant effect on key indicators of the erodibility and hydrological response of selected SFMs, namely runoff volume, runoff total sediment load (TSL), leachate volume and leachate TSL.

2. There is a negative relationship between PBT application rate and rate of erosion.

3. For the selected SFMs, the addition of gypsum will enhance the efficacy of the PBTs.

4. For the selected SFMs, the greatest decline in surface roughness after rainfall will be associated with the untreated control.

Chapter 2. Literature review

2.1 Introduction to the mining sector and environmental problems associated with rainfall erosion on mine-sites

Rio Tinto Iron Ore Atlantic will be applying *'Mountain Top Removal'*, to obtain iron ore from a proposed mine development in Simandou, Guinea (West Africa). Modern mining often uses huge machinery such as draglines to remove, transport and deposit huge quantities of unwanted waste-rock, forming unconsolidated waste-rock landscapes with steep slopes that are highly erodible (Williams, 2001; So et al., 2002). Mining can produce a high waste to product ratio (Mining Watch, 2002) and waste-rock dumps can be very large topographic features, extending up to 300m in height and containing 500 million m^3 of material, which have different hydro-geological properties to natural hill-slopes and variable materials, grading and structure (Hancock et al., 2008). Consequently, predicting their hydraulic response to rainfall is not straightforward (McCarter, 1990; in Fala et al., 2003).

Mine-site slope forming materials (SFMs) consists of unconsolidated waste-rock, soil and ore material (Singer and Munns, 1999), which are referred to collectively in this thesis as SFMs. Studies by Strohm et al. (1978; in Smith et al., 1995) suggest that SFMs with >20% material passing a 4.75 mm particle size sieve should be considered soil. Fragaszy et al. (1992; in Smith et al., 1995) suggest SFMs with 50-60% materials <12.7 mm behave in the same way as a soil. Alternatively, Morgestern (1995; in Smith et al., 1995) infers that SFMs with sand content at about 20% is the boundary between rock-like and soil-like material. Smith et al. (1995) differentiates between soil-like and rock-like SFMs, in terms of their hydrological properties, which is why it is important to understand the physical and chemical properties of the SFM beyond the conventional soil and non-soil definition.

Rainfall causes erosion by direct raindrop impacts, surface and subsurface water movement (via sheet wash, rills, gullies, leachate), or by initiating landslides (Wild, 1995). On fresh unconsolidated, un-vegetated SFMs runoff erosion can initiate very quickly; and once rill and gully processes have started, erosion rates could reach 100 to 500 t ha^{-1} (Morgan, 2006). At Simandou, erosion by water is highly likely because of the steep sloping topography and high intensity tropical rainfall (IFC, 2006), with regional annual rainfall approximately 3500 mm (Lucas Kitchen, Personal Communication, December 3rd 2012). Erosion and runoff is costly to manage, are hazards to mine operations and presents risks of flooding, contamination and ecological

degradation to the local environment (Lal, 1988; Kennedy, 1990; Riley, 1995; Wild, 1995; Wood and Armitage, 1997; Xu and Liu, 1999; Williams, 2001).

Runoff describes water that moves at the surface and leachate describes water that has infiltrated the surface and has moved down through the profile. Conventionally soil erosion rates are assessed by determining runoff volumes and runoff total sediment loads (TSLs) (Morgan, 2006). Unconsolidated SFMs from a mine-site may be just as at risk from leachate erosion as surface runoff. Therefore, it is important to understand the comparative hydrological response and erodibility of different SFMs in order to inform sediment and water management plans for the mine-site (Clark, 2010).

Polymer Based Treatments (PBTs) can reduce material loss at source (Sojka et al., 2007), can be applied to large sites and so reducing the need for costly erosion and runoff control measures that have to be maintained throughout the life of the mine (Kennedy, 1990). Controlling erosion at source can reduce the environmental impacts from sediment transported off-site, and reduce the frequency with which haul roads have to be cleared of deposited sediment. Erosion control also avoids dredging of ponds (often when sediment levels reach 60% of their design capacity) and reduces the number or size of required sedimentation ponds (also maximising space for mining operations). Finally erosion control at the source will reduce the need or amount of flocculent needed to control turbid runoff discharge (Kennedy, 1990). The mining sector, including metals and minerals, is a growing global industry and the global iron ore market has grown by 95%, between the years 1999 to 2008; with the rate of growth increasing (The Engineering and Mining Journal report in; Creamer Media, 2009). Rapid industrial growth highlights the need for more understanding about the erodibility and hydrological response of mine-site SFMs. As a result best sediment and water management solutions can be devised and implemented.

2.2 The mechanics of rainfall-induced erosion

Erosion by water involves the detachment of individual particles from the greater mass, followed by entrainment and transport, by surface runoff (Ellison, 1947; in Barthès and Roose, 2002). In each case a critical expenditure of energy is required by the eroding agent for detachment and/or transport to happen (Kinnell, 2005). When there is no longer sufficient energy for particle transportation, material deposition will occur (Morgan, 2006). Although

discussed separately here, in reality detachment, entrainment, transport and deposition will often be operating simultaneously during rainfall (Morgan, 2006).

2.2.1 Detachment

Particle detachment can occur from either the impacting force of rain drops or by runoff flow velocities (Singer and Munns, 1999; Kinnell, 2005; Morgan, 2006). The rate of detachment by surface runoff depends on the shear velocity of the flow, the unit discharge, its load and material size (Morgan, 2006,). Rain-splash is the most important detaching agent (Morgan, 2006), with kinetic energies (KE) of 0.3-0.6 J m^2 (Schwab et al., 1981; Hudson, 1989). The KE of rain drop splash can be 200 times that of runoff (White, 2006). Cumulative KE load is a function of rainfall intensity and Drop-Size Distribution (Lal, 1988). Rain drop diameters increase with rainfall intensities up to 100 mm hr^{-1} (Hudson, 1989) The velocity of rainfall impact may vary from 4 m s^{-1} for smaller 1.0 mm drops to 9 m s^{-1} for larger 5 mm drops, which are associated with rainfall events in tropical countries such as Guinea (Hudson, 1989). Larger drops have greater mass and vertical terminal velocity and so are associated with higher KE, although there tends to be fewer drops per unit area (Fox, 2004).

McIntyre (1958) outlines how aggregate breakdown results from two complementary mechanisms that can be instigated by either *physical* or *chemical properties,* as illustrated in Figure 2.1 Physical aggregate breakdown results when raindrop impact energy is greater than that required to overcome the inherent stability of the aggregate, which causes particles to detach from the main pedon surface (Loch and Rosewell, 1992; Amézketa, 1999; Abiven et al., 2009). Physical breakdown can also occur by slaking caused by rapid wetting and the rapid expulsion of air (Simmons, 1998). Chemical disaggregation is promoted by rapid wetting and is dependent on SFM properties such as the electrical conductivity, cation exchange capacity and clay mineralogy as swelling clays are particularly susceptible (Simmons, 1998; White, 2006).

2.2.2 Entrainment

Entrainment of a particle from the greater mass by surface runoff occurs when flow velocities and shear stress are greater than the soil's inherent 'resistance to entrainment' (Morgan, 2006). Particle size and roughness will affect entrainment, where fine sands and silts require less energy to facilitate

detachment and entrainment than larger sand particles, and the finest particles (clays) are generally more cohesive and more difficult to erode (Singer and Munns, 1999; Morgan, 2006). In reality the material's surface will consist of varying particle sizes, and their assemblage will affect the ease of entrainment; coarse particles may protect smaller particles, unless rain splash acts and mixes the fines into the flow (Morgan, 2006).

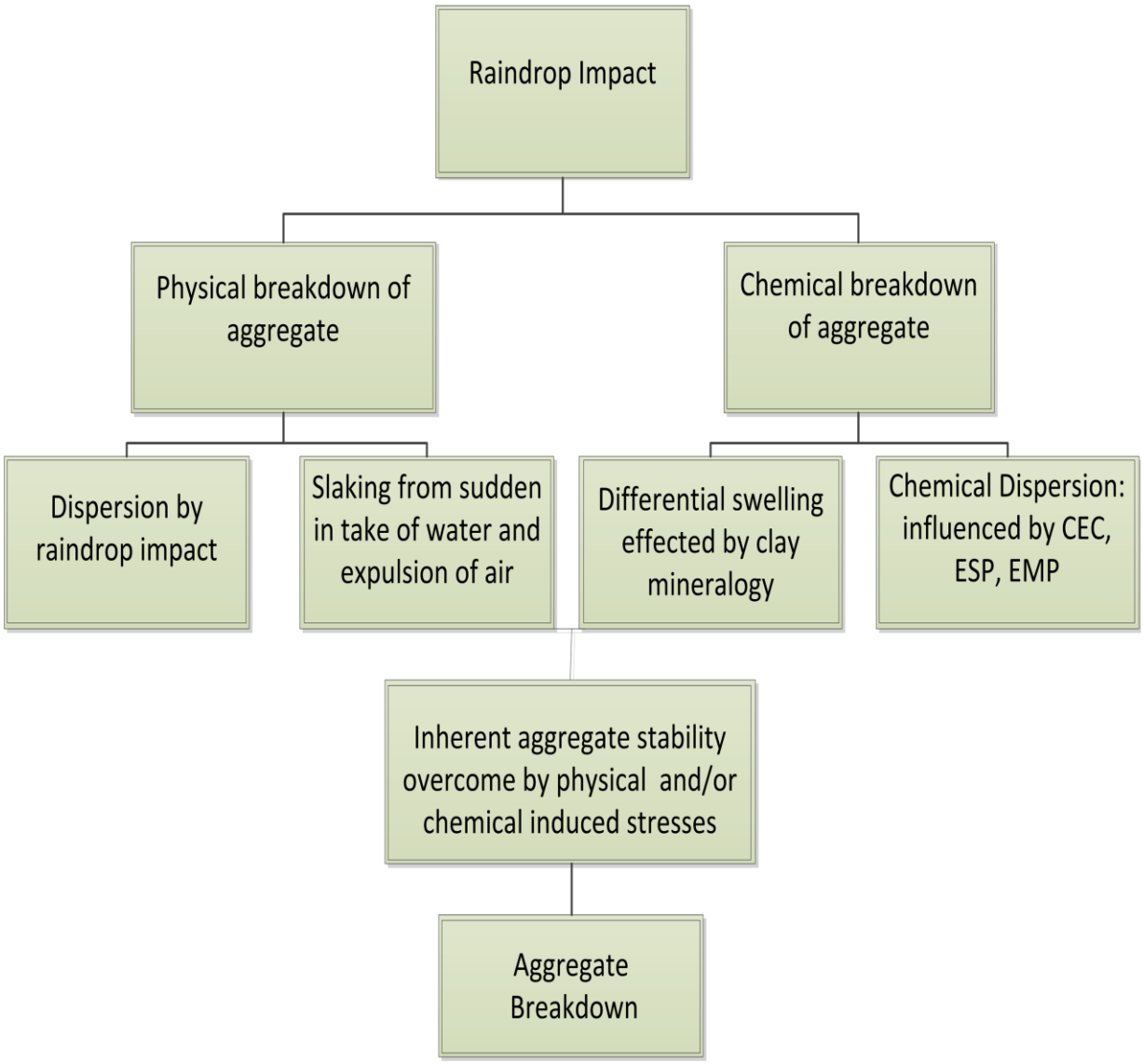

Figure 2.1 Flowchart illustrating key erosion processes that lead to aggregate breakdown *(Source: modified from Simmons, 1998)*

2.2.3 Transport

The impacts of erosion will be affected by the amount of material detached, as well as the eroding agent's capacity to transport the detached material, both over time and space; where erosion is defined as either transport or detachment limited (Morgan, 2006).

Detached material can become entrained by water via impacting raindrops or by surface runoff or sub-surface leachate (Morgan, 2006). Erosion studies at a mine waste dump in Northern Territory, Australia, revealed preferential removal of silt and clay by water erosion (Riley, 1995). Finely sized silt and clay particles can be transported far from its source, entering local water courses and causing high turbidity in runoff ponds, which may require flocculants to reduce turbidity and enable the ponds to be drained in line with drainage turbidity regulations (Kennedy, 1990; Riley, 1995; Wood and Armitage, 1997; Williams, 2001).

The development of runoff is affected by infiltration capacity (a function of pore sizes and SFM density), formation of a structural seal, permeability (a function of structure characteristics and stoniness) and hydraulic conductivity (as determined by particle size and porosity) (Loch et al., 1998).

This research will be important in understanding the extent to which our knowledge of erosional processes associated with soils can be transferred to non-soil SFMs. It has been found that the general mechanisms of runoff generation also apply to artificial slopes such as waste-rock dumps (Nicolau, 2002). The Green and Ampt equations have been found to successfully describe Hortonian overland flow on artificial slopes (Evans, 1997; in Nicolau, 2002). Saturation excess overland flow (sheet flow) occurs when soil moisture storage reaches capacity with no further room for water to infiltrate; common when rain falls on soils with high antecedent moisture (Kollet and Maxwell, 2006). This has been reported on artificial slopes in humid regions where the material under the topsoil has a high bulk density (Haigh, 1992; in Nicolau, 2002). Tunnel flow occurs on coarse SFMs with poor structure or high stone content, and has been reported on cracked artificial slopes with large macro pores, which caused piping (Nicolau, 2002).

Leachate describes water that has infiltrated the surface and moves through the profile (Morgan, 2006; White, 2006). The flow of water in mine waste-rock piles depends on its internal structure, which is effected greatly by the dumping methods used to construct the pile, its size and the size of the materials it contains (Fala et al., 2003). Hydraulic conductivities of mine waste-rock dumps can vary between 10^{-2} m sec for those with rockier (high porosity) textures, to

10^{-9} m sec in clay textured materials (Smith et al., 1995). Sediment concentrations as high as 1.0 g l^{-1} have been measured from subsurface flow on silt loam soils in California (Pilgrim and Huff, 1983; in Morgan, 2006), but less is known about the erosive potential of sub-surface water particularly within SFMs that have originated from a mine-site. Recognising that sub-surface flow is an integral component of water movement in unconsolidated SFMs is the primary reason that total leachate volume and leachate sediment loads will be measured in this study. The results of this study are important as there are no known published papers that have compared differences in the erodibility and hydrological response, in terms of both leachate and runoff, on unconsolidated and non-vegetated tropical ore, waste-rock and soil SFMs.

2.2.4 Deposition

Locally re-deposited material may reduce infiltration and increase runoff erosion by forming seals and surface crusts (de-hydrated surface seals); either as a structural crust formed *in situ*, or by the deposition of fine particles. Surface sealing processes begin in soils when dispersed particles move into the surface with the infiltrating water and clog pores to form a "washed-in" layer of low permeability (McIntyre, 1958). Once the availability of disaggregated material becomes limited, compactive forces dominate the seal formation process, which in turn increases the probability of surface runoff initiation (Simmons, 1998). Surface seal formation increases with time (Govers and Poesen, 1985; in Morgan, 2006), and infiltration rate declines promoting runoff generation and continuing surface erosion (Tindall and Kunkel, 1999).

2.3 Factors that affect the erodibility and hydrological response of Slope Forming Materials

Erodibility defines the resistance of the SFM to detachment and transport (Morgan, 2006 p 50). Texture, aggregate distribution, mineralogy, organic matter content and chemistry will affect a SFM's resistance to erosion (Morgan, 2006). The SFMs in this study have very different physical and chemical properties, ranging from weathered rock, to soil and iron ore. Less is known about the physical and chemical characteristics of mine-site ore, waste-rock and tropical soil SFMs, and how these properties affect SFM erodibility and hydrological response to rainfall, so the results collated in this study will provide a reference point for future studies.

2.3.1 Particle size distribution (PSD)

Particle size distribution (PSD) is the percentage of sand, silt and clay and determines the SFM's texture (White, 2006). Sandy and coarse textured soils are associated with good drainage (White, 2006) and in general, high silt containing materials have poor structure and are easily erodible (McIntyre, 1958; Levy et al., 1993, in Simmons, 1998; Bryan 2000,). Processes such as swelling and micro-mass movement are known to occur in saturated clay-rich surfaces (Selkirk and Riley, 1996; White, 2006). PSD is important for erodibility studies because aggregate stability and surface seal development are influenced by the proportion of fine materials, particularly the amount <100 µm, which can cause blockages within the surface matrix, promote runoff and cause higher sediment transport rates (Loch, 1994).

2.3.2 Dry aggregate size distribution (DAD)

Dry aggregate size distribution (DAD) is an assessment of the proportion of different aggregate size classes within a SFM sample that has been air dried and passed through a mechanical sieve (Nimmo and Perkins, 2002). The formation of aggregates is different in soil and non-soil SFMs and from here on in, the term 'aggregate^{S}' or 'DAD^{S}' will be used in reference to aggregates of all soil SFMs, and 'aggregate^{NS}' or 'DAD^{NS}' will refer to aggregates of all non-soil SFMs.

In soils, aggregates^{S} are the binding of sand, silt and clay primary particles into a larger entity by organic matter and micro-biology, which drives aggregation processes (White, 2006). The distribution of aggregate^{S} sizes in soils may cause differences in physical aggregate^{S} stability and hence differences in erodibility (Skidmore and Layton, 1992). Organic matter in soil may increase hydrophobicity; decrease breakdown caused by slaking (Igwe and Nkemekosi, 2007) and is a good indicator of soil aggregate^{S} stability (Abiven et al., 2009).

Non-soil SFMs contain unconsolidated primary particles of gravel, conglomerate and breccia fragments of different shapes and sizes (Price, 2009). The agglomeration of non-soil SFMs is a function of their inherent mineralogy and how it was extracted (Price, 2009). Exposure to weathering will distinguish regolith or saprolite non-soils from predominately solid rock containing non-soils (Graham et al., 2010; Price, 2009). Non-soil mechanical behaviour will largely be controlled by the point-to-point contact between coarser aggregates^{NS}, where sub-surface flow will take place between larger voids. A coarse grained assemblage creates a highly porous zone for water and air to flow, where

preferential flow paths can be vertical, horizontal or inclined (Fala et al., 2003). A fine-grained non-segregated waste-rock pile will be dependent on pore-flow conditions, largely controlled by surface infiltration rates and hydraulic conductivity (Smith et al., 1995). It is therefore hypothesised that the non-soils of this study will have higher leachate volumes, as compared with the more cohesive soil SFMs.

2.3.3 SFM chemistry

Differences in non-soil and soil chemistry are not straight forward. Graham et al. (2010) discuss the transition of hard rock to soil, and identifies the regolith stage as the transition between the two. Saprolite materials are identified as being derived from *in-situ* rock weathering where the original rock, texture, fabric and structure has been retained. They are commonly found in tropical regions (Massey and Pang, 1988; in Gan and Fredlund, 1996). The physical and chemical properties that distinguish a saprolite material from a soil or non-soil are not defined in the literature. Differences in the extent the SFM was disturbed during excavation and weathering processes once the non-soil has been exposed to the surface (Price, 2009) will affect the non-soil's physical and chemical properties.

Soil pH is a good indicator of soil processes such as leaching, podzolization, calcification, salinization and humification (Addison et al., 2002). Electrical Conductivity is also used as an indicator of soil salinity (Ehsani and Sulliven, 2010). There is a connection between pH and the amount of base saturation, because a high base saturation value would indicate that the exchange sites on a particle are dominated by non-acid ions (Addison et al., 2002). Soil pH and the net negative charge affect the rate of clay dispersion, which affects surface seal development and runoff formation (Chrom et al., 1994; in Igwe and Nkemekosi, 2007).

Cation Exchange Capacity (CEC) explains the overall base cation concentration (the net negative charge) of a mineral and its ability to attract positively charged cations. Most commonly occurring cations in soils are calcium (Ca), magnesium (Mg), potassium (K) and sodium, (Na) (White, 2006). Exchangeable Na content is important in terms of erodibility as soils with high Na (sodic soils) have reduced aggregate^{S} stability from Na causing physico-chemical induced swelling, clay dispersion, and disaggregation (Singer and Munn, 1999). Dontsova and Norton (2002) demonstrated that the Ca^{2+}/Mg^{2+}ratio had a significant effect on clay dispersion and surface sealing, with Mg-treated soils

registering final infiltration rates approximately 50% lower than those of Ca-treated soils. This is primarily due to the hydration energy and hydration radius of Mg^{2+} being greater than Ca^{2+} (Bohn et al., 1985; in Karimor et al., 2009). In Mg-dominated soils, clay surfaces tend to absorb more water than when exchangeable Ca^{2+} is present. Studies on Nigerian tropical soils reveal that there were significantly more exchangeable cations, CEC, exchangeable acidity and available phosphorus in the clay fraction as compared with the silt fraction, and that high CEC was found to encourage aggregation^{S} rather than dispersion (Igwe and Nkemekosi, 2007).

2.3.4 Mineralogy

The mineralogy of non-soils will reflect the parent material mineralogy and its exposure to biological, chemical and physical processes that can cause mineralogy to change with time; as often happens during mining when materials are stored in waste-rock dumps (White, 2006; Price, 2009). Mineralogy has an important effect on soil and non-soil resistance to physical and chemical breakdown by water (White, 2006). Non-soil resistance to breakdown is dependent on the mineralogy of its surface area that has been exposed to rainfall (Price, 2009). Mineral resistance to breakdown is influenced by the degree of sharing between cations and anions in the crystal lattice; Si-O bonds have the highest energy on formation followed by Al-O, O-Na and O-Ca bonds (the metal cations) (White, 2006; Price, 2009).

In soils the mineralogy of the silt and sand fraction is largely influenced by the parent rock material, as well as the salts, oxides and hydroxides formed from weathering and erosion (White, 2006). Most Fe (hydroxide) oxides form by precipitation from solutions and are known to accumulate in highly weathered soils, maghemite and hematite form, also during weathering of the primary mineral magnetite (Fe_3O_4) (White, 2006). Goethite is the most common mineral and ferrihydrite is a poorly ordered Fe oxide that readily re-precipitates (White, 2006). Hematite minerals are common in areas where organic matter is rapidly oxidised, and goethite and maghemite are common in tropical regions. Gibbsite is the main aluminium mineral in soils, which is formed in acid soils when aluminium hydroxides crystallise (White, 2006). The primary titanium oxides in soils are rutile and anatase (both TiO_2) and tend to be most abundant in tropical weathered soils (White, 2006). Muscovites are often found in the sand and silt sized fractions of less weathered rocks (White, 2006).

Soils and weathered non-soils are likely to contain different clay minerals (White, 2006; Price, 2009). Adsorption of water and solutes depends on the specific surface area of the clay and the types of minerals present (White, 2006). Clay minerals are important for physical and chemical reactions such as flocculation, dispersion, cation exchange, moisture retention, aggregation and the adsorption of soil conditioners (Simmons, 1998; White, 2006). The mineralogy of the clay fraction depends on the parent material and subsequent weathering, and is broadly sub-divided into predominately phyllosilicates and mineral oxides, hydroxides and salts (White, 2006). The phyllosilicates crystal layers have varying silicon to aluminium ratios including ≤1 the imogolite and allophones, 1:1 the kaolinities and 2:1 the illites, vermiculites and smectites.

Clay mineralogy affects SFM erodibility, with kaolinite, halloysite, chlorite and fine grained micas including muscovite most resistant to expansion from rapid-wetting as opposed to smectite, vermiculite and illite minerals, which are more erodible on rapid wetting (Morgan, 2006). Clays including montmorillonite, illite and vermiculite are more effective at retaining positive cations, and are associated often with greater stability (Ehansani and Sulliven, 2010). In general 1:1 clays are most stable in water because they have strong hydrogen bonds and uniform crystal structure, compared to 2:1 clays that have weaker van der Waal and electrostatic forces (White, 2006).

2.3.5 Antecedent moisture content

Antecedent moisture content is defined as the moisture content of a material prior to a rainfall event, and can have different effects on soil erodibility as summarised in Morgan (2006) and Kollet and Maxwell, (2006).
These effects include:

- Dry soil that receives heavy rainfall can lead to slaking, caused by compression of air that bursts out at the wetting front.
- Partially wet soils can experience aggregate breakdown following rainfall, which may reduce surface roughness and the likelihood of runoff generation, but not yet reducing infiltration rate.
- Saturated SFMs with <15% clay are most likely to experience sealing if rainfall intensities are high.
- In general, soil strength will increase with decreasing soil moisture and material detachment decreases with increasing soil strength (relative to rainfall KE).

Some studies have found pre-wetting the soil greatly reduces runoff (Le Bissonnais and Singer, 1992; in Le Bissonnais et al., 1995). Conversely, other

studies indicate that runoff starts very quickly on wetted soils (Bajracharya and Lal, 1992; in Le Bissonnais et al., 1995). Sandy soils with low capillary storage, at their limiting moisture content produce runoff, despite rainfall intensity being less than infiltration capacity (Morgan, 2006). Soils with high silt contents and high moisture may be less stable than more cohesive (non-swelling) clay-based soils (Morgan, 2006). Unlike soil SFMs, less is known about how moisture content affects the erodibility and hydrological response of non-soil SFMs. Smith et al. (1995) suggests waste-rock SFMs containing a higher percentage of clay (no amount is defined), are more likely to experience dispersion in water or swelling behaviour, and are most susceptible to weathering.

Changing moisture conditions are pertinent to this project as the mine-site is located in a region that has a distinct rainy and dry season causing contrasting moisture conditions. Therefore, it will be important to understand if erosion susceptibility changes at different antecedent moisture conditions, and also whether non-soils are as responsive to changing moisture conditions as soil SFMs.

2.3.6 Magnetic susceptibility

Few research papers compare the magnetic properties of soils and non-soil SFMs, and assess the relationships between magnetic susceptibility (MS) and erodibility (Rhoton et al., 1998). MS is a measure of the 'magnetizability' of a material (Thompson and Oldfield, 1986; in Dearing, 1999) and its concentration of iron (Fe) bearing minerals (Dearing, 1999). Typically SFMs contain more than one type of magnetic mineral (Dearing, 1999). Dual MS readings give measurements at two magnetisation frequencies, high and low (Dearing, 1999; Price, 2009). Low frequency measurements will infer the bulk magnetisation of the sample, and high frequency readings are indicative of secondary minerals (Dearing, 1999). Magnetite and maghemite are common magnetic minerals that if found will dominate the MS measurement and are known as ferromagnetic (Dearing, 1999). Lower MS values are found in antiferromagnetic minerals including haematite and goethite (Dearing, 1999). Weak positive MS is recorded in paramagnetism Fe minerals and salts such as biotite and olivine, and weak negative MS readings are recorded in diamagnetic materials such as water, organic matter and quartz (Dearing, 1999).

Fe oxides are a major weathering product of tropical soils (Hendrick et al, 2005). Magnetite and maghemite are of very fine grain size (~0.4-0.001 mm) (Maher, 1998). In non-soils intrinsic magnetic minerals are referred to as

primary minerals, and other Fe oxides that have formed from external processes, such as digenesis, soil formation, bacteria or fuel combustion are called secondary minerals (Dearing, 1999). Taking into account that the SFMs in this study have originated from a mine-site known to be rich in Fe minerals, it is theorised that the soils and non-soils will have magnetic properties. Studies in the Memphis Catena found the types of Fe oxides recorded were related to changes in erodibility (Rhoton et al., 1998). A significantly ($p<0.01$) positive correlation was found between soil loss and the portion of citrate bicarbonate of dithionite (used to determine the amount of ferrimagnetic minerals present) (Rhoton et al., 1998). The findings suggested that portions of Fe oxide occur as discrete particles, which discourage aggregation^{S}, as opposed to acid ammonium oxalate extractable Fe, which was considered to be a more important mineral in aggregation^{S} (Rhoton et al., 1998). The range of SFMs investigated in this study will develop the knowledge base regarding the links between MS and erodibility.

2.4 The effects of rainfall erosivity on runoff and erosion

Erosivity is defined by Hudson (1989) as the potential ability of rain (or wind) to cause erosion. Erosivity is a function of rainfall drop size, intensity, and duration (Lal, 1988) and can be assessed from the 'cumulative KE of a storm' (Lal, 1988; Hudson, 1989). Rainfall KE is measured in J m² and defines the energy available for compactive and dispersive processes that may result in aggregate breakdown; KE = (0.5 (rain drop mass (terminal velocity)²).

Rain drop size is conventionally described by the drop size distribution (DSD), or the median drop diameter (D_{50}), which is the median point on a cumulative percentage volume curve (Hudson, 1989). Variations in rain drop size and shape are the result of the breakup and coalescence processes operating during the raindrop's free-fall to the ground (Assouline, 2009). In tropical rainfall events larger drops have greater mass and vertical terminal velocity, resulting in higher erosivity thus causing more erosion (Fox, 2004). DSD provides only an '*estimated'* KE value, because actual calculations of single drop velocities are difficult to quantify due to the changing drag coefficient during the descent of the raindrop (Simmons, 1998).

D_{50} changes with intensity and rain drop diameters appear to increase with rain intensities >100 mm hr $^{-1}$; and then decreases in size at rain intensities >200 mm hr $^{-1}$ (Hudson, 1989). Hudson's (1989 p 54) DSD chart for high intensity rainfall shows D_{50} of 2-4 mm for 100 mm hr^{-1} rainfall intensities (the design storm used in this study). In tropical climates, rainfall intensities may be

between 100-150 mm hr^{-1} and KE *tends* to level off to 0.29 MJ ha^{-1} mm^{-1} when reaching intensities >75 mm hr^{-1} (Morgan, 2006). Studies in Nigeria, which is in the same geographic region as Guinea, found at least 10 rainfall events (per rainy season) to reach intensities >120 mm hr^{-1}, as compared to perhaps 1 event per year in the UK (Ajayi, 1982). This highlights the high erosivity of West African rainfall, and the importance of replicating storm KE and drop size in the laboratory, to ensure that measured erosion, leachate and runoff reflect those likely to be experienced in the field.

2.5 Polymer-based treatments (PBTs) to control runoff and erosion on a mine-site

2.5.1 Using PBTs to control runoff and erosion on a mine-site

Soil conditioners and soil stabilisers reduce soil degradation, dust and erosion (Morgan, 2006). There are many types, including organic products (Sojka et al., 2007), flocculants such as gypsum, alumn or poly-aluminium chloride (Morgan, 2006), mineral conditioners such as oxides of Fe (Sojka et al., 2007) and dust suppressants, such as asphalt, latex and plastic sprays (Singer and Munns ,1999; Kissell, 2003).

Synthetic Polymer Based Treatments (PBTs), which include polyacrylamide (PAM), polyvinylacrylic-latex (PVAL), or polyvinylacetate (PVA) come in different forms usually as oil based, water based, granular or as dry tablets and are an effective erosion control solution because they stop erosion at source (Zejun et al., 2002; Vacher et al., 2003; Martínez-Rodríguez et al., 2007; Lee, 2009; Weston et al, 2009).

PAMs have been extensively reported as an effective erosion control solution in the literature, as detailed in Table 2.1. PAMs used on non-vegetated, steep slopes are reported to be a cost effective erosion control option, in comparison to the high costs of slope profiling (Green and Stott, 2001). Solutions such as mulches have high costs due to the need for high quantities of mulch at larger sites, and can be ineffective if rills form (Green and Stott, 2001). PBTs are considered advantageous for use on mine-sites because they are easily applied and cheaper by about one tenth as compared to Class-A Type 1 erosion mats (Nwankwo, 2001; Sojka et al., 2007). PBTs also provide ‘temporary’ non-permanent erosion control, which is beneficial on a mine-site where the landscape is continuously re-engineered. Anionic PAMs are well documented

for use in the agricultural sector (Aase et al., 1998; Zejun et al., 2002; Sojka et al., 2007; Mahardlika et al., 2008). Green and Stott (2001) note the potential for PAMs to stabilise steep slopes in construction, mine spoils, highway-cuts and other disturbed landscapes. However, application in these sectors is less reported in the literature, particularly the mining sector.

PAMs are flocculants, forming ionic bonds between (suspended) clay and silt particles that create larger aggregates (Green and Stott, 2001; Nwankwo, 2001). This inhibits the re-suspension of material (Weston et al., 2007), enhances aggregate stability and permeability (Green and Stott, 2001; Bratby, 2006). Erosion is reduced as more energy is needed to move larger particles than smaller particles (Yonts, 2008). Through retaining aggregate stability, the surface is more resistant to the erosive forces of dispersion and shear by rainfall (Nwankwo, 2001; Vacher et al., 2003). Controlling the supply of disaggregated material prevents surface sealing, maintains infiltration and deters surface runoff formation (Nwankwo, 2001). Images taken using a scanning electron microscopy (SEM) revealed soils without PAM treatments were more compact with higher bulk densities and smaller pores, and soils to which PAM had been applied had no crust with higher porosity (Zejun et al, 2002). Vacher et al. (2003) found that PAM increased aggregate strength, but did not protect against the compactive effects of raindrop impacts.

Compared to PAMs few research papers (Khansbasi and Abdalla, 2006; Movahedan et al., 2012) report on the effects of PVAL or PVA PBTs when used as an erosion control solution, and no known papers report on PVALs to control erosion on mine-site soil, ore or waste-rock SFMs. PVALs and PVAs function as soil stabilisers and form a permeable film after dehydration, which strengthens the surface (Khansbasi and Abdalla, 2006). PVALs and PVAs are commercially sold as dust suppressants (Sojka et al., 2007). Khansbasi and Abdalla (2006) report enhanced mechanical strength, measured by unconfined compression testing, when a PVAL was used on a desert sand material obtained from a sandy dune quarry. This gives some indication that the PVAL will be successful stabilising the surface of the non-soil SFMs evaluated in this study.

A better understanding of the types of commercially available PBTs and their effects on the erodibility and hydrological response of SFMs found at a mine-site will be beneficial to the wider disturbed-lands/construction sectors. This is because although organisations, such as the USA Department of Agriculture Natural Resources Conservation Services (USDA NRCS), endorse the use of polymer products for erosion control, there are no current guidelines that explain the effectiveness of the product on waste-rock and ore materials (Lee, 2009).

Table 2.1 Summary of PAMs and their effects on erosion and runoff reported in the literature

	PAM Description	Experimental Conditions	Outcomes of PBT Study	Reference
1	High molecular weight (12-15 mg mol^{-1}.) anionic PAM Super Floc A836, with 18% charge density	Four PAM application rates were tested: 0, 1, 2, 4 and 6 kg ha^{-1}.	The low 2 kg ha^{-1} application rate at 8 mm dilution worked better than the higher application rate 6 Kg ha^{-1} at 20 mm dilution. 2 kg ha^{-1} in the first irrigation reduced runoff by 70% and soil loss by 75%, but these effects were not sustained in irrigations two and three.	Aase et al. (1998)
2	Three anionic PAMs were tested including SOILFLOC^{TM} 300-E, PAM-Ald and SOILFIX^{TM} LDP	PAMs were tested on Puerto Rico soils at 20% slope. Erosion loss was recorded after 1, 2, 8, 30 and 60 days post treatment using 20, 80, 120 kg ha^{-1} application rates.	All treatments caused a significant reduction in sediment loss following the first rainfall event, but at rainfall event three the lowest PAM application rate 20 kg ha^{-1} had soil loss amounts 150% than that of rainfall event one. No significant difference were found in the erosion amounts of the 80 kg ha^{-1} and 120 kg ha^{-1} treatments when measured at the first four time intervals, although after 60days (time interval five) the 120 kg ha^{-1} generated significantly less erosion than the 80 kg ha^{-1} .	Martínez-Rodríguez et al. (2007)
3	Cytec A110 Superfloc (18% charge density and 15 Mg mol^{-1} molecular weight) anionic PAM	5000 kg $ha^{-1}$of dry gypsum was used with 20 kg ha^{-1} and 40 kg ha^{-1} PAM.	For the silt loam soils, the gypsum without PAM treatment was more effective at reducing soil loss than the PAM alone treatment. Gypsum alone was just as effective as the PAM; although the PAM plus gypsum was consistently the most effective erosion control treatment for all soils. Variations in PAM effectiveness were attributed to clay content, pH and CEC.	Lee (2009)

4	Siltstop 634 emulsion PAM (15-20 Mg mol^{-1} molecular weight and 20-30% charge density)	14 l ha^{-1} PAM was applied with a hydroseed mix on slopes ranging between 2-30% in Georgia US.	The PAM plus hydroseed treatment had no statistical benefit in terms of erosion control than the hydroseed alone treatment. Low clay content and low CEC were in part the reasons that the PAM did not perform as expected. The absence of rain may have caused also the PAM to photo-degrade, reducing the PAM's effectiveness.	Markewitz and Glazer (2009)
5	Dry granular anionic PAM with molecular weight of 5 Mg mol^{-1} (no product name given)	PAM was applied at 25, 50 and 75 kg ha^{-1} and gypsum was applied at 10, 20 and 30 Mg ha^{-1} on steep soils in Iran	The higher application rate PAM plus gypsum treatments (75 kg ha^{-1} PAM plus 30 Mg ha^{-1} gypsum) was most effective reducing soil loss on the steeper slopes (30%) and under the most intense rainfall conditions (75 mm hr^{-1}). Sediment reductions recorded for the highest application rate PAM ranged between 11-44%, 48-64% and 85-92%, respectively, compared to 0-7%, 0-9% and 5-13%, which were the results of the lowest application rate 25 Mg ha^{-1} PAM treatment.	Akbarzadeh et al. (2009)
6	Superfloc A-110 dry anionic PAM	40 kg ha^{-1} PAM and 10,000 kg ha^{-1} gypsum, which was mixed into the upper 5 cm, was applied to one soil and one overburden material from Central Queensland, Australia.	Soil loss reductions of 39%, 43% and 74% was recorded for the respective gypsum alone, PAM alone and PAM plus gypsum treatments compared to the control, and 41%, 50% and 70% for the overburden material. The chemical and physical properties of the materials are not given.	Mahardhika et al. (2008)
7	Anionic PAM (product information not given)	20 kg ha^{-1} PAM and gypsum (2500 kg ha^{-1}) was tested on soil plots in areas of the Indian Himalayas	PAM alone did not significantly reduce soil losses compared to the gypsum alone and PAM plus gypsum treatments, with soil loss ranging 0.9-10.7%, 35.3-88.2% and 43.5-89.3%, respectively. It was recommended that gypsum alone would be a more cost effective erosion control option for this location.	Kumar and Saha (2011)

2.5.2 How PBTs control runoff and erosion

Synthetic PBTs are long chain, soluble, synthetic copolymers of acrylamide functional group monomers (PAMs) and acrylic latex functional groups (PVALs) (Khanbashi and Abdalla, 2006; Yonts, 2008). Polymer structures can be cross linked or linear. Only linear polymers are used for erosion control because cross linked polymers cannot form chelates or tackifier agglomerations (Steve Iwinski, personal communication, 24th August, 2011). Linear polymers are dissolved in water and the charge created by the water and soil creates a bridge for the dissolved polymer to bond to the soil causing flocculation to happen (Sojka et al., 2007).

Polymers are identified by molecular weight, the type of monomer and the amount of active ingredient or charge density (Vacher et al., 2003). Polymer charge density and molecular weight affect the amount of polymer adsorption (Bratby, 2006). Changes in molecular weight are caused by increasing the length of the polymer chain (Green and Stott, 2001). Charge density is expressed as the percentage monomer copolymerized (or percentage hydrolysis), and the resultant charge is either cationic (net positive), non-ionic (neutral) or anionic charge (net negative) (Barvenik, 1994; in Green and Stott, 2001; Vacher et al., 2003).

Cationic and neutral PAMs have toxicities warranting caution, (Sojka and Surapaneni, 2001; Weston et al., 2009; Clark, 2010), and only anionic PAMs are reported in the literature (Table 2.1). In anionic PAMs the acrylamide is negatively charged at high pH by acid dissociation reaction (-COOH → -COO- + H^+). Clay particles are the primary constitute onto which polymer molecules are absorbed (Schamp et al., 1975; in Vacher et al., 2003; Bratby, 2006). Anionic polymers do not exhibit adsorption, due to charge repulsion between polymer molecules and negatively charged clay surfaces, but this is overcome by covalent bonding, cation bridging, water bridging (hydrogen bonding) and/or van der Waal attraction (Simmons, 1998; Kanungo, 2005; Lee, 2009). Anionic polymers are absorbed to clays in two forms of cationic bridging. The first happens in aqueous solutions where an anionic group interacts with exchangeable cations through water molecules, forming an outer-sphere diffuse complex (Simmons, 1998). The exchange of cations reduces the size of the diffused double layer that surrounds the clay particle, increasing the attraction to neighbouring clay particles (Bratby, 2006) as illustrated in Figure 2.2. The second happens under dehydrated conditions where polymer anions are directly associated with exchangeable cations forming an inner sphere complex (Simmons, 1998). During dehydration water molecules are displaced by anionic polymer molecules, and absorbed molecules interact through van der Waal attraction, and drying increases interaction (Simmons, 1998).

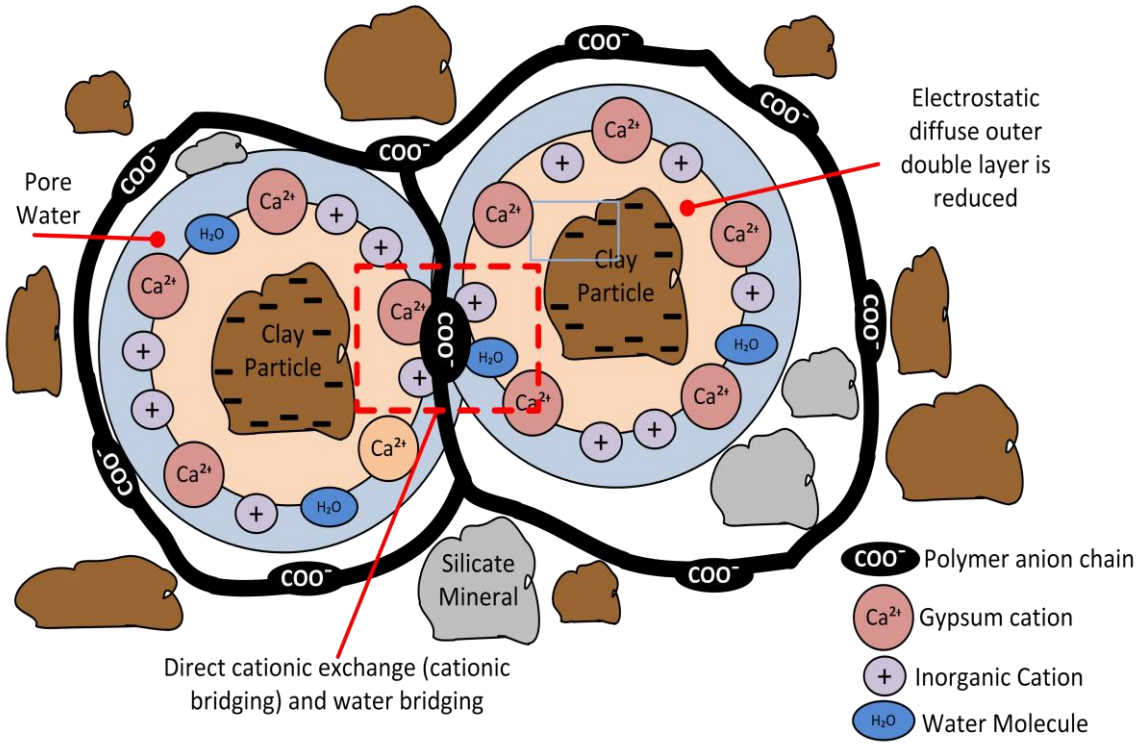

Figure 2.2. Conceptual diagram of polymer molecule adsorption onto clay minerals *(Source: Author, 2012)*

Non-ionic PVALs and PVAs like PAMs are absorbed onto clay surfaces primarily by hydrogen bonding (Kanungo, 2005). Non-ionic PVALs and PVAs do not have a charge density (Lu et al., 2002), so do not form cation bridging, but they contain vinyl acetate and latex based monomers that form a permeable film at the surface, which after dehydration strengthens the surface (Khansbasi and Abdalla, 2006). Depending on the polymer's viscosity, water and oxygen are still able to penetrate the surface, but the polymer changes the mechanical properties of those particles it is adhered to, and holds particles in place, preventing detachment and entrainment from raindrop impact and the shear forces of runoff (Khansbasi and Abdalla, 2006).

2.5.3 The Effect of application rate on PBT efficacy

The literature discusses a range of anionic PAM application rates for use on a range of soil types and slope conditions, some of which are detailed in Table 2.1 and by Sojka et al. (2007). However, there are few studies that discuss PAM application rates on ore and waste-rock SFMs (Mahardhika et al., 2008), and no known studies that have tested PVALs application rates on mine-site soil, ore and waste-rock SFMs.

Mixed outcomes are reported using high and low application rate anionic PAMs on soils. Soupir et al. (2004; in Sojka et al., 2007) observed that if the application solution is too concentrated, its high viscosity can restrict infiltration, thereby generating more runoff. No real benefit was found using the higher application rate treatment compared to the lower application rate treatment in terms of material loss and cumulative runoff in a study by Lee (2009). These findings are consistent with Aase et al. (1998) as well as Tang et al. (2006; in Lee, 2009). However, findings listed in Akbarzadeh et al. (2009) including Flangan et al. (2002) and Peterson et al. (2002) found higher anionic PAM application rates including 60 kg ha^{-1} and 80 kg ha^{-1}, respectively, were most successful at reducing soil loss on steep slopes. The benefits of using PAM in terms of erosion and runoff reduction are shown to be not straightforward, where high application rate treatments may cause the greatest reduction in erosion, but this may equate to higher runoff volumes (Lee, 2009).

2.5.4 Different types of SFMs on PBT effectiveness

PBT effectiveness is dependent not only on the PBT formulation; but also on the SFM's chemical and physical characteristics (Vacher et al., 2003; Sojka et al., 2007). Soils with 50% clay showed no significant difference between anionic PAM treatments with different molecular weights and charge densities, but effectiveness improved with PAM application rate. This is thought to be in part due to the fact that as clay content increases, the importance of distance to bonding sites and length of the PBT molecule decrease. However, the amount of PAM and hence amount of charged sites becomes more important (Vacher et al., 2003). Sojka et al. (2007) notes PAM performance was enhanced by adding small amounts of clay material to coarser textured soils. Lecourtier et al. (1990; in Sojka et al, 2007) recognised a critical salt concentration will exist for the adsorption of anionic PAMs to overcome electrostatic repulsion from charged minerals. Studies by Bhardwaj and McLaughlin (2007) revealed clay mineralogy affects the success of different PAM treatments, and soils with smecite and

kaolinite clays flocculated better and quicker than illite and montmorillonite based soils.

Soil pH is important because there is a decrease in PAM adsorption with increasing solution pH (Lu et al. 2002; Deng et al. 2006; in Lee, 2009). Lee (2009) found that anionic PAM plus gypsum treatments were successful at reducing erosion on a range of soils, apart from one soil containing very high organic matter. This is because high organic matter containing soils are more stable, which may reduce access to anionic PAM sorption sites (Auerswald, 1995; in Lee, 2009; Mbagwu and Auerswald, 1999; in Lee 2009). PAM adsorption has been found to vary between soil types, soil surface areas and soil texture, but there are no known studies that discuss the physical and chemical properties of non-soil SFMs in relation to PBT effectiveness. Therefore, the results from this study will be an important contribution to the potential application of PBTs for erosion control in the mining sector.

2.5.5 The effect of gypsum on PBT efficacy

Charged cations overcome the repulsion associated with polymer to mineral negative charge sites (Sojka et al., 2007). Studying a range of cations, Rengasamy and Sumner (1998; in Sojka et al., 2007) found divalent cations were 28 times more effective at enhancing anionic PAM sorption than monovalent cations, such as Na^+ and K^+. The double charge and small hydrated radius of divalent Ca shrinks the electrical double layer surrounding charged particles, increasing cation bridging between the clay and polymer molecule. This promotes flocculation; as compared to Na which has a large hydrated radius that prevents ion bridging leading more often to dispersion (Sojka et al., 2007; Kumar and Saha, 2011). Gypsum ($CaSO_4$) is a frequently used source of Ca^{2+} that can be applied as a solution or by direct-application to the surface (Green and Stott, 2001).

Studies in Brazil found that final infiltration increased four times and erosion was reduced by 70% using 4000 kg ha^{-1} gypsum in conjunction with a dry PAM at 20 kg ha^{-1} (Yu et al., 2003; in Sojka et al., 2007). An assessment of a PAM (40 kg ha^{-1} Superfloc A-110 dry anionic PAM) and gypsum (10,000 kg ha^{-1}) on one soil and one waste-rock material from Central Queensland, Australia reported significant reductions in erosion loss using PAM plus gypsum treatments (Mahardhika et al., 2008). These findings indicate that PAM plus gypsum treatments will be successful on the non-soil SFMs in this study, but as the characteristics of the waste-rock materials are not disclosed, no direct comparisons can be drawn between the two studies. PAM (20 kg ha^{-1}) used

with gypsum (2500 kg ha^{-1}) on soil plots in the Indian Himalayas revealed minimal differences in soil loss between the gypsum alone and PAM plus gypsum treatments (Kumar and Saha, 2011), and gypsum alone was a more cost effective erosion control solution for the location (Kumar and Saha, 2011). Consequently, a gypsum without polymer treatment will be tested in the Phase II experimental design of this study.

2.5.6 Method of application effects on PBT efficacy

Granular or tablet forms are often used in furrow irrigation, but these are not practical for sprinkler irrigation systems or high pressure sprayers (Weston et al., 2007). Polymer viscosity can affect the ease at which it can be applied, (Green and Stott, 2001), and whether sufficient total solution volume creates sufficient penetration of the polymer into the surface (Lentz, 2003; in Sojka et al., 2007; Markewitz and Glazer, 2009). Polymer effectiveness increases when subject to a drying cycle (Zhang and Miller, 1996; in Green and Stott, 2001), because drying induces inner-sphere complexes and van der Waal forces of attraction between the polymer and the clay, causing the polymer chain to become irreversibly absorbed to the substrate (Shainberg et al., 1990; in Green and Stott, 2001). Drying times of 12 to 24 hours are recommended (Vacher et al., 2003).

PAM used with a straw mulch concluded the straw plus polymer and straw-only treatments typically performed 5 to 10 fold better than the polymer-only treatments for erosion control and about 2 fold better for infiltration improvement (Vacher et al., 2003). This is because the straw provided additional surface cover reducing the energy of impacting raindrops. Although the PAM reduces aggregate breakdown it does not, like the straw, provide a barrier from the compactive effects of raindrop impact (Vacher et al., 2003). Furthermore straw mulch would not be cost effective for a large dynamic mine-site.

2.6 SFM surface roughness quantification using a Geographic Information System (GIS)

Surface Roughness (SR) is an expression of the variability of elevation of a topographic surface at a given scale (Grohmann et al., 2009). SR change has been directly linked to the severity of erosion processes (Bergsma and Farshad, 2007), and is an important parameter for understanding rainfall erosion

mechanisms at small scales (<1 m²) (Jester and Klik, 2005). For these reasons, it can be used to understand the effectiveness of PBTs at a sub-process level.

Surface micro-relief variability can be assessed by its relative smoothness, roughness or ruggedness over time. Valentin (1985; in Bergsma and Farshad, 2007) describes the sharpness of aggregates is lessened by swelling processes; and slaked material or dispersed aggregates create a more rugged surface. Raindrop impact pedestals can create a more rugged surface over time. Alternatively overland flow, compaction and crusting can cause smoothing (Bergsma and Farshad, 2007). A surface that shows no change in SR after rainfall could be considered as either being very stable; or in a dynamic equilibrium of erosion and deposition processes. It is hypothesised that the greatest change in SR during a rainfall event will be associated with the untreated control, followed by the gypsum only treatment and then the polymer only treatment. The polymer plus gypsum treatment will show the least change in SR as these treatments will be the most effective stabilising the surface, as illustrated in Figure 2.3.

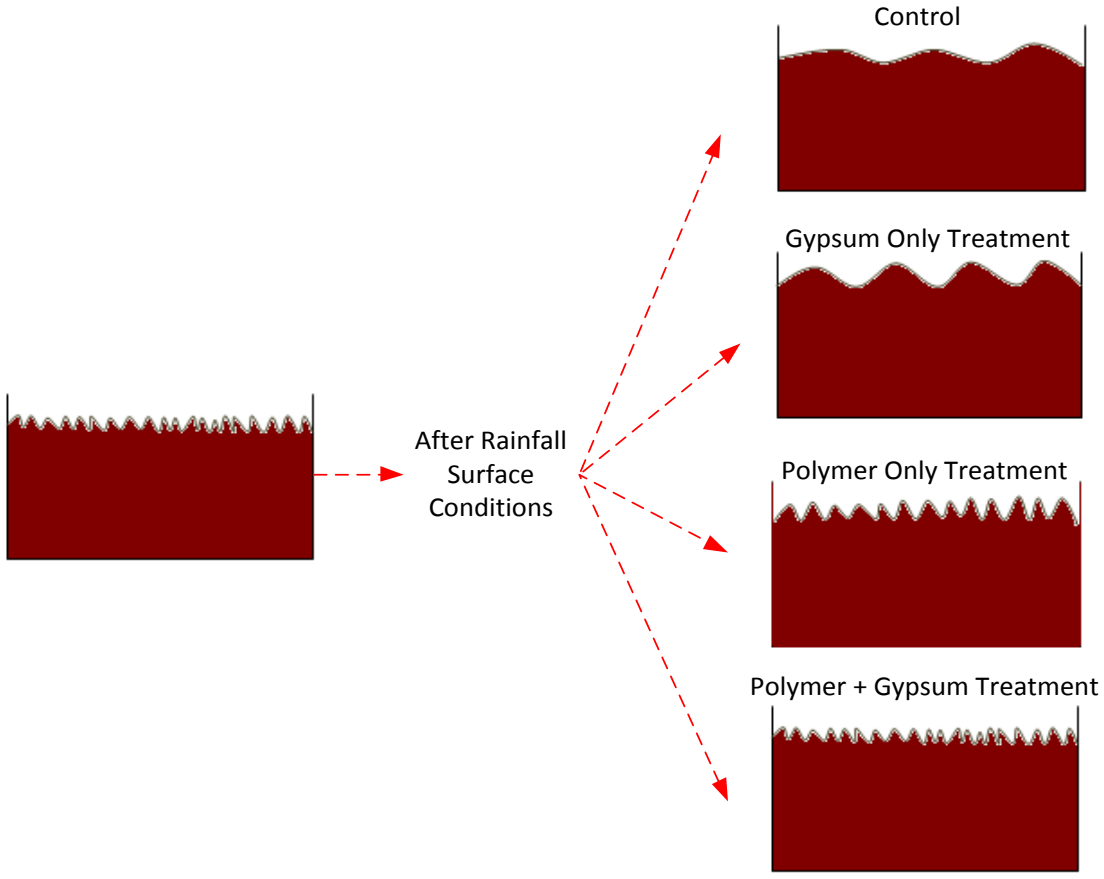

Figure 2.3 Conceptual diagram illustrating the predicted response of PBTs surface roughness to rainfall *(Source: Author, 2012)*

SR can be assessed by either 2D or 3D methods. Conventional 2D methods use erosion pins or micro-relief meters to determine surface height change (Hudson, 1989; Merel and Farres, 1998). The tortuosity method uses a pin meter or roller chain of fixed length to calculate the surface profile ratio of a transect (Kamphorst et al., 2000). These methods involve spatial sampling and give low spatial accuracy, where the devices themselves affect surface processes and may bias results (Hudson, 1992; in Nouwakpo et al,. 2010; Merel and Farres, 1998). Other methods include Random Roughness Assessments (the standard deviation of point elevations for a given plot reference plane), but this can be time consuming (Merel and Farres, 1998; Vidal Vàzquez et al., 2008). Kamphorst et al. (2000) discusses the need for 3D SR measurements, but reasoned photogrammetry methods in the 1990s were expensive. Quality high resolution digital single lens reflex cameras such as the Canon EOS 500D can now be purchased for <£500, making photogrammetry methods financially viable.

2.6.1 Near Surface Digital Photogrammetry (NSDP) as a tool for quantifying micro surface roughness change during rainfall

Near Surface Digital Photogrammetry (NSDP) facilitates precise measurements by using a pair of cameras at low height (<300m) above the surface to produce a pair of stereo images with at least 60% overlap. Stereo images generate single 3D Digital Elevation Models (DEMs) (Wolf and Dewitt, 2000; Mohamed et al., 2009). DEMs can be used to locate points in an image to find distances, areas, volumes, elevations and the size of objects and so quantify surface micro-relief (Wolf and Dewitt, 2000; Lascelles et al., 2002; Mohamed et al., 2009). NSDP derived DEMs used in a GIS can provide terrain and SR statistics quickly and readily. The images generated are a permanent record of topography that can be re-visited any time (Mohammed, 2009). NSDP used in micro-terrain studies has potential for quick application; although for the non-NSDP specialist this will only be achieved after time finding familiarity with the software and camera equipment (Lascelles et al., 2002).

Laser scanners are reported to generate lower DEM precision and resolution than NSDP produced DEMs (Rieke-Zapp et al., 2001). Furthermore scanners can take an hour to scan one surface, and are also more expensive than the equipment needed to facilitate NSDP (Rieke-Zapp et al., 2001). However the accuracy of a DEM compiled by NSDP and a laser scanner has been found to be statistically comparable by Nouwakpo et al. (2010), in both laboratory and field studies, with the ground co-ordinate precision of 2 m^2 soil images to be 0.83×10^{-3} m.

DEM resolution can be affected by the target area (lighting, amount of contrast features in shot), type of camera, camera height, distance between the cameras, resolution of camera, accuracy of measured ground control points, light conditions and software capacity (Mohamed et al., 2009; Gessesse et al., 2010; Wolf and Dewitt, 2000). Nouwakpo et al. (2010) found rougher surfaces caused higher error than smoother surfaces, thought to be because rough surfaces have more relief displacement, which reduces the performance of the image matching algorithm. In contrast, Mohamed et al. (2009) found smoother surfaces had higher error, thought to be because rough surfaces provide better image contrast. Having independent check points in the NSDP model is a quantitative way to assess DEM accuracy, enabling automated comparisons of the check points' positioning to their estimated co-ordinates (Chandler, 1999).

NSDP has been used to assess rill initiation by overland flow (Lascelles et al., 2002), field based rill erosion and deposition rates (Gessesse et al., 2010), soil loss by erosion (Nouwakpo et al., 2010), micro-topography river bed flow processes (Lane and Chandler, 1998), rill network evolution (Rieke-Zapp and Nearing, 2005), rill and surface depression assessments (Mohamed et al., 2009) and sheet erosion evolution (Moritani et al., 2010). This study will use NSDP derived images in a GIS to understand how PBTs affect rainfall erosion processes. This combined NSDP and GIS methodology is entitled 'Near-Surface Photogrammetry Assessment of Slope Forming Materials' Surface Roughness and from here on in will be referred to as 'NSPASS'.

2.6.2 The advantages of using a GIS to assess SFM surface roughness

3D SR assessment methods use a Geographic Information System (GIS), which is an integrated computer-based tool that facilitates the input, processing, display and output of spatially referenced data (Shi et al., 2004; Jester and Klik, 2005). Complex GIS methods have been used to determine SR including the 'Fractal Dimension' concept (Mandlebrot, 1983; in Jenness, 2004), which compares the dimension of the irregular and flat surface that goes through every point within a given volume (Jenness, 2004). Inferences about SR have been made from cell-based slope and aspect algorithms, although this generated values 1.6-2.0 times the size of the cell (Hodgson, 1995; in Jenness, 2004; Grohmann et al., 2009). The Area-Ratio method is a ratio of the flat planimetric area and actual surface area within a cell. Flat surfaces have ratio values close to 1.0 and, more rugged terrains have increasing SR ratio values,

that in theory could have an infinite value, but are usually <10 (Jenness, 2004; Grohmann et al., 2009).

The Area-Ratio method, unlike other GIS methods is scale independent (Grohmann et al., 2009), and is a downloadable GIS extension that automates the determination of SR statistics (Jenness, 2004). The precision and accuracy of this ArcGIS tool is statistically comparable to thin section based assessments (Jenness, 2004). However SR raster based methods make the analysis automated, objective and quicker to perform. Huang and Bradford (1990; in Mohamed et al., 2009) argue that roughness cannot be completely described by a single index such as random roughness. However, having a mean SR value, representative of variance within the entire target area, is considered to be more representative than transect sampling techniques (Jenness, 2004), particularly as the SFMs in this study have highly variable physical characteristics.

The ArcGIS SR extension tool has been successfully used in the zoological field in the context of population movements and terrain studies (Jenness, 2004). However, to date this SR extension tool has not been used in combination with NSDP derived DEMs for pedological or geomorphological applications. This study will use SR information derived using NSPASS, to make inferences about erosion mechanisms operating when using different PBTs to control erosion. It is hoped that the development of this method will be useful for future erosion studies.

Chapter 3. Materials and methods

3.1 Case study location and materials

Guinea is located in West Africa (latitude 10.5°N; longitude 11.5°W), bordering the Atlantic coast to the west as well as Guinea-Bissau, Senegal, Mali, Côte d'Ivoire, Liberia and Sierra Leone (Figure 3.1). Guinea has an average annual rainfall of 3500 mm and a dry season between December and May (Lucas Kitchen, Personal Communication, 26th November 2010). The Simfer mining concession extends for 110 km of the forested Simandou Mountain range in South Eastern Guinea (IFC, 2006), within Guinea's Guinée Forestiére and Haute Guinée regions (Rio Tinto, 2010). The project area is 550 km east of Guinea's capital Conakry (Lucas Kitchen, personal communication, 26th November 2010). Two protected forests *Pic de Fon* and *Pic de Tibé* cover approximately 12% of the concession area, and Simandou's southern reaches are within Conservation International's '*Guinean Forest Hotspot'* (IFC, 2006).

Figure 3.1 Simfer Mine, Simandou, Guinea, West Africa
(Source: https://www.cia.gov/library/publications/the-world-factbook/geos/gv.html)

Ten SFMs have been chosen by Rio Tinto for critical evaluation of their erodibility in Phase I of this study. The SFMs are categorised as ore, waste-rock or soil. A description of the ten SFMs used in Phase I are given in Table 3.1.

Those materials that are associated with high erodibility were incorporated into Phase II of this study to evaluate the effectiveness of PBTs in controlling runoff, leachate and erosion and are listed in Table 3.2.

Table 3.1 Description of SFMs evaluated in Phase I of this study

Material Name		Material Type	Description
1.	LITH	Soil	Lithosol (also referred to as Entisols or skeletal soils): Lack horizon development and are notoriously shallow and stony.
2.	SRE	Soil	A soil rejuvenated by erosion
3.	FER	Soil	Ferralitic soil or Ferrosols (or lateritic soils): Tropical soils that typically have low silica, high iron and aluminium content and low cation exchange capacity.
4.	ALL	Soil	Alluvisol: Consisting of alluvial deposits, which were once transported by water
5.	RD	Waste-rock	Rubbly drift material
6.	HGF	Ore and Waste-rock	HGF (Friable Geothitic Haematite): Ranging from biscuit-like structure to a more common massive bedded structure
7.	PHY-WEA	Waste-rock	PHY-WEA (weathered phyllite): A highly weathered phyllite with lowered silica, and is kaolinite rich. Phyllite is found stratigraphically below the haematite/martite mineralisation. Phyllites are foliated metamorphic rock that represents a gradation in the degree of metamorphism between slate and mica schist. The weathered phyllites at Simandou have been highly leached leading to a geo-technically weak, often clayey material comprising mainly silt sized particles.
8.	HRS	Waste-rock	Haul road surface material
9.	NEW-WEA	Ore and Waste-rock	Weathered Mineralisation: A surficial strata found overlying high grade haematite mineralisation; generally present as clay, goethite and/or gibbsite filled fractures and voids extending into the formation below.
10.	COMB-WEA	Ore and Waste-rock	This is a combined 50:50 (% w/w) blend of two NEW-WEA samples excavated from different locations.

Soil taxonomy references from Buol et al. (2003). Geological material references from Lucas Kitchen (Personal Communication, 26th November 2010).

Table 3.2. Description of SFMs evaluated in Phase II of this study

Material Name		Material Type	Description
1.	LITH	Soil	Lithosol: Lack horizon development and are notoriously shallow and stony.
2.	HRS	Waste-rock	Haul road surface material
3.	PHV	Waste-rock	Same as PHY-WEA
4.	TRN	Ore and Waste-rock	Transitional material (TRN) is generally a friable material type, with some harder patches. Fe content is between 62% to 65% and silica/alumina around or less than 1%. It may contain an assortment of clay materials including Gibbsite.

Soil taxonomy references from Buol et al. (2003). Geological material references from Lucas Kitchen (Personal Communication, 26th November 2010).

A two week site visit to Simandou was made in September 2011, in order to understand more about the Simfer mining project and undertake preliminary investigations using the PBTs. The objectives for the site visit were to evaluate the PBTs under field-conditions and assess whether PBT application rates proposed by the product manufactures are suitable for Simandou climatic condition, in order to inform the selection of appropriate applications rates for testing during the laboratory programme. The field trip was also an opportunity to refine and develop the NSPASS methodology.

It was not possible in the time period available to construct fully replicated field plots, so instead 18 $1m^2$ sub-plots were constructed using concrete pillars dug into the ground and high visibility twine to delineate each of the 18 sub-plots, as shown in Figure 3.2. The sub-plots contained the highly erodible SFM PHY-WEA. There were 18 treatments including four PBTs applied at two application rates plus two control treatments. The treatments were applied with a backpack sprayer. Visual assessments of the sub-plots were recorded along with NSPASS acquired SR and SA data, to assess the extent the PBTs stabilised the surface in comparison to the control during rainfall. Assessments were made on day 1 and then after 2 successive rainfall events. The PBTs were found to show less surface deformation than the control, and this gave strong indication that these treatments were suitable for further and more thorough laboratory analysis, under controlled conditions.

The site visit highlighted how large the mining concession site is, and was useful for understanding how SFMs are managed and will be stored once mining commences. The site visit, as illustrated in Figures 3.3 to 3.5, also helped to convey the high intensity associated with rainfall events in the region and the severity of runoff and sediment movement on the site after rainfall; despite erosion control measures being in place and mining operations limited to a small number of test site.

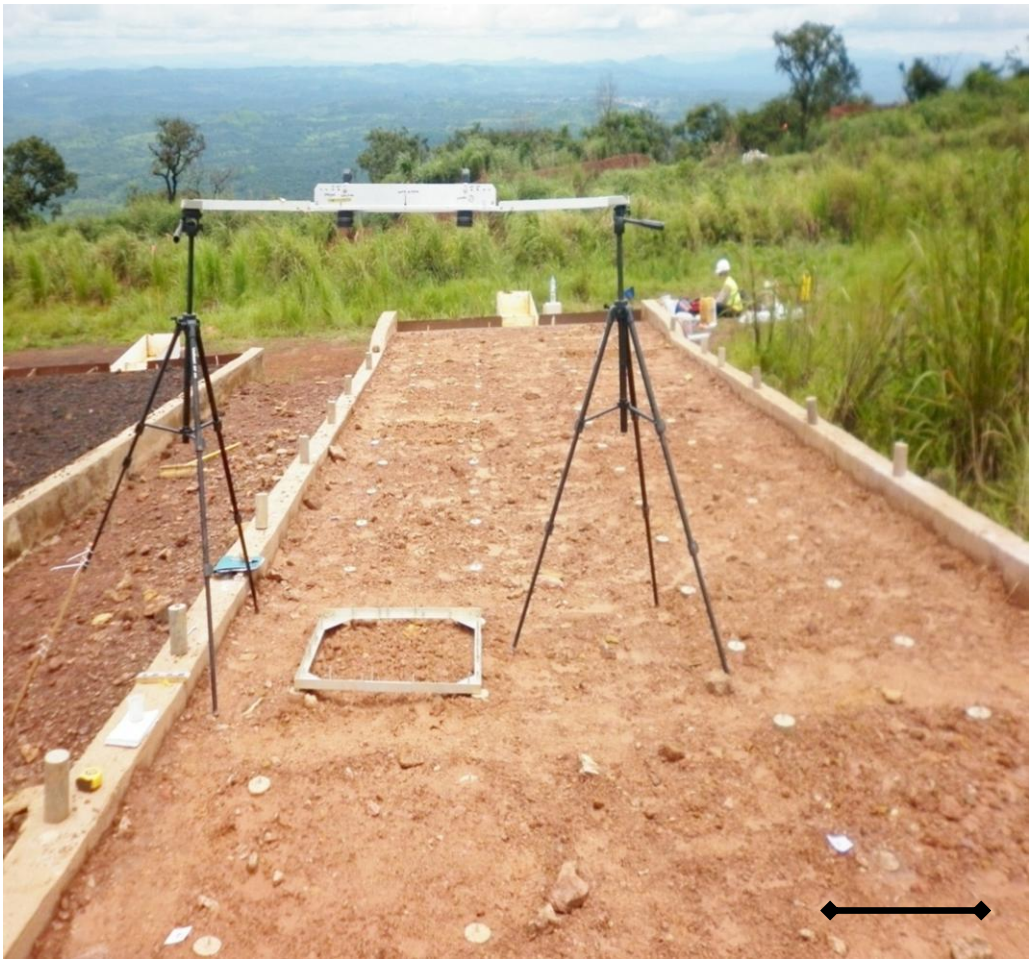

Figure 3.2. NSPASS set-up in the field showing gird set up of 18 1 m^2 sub-plots (2cm = 1m)

Figure 3.3. Rill and gully formation observed in the Simandou landscapes adjacent to a mine-site haul road (2cm = 1m)

Figure 3.4. Surface runoff after a rainfall event (2cm = 1m)

Figure 3.5. Hill slope erosion in the Simandou site

3.2. Phase I: Critical Evaluation of the erodibility and hydrological response of Slope Forming Materials (SFMs)

3.2.1 Characterization of the SFMs

All of the SFMs in Tables 3.1 and 3.2 were determined for particle size distribution (PSD), dry aggregate distribution (DAD), organic carbon, pH, electrical conductivity (EC), cation exchange capacity (CEC), exchangeable cations (Ca, Mg, Na and K), mineralogy and magnetic susceptibility. The methods used for the different analyses are detailed in Table 3.3. All analyses were carried out in triplicate, and variance in the chemical and physical characteristics of the different SFMs was determined using One-Way ANOVA Post-hoc Fisher LSD, using STATISTICA software (Version 9.1).

Table 3.3 List of the methods used to assess the physical and chemical characteristics of the different SFMs

Characterisation Test	Method	Reference
Organic Carbon Content (% w/w)	Wet Oxidation Method: organic matter is almost completely oxidised by with a solution of potassium dichromate, sulphuric acid and orthophosphoric acid. Excess dichromate is determined by titrating with ferrous sulphate solution.	Walkley and Black 1934. (NRM SOP JAS 093)
pH	Soil was air dried at 30°C and sieved (2mm). A 2:5 soil to water ratio was prepared and stirred. pH was then measured using an electrical pH-meter.	MAFF, 1986 (NRM SOP JAS 39F)
Electrical Conductivity (EC) ($\mu S\ cm^{-1}$)	The solution was prepared as a 2:5 soil to water ratio, swirled gently for 30 seconds. Conductivity was measured using two standardised electrodes placed 1cm apart in the solution. EC measures ions in solution.	Carter, 1993 (NRM SOP JAS 058)
Cation Exchange Capacity (CEC) (meq 100g)	SFMs were leached in ammonium acetate, and the excess removed. The solution was extracted with KCl and determined colorimetrically. The exchanged ammonium ions correspond with CEC.	MAFF, 1986; (NRM SOP JAS 330, JAS 128)
Exchangeable Cations Ca, Mg, K, Na (meq 100g)	SFMs were leached in ammonium acetate, and the excess removed. The exchangeable acetate extract is examined for exchangeable cations Ca, Mg, K, Na determined by inducing plasma emission spectroscopy.	MAFF, 1986; (NRM SOP JAS 330 and 128)
Bulk Density ($Mg\ m^3$)	SFMs were sieved and disturbed weight was measured with a balance in a set tray volume.	Walkley and Black, 1934. (NRM SOP 0211)
Dry Aggregate Distribution (% w/w)	Materials were air dried, weighed and 12 fractions were mechanically sieved (<53 µm; 53-63 µm; 63-125 µm; 125-150 µm; 150-250 µm; 250-500 µm; 0.5-1.0 mm; 1.0-2.0 mm; 2.0-5.6 mm; 5.6-19 mm; 19-37.5 mm; >37.5 mm).	Smith and Mullins, 2006; Nimmo and Perkins, 2002

Particle Size Distribution (% w/w)	5 fractions were measured using the Pipette sedimentation method (<0.002 mm; 0.002-0.063 mm; 0.063-0.212 mm; 0.212-0.63 mm; 0.63-2.0 mm). The sample was mixed with water and particles >63 µm removed by sieving. The remaining solution was stirred and the clay and silt amounts determined by sedimentation.	Brade-Birks, 1959; Day, 1965
Magnetic Susceptibility (% w/w)	Air dried samples were packed into 10ml containers, weighed and magnetic susceptibility was measured in a MS2 Dual Frequency Magnetic Susceptibility Meter, where Kappa LF and Kappa HF were recorded and normalised by respective test material bulk density.	Dearing, 1999
Mineralogical Composition ($m^3\ kg^{-1}$)	Bulk mineralogy was assessed using x-ray powder diffraction (XRPD). Samples were wet ground in ethanol. The X-ray XRPD pattern was recorded from 2-75°2θ using Cobalt Kα radiation. Quantitative analysis was done by a normalised full pattern reference intensity ratio (RIR) method with a 95% confidence level.	Omotoso et al., 2006

3.2.2. Assessment of SFM hydrological response and erodibility during rainfall

Erodibility can be assessed directly in the laboratory under controlled conditions using erodibility indices including runoff volume, runoff rate, runoff total sediment load (TSL), leachate volume and leachate TSL (Bryan, 1968; in Selkirk and Riley, 1996; Barthes and Roose, 2002; Singh and Khera, 2008). Working in the laboratory allows for controlled replication of results and robust statistical analysis. Ensuring all test conditions are controlled will allow for further understanding about what physical and chemical properties influence the hydrological response and erodibility of the SFMs (Phase I).

The comparative erodibility and hydrological response of the SFMs was assessed using the following indicators:

- **Total runoff and leachate volumes**
  Surface runoff and leachate were collected in separate containers, connected by separate hoses to each erosion tray. At the end of each

simulated rain event, runoff and leachate total volumes were measured and recorded.

- **Runoff rate (ml min^{-1})**
  Runoff rate was measured at five minute time intervals. Runoff volume change was marked onto the container at each time interval and change in volume over time was determined against a pre-calibrated container.

- **Runoff Total Sediment Load (TSL) and leachate TSL**
  Once the runoff and leachate had been measured, 10 ml of 60 g l^{-1} ammonium sulphate flocculent solution was added to each container to facilitate the rapid deposition of suspended material. Once settled the clear liquid was siphoned away. The remaining material was oven dried at 40°C and weighed to give TSL. Total Sediment Concentration (TSC) was then calculated as:

  Runoff TSC (g l^{-1}) = Runoff TSL mass (g) / Total runoff volume (l)

  Leachate TSC (g l^{-1}) = Leachate TSL mass (g) / Total leachate volume (l)

3.2.3 Rainfall simulation experimental set-up

The Phase I experimental programme was undertaken using a 2.0 m (l) x 1.0 m (w) x 0.25 m (d) stainless steel erosion rig, which can be adjusted in height at 5° intervals and was set to a uniform slope angle of 10°. The erosion rig has a modified base plate, which is large enough to position three 0.25 m x 0.5 m x 0.09 m erosion trays. A pressurised rainfall simulator was calibrated to the desired storm conditions, as detailed in Appendix A. To obtain the specified rainfall intensity and K.E., a full cone nozzle (Lechler number 460.886.17) set at 0.85 bar pressure was used and the simulator's boom arm was set at 2.4 m above the ground level (Figure 3.6). Test materials were left for several days until air-dry and were then thoroughly mixed. Three test replicates of the same material were pre-prepared with the same bulk density. Erosion trays were filled and compacted using a flat rectangular metal plate to achieve a level surface. Erosion trays had two collection containers connected to separate hoses for surface runoff and leachate, as shown in Figure 3.3

This design-storm was specified by Rio Tinto as having 100 mm hr^{-1} intensity for 30 minute duration, which was associated with a 1:20 year return period for the Simandou area. The design was based on observations obtained from intensity, duration and frequency curves created with rainfall data from Dabatini

in Simandou. Ideally the design rainfall event should replicate the Drop Size Distribution (DSD) and KE of tropical rainfall. Tropical rainfall has much larger drops than temperate rainfall (Hudson, 1989). Target conditions for the simulated design storm were to have KE between 35 to 50 J m^2 with a drop size range of 2-4 mm (Hudson, 1989; Morgan, 2006). Details of the rainfall simulation calibration processes are given in Appendix A.

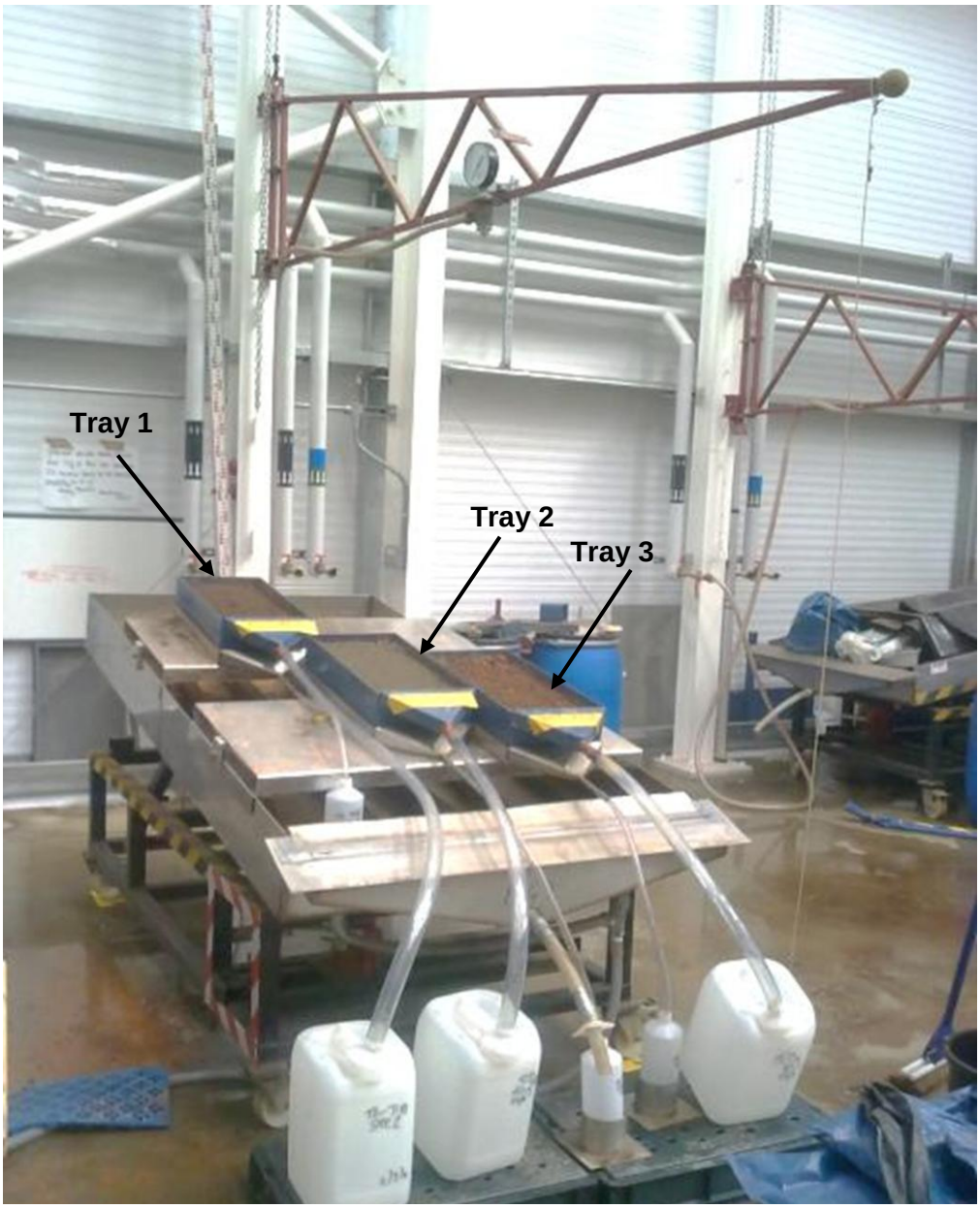

Figure 3.6. Phase I experimental set-up of the rainfall simulator and erosion trays

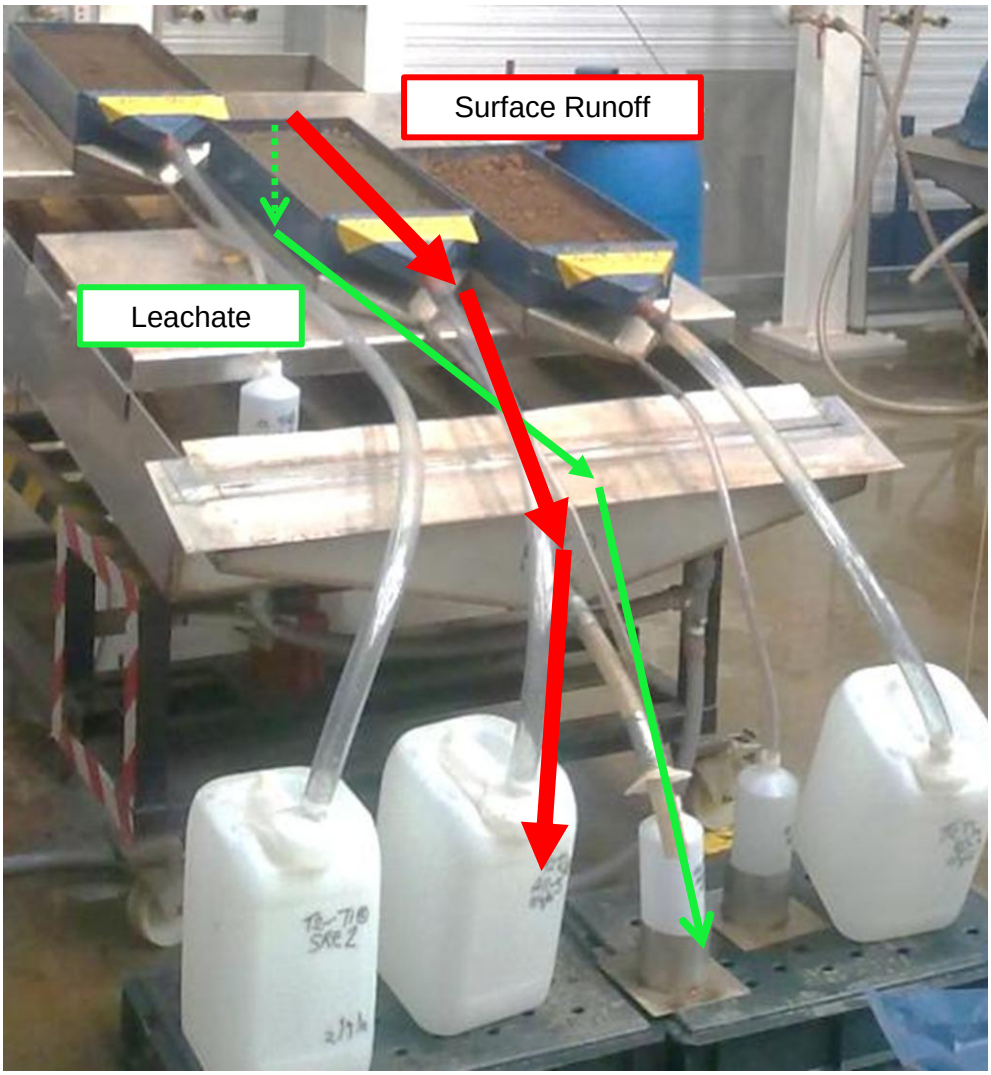

Figure 3.7. Phase I experimental runoff and leachate collection system

3.2.4 Phase I experimental design

An assessment of SFM erodibility was carried out first at air-dry antecedent moisture conditions **(AD_{amc})** and subsequently at field capacity antecedent moisture conditions **(FC_{amc})** in order to replicate field conditions in Guinea during the dry and wet season, respectively. Field capacity is the amount of water held by a material at saturation, after excess water has drained away under the influence of gravity (Singer and Munns, 1999). Field capacity was simulated by subjecting the test materials to a non-erosive rainfall event (fine mist), until 300 ml of leachate was collected, the materials were then left to drain freely for 24 hours. Wetting-up by simulated rainfall as opposed to immersion wetting, is likely to give results relevant to field soil behaviour, as detailed in Loch (1994).

The experimental schedule is shown in Appendix B. The treatments were compiled in triplicate. To ensure that there was no bias in the order that the test materials appeared in the experimental schedule, or the position of the test materials on the erosion rig, the experimental schedule was compiled using a randomised sample design. Experimental observations and digital photographs of the erosion trays pre- and post- rainfall were recorded for each experiment.

3.2.5 Statistical analysis of the Phase I results

Before applying all statistical analyses, data from the experiments were processed by removing outliers observed in the p-plot of residuals, and a normal probability distribution was achieved as necessary by transforming the dataset using a log or square root function. All analyses were carried out in triplicate, and variance between the results for the different SFMs was determined using One-Way ANOVA and Post-hoc Fisher LSD, using STATISTICA software (Version 9.1). A direct comparison of SFM erodibility and hydrological response at different antecedent moisture conditions was made using Factorial ANOVA and Post-hoc Fisher LSD, using STATISTICA software (Version 9.1). Stepwise linear multiple regression analysis (MRA) using STATISTICA (version 10) was used to determine which SFM properties best explained differences in the runoff volume, runoff TSL, leachate volume and leachate TSL results. Principal Component Analysis (PCA) using the SFM characterisation data was used to determine whether or not it was necessary to treat the soil and non-soil data as discrete populations for the MRA.

3.3. Phase II: Critical evaluation of polymer-based treatments to control runoff and erosion from engineered slopes

3.3.1 The Polymer Based Treatments (PBTs)

In order to conduct a preliminary assessment of whether the Polymer Based Treatments (PBTs) would be effective at controlling erosion, four different polymer products were assessed in the field in Guinea, and sprayed onto 18 subplots of non-soil PHY-WEA, which was a SFM available for field assessment at that time. Limited time and resources restricted a more thorough assessment. The three products found to be most successful based on visual assessment of surface deformation change after three successive rainfall events were selected for further testing in the laboratory and are listed in Table 3.4 and include; Siltstop® APS 705 (SS7) anionic powder based polyacrylamide (PAM),

Siltstop® APS 605 (SS6) anionic emulsion based PAM and Soilfloc® DC90 (DC90) non-ionic liquid based polyvinylacrylic latex (PVAL).

In Phase II the effectiveness of the three polymer products to control runoff, leachate and erosion were assessed at two different application rates, with and without the addition of gypsum. The manufacturer's recommended application rate was compared to a higher application rate, approximately three times the manufacturer's recommended application rate (Table 3.6), which was in-line with the highest application rates reported in the literature discussed in Section 2.5.1 (Table 2.1). In total 14 PBT combinations were tested using three polymer products plus an untreated control (Table 3.4). Average viscosity (n=3) of the different treatment concentrations was determined using a Brookfield DV-E Viscometer Version 1 (Spindle number 61). Each treatment was replicated four times, and in total there were 224 test results from 28 simulated rainfall experiments (Table 3.5). It was hypothesised that there would be a negative relationship between PBT application rate and rate of erosion, and that the addition of gypsum will improve PBT efficiency to manage erosion and runoff.

3.3.2 The SFMs selected for assessment of PBT effectiveness to control runoff and erosion

The comparative erodibility and hydrological response of the polymer treated SFMs was assessed by determining post-rainfall runoff volume, runoff TSL, leachate volume and leachate TSL. Four materials were selected including Haul Road Sample (HRS), Transitional Material (TRN), Very Weak Weathered Phyllite (PHV) and Lithosol (LITH) (Table 3.2 in Section 3.1). Non-soils PHY-WEA and HRS were chosen because they were associated with high runoff volumes and runoff TSLs in Phase I. HGF was chosen because it was associated with high leachate volumes and leachate TSLs in Phase I, thus associated with a contrasting hydrological response to PHY-WEA and HRS. The literature has shown that there are more studies regarding the use of PBTs particularly PAMs on soil SFMs as compared with non-soil SFMs. Therefore, LITH (a soil SFM) would provide results to compare the erodibility and hydrological response of a soil material to the three non-soil SFMs. During the course of this research, and as a result of continued exploration on site and a more detailed understanding of their physio-chemical characteristics, Rio Tinto changed the nomenclature of PHY-WEA and HGF to PHV and TRN, respectively (Lucas Kitchen, personal communication, 3rd December 2012).

All four SFMs were imported in two respective batches for Phase I and Phase II. One-way ANOVA Post-hoc Fisher LSD analysis were used to determine if the

SFMs used in Phase I and Phase II are from the same respective populations (Appendix G). Test materials were left to air-dry and were then thoroughly mixed. The materials were characterised by the same parameters adopted in Phase I (Table 3.3 in Section 3.2.1).

Table 3.4. Polymer-based treatments code descriptions

Treatment Code	Polymer Product	PBT Type	Application Rate	Gypsum addition
Control	Control	n/a	n/a	No
$Control_{GYP}$	Control	n/a	n/a	Yes (5000 kg ha^{-1})
DC_L	Dc90	PVAL	Low	No
DC_L_{GYP}	Dc90	PVAL	Low	Yes (5000 kg ha^{-1})
DC_H	Dc90	PVAL	High	No
DC_H_{GYP}	Dc90	PLAL	High	Yes (5000 kg ha^{-1})
SS6_L	Siltstop 605	PAM Emulsion	Low	No
$SS6\_L_{GYP}$	Siltstop 605	PAM Emulsion	Low	Yes (5000 kg ha^{-1})
SS6_H	Siltstop 605	PAM Emulsion	High	No
$SS6\_H_{GYP}$	Siltstop 605	PAM Emulsion	High	Yes (5000 kg ha^{-1})
SS7_L	Siltstop 705	PAM Powder	Low	No
$SS7\_L_{GYP}$	Siltstop 705	PAM Powder	Low	Yes (5000 kg ha^{-1})
SS7_H	Siltstop 705	PAM Powder	High	No
$SS7\_H_{GYP}$	Siltstop 705	PAM Powder	High	Yes (5000 kg ha^{-1})

Note: application rates and PBT product information is detailed in Table 3.6

Table 3.5. The Phase II experimental activity plan

PHASE II EXPERIMENTAL DESIGN									
SFM	PBT	Application rates	Gypsum	Rainfall 100mm hr^{-1}	Slope (10°)	No: of Replicates	No: of tests	No: of trays/ test	Total No: of Results
4	3	2	2	1	1	4	28	8	224

Table 3.6. Description of polymer based treatments used in Phase II

Polymer Based Treatments Description				
	APS 705 Silt Stop (SS7)	**APS 605 Silt Stop (SS6)**	**Dc90 Application 1 of 2**	**Dc90 Application 2 of 2**
Product Details	Dry granular Powder	Emulsion	Liquid	Liquid
Type of Polymer	Anionic linear Polyacrylamide	Anionic linear Polyacrylamide	Non-ionic linear Polyvinylacrylic latex	Non-ionic linear Polyvinylacrylic latex
Molecular Weight	Mixture	Mixture	High	High
Stir Time	90 seconds at speed 5	30 seconds at speed 1	30 seconds at speed 1	30 seconds at speed 1
Low Application Rate	22 kg ha^{-1} or, 0.05 g per 0.22 m^2 erosion tray	14.0 l ha^{-1} or, 0.03ml per 0.022 m^2 erosion tray	140 l ha^{-1} or, 0.3ml per 0.022 m^2 erosion tray	281 l ha^{-1} or, 0.6ml per 0.022 m^2 erosion tray
Water solution	65 ml	65 ml	8 ml	10 ml
Viscosity (m.Pa.S)	10.6	10.6	10.8	10.2
High Application Rate	67 kg ha^{-1} or 0.15 g per 0.22 m^2 erosion tray	37.4 l ha^{-1} or 0.08 ml per 0.022 m^2 erosion tray	468 l ha^{-1} or 1ml per 0.022 m^2 erosion tray	468 l ha^{-1} or 1 ml per 0.022 m^2 erosion tray
Water solution	65 ml	65 ml	10 ml	10 ml
Viscosity (m.Pa.S)	13.2	13.7	10.5	10.2

3.3.3 Application of polymer-based treatments

Test replicates of the same SFM were prepared with the same bulk density. The Phase II experimental design had a higher number of experimental treatments than Phase I, so smaller 0.2 m (l) x 0.11 m (w) x 0.07 m (d) erosion trays were used in Phase II to ensure sufficient SFM could be imported from Guinea. Each erosion tray had two collection containers connected to separate hoses for surface runoff and leachate, as shown in Figure 3.8. Erosion trays were filled and compacted using a flat metal plate to achieve a level surface. It was important to replicate field conditions as accurately as possible, and so the surfaces DAD of treatment replicates were not manipulated in any way in order to replicate the inherent variability of waste-rock dumps, which in the field would have heterogeneous sorting of aggregate sizes.

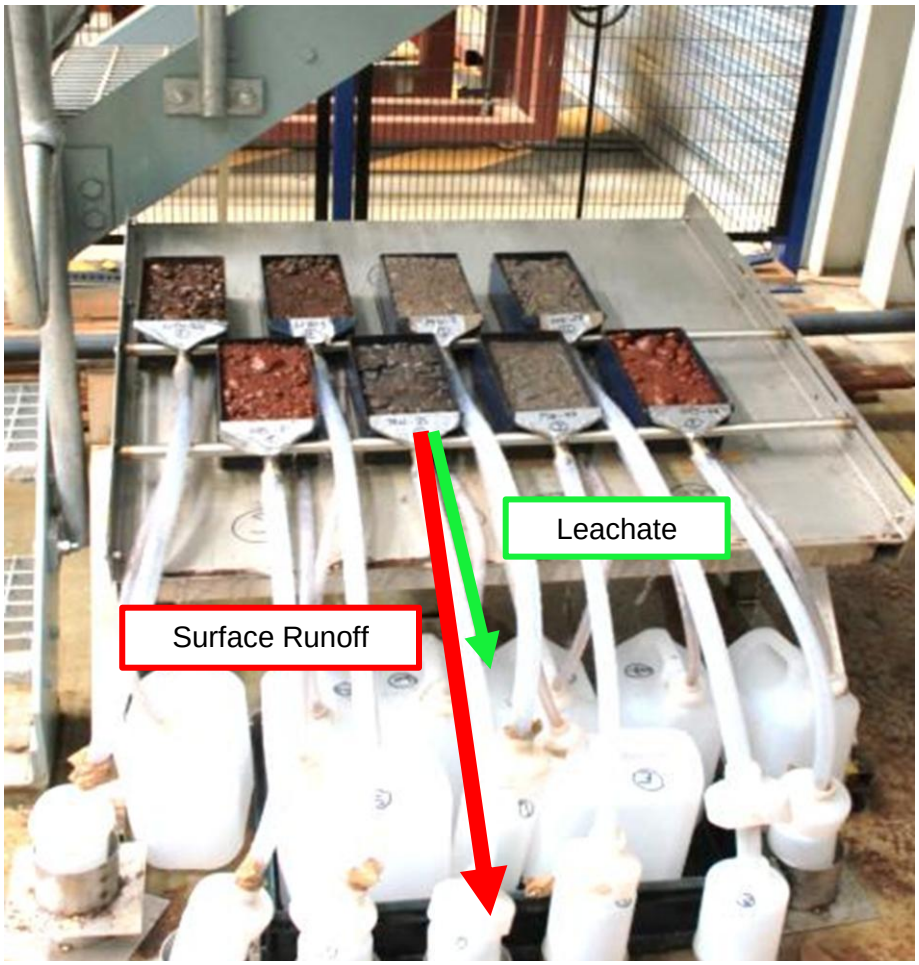

Figure 3.8. Phase II rainfall tower experimental set-up

Gypsum application rates discussed in the literature mostly range between 2500 to 10,000 kg ha^{-1} (Sojka et al., 2007; Mahardhika et al., 2008; Akbarzadea

et al., 2009; Lee, 2009; Kuma and Saha, 2011). Consequently, 5000 kg ha^{-1} (11g per experimental erosion tray) was selected as a medium value. For the gypsum based treatments, dry powdered gypsum was applied to the entire surface using a sieve, and was then mixed with the top 2-3 cm of the test material prior to the application of the polymer solution.

Polymer products were measured and added to water and stirred with an electronic whisk for the respective time period listed in Table 3.6 and then immediately applied to the test material's surface. The SS7 dry powder PAM had a longer stir time than the other two liquid PBTs, as the powder took longer to dissolve (Soupir, 2004). Polymer treatments were applied to the entire surface of the test material using a pressurised air spray gun. The spray gun was rinsed with water after each polymer treatment, and then treated with air brush cleaner at the end of use each day to avoid clogging the nozzle. Soilfloc® DC90 Polyvinylacetate requires two treatments within a 24 hour time period. The second application was made approximately three hours after the first application. All polymer treatments were then allowed to dry for 24 hours.

The same procedures for determining runoff and leachate volumes and associated TSLs adopted in Phase I were adopted in Phase II. Leachate and runoff volumes were measured, and then oven-dried to remove the liquid in order to weigh the respective sediment mass and determine leachate TSL and runoff TSL. The variance between the different treatment results was determined using One-Way ANOVA Post-hoc Fisher LSD, using STATISTICA software (Version 10). High variability in the Phase I results raised concerns about whether three test replicates was sufficient to detect significant differences in the outcome of the Phase II results. Power analysis using the results of the Phase I experiments in STATISTICA V.10 showed the minimum number of test replicates needed was four in order to detect a significant difference in sediment load data of 25g (alpha=0.05) with a power of 80%.

3.3.4 Phase II rainfall simulation set-up

The slope and rainfall conditions were consistent with the experimental set-up used in Phase I of this research at 10° and 100 mm hr^{-1} for 30 mins duration, respectively, in order to maintain continuity between experimentation. The erosion trays were placed on a table that was adjusted to a 10° slope. It was more practical to achieve uniform rainfall intensity for a high number of smaller sized erosion trays using a 8.8m tower rainfall simulator in Phase II, as opposed to the pressurised boom arm rainfall simulator used in experimental Phase I.

The rainfall tower was calibrated to 100 mm hr^{-1} by testing rainfall intensity in the same way described in Phase I (Appendix A) using different tray positions

Eight erosion trays were found to fit under the rainfall tower, whilst being subject to the design rainfall intensity 100 mm hr^{-1} for a 30 min duration with a mean (n=3) ±10% variability. The rainfall tower was fitted with a coarse mesh to create larger rain drops. A Parsivel-2 Laser Optical Disdrometer was used to measure drop-size distribution (DSD) and ensure the simulator was creating large rain drops (this device was not available during Phase I and so the flour pellet method was used to determine rainfall DSD). Figure 3.9 is a sample disdrometer reading showing the desired rainfall intensity of 100 mm hr^{-1}. The graph illustrates a higher proportion (>750) of the smaller rain drops at the two time periods are 0.5-3.0 mm in size; fewer (0-10) drops are recorded in the larger 3.5-6.0 mm drop-sizes, which is a trend consistent with the DSD reported for tropical rainfall in the literature (Lal, 1998; Obi and Salako, 1995) and also in Phase I of this study where drop size D_{50} was 1.30-1.34 mm.

3.3.5 Near-surface photogrammetry assessment of slope forming material surface roughness (NSPASS) methodology

To determine why some PBTs performed differently in terms of runoff and erosion control, the 3D surface area (SA) in m^3 and surface roughness (SR) of selected treatments was assessed before and after rainfall. Treatments were selected if they showed significant differences in the statistical One-way ANOVA analysis results.

An approach that uses near surface digital photogrammetry (NSDP) and a geographic information system (GIS) entitled 'Near-Surface Photogrammetry Assessment of SFMs Surface Roughness'(NSPASS), was developed in order to quantify the extent SR and SA change during rainfall. NSPASS has the potential to provide millimetre accuracy of surface terrain micro-relief (Nouwakpo et al., 2010). A quantifiable assessment of the plot's SA and SR before and after rainfall and using measured runoff TSL data, would help better understand what effect the different PBTs were having on the plot's surface in comparison to the control. It is expected that the net change in SR and SA after rainfall will reflect differences in the efficacy of PBTs, and that the largest SA and SR change would be associated with the untreated control, followed by the gypsum only treatment, then polymer without gypsum and the polymer with gypsum treatment showing the least SA and SR change; and hence be the most successful stabilising the surface. The NSPASS steps involved converting NSDP images into SR and SA data are summarised in Figure 3.10.

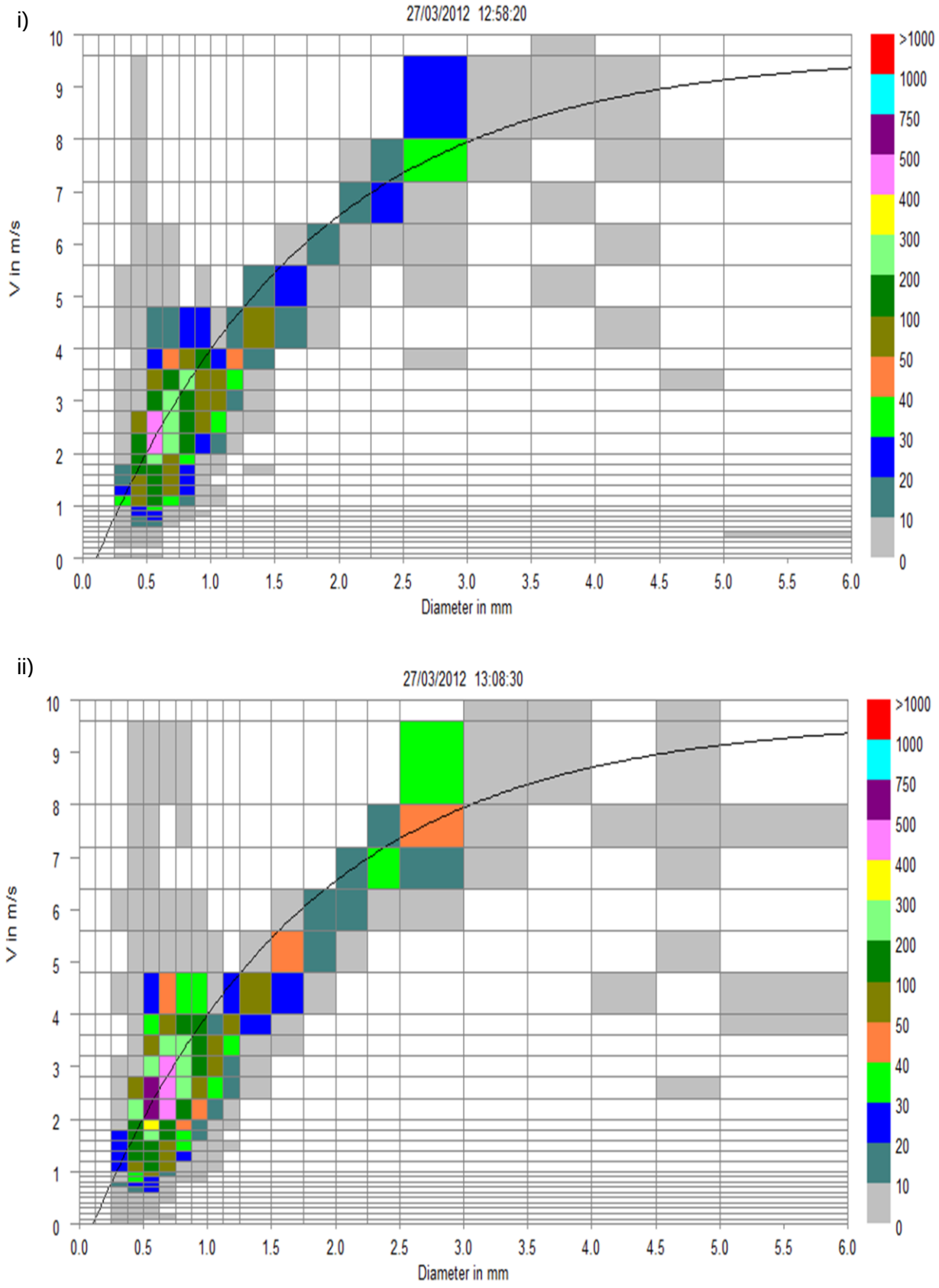

Figure 3.9. Rainfall drop-size distribution of 100 mm hr^{-1} design storm measured for 20 second intervals at i) 0 mins and ii) 10 mins

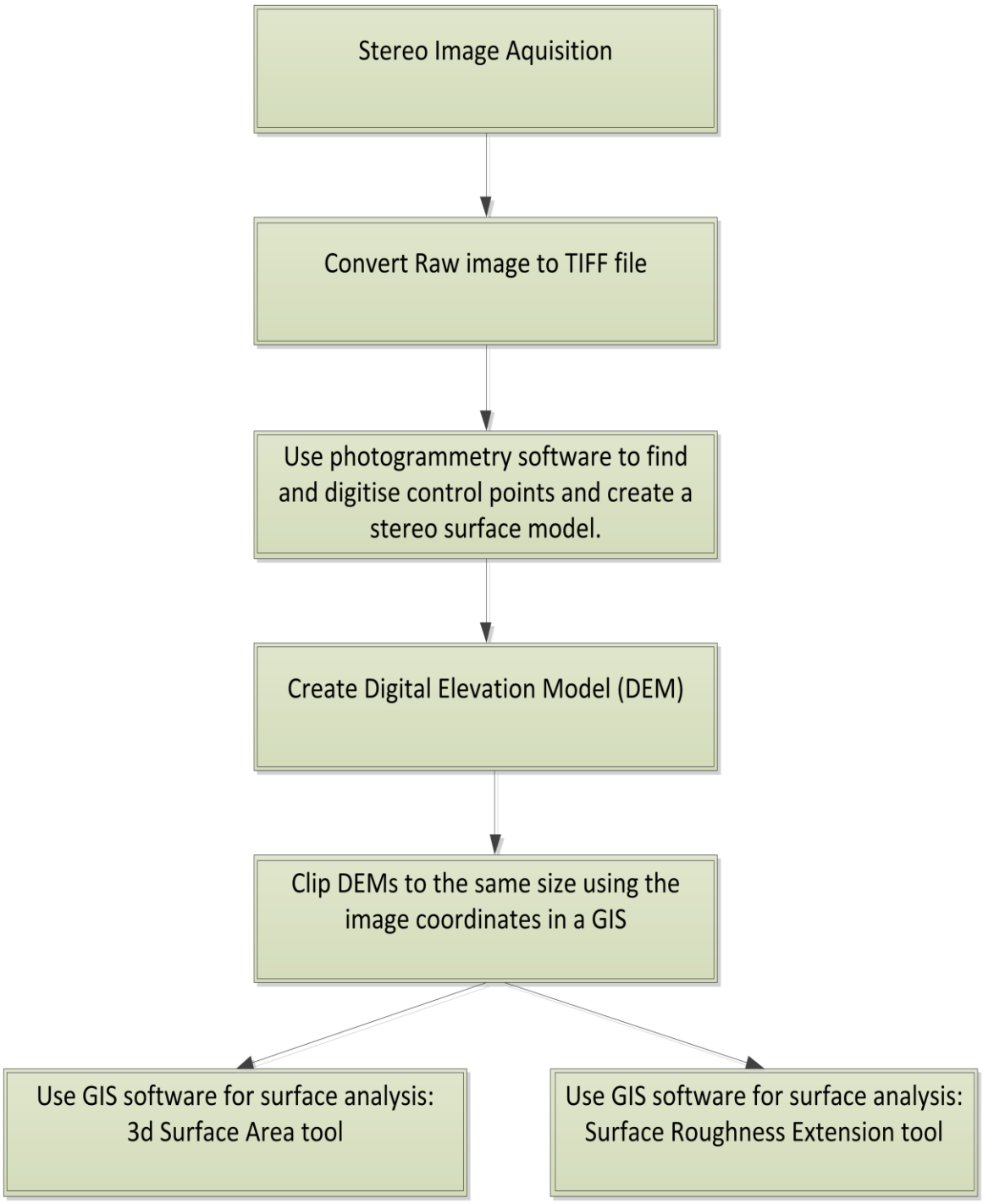

Figure 3.10. NSPASS step by step approach to converting stereo images into surface roughness data *(Source: Author, 2012)*

3.3.5.1 Stereo image acquisition

The NSDP image acquisition system consisted of two Canon EOS 500D digital cameras, both with a Canon EF 20mm fixed focal length (f/2.8) lens and 22.3mm array, used in program setting where the camera shutter speed automatically selects the aperture. The cameras were mounted onto a bespoke rigid lightweight aluminium frame, with vertical adjustment achieved using two tripods mounted at adjacent ends of the frame, as shown in Figure 3.11. This is the first time NSPASS has been used to assess rainfall induced surface micro-topography changes during rainfall. The approach was first tested in the laboratory, and then further developed in the field in Guinea during September 2011. Later this method was refined again in the laboratory for the purpose of the Phase II experimental set-up.

To convert a pair of 2D stereo images into a single 3D image requires a reference co-ordinate system. A portable spatial calibration target frame was designed and made using 57 x 8 mm bolts of differing lengths, secured to a 0.9 x 0.5 m^2 perforated steel sheet with pre-drilled 8mm holes that were evenly spaced (Figure 3.11b). The target frame had dual purpose; to provide a calibrated spatial reference system to measure micro-relief surface change, and also to secure the erosion trays in place so the tray positioning was the same in every image. Details of how the target frame was designed and calibrated to obtain X, Y, Z co-ordinates are given in Appendix C. Post image accuracy analysis, as detailed later in the next section, was found to be satisfactory using the final experimental set-up with an accuracy of 2-3mm.

It was important to have (approximately) >60% overlap in the view finder of both cameras to perform image triangulation (Wolf and Derwitt, 2000). The cameras were positioned 180° to the ground with a spirit level, the cameras height (0.63m) was always measured from the base of the target to the array of each camera. In addition, the distance between the cameras (0.13 m) did not change ensuring the parallax, or the apparent displacement in the position of the target in relation to the cameras, was constant (Wolf and Derwitt, 2000). It was important the cameras positioning were kept constant to ensure each image was comparable to the next. After image acquisition a detailed database of the stereo digital image file names (and all subsequent files associated with that image) was created, and each image was given a unique identifier, detailing its date and treatment number.

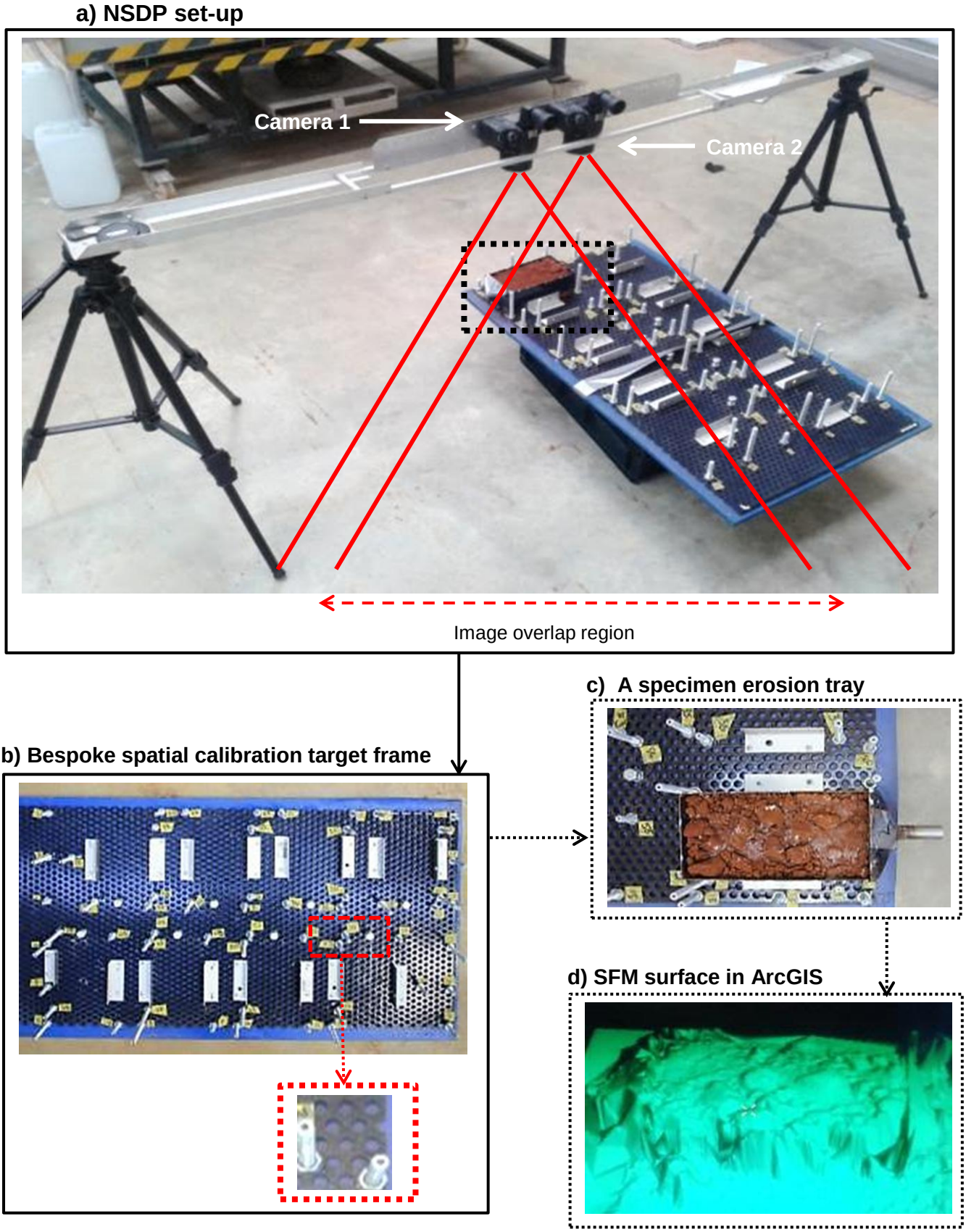

Figure 3.11 The NSDP set-up used in experimental Phase II

3.3.5.2. Transforming stereo images into digital elevation models (DEMS)

The Canon camera raw file format images were converted into TIFF format to be compatible with Leica Photogrammetry Suite 2011 (LPS) in ERDAS Imagine, which was the software used to digitise the images. Stereo TIFF images were digitised using 11 ground control points (GCPs). 8 mm diameter laser printed stickers with the image of a bulls-eye were positioned on the top of each bolt head (or GCP) on the target frame, in order to be able to locate and geo reference the centre of the bolt's exact location. X, Y, Z co-ordinates were assigned to each GCP. Once digitised, image pairs were then triangulated using the software to create a single three dimensional block-file. Leica Photogrammetry Suite block-files were then converted into digital elevation model (DEM) format in order to be used in the GIS for automatic terrain extraction functions.

The accuracy assessment of the NSDP experimental set-up is important as the results are looking at micro scale SA and SR, and thereby millimetre accuracy is needed to capture aggregate scale micro-relief changes in 0.022m² erosion trays. Geo-referenced stereo-image error can be measured using the LE90 (Linear Error of 90%) and CE90 (Circular Error of 90) (Wolf and Dewitt, 2000), and the process followed to assess image error is detailed in Appendix D.

The CE90 and LE90 for digitised stereo images was recorded and ranged between 0.84 mm and 2.49 mm, which was considered satisfactory, based on the limitations of using this method with the equipment and time at hand (Wolf and Dewitt, 2000). It is reasoned that CE90 and LE90 accuracy could still be improved on with more time to experiment with different cameras, camera lens and apparatus set-up. 2-3 mm accuracy was considered a success in retrospect, as studies that have used NSDP to create river-bed DEMs reported accuracy ±10 mm (Lane and Chandler, 1998). Furthermore NSPASS has not ever been used before, and so this research will provide the framework for future studies to use and refine the approach.

3.3.5.3 Using NSPASS to assess SFM surface roughness and surface area

Using ESRI ArcMap GIS Version 10 each DEM was clipped to delete the immediate edge of the erosion tray and avoid potential edge effects caused by shadowing of the tray (see example in Figure 3.12). A 0.112 m^2 clip template was created using the image co-ordinate system, and ensured all DEMs were clipped at identical locations. DEMs of the same treatment obtained before and after rainfall were used to quantify SR change using the surface ratio extension

tool for ArcMap, and SA change using the surface volume function in ArcMap 3D Analyst, as discussed in Section 2.6.

SR for the entire clipped image is calculated by ArcMap from dividing the surface area of the target using a raster adjustment factor for the cell's planimetric area, as shown below (Jenness, 2004).

$$Surface\ Roughness = \frac{C^2}{cos\left[\left\{\frac{\pi}{180}\right\}s\right]}$$

$$Where\ C\ is\ cell\ size, and\ S\ is\ slope\ in\ degrees$$

The tool generates statistics including mean SR, maximum SR and minimum SR. Values closer to 1.0 are representative of flatter surfaces, and increasingly higher ratio values (>1.0) represent the increasing slope within the cell and higher surface irregularity. An example image of SR output is shown in Figure 3.13, where the SR range is between 1 and 9.39. The flatter surfaces are depicted in white; and more irregular surfaces areas in an increasingly darker shade of red. Note that the lowest SR is at the central surface of larger stones and rocks, and the rougher areas near the stones perimeter, where there is a sudden elevation change.

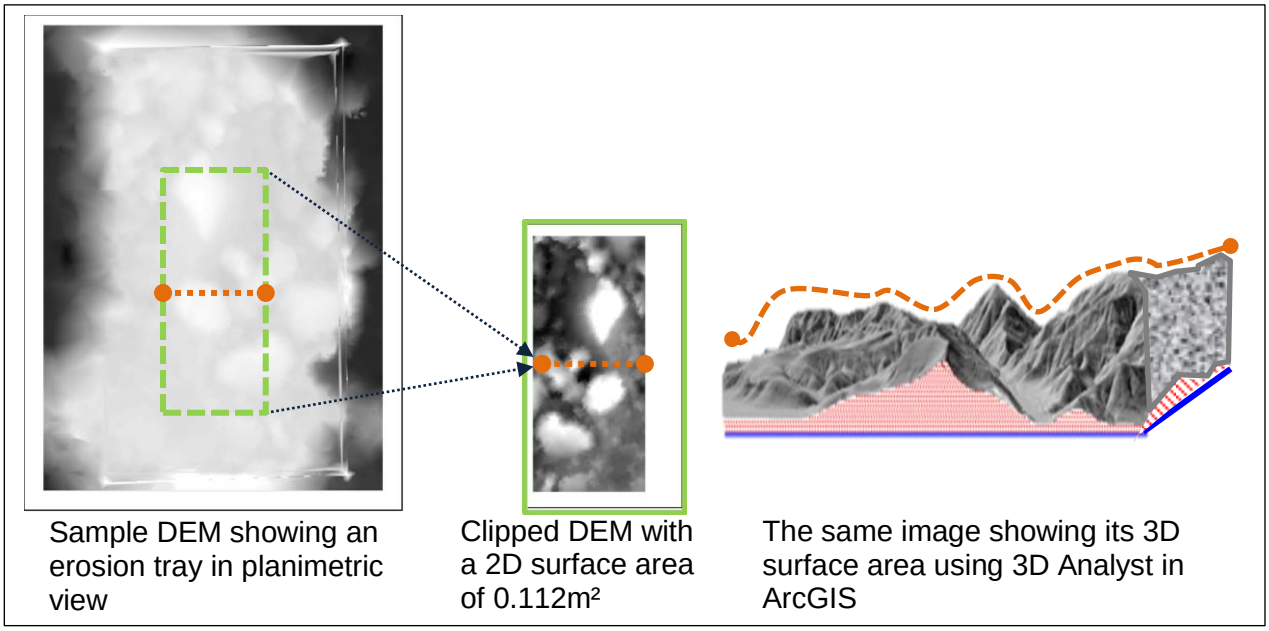

Figure 3.12. Left: Sample DEM clipped to 0.112 m² in planimetric view. Right: the same image illustrating its 3D surface area

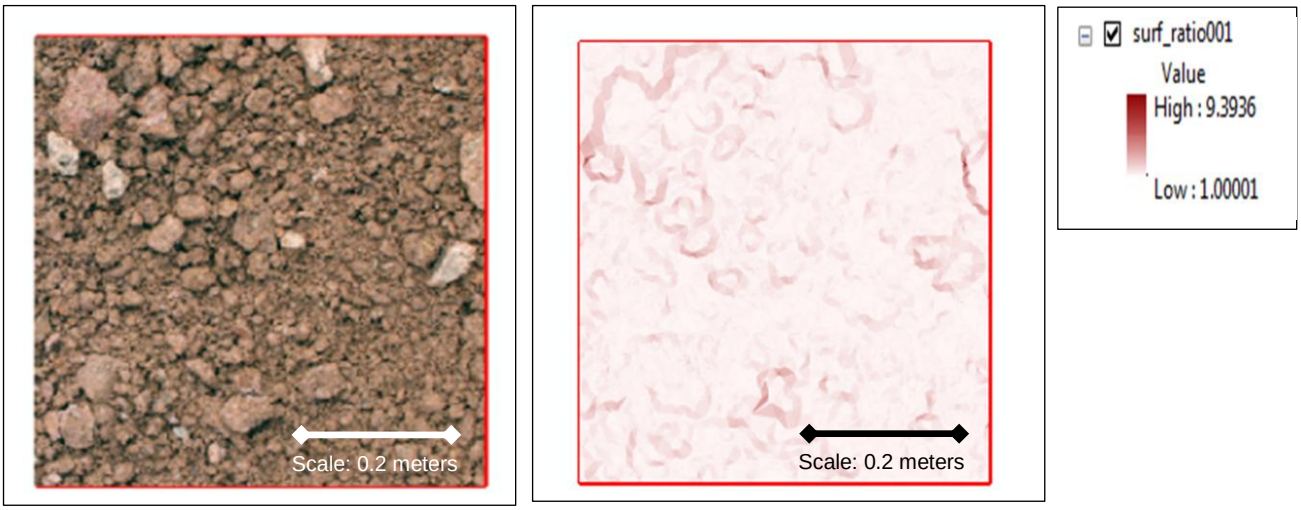

Figure 3.13. Left: 0.5 m² clipped sample image;
Right: surface roughness results using the same image

Figure 3.12 illustrates that 2D surface area will always be 0.112 m² using the same X and Y co-ordinates of the clipped template. 3D surface area is calculated using the X, Y and Z values of the DEM in square metres. Post rainfall changes in SA is expected to be consistent with changes in SR, and using both the SA and SR statistics will provide a more comprehensive interpretation of surface micro-relief change, as having both indicators will best interpret the data if anomalous results are found.

Used in conjunction with the runoff TSL results, SA and SR can be interpreted to identify erosion processes that would have been operating during rainfall, which are summarised in Table 3.7, and will give a better understanding about why some treatments worked better than others reducing runoff TSLs (Lane and Chandler, 1998).

If mean SR and SA change is the exact same value before and after rainfall, then it is inferred that the surface was stable during rainfall. The alternative inference is that material has moved within the erosion tray, but erosion and deposition was exactly balanced and hence no net difference in SR or SA. It is reasoned that the likelihood of the latter eventuality, generating the exact same SR and SA value before and after rainfall, is very low. A negative change in SR or SA implies on average surface roughness has decreased, with a smoother surface formed by erosional processes, such as material transportation, compaction and/or armouring. A positive change in SR or SA implies on

average the surface has become rougher, which could indicate a net gain in deposited material transported from the upper parts of the tray, splash pedestal formation, armouring and/or aggregate breakdown occurrence. Moore et al. (2003) recognises splash pedestals, rills, crusting, scouring and gullies are indicative of erosion by water. At millimetre scale it is reasoned that rill and especially gully formation are unlikely.

Table 3.7. Potential erosion processes that could be interpreted from post-rainfall SR and SA change

Mean SR and SA change	**Erosional processes that can cause observed change in surface roughness (SR) and surface area (SA)**				
Negative Change (-)	Smoothing by material loss	Sealing or surface compaction	Armouring	Rolling or displacement of unstable stones	
Positive Change (+)	Breakdown of large aggregate into smaller aggregates	Localised deposition within sub-plot	Downslope movement of eroded material	Exposure of originally covered rocks	Splash pedestals formation
No Change	There has been no erosion. The surface is stable	Inter-plot erosion and deposition is balanced, so no net material loss			

Chapter 4. Phase I results and discussion: differences in SFM erodibility and hydrological response to rainfall

4.1 Introduction

The hydrological response of un-vegetated mine-site SFMs in terms of runoff and leachate is not well documented. Riley (1995) reports that unconsolidated waste rock dumps are 10-100 times more erodible by surface runoff than natural sites within the same geographic area. The relative proportion of surface runoff and associated sediment load, and subsurface leachate and associated sediment load, governs the risks associated with the transport of contaminants as well as slope instability (Vacher et al., 2004). Less is known about the erosive potential of water moving through the SFM as leachate as compared with surface runoff (Hawkins, 1998; Morgan, 2006), particularly on SFMs such as those evaluated in this study. Non-soils are associated with coarse material, high porosity and generally have good drainage properties as compared to soils (Smith et al., 1995). Consequently, understanding the response of SFMs to rainfall and factors affecting SFM erodibility is important in order to design appropriate sediment and runoff management solutions in the mining sector.

The following hypotheses were formulated to test the hydrological response and erodibility of the ten SFMs evaluated in Phase I of this study:

1. Significant differences will be observed between the physical and chemical properties of the soil and non-soil SFMs.

2. Different SFMs will have different hydrological responses in terms of:
    a. runoff volume and associated TSL, and
    b. leachate volume and associated TSL.

3. Antecedent moisture conditions (i.e. air dry v. field capacity) will affect the erodibility and hydrological responses of the SFMs.

4. Erodibility and hydrological responses of SFMs can be explained by their physical and chemical properties.

This chapter starts in Section 4.2 by discussing the physical and chemical properties of the SFMs and comparing the soil and non-soil SFMs. SFM response to rainfall in terms of runoff rate, runoff volume, runoff TSL, leachate volume and leachate TSL is discussed in Section 4.3 and 4.4 when SFMs were

tested under air-dry (AD_{amc}), and field-capacity antecedent moisture conditions (FC_{amc}). SFMs were tested at AD_{amc} and then FC_{amc} in order to replicate the wet and dry season that prevails in Simandou, Guinea. Hypothesis 2 is tested in Section 4.5.1 which discusses differences in the SFMs hydrological response to rainfall. Hypothesis 3 is tested in Section 4.5.2 which compares the effects of changing antecedent moisture conditions on the SFM responses to rainfall. Section 4.5.3 uses the results of Multiple Regression Analysis to identify and discuss which soil and non-soil SFM properties are statistically significant in explaining differences in SFM erodibility and hydrological response. Key findings and relevant outcomes for Phase II of this study are summarised in the chapter conclusions.

4.2. Results of SFM physical and chemical properties analysis

4.2.1 Bulk Density (Mg m³)

The results indicate that the bulk density of the soils is as expected significantly ($p<0.05$) lower than the non-soil SFMs with mean (n=3) values for the soils and non-soil SFMs ranging between 0.759–0.906 Mg m³ and 1.029–2.604 Mg m³, respectively (Table 4.2).

4.2.2 pH

The soils LITH (pH 5.1), FER (pH 4.76) and ALL (pH 4.9) are significantly more acidic than the other SFMs, and the non-soil WEA has the lowest acidity at 6.36. All of the 10 SFMs are considered acidic with pH values ranging from 4.76 – 6.39 (Table 4.2). Acidic reaction of the SFMs is in the order ALL=FER > LITH > SRE=HGF=NEW-WEA > RD=PHY-WEA=NEW-WEA > COMB-WEA=HRS > WEA.

4.2.3 Electrical Conductivity (µS cm^{-1})

Electrical Conductivity (EC) is an indicator of salinity, and the SFMs are not considered saline (White, 2006), as EC ranges from 1443 – 2040 µS cm^{-1}. Non-soil COMB-WEA has significantly the highest EC at 2040 µS cm^{-1}, and soil LITH and non-soils RD and HRS the lowest EC at 1443-1480 µS cm^{-1} (Table 4.2).

Table 4.1. SFM Particle Size Analysis

Slope Forming Material	Particle Size Analysis (% w/w)				
	Coarse Sand 2.0–0.63mm	Medium Sand 0.63–0.212mm	Fine Sand 0.212–0.063mm	Silt 0.063–0.002mm	Clay <0.002mm
LITH	8.00_{a}	6.33_{a}	5.00_{ab}	50.0_{f}	30.6_{f}
ALL	6.33_{a}	18.0_{bc}	13.6_{e}	24.3_{e}	37.6_{g}
FER	7.66_{a}	25.0_{e}	11.6_{de}	13.0_{bc}	42.6_{h}
SRE	18.0_{b}	4.66_{a}	2.33_{a}	51.0_{f}	24.0_{e}
RD	37.0_{d}	15.0_{b}	9.00_{cd}	20.3_{d}	18.6_{d}
PHY-WEA	6.33_{a}	4.66_{a}	7.66_{bc}	65.6_{g}	15.6_{c}
NEW-WEA	16.0_{b}	21.6_{d}	26.6_{f}	26.3_{e}	9.33_{b}
COMB-WEA	30.0_{c}	31.0_{f}	26.0_{f}	10.0_{a}	3.00_{a}
HRS	27.0_{c}	27.6_{e}	20.3_{g}	14.3_{c}	10.6_{b}
HGF	17.6_{b}	20.6_{cd}	40.0_{i}	18.3_{d}	3.33_{a}

Within the same column, values not followed by the same letter are significantly different $p<0.05$ as determined by One-way ANOVA post-hoc Fisher LSD analysis (n=3). Note: soils are shaded in white and non-soils in green for ease of reference.

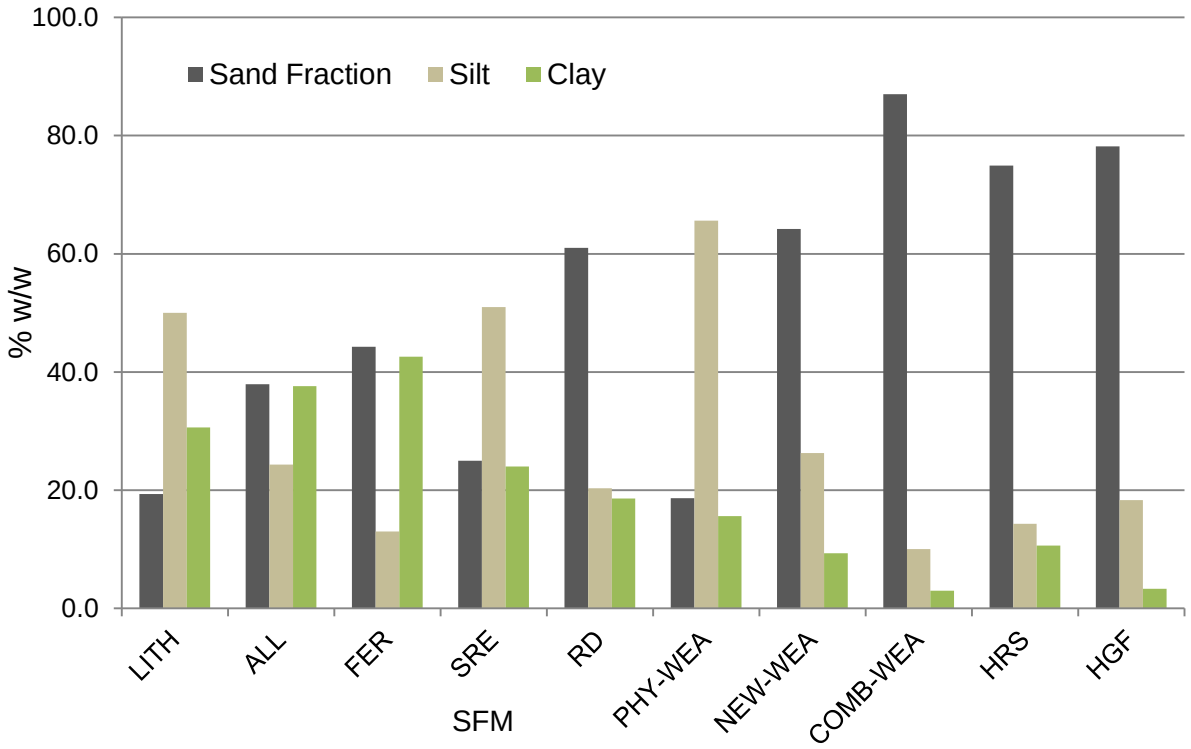

Figure 4.1. Summarised SFM Particle Size Distributions (% w/w)

Note: For brevity, coarse, medium and fine sand results (% w/w) have been combined. For statistical differences between SFM refer to Table 4.1.

Table 4.2. Physical and chemical characteristics of SFMs used in Phase I

							Exchangeable Cations (meq 100g)				
Slope Forming Material	Type of SFM	Bulk Density (Mg m^3)	pH	EC (uS cm)	Organic Carbon (% w/w)	Magnetic Susceptibility (m^3 kg^{-1})	Ca	Mg	K	Na	CEC (meq 100g)
LITH	Soil	0.811_{ab}	5.10_{e}	1454_{c}	6.50_{f}	174.8_{d}	6.53_{d}	0.38_{c}	0.29_{c}	0.04_{c}	24.2_{c}
ALL	Soil	0.869_{bc}	4.90_{c}	1768_{ab}	3.46_{d}	-0.2_{b}	2.96_{bc}	1.31_{d}	0.17_{b}	0.10_{f}	18.0_{b}
FER	Soil	0.906_{c}	4.76_{c}	1769_{ab}	4.00_{e}	29a	2.56_{abc}	1.48_{e}	0.44_{d}	0.033_{ac}	18.3_{b}
SRE	Soil	0.759_{a}	5.40_{a}	1722_{a}	10.3_{g}	438.3_{e}	11.6_{e}	2.21_{f}	0.63_{e}	0.04_{c}	32.3_{d}
RD	Non-soil	1.36_{e}	5.63_{b}	1443_{c}	0.57_{c}	60.8_{c}	8.20_{d}	0.37_{c}	0.20_{b}	0.026_{ab}	15.5_{b}
PHY-WEA	Non-soil	1.029_{d}	5.63_{b}	1680_{a}	0.17_{ab}	27.2_{a}	1.16_{ab}	0.11_{b}	0.05_{a}	0.026_{ab}	2.43_{a}
NEW-WEA	Non-soil	2.098_{g}	5.50_{ab}	1776_{ab}	0.23_{b}	61.7_{c}	1.13_{ab}	0.05_{ab}	0.02_{a}	0.03_{a}	2.43_{a}
COMB-WEA	Non-soil	2.46_{i}	5.99_{d}	2040_{d}	0.13_{ab}	31.4_{a}	1.10_{ab}	0.068_{ab}	0.01_{a}	0.05_{e}	1.70_{a}
HRS	Non-soil	1.76_{f}	6.06_{d}	1480_{c}	0.47_{c}	33.5_{a}	3.86_{c}	0.08_{ab}	0.02_{a}	0.02_{bd}	5.23_{a}
HGF	Non-soil	2.604_{j}	5.43_{a}	1830_{b}	$<0.001_{a}$	10.7_{ab}	0.77_{a}	0.03_{a}	0.01_{a}	0.03_{a}	1.93_{a}

Within the same column, values not followed by the same letter are significantly different at $p<0.05$ as determined by One-Way ANOVA post-hoc Fisher LSD analysis (n=3). Note: soils are shaded in white and non-soils in green for ease of reference.

Table 4.3. Bulk mineralogical composition of the SFMs (% w/w)

Mineralogy Composition of Test Materials (% w/w)											
Slope Forming Material	Quartz	Plagioclase	Hematite	Goethite	Magnetite	Maghemite	Anatase	Rutile	Gibbsite	Muscovite	Kaolinite
LITH	22.1	0	7.5	14.9	0	8.5	0.7	0.5	9.7	0	14.8
ALL	48.8	1	0	4.9	0	1.1	0.2	0.7	0.4	0	35
FER	48	0.5	1	6.2	1.3	1	0.4	0.3	4.5	0	28.2
SRE	48.6	1	0	4.9	0	1.1	0.2	0.7	0.4	0	35
RD	1.7	0	26.3	51.7	0	0	0.3	0	15	0	5
PHY-WEA	2.8	0	7.3	13.7	0	2.2	0	0.3	3.7	50.8	19.2
COMB-WEA	1.4	0	74.5	11.8	6.1	0	0.1	0.1	4.7	0	1.3
HRS	4.8	0	56.2	24.1	0	0.6	0.1	0.1	8.6	0	5.5
HGF	4.1	0	86.8	0.8	3	0	0	0.1	3.5	0	1.6

Organic carbon results have been omitted as these were obtained in separate analysis reported in Table 4.2. Note only single mineralogical results were obtained for each SFM and so could not be statistically analysed for variance. The XRPD method used has been extensively validated (Omotoso et al., 2006) and mineralogical composition of the same SFM is very likely to give identical XRD patterns (Stephen Hillier, Personal Communication, 31st January 2012). Due to insufficient material amounts there are no results for NEW-WEA. Note: soils are shaded in white and non-soils in green for ease of reference.

Table 4.4. SFM Dry Aggregate Distribution Results

Dry Aggregate Distribution (DAD) % w/w												
Slope Forming Material	>37.5mm	19-37.5mm	5.6-19mm	2.0-5.6mm	1.0-2.0mm	0.50-1.0mm	250-500µm	150-250µm	125-150µm	63-125µm	53-63µm	<53µm
LITH	0.01_{a}	0.2_{e}	9.6_{f}	10.5_{ab}	17.8_{bc}	21.5_{f}	20.5_{d}	8.70_{c}	2.72_{abc}	4.94_{a}	1.46_{ab}	2.0_{abc}
ALL	0.01_{a}	2.06_{ce}	25.6_{abd}	20.4_{c}	17.4_{bc}	14.7_{de}	11.2_{b}	4.96_{ab}	1.19_{a}	1.85_{bc}	0.369_{c}	0.16_{ab}
FER	0.01_{a}	13.09_{f}	20.8_{bcd}	17.4_{cd}	18.7_{c}	13.8_{a}	10.4_{b}	3.50_{a}	0.64_{a}	1.12_{c}	0.23_{c}	0.22_{ab}
SRE	9.81_{b}	11.4_{df}	11.7_{fg}	9.8_{e}	15.8_{b}	16.2_{e}	14.5_{c}	5.67_{abc}	2.16_{ab}	3.25_{ab}	1.84_{ab}	2.55_{c}
RD	5.73_{ab}	5.23_{abc}	29.1_{ae}	19.9_{c}	10.8_{a}	6.65_{b}	5.73_{a}	3.88_{a}	1.41_{ab}	4.19_{a}	1.98_{ab}	5.28_{d}
PHY-WEA	3.87_{ab}	8.04_{abd}	17.7_{bg}	7.9_{ae}	11.0_{a}	10.4_{c}	10.1_{b}	15.3_{d}	10.2_{d}	4.88_{a}	0.39_{c}	0.141_{a}
NEW-WEA	2.4_{ab}	9.2_{bdf}	35.3_{e}	12.3_{ab}	13.1_{d}	5.45_{ab}	4.52_{a}	4.43_{a}	4.43_{bc}	4.43_{a}	2.21_{a}	2.21_{bc}
COMB-WEA	9.87_{b}	4.49_{ace}	29.9_{ae}	17.7_{cd}	9.40_{a}	5.74_{ab}	5.25_{a}	4.98_{ab}	1.87_{ab}	3.60_{ab}	1.80_{ab}	1.8_{abc}
HRS	4.15_{ab}	5.94_{abc}	19.9_{bc}	12_{ab}	13.1_{d}	10.7_{c}	10.0_{b}	7.72_{bc}	5.67_{c}	8.86_{d}	1.19_{bc}	0.7_{abc}
HGF	8.89_{b}	7.39_{abd}	26.8_{ad}	13.9_{bd}	6.81_{e}	4.08_{a}	4.30_{a}	4.58_{a}	2.02_{ab}	8.59_{d}	2.37_{a}	10.3_{e}

Within the same column, values not followed by the same letter are significantly different at $p<0.05$ as determined by One-Way ANOVA post-hoc Fisher LSD analysis (n=3). Note: soils are shaded in white and non-soils in green for ease of reference.

4.2.4 Organic Carbon (% w/w) and Cation Exchange Capacity (CEC) meq 100g

Soil SFMs had as expected significantly higher organic carbon values (% w/w) as compared to the non-soil SFMs (Table 4.2). Specifically, mean organic carbon values for the soils are in the order SRE, LITH, FER and ALL with values of 10.3%, 6.5%, 4.0% and 3.46%, respectively. In contrast, all non-soil SFMs were associated with organic carbon values of <0.57%.

Organic carbon, clay content and pH are important factors affecting soil CEC (Asadu, et al., 1997; in Igwe and Nkemekosi, 2007). The CEC results had the strongest linear relationship with organic carbon (R^2 = 0.875), followed by kaolinite clay amounts (R^2 = 0.49) and pH (R^2 = 0.379). The soils had higher kaolinite clay (Table 4.3) and organic carbon amounts at 14.8-35% (w/w) and 3.46-10.3% (w/w), respectively, compared to the non-soils at 1.6-19.2% (w/w) and <0.57% (w/w); and so the soils are associated with significantly higher CEC values at 32.3, 24.2, 18.0 and 18.3 meq 100g for SRE, LITH, ALL and FER, respectively. With the exception of RD, soil CEC values are generally an order of magnitude greater than the non-soil SFMs, which had values ranging between 5.23-1.73 meq 100g (Table 4.2).

4.2.5 Exchangeable Cations (Ca, Mg, K, Na) meq 100g

Exch-Mg, Na and K are low for all SFMs (White, 2006). All SFMs are associated with trace levels of Exch-K. Specifically, soils SRE, FER and LITH are associated with significantly higher Exch-K levels at 0.63, 0.44 and 0.29 meq 100g, respectively, as compared with all other SFMs with concentrations <0.20 meq 100g (Table 4.2).

The soils ALL, FER and SRE have the highest Exch-Mg values, ranging between 1.31 - 2.21 meq 100g. Furthermore, as with the Exch-K results, non-soil RD and soil LITH are associated with statistically similar Exch-Mg values of 0.37 and 0.38 meq 100 g respectively. All other non-soil SFMs are associated with Exch-Mg concentrations <0.11 meq 100g.

All SFMs are associated with trace levels of Exch-Na ranging from 0.02–0.10 meq 100g. Soil ALL has a significantly higher Exch-Na concentration than all other SFMs at 0.1 meq 100g.

The Exch-Ca values for the non-soils and soils are not represented by distinctly different populations. High concentrations of Exch-Ca are associated with the soils SRE and LITH, and the non-soil RD with values of 11.6, 6.53 and 8.20 meq 100g, respectively. The remaining SFMs have low Exch-Ca concentrations <3.86 meq 100g.

4.2.6 Magnetic Susceptibility ($m^3\ kg^{-1}$)

Few research papers compare the magnetic properties of soils and non-soils, and assess the linkages between magnetic susceptibility (MS) and erodibility (Rhoton et al., 1998). The relevance of MS to the comparative erodibility of SFMs is discussed in Section 2.3.6. The results show no clear statistical distinction between the soils and non-soil populations with regards MS (Table 4.2). Soil SRE had significantly the highest MS (438.3 $m^3\ kg^{-1}$), 2.5 times higher than soil LITH (174.8 $m^3\ kg^{-1}$). Further, LITH was associated with a MS nearly three times greater than the non-soils RD (60.8 $m^3\ kg^{-1}$) and NEW-WEA (61.7 $m^3\ kg^{-1}$), and soil ALL had significantly the lowest MS of all SFMs (-0.2 $m^3\ kg^{-1}$).

4.2.7 Mineralogy (% w/w)

SFM mineralogical composition is summarised in Table 4.3. It is important to note that only single mineralogical results were obtained for each SFM and so could not be statistically analysed for variance. The X-ray Powder diffraction (XRPD) method used has been extensively validated (Omotoso et al., 2006) and mineralogical composition of the same SFM is highly likely to give identical XRD patterns (Stephen Hillier, Personal Communication, 31st January 2012).

Differences in the dataset are described below. The soils have higher quartz content than the non-soils. Soils ALL, FER and SRE are dominated by quartz and kaolinite with composition values for quartz and kaolinite of 48.8, 48.0, 48.6 and 35, 28.2 and 35 (% w/w), respectively. In contrast, LITH is associated with a broad distribution (% w/w) of minerals, namely quartz (22.1), kaolinite (14.8), gibbsite (9.7), goethite (14.9) and hematite (7.5).

With the exception of PHY-WEA, non-soils are dominated by hematite or goethite. COMB-WEA and HGF are associated with 74.5 and 86.8% w/w Hematite, respectively. Non-soils RD and HRS are dominated by hematite (26.3 and 56.2% w/w) and goethite (51.7 and 24.1% w/w). PHY-WEA is dominated by muscovite and kaolinite with % w/w values of 50.8 and 19.2, respectively. In all SFMs, anatase and rutile are found in trace amounts.

4.2.8 Particle Size Distribution (PSD) (% w/w)

The 5-fraction PSD results in Table 4.1 (coarse sand 2.0-0.63 mm; medium sand 0.63-0.212 mm; fine sand 0.212-0.063 mm; silt 0.063-0.002 mm; clay <0.002 mm) are summarised in Figure 4.1 and indicate significant differences in the PSDs of soil and non-soil SFMs. Soils LITH and SRE are dominated by the silt (50 and 51 % w/w), clay (30 and 24 % w/w) and coarse-sand sized fractions (8 and 18 % w/w). Soil ALL is dominated by the silt/fine sand (37.9%) and clay sized fractions (37.6%) and FER by the clay (42.6%) and medium sand sized fractions (25%).

With the exception of PHY-WEA, the non-soils RD, WEA, NEW-WEA, COMB-WEA, HRS and HGF are dominated by the sand sized fractions with mean values of 61.0, 85.6, 64.2, 87.0, 74.9 and 78.2% (w/w), respectively. In contrast PHY-WEA is dominated by the silt sized fraction (65.6%).

4.2.9 Dry Aggregate Distribution (DAD) (% w/w)

Non-soil SFMs contain unconsolidated primary particles of gravel, conglomerate and breccia fragments of different shapes and sizes (Price, 2009). Soil aggregates are the binding of sand, silt and clay primary particles into a larger entity by pedogenic processes (White, 2006). From here on in, the term 'aggregate^{S}' or 'DAD^{S}' will refer to soil aggregates, and 'aggregate^{NS}' or 'DAD^{NS}' will refer to non-soil aggregates. The relevance of DAD to the comparative erodibility and hydrological response of SFMs is discussed in Section 2.3.2.

DAD was assessed using 12 size fractions ranging from >37.5 mm to <53 µm (Table 4.4). In contrast to PSD, the DAD results represent non-dispersed aggregate distribution. The detailed data-set was necessary to represent the heterogeneous aggregate size range of the SFMs, and assess which aggregate size classes are important properties in the runoff, leachate and erosion results using Multiple Regression Analysis (Section 4.5.3).

Soils LITH (59.8% w/w) and SRE (47% w/w) show aggregate^{S} sized 250 µm – 2 mm are the dominate size class, and 0.5-19 mm is the dominant size class for soils ALL (78% w/w) and FER (71% w/w). Aggregates^{NS} sized 5.6-19 mm dominate the non-soil SFMs, with proportions ranging 17.7–35.3% (w/w). HRS and HGF have significantly higher 63-125 µm sized aggregates^{NS} than all other SFMs at 8.86 and 8.59% w/w respectively. HGF has significantly the highest amount of <53 µm aggregates^{NS} of all the SFMs at 10.3% (w/w). PHY-WEA has significantly high amounts of aggregates^{NS} 125 µm – 1 mm (46% w/w).

4.2.10 Testing Hypotheses 1: differences in the physical and chemical properties of the soil and non-soil SFMs

It was hypothesised that there would be significant differences found in the physical and chemical properties of the soil and non-soil SFMs. This has been shown for bulk density, organic carbon, clay sized particles, quartz, hematite, magnetite, anatase, kaolinite, DAD >37.5 mm and DAD 1.0-2.0 mm. No significant differences were observed in the soil and non-soil EC, exchangeable cations, goethite and gibbsite amounts, sand (coarse, medium, fine), silt and aggregates sized 37.5-2.0 mm and 1 mm - <53 μm. These results are evidence that differences between soil and non-soil properties are not clear cut; and non-soils HRS and RD, and to a lesser extent PHY-WEA, frequently show similar properties to the soil SFMs.

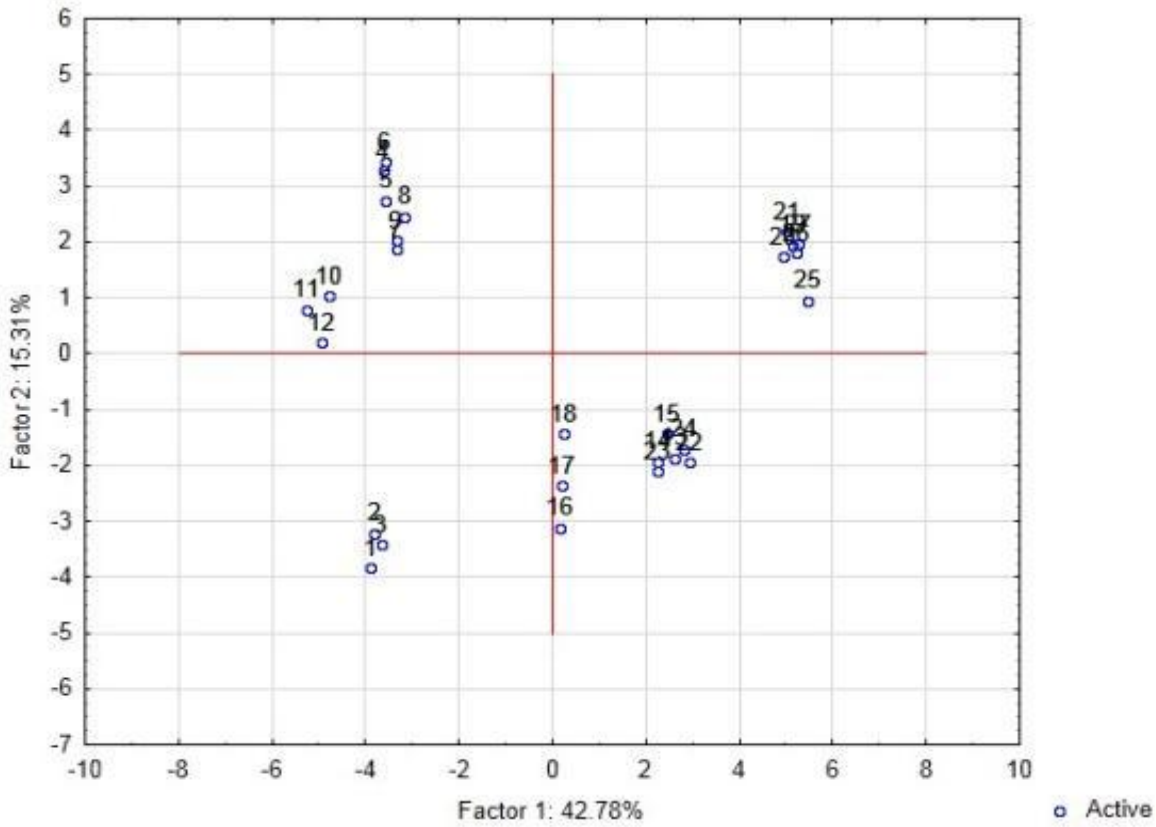

Figure 4.2. Principal Component Analysis illustrating the cases using Factors 1 and 2.

Note: Cases 1 – 12 on the left side are the soil SFMs. Cases 13 – 27 on the right side are the non-soil SFMs

To test and compare the soil SFMs and non-soil SFMs behaviours during rainfall, the soils and non-soils hydrological response to rainfall and erodibility results are analysed as the same statistical population using ANOVA statistical analysis. The results are discussed in Sections 4.3 to 4.5.2.

MRA was undertaken to identify which key SFM properties dictate the hydrological response and erodibility of the SFMs tested in Section 4.5.3. The results from Section 4.2 showed statistical similarities and differences in the physical and chemical characteristics of the soil and non-soil SFMs. Principal Component Analysis (PCA) using STATISTICA (v.10) was then used to determine if it was necessary to separate the soil and non-soil characterisation data-set prior to undertaking stepwise linear Multiple Regression Analysis (MRA). Figure 4.2 illustrates that using Factors 1 (42.74%) and Factors 2 (15.31%), the soils (cases 1 to 12) are grouped to the left of the graph and the non-soils (cases 13 to 27) are grouped to the right. The PCA results indicate significant divisions in the physical and chemical properties of the soil and non-soil SFMs, which justifies treating the soil and non-soil characterisation data separately in the MRA analysis, as discussed later in Section 4.5.3.

4.3 Hydrological responses and erodibility of slope forming materials under air-dry antecedent moisture conditions (AD_{amc})

4.3.1 Runoff volume and runoff rate at AD_{amc}

One-way ANOVA Post-hoc Fisher LSD analysis demonstrate that total AD_{amc} runoff volume was in the order HRS=PHY-WEA=SRE > COMB-WEA=PHY-WEA=SRE > COMB-WEA=SRE=LITH > ALL=FER=RD=HGF (Table 4.5). Non-soils HRS (4249 ml) and PHY-WEA (3333 ml) and soil SRE (2520 ml) generated significantly the highest runoff volume compared with all other SFMs. Put into perspective, HRS produced on average 34 times more runoff than RD.

Cumulative AD_{amc} runoff volume recorded for the 30min storm event is shown in Figure 4.3 and AD_{amc} runoff rates (at 5 min intervals) are summarised in Table 4.6. The results show that from 0-5mins non-soils PHY-WEA (50 ml min^{-1}) and HRS (102 ml min^{-1}) had runoff rates significantly higher than all other SFMs, which were statistically comparable to the runoff rate recorded for soil SRE (52.5 ml min^{-1}). Between 5-10mins non-soils HRS (97.0 ml min^{-1}) had significantly higher runoff rates than all other SFMs, and this result was statistically comparable to SRE (90.2 ml min^{-1}), PHY-WEA (90. ml min^{-1}) and COMB-WEA (24.0 ml min^{-1}). This trend is relatively consistent for the remainder of the rainfall storm event.

Table 4.5. SFM runoff and leachate volumes, Total Sediment Load (TSL) and Total Sediment Concentration (TSC) at AD_{amc}

Slope Forming Material	Runoff Volume (ml)	Runoff TSL (g)	Runoff TSC (g l^{-1})	Leachate volume (ml)	Leachate TSL (g)	Leachate TSC (g l^{-1})
LITH	617_{ab}	2.03_{ab}	3.29_{ab}	3884_{cd}	0.8_{a}	0.206_{a}
ALL	143_{a}	0.41_{ab}	2.87_{ab}	5888_{a}	0.9_{a}	0.15_{a}
FER	267_{a}	0.02_{a}	0.07_{a}	5456_{a}	0.94_{a}	0.17_{a}
SRE	2520_{bcd}	10.2_{bc}	4.04_{c}	2168_{b}	0.32_{a}	0.15_{a}
RD	123_{a}	0.56_{ab}	4.53_{bc}	6455_{a}	4.08_{b}	0.63_{b}
PHY-WEA	3333_{cd}	47.8_{d}	14.3_{d}	1945_{b}	0.38_{a}	0.19_{a}
NEW-WEA	333_{a}	0.75_{ab}	2.25_{ab}	8200_{d}	5.20_{b}	0.63_{b}
HRS	4249_{d}	12.2_{c}	2.88_{ab}	3346_{bc}	1.97_{a}	0.59_{b}
HGF	140_{a}	0.44_{ab}	3.14_{abc}	5200_{ad}	0.76_{a}	0.15_{a}
COMB-WEA	1410_{abc}	2.27_{ab}	1.61_{ab}	5833_{a}	4.62_{b}	0.79_{b}

Within the same column, values not followed by the same letter are significantly different at $p<0.05$ as determined by One-Way ANOVA post-hoc Fisher LSD analysis (n=3).
Note: soils are shaded in white and non-soils in green for ease of reference

Table 4.6. Differences in AD_{amc} SFM runoff rate (ml min^{-1}) at 5-min time intervals

Slope Forming Material	Runoff Rate (ml min^{-1})					
	0-5 minutes	5-10 minutes	10-15 minutes	15-20 minutes	20-25 minutes	25-30 minutes
LITH	4.7_{ab}	6.0_{ab}	10.7_{a}	16.7_{a}	32.0_{abc}	53.3_{a}
ALL	3.0_{a}	9.0_{ab}	2.0_{a}	7.0_{a}	3.0_{ab}	4.0_{a}
FER	ND	ND	ND	ND	ND	ND
SRE	52.5_{cd}	66.7_{abc}	84.0_{bc}	90.2_{ab}	84.3_{abc}	126_{ab}
RD	ND	ND	ND	ND	ND	ND
PHY-WEA	50_{c}	90.0_{bc}	107_{c}	153_{b}	140_{bc}	127_{ab}
NEW-WEA	13.3_{b}	3.3_{a}	13.3_{a}	13.3_{a}	6.7_{a}	16.7_{a}
HRS	101.5_{c}	96.9_{c}	212_{d}	143_{b}	154_{c}	207_{b}
HGF	2.7_{a}	4.7_{a}	4.7_{a}	8.0_{a}	13.3_{a}	26.7_{a}
COMB-WEA	6.7_{ab}	24.0_{abc}	43.3_{ab}	70.7_{ab}	69.3_{abc}	68.0_{a}

Within the same column, values not followed by the same letter are significantly different at $p<0.05$ as determined by One-Way ANOVA post-hoc Fisher LSD analysis (n=3). Insufficient surface runoff (Non detectable ND) was generated from FER and RD for the determination of 5-min interval runoff rates.
Note: soils are shaded in white and non-soils in green for ease of reference.

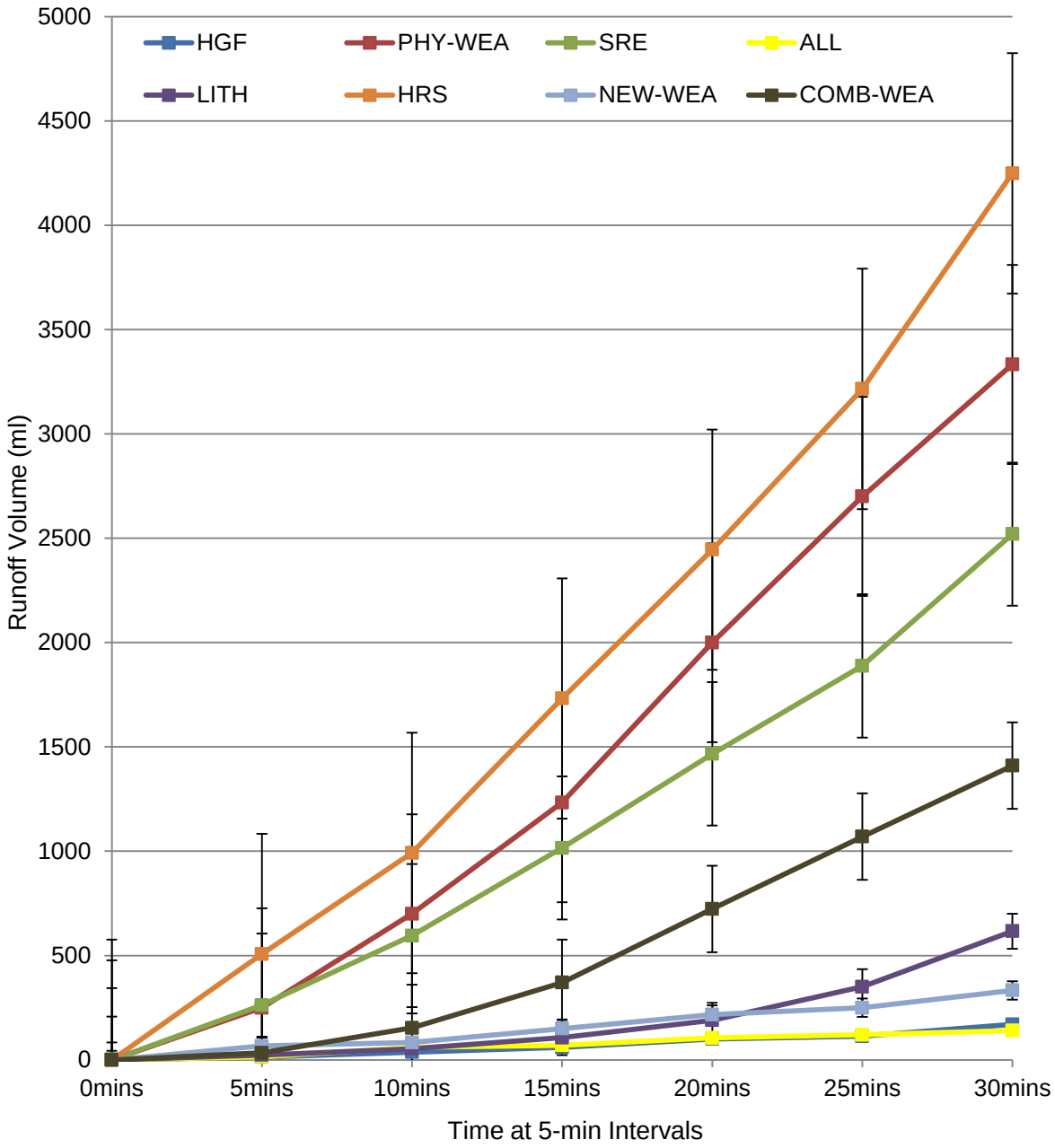

Figure 4.3. AD_{amc} SFM cumulative runoff volume (at 5 min intervals)
Note: For statistical differences between SFMs refer to Tables 4.6 (n=3). Error bars denote ±1 Standard Error

Experimental observations and post-rainfall evidence from photographs of non-soil PHY-WEA (Figure 4.4) show the fine material has been removed and the surface is left compact and heavily armoured. Figure 4.5 illustrates that during rainfall, fine material is mobilised by impacting raindrops and progressively in-fills surface pores. As the surface seals, infiltration-excess surface runoff increases, as shown in the runoff rate data. Post-rainfall PHY-WEA showed a decline in surface elevation of 2-3 cm, with compaction evident from visual

inspection. This inferred that that when the supply of low density material became limited, raindrop energy is used for compaction processes, which would further deter infiltration and sustain high runoff volume generation.

PHY-WEA-2 pre rainfall

PHY-WEA-2 post rainfall

Figure 4.4. Photographs of AD_{amc} PHY-WEA taken before and after rainfall *(Scale 1cm = 3cm)*

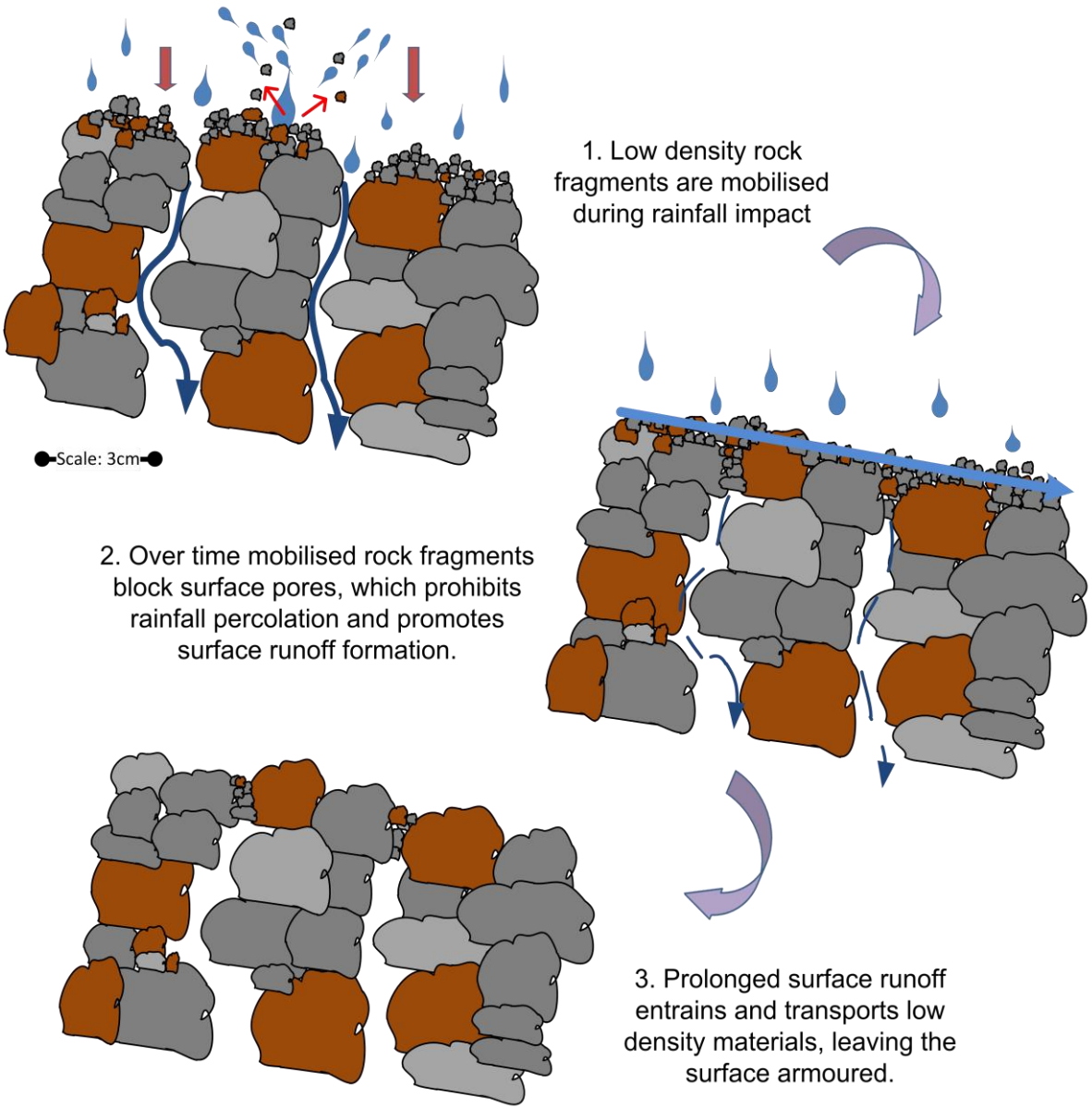

Figure 4.5. The effects of raindrop impact and surface runoff on non-soil SFMs *(source: Author, 2012)*

Soil SRE had significantly the highest runoff volume and rate of the soils. Post rainfall photographs of SRE (Figure 4.6) show the surface sealed with considerable amounts of disaggregated material on and around the erosion tray; evidence of raindrop impact processes (rain-splash) and infiltration-excess overland flow (as explained in Figure 4.7). Studies of highly weathered soils (Asadu and Akamigbo 1990; Asadu, et al., 1997; in Igwe and Nkemekosi, 2007) found aggregate stability dependent on clay content, clay mineralogy and CEC, but SRE has the highest amounts of kaolinite clay as compared with the other soils at 35% w/w. Post rainfall images of SRE show that it had many coarse stones (>3 cm) at the surface. A stoney surface will create an impermeable

surface area deterring infiltration in favour of runoff formation (Poesen and Ingelmo-Sanchez, 1992; in Morgan, 2006).

SRE-2 pre rainfall

SRE-2 post rainfall

Figure 4.6. Photographs of AD_{amc} SRE taken before and after rainfall
(Scale 1 cm = 3 cm)

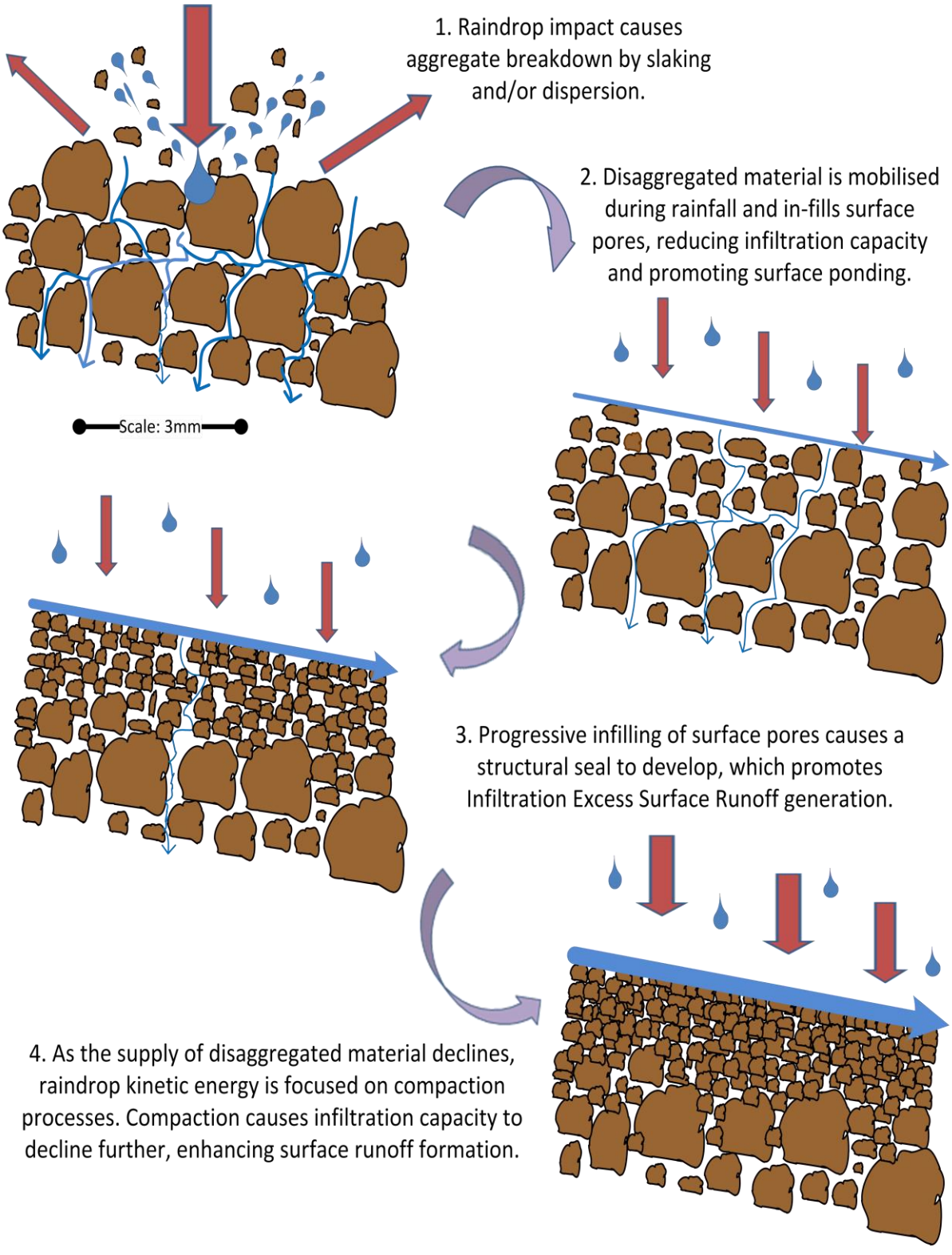

Figure 4.7 Infiltration-excess overland flow formation by raindrop impact
(Source: Author, 2012)

Figure 4.8 is a photograph of SRE taken mid-rainfall (after approximately 20 mins) and shows SRE has extensive ponding and is visibly water-logged. It cannot be discerned whether hydraulic conductivity and soil moisture storage properties are in part also responsible for SRE generating significantly high runoff volumes by saturation-excess overland flow processes, as illustrated in Figure 4.9. SRE is a colluvium soil, which is known to have a shallower profile than non-disturbed soils, described as having a 'loose' structure by Rybar et al. (2002). The exact origin of SRE is uncertain, but it is thought to be formed by colluvial deposition at the foothills of the Simandou Range (Lucas Kitchen, Personal Communication 26th November 2010). SRE's origin and shallow profile suggests it has a less developed structure than the other soils. It is reasoned that aggregate breakdown and saturation excess overland flow processes would have been operating simultaneously; when combined this caused the marked runoff volumes recorded by SRE compared to the other soils. Further testing of the soil *in situ* would be required to prove this.

SRE-3 mid rainfall

Figure 4.8. SRE saturated after approximately 20mins of rainfall
(Scale 1 cm = 3 cm)

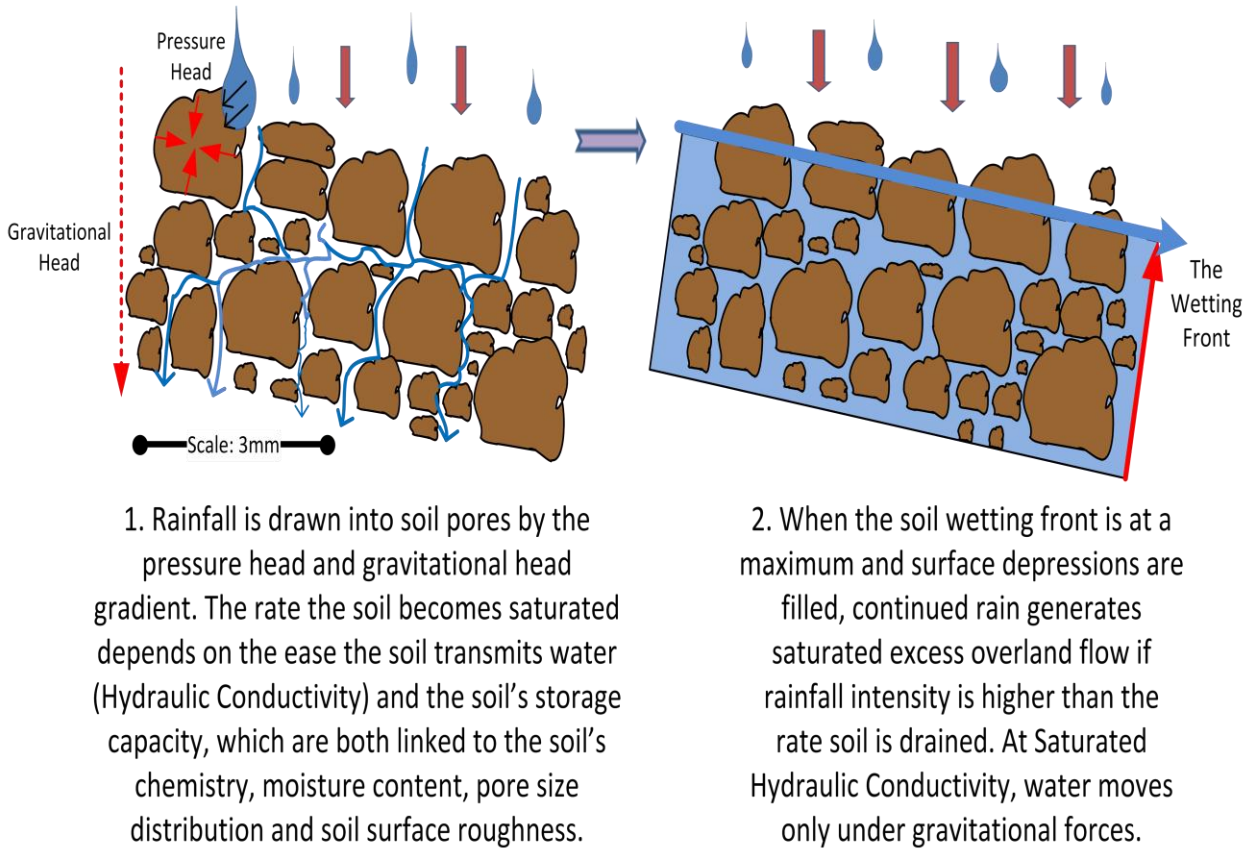

Figure 4.9. Saturation-excess surface runoff formation
(Source: Author, 2012)

4.3.2 Total Sediment Load (TSL) in runoff (AD_{amc})

One-Way ANOVA and post-hoc Fisher LSD analysis demonstrate that runoff TSL (g) from the erosion trays was in the order PHY-WEA > HRS=SRE > COMB-WEA=NEW-WEA=LITH=ALL=FER=RD=HGF (Table 4.5). Non-soil PHY-WEA was associated with significantly the highest runoff TSL of all the SFMs with a mean value of 47.8 g; 2300 times more runoff TSL than soil FER (0.02g). Non-soil HRS (12.2 g) and soil SRE (10.2 g) are also associated with significantly higher TSLs than the other SFMs. Non-soil PHY-WEA also had significantly the highest AD_{amc} Total Sediment Concentration (TSC) of 14.3 g l^{-1} (Table 4.5), followed by non-soil HRS (2.88g l^{-1}) and soil SRE (4.04 g l^{-1}). High TSLs and TSCs can be detrimental to the local environment and also disrupt mining operations.

PHY-WEA comprises 65.5% silt-sized particles. Materials with a high silt composition are reported to be easily eroded as silt has low cohesive properties and materials have weak inter-particle bonds (Vacher et al., 2004). Furthermore

highly weathered materials such as PHY-WEA are known to have lower strength (resistance to failure under the action of stresses such as raindrop impacts), than if the material was in a non-weathered state (Price, 2009). This suggests PHY-WEA is highly susceptible to physical aggregate^{NS} breakdown processes caused by raindrop impacts, creating smaller easier to entrain aggregates^{NS} or primary particles, in the same way as aggregate^{S} breakdown effects soils (as was illustrated previously in Figure 4.7).

PHY-WEA has a mineralogical composition of 50.8% muscovite (Table 4.3). It is speculated that the flat sheet-like silicate shape of muscovite minerals (Price, 2009), is more conducive to plugging surface pores than other mineral shapes. However, without further analysis using high resolution electron microscope imagery, this cannot be proven.

4.3.3 Leachate volume at AD_{amc}

Non-soil NEW-WEA (8200 ml) had significantly higher leachate volume compared with non-soil PHY-WEA (1945 ml) and soil SRE (2168 ml), which both had significantly lower leachate volumes compared with all other SFMs (Table 4.5).

Photographs of NEW-WEA show that post-rainfall the surface is left void of finer materials and heavily armoured (Figure 4.11). Observations of non-soil NEW-WEA showed it had a high surface porosity due to a high content of rocks at the surface. Poesen et al. (1994) defines rock fragments as minerals >2 mm in size. NEW-WEA has a DAD of 59.2% w/w >2 mm (Table 4.4, Section 4.2). Porosity is largely controlled by the size of pores and their connectivity; larger pores will transfer higher quantities of rainfall to leachate as shown in Figure 4.10 (Hawkins, 1998; Fala et al., 2003). It is deduced NEW-WEA showed no significant change in runoff rate over time, had significantly low runoff volume and high leachate volume because of high surface porosity caused from having a higher content of large rocks than the other SFMs.

The soil leachate volumes recorded by ALL (5888 ml) and FER (5456 ml) were not statistically different to non-soils RD (6455 ml) and COMB-WEA (5833 ml). Cumulative runoff volume and runoff rate were not recorded for FER or RD because insufficient volumes were detected. Soil ALL is associated with significantly lower runoff rates compared to soil SRE at 0-5mins and 10-15mins (Table 4.6). Photographs of ALL and FER (Figures 4.12 and 4.13) show the surfaces are relatively unchanged after rainfall, with no obvious surface deformation. The results indicate soils ALL and FER have high aggregate^{S}

stability during rainfall, causing high infiltration rates, high leachate volumes and low runoff rates.

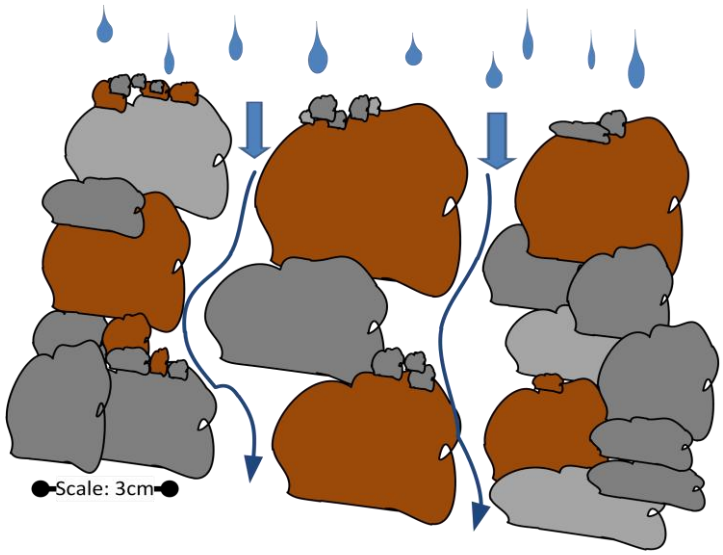

SFMs with a high proportion of coarse rock fragments will have large voids between where rock fragments meet, creating high porosity, which rapidly transfers rainfall to leachate and creating little, if any, surface runoff.

Figure 4.10. The effect of rainfall on high porosity SFMs
(Source: Author, 2012)

4.3.4 Total sediment load in leachate (AD_{amc})

The AD_{amc} results show that leachate TSLs from non-soils RD (4.08 g), NEW-WEA (5.2 g) and COMB-WEA (4.62 g) were significantly higher than all other SFMs, which ranged between 0.32-1.97 g. Non-soils COMB-WEA (0.79 g l^{-1}), NEW-WEA (0.63 g l^{-1}), HRS (0.59 g l^{-1}) and RD (0.63 g l^{-1}) had significantly higher leachate TSC at AD_{amc} as compared with all other SFMs, which had values of <0.206 g l^{-1} (Table 4.5).

The open porous nature of RD, NEW-WEA and COMB-WEA predisposes these SFMs to higher erosion losses, caused by high leachate volumes and through-flow rather than by surface runoff. This should be considered when designing runoff storage structures and deciding in what order to stock pile these SFMs, where it is recommended not to position RD, NEW-WEA or COMB-WEA on top off a SFM with low permeability, as this is likely to result in high leachate volumes at the interface between the materials within the waste-rock dump.

In summary the AD_{amc} results have highlighted that despite showing significant differences in their physical and chemical properties, the soil and non-soil SFMs in this study (HRS, PHY-WEA (non-soils) and SRE (soil)), which were

associated with high runoff volumes and TSLs; and LITH, ALL, FER (soils) and RD, HGF and COMB-WEA (non-soils) associated with higher leachate volumes and TSLs show comparable responses to rainfall, both in terms of their relative erodibility and hydrological response.

NEW-WEA-2 pre rainfall

NEW-WEA-2 post rainfall

Figure 4.11. Photographs of AD_{amc} NEW-WEA taken before and after rainfall *(Scale 1 cm = 3 cm)*

ALL-1 pre-rainfall

ALL-1 post-rainfall

Figure 4.12 Photographs of AD_{amc} ALL taken before and after rainfall *(Scale 1cm = 3cm)*

FER-3 pre-rainfall

FER-3 post-rainfall

Figure 4.13 Photographs of AD_{amc} FER taken before and after rainfall *(Scale 1 cm = 3 cm)*

4.4 Hydrological responses and erodibility of slope forming materials at Field Capacity Antecedent Moisture Conditions (FC_{amc})

4.4.1 Runoff volume and runoff rate at FC_{amc}

At FC_{amc} one-way ANOVA post-hoc Fisher LSD analysis ($p < 0.05$) indicates that significantly higher runoff volumes were associated with non-soil PHY-WEA (6238 ml) and soil SRE (5000 ml) as compared with all other SFMs, which ranged from 70–1026 ml (Table 4.7). FC_{amc} runoff rates are summarised in Table 4.8 and cumulative runoff volume is illustrated in Figure 4.14. After the initiation of rainfall from 0-5mins, soil SRE (80 ml min^{-1}) and non-soil PHY-WEA (88.7 ml min^{-1}) had significantly higher mean runoff rates, as compared with all other SFMs which ranged from 1.3–20.0 ml min^{-1}. This trend continued for each of the five subsequent time periods for the remainder of the 30 minute storm. Both SRE (233 ml min^{-1}) and PHY-WEA (301 ml min^{-1}) achieved significantly higher runoff rates than all other SFMs after 30mins.

Table 4.7 SFM runoff and leachate volumes, TSLs and TSCs at FC_{amc}

Slope Forming Material	Runoff Volume (ml)	Runoff TSL (g)	Runoff TSC (g l^{-1})	Leachate Volume (ml)	Leachate TSL (g)	Leachate TSC (g l^{-1})
LITH	1026a	0.5a	7.2a	4830_{b}	1.35_{ac}	0.30_{a}
ALL	120a	1.07a	26.7b	9900_{a}	0.75_{a}	0.07_{b}
FER	133a	0.34a	7.2a	8933_{a}	0.86_{a}	0.09_{bc}
SRE	5000b	41.8b	7.3a	3300_{b}	0.78_{a}	0.24_{ac}
RD	70.0a	0.5a	7.9a	8366_{a}	3.79_{bc}	0.46_{a}
PHY-WEA	6238b	166c	26.2b	3066_{b}	19.1_{d}	4.8_{d}
HRS	450a	0.7a	2.6a	8700_{a}	5.37_{b}	0.01_{a}
HGF	527a	2.9a	4.9a	8683_{a}	7.37_{b}	0.79_{a}

Within the same column, values not followed by the same letter are significantly different at $p<0.05$ as determined by One-Way ANOVA and post-hoc Fisher LSD analysis (n=3). Note: soils are shaded in white and non-soils in green for ease of reference

As observed at AD_{amc}, significantly higher runoff volumes were recorded for non-soil PHY-WEA and soil SRE at FC_{amc}, and after 30 mins runoff rates were still increasing (Figure 4.14i). It is still unknown for how long these materials can sustain increasing runoff rates and high runoff volumes. Runoff volume is an important consideration for Rio Tinto because runoff management, which will include the creation of large scale drainage facilities and sedimentation ponds, will be expensive, so understanding SFMs that generate high runoff volumes and associated high TSLs and TSCs will be an important consideration in the design of runoff management infrastructure (Lucas Kitchen, Personal Communication, 26th November 2010).

Table 4.8. Differences in SFM runoff rate at 5-min intervals at FC_{amc}

Slope Forming Material	Runoff Rate (ml min^{-1})					
	0-5 mins	5-10 mins	10-15 mins	15-20 mins	20-25 mins	25-30 mins
LITH	20.0_{ab}	20.7_{a}	33.3_{a}	28.0_{a}	47.7_{a}	55.7_{a}
ALL	1.3_{a}	3.3_{a}	4.7_{a}	4.3_{a}	3.0_{a}	7.3_{a}
FER	4.7_{a}	2.7_{a}	4.0_{a}	5.0_{a}	5.3_{a}	5.0_{a}
SRE	80.0_{c}	147_{b}	167_{b}	180_{b}	193_{b}	233_{b}
RD	1.3a	3.3_{a}	2.3_{a}	3.7_{a}	0.0_{c}	3.3_{a}
PHY-WEA	88.7_{bc}	159_{b}	217_{c}	237_{b}	245_{b}	301_{b}
HRS	7.7_{a}	9.7_{a}	14.0_{a}	28.0_{a}	12.7_{a}	18.0_{a}
HGF	8.0_{a}	18.7_{a}	19.3_{a}	16.7_{a}	18.7_{a}	24.0_{a}

Within the same column, values not followed by the same letter are significantly different at $p<0.05$ as determined by One-Way ANOVA and post-hoc Fisher LSD analysis (n=3). Note: soils are shaded in white and non-soils in green for ease of reference

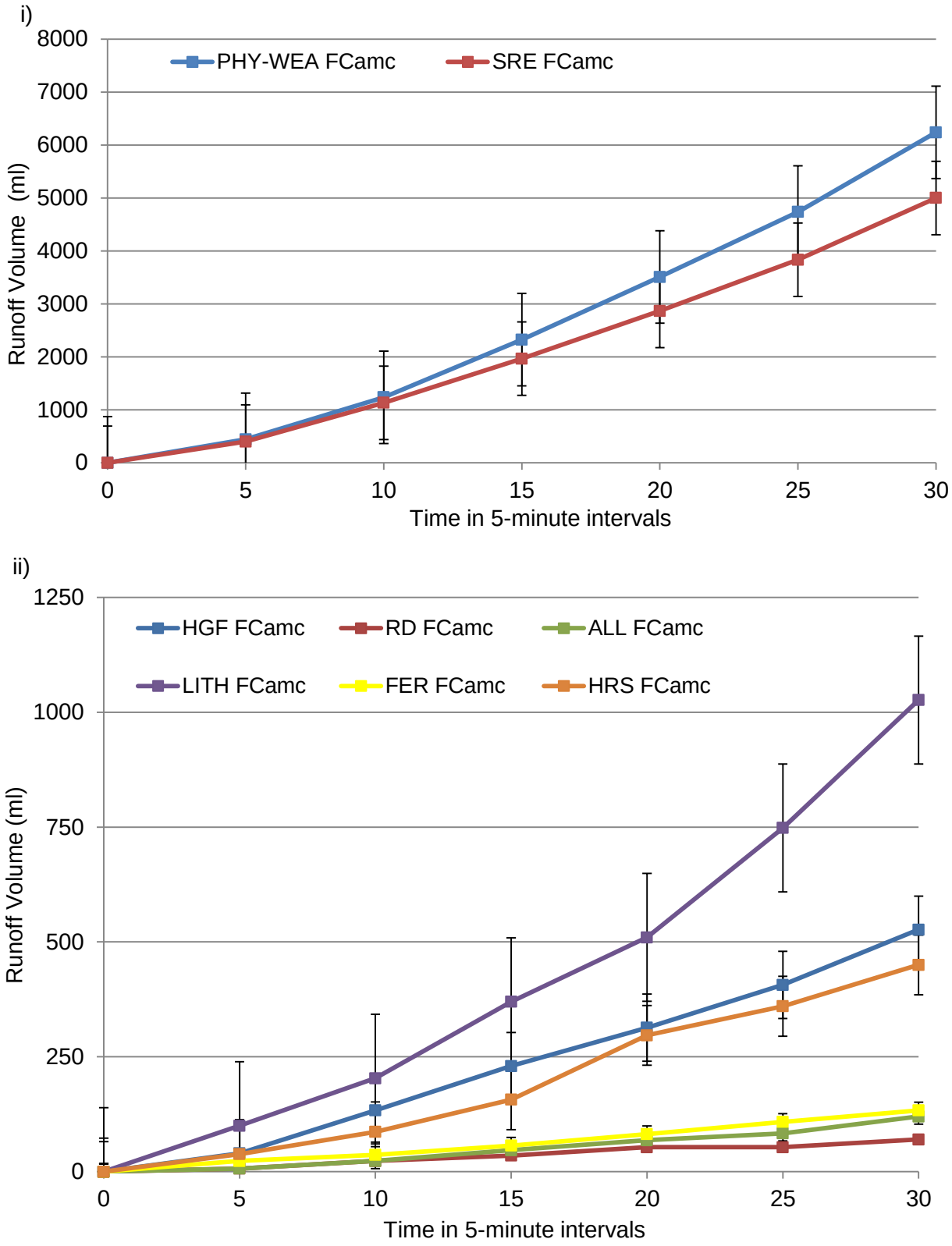

Figure 4.14 FCamc cumulative runoff volume at 5-min intervals: showing i) PHY-WEA and SRE ii) HGF, RD, ALL, LITH, FER and HRS

Note: the vertical scale bars of Figure i and ii are not the same. For statistical differences between SFMs refer to Tables 4.8. Error bars denote ±1 Standard Error.

Figure 4.14 illustrates that with the exceptions of PHY-WEA and SRE, soil LITH has significantly higher cumulative runoff volume amounts than the other SFMs; generating runoff volume ten times that of the soils ALL and FER. Post-rainfall, LITH showed evidence of surface sealing, which implies that aggregate^S breakdown caused a decline in infiltration capacity during rainfall. It is reasoned that differences in soil texture would cause differences in aggregate^S cohesion, as silt gives less cohesion than clay, which binds the aggregate together (Morgan, 2006; White, 2006). LITH has kaolinite clay amounts, half that of the other soils at 14.8% w/w (Table 4.3). Furthermore, at 50% w/w, LITH has significantly high PSD of silt sized particles, double the amount of soils ALL and FER (Table 4.1). Aggregates^S with less cohesive strength would be more susceptible to breakdown by raindrop impacts. Differences in soil texture may also cause differences in soil saturated hydraulic conductivity, so at field capacity soils ALL and FER are draining at a higher rate than soils LITH and SRE. However, further testing of infiltration rate is necessary to be certain about the hydraulic processes affecting these soils.

4.4.2 Total sediment load in runoff (FC_{amc})

Soil SRE and non-soil PHY-WEA at FC_{amc} gave significantly higher mean runoff TSL values of 41.8 g and 165 g, respectively as compared with all other SFMs, with values ranging from 0.34 g to 2.9 g (Table 4.7). These results highlight the marked differences in SFM erodibility between SRE and PHY-WEA and the remaining SFMs.

Soil ALL and non-soil PHY-WEA had significantly higher runoff TSCs compared with all other SFMs, with values of 26.7 g l^{-1} and 26.2 g l^{-1}, respectively (Table 4.7). Although it is of note that runoff TSL associated with ALL (1.07g) was orders of magnitudes less than runoff TSL from PHY-WEA (166 g), but low runoff volumes from ALL caused an increase in runoff turbidity. Runoff TSC will be an important consideration for sediment management planning on a mine-site because water from disturbed areas may have to pass through sediment control structures before entering nearby streams or rivers, to comply with stipulated suspended solid concentrations (Kennedy, 1990).

4.4.3 Leachate volume at FC_{amc}

The highest leachate volumes were generated from the soils ALL and FER, and non-soils RD, HRS and HGF, with no significant differences in their mean values of 9900 ml, 8933 ml, 8367 ml, 8700 ml and 8683 ml, respectively (Table

4.7). No significant differences in leachate volume were observed between LITH, SRE and PHY-WEA with values ranging between 3066–4830 ml. It is presumed that ALL and FER, as compared to the other two soils, are less susceptible to aggregate^{S} breakdown during rainfall at $AD_{amc,}$ and are structured in such a way as to transmit high leachate volumes (Morgan, 2006).

4.4.4 Total sediment load in leachate (FC_{amc})

Table 4.7 shows non-soil PHY-WEA produced significantly higher leachate TSL (19.1 g) than all other SFMs at FC_{amc}. Non-soils RD, HRS and HGF produced statistically comparable leachate TSLs to one another (ranging from 3.79 g and 7.37 g). All four soils generated <1.35 g leachate TSL. The leachate TSC results show that PHY-WEA (4.8 g l^{-1}) had significantly higher leachate TSC as compared with all other SFMs, which ranged from 0.01 to 0.79 g l^{-1} (Table 4.7).

Despite generating significantly lower leachate volume, PHY-WEA was associated with the highest leachate TSL at FC_{amc} of all the SFMs (19.1 g). Furthermore, at FC_{amc} PHY-WEA produced significantly higher TSL by both leachate and runoff as compared to all other SFMs. This highlights the exceptionally high erodibility of non-soil PHY-WEA under FC_{amc}. High TSLs and TSCs by runoff or by leachate generated on waste-rock dumps can disrupt mining operations and be detrimental to the local environment by reducing water reservoir capacity through sedimentation and impacting on surface and sub-surface water quality. Managing sediment load can be expensive (Schwab et al, 1981; Brotons et al., 2010), and it is important to know which SFMs are most at risk to high TSLs by both runoff and also by leachate.

4.5 Testing hypotheses 2 to 4

4.5.1 Testing Hypothesis 2: Differences in SFM erodibility and hydrological response.

4.5.1.1 Air-dry antecedent moisture condition results.

It was hypothesised that the different SFMs would have different hydrological responses in terms of i) runoff volume and associated TSLs and ii) leachate volume and associated TSLs. Comparing the results in Table 4.9 at AD_{amc} using Factorial ANOVA post hoc Fisher LSD ($p < 0.05$) analysis shows this hypothesis is supported. Leachate volumes significantly exceed runoff volumes for soils ALL (4118%), LITH (630%) and FER (2043%), and non-soils RD (5248%),

NEW-WEA (2463%), HGF (3714%) and COMB-WEA (414%). However, non-soils PHY-WEA (171%) and HRS (127%) had significantly higher runoff volumes than leachate volumes. SRE showed no significant difference in runoff and leachate volume.

Table 4.9 Leachate and runoff volumes and associated TSLs at AD$_{amc}$

Slope Forming Material	Volume (ml)	TSL (g)
LITH Leachate	3884_{b}	0.8_{cd}
LITH Runoff	617_{de}	2.03_{bcd}
ALL Leachate	5888_{a}	0.9_{bc}
ALL Runoff	143_{f}	0.41_{bcd}
FER Leachate	5456_{ab}	0.94_{a}
FER Runoff	267_{f}	0.02_{bcd}
SRE Leachate	2168_{c}	0.32_{gh}
SRE Runoff	2520_{c}	10.2_{b}
RD Leachate	6455_{a}	4.08_{bcd}
RD Runoff	123_{f}	0.56_{ef}
PHY-WEA Leachate	1945_{d}	0.38_{h}
PHY-WEA Runoff	3333_{c}	47.8_{bc}
NEW-WEA Leachate	8200_{ab}	5.2_{bcd}
NEW-WEA Runoff	333_{g}	0.75_{efg}
HRS Leachate	3346_{f}	1.97_{fg}
HRS Runoff	4249_{d}	12.2_{de}
HGF Leachate	5200_{a}	0.76_{bc}
HGF Runoff	140_{ef}	0.44_{bcd}
COMB-WEA Leachate	5833_{a}	4.62_{bc}
COMB-WEA Runoff	1410_{f}	2.27_{ef}

Within the same column, values not followed by the same letter are significantly different ($p<0.05$), determined by Factorial ANOVA post-hoc Fisher LSD analysis (n=3).

Surface sealing is common to both soil and non-soil SFMs. This process is the defining precursor of whether leachate or runoff is the dominant hydrological response to rainfall. However, it is important to note that the processes that lead to surface sealing are different. Figure 4.15 illustrates that the susceptibility to raindrop impacts is the primary cause of detachment in the soil SFMs (Morgan, 2006), and will determine if there is a supply of disaggregated materials to seal

the surface, and so whether leachate or runoff is the dominant hydrological response to rainfall.

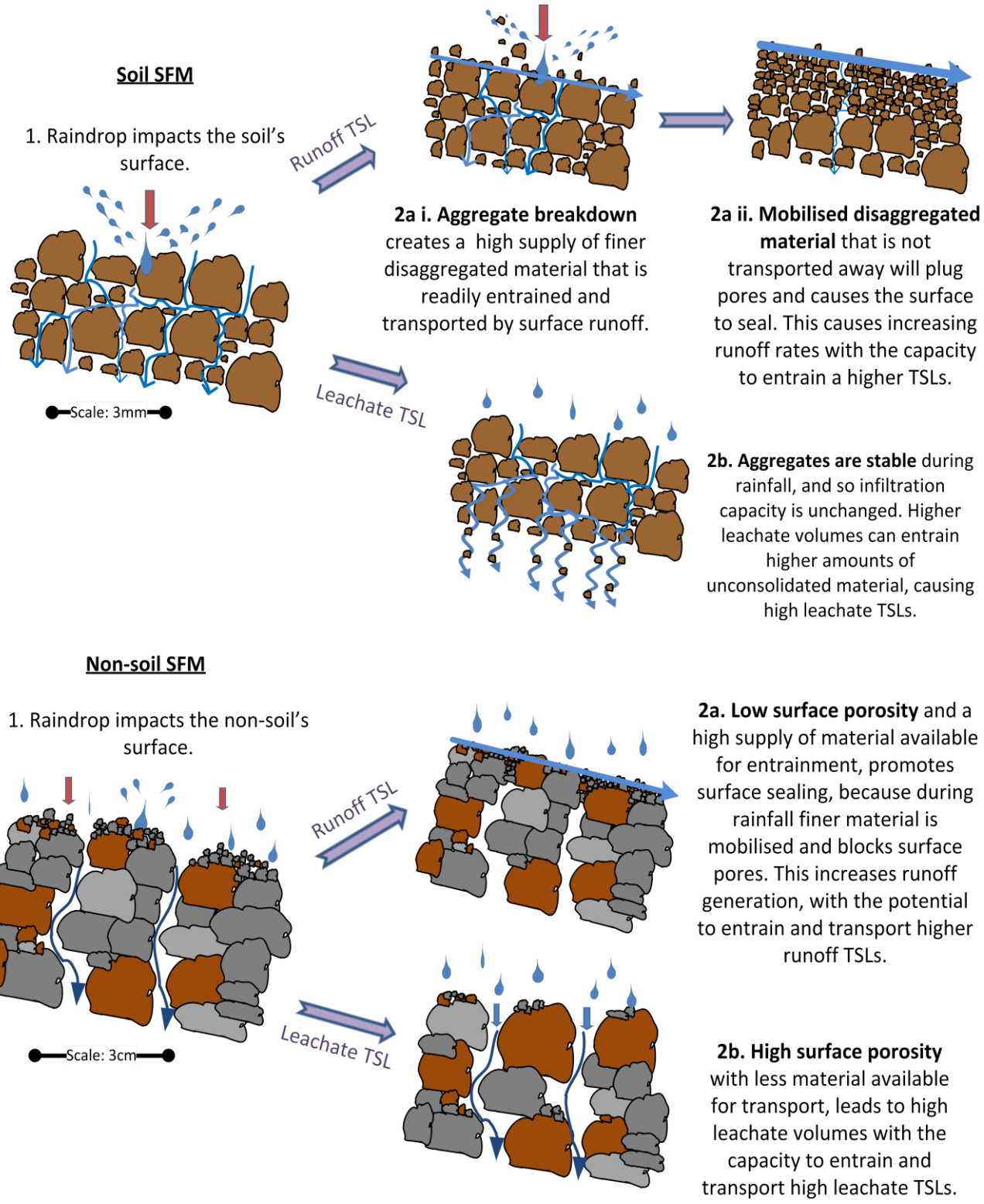

Figure 4.15. Important factors determining whether the soils and non-soil SFMs generate leachate TSL or runoff TSL *(Source: Author, 2012)*

Figure 4.15 shows runoff (wash) is the primary cause of detachment for the non-soil SFMs. The organisation of material at the surface determines surface porosity as well as material available for transport by rain-splash. These are critical factors determining the extent of surface sealing and whether leachate and runoff is formed from non-soil SFMs during rainfall. When surface porosity is low, surface ponding can occur early on in the rain event.

As expected, Advanced Linear statistical analysis showed a significant correlation between the runoff volume and leachate volume results ($p=0.020$) for all SFMs, except SRE. Generation of runoff or leachate is inter-dependent and dynamic in space and time, which was also observed during studies of simulated coal stock pile systems by Curran et al. (2002). For SRE, there is no correlation between its leachate and runoff volume results, because it is postulated that SRE has exceptionally high water storage capacity when compared with the other SFMs, and therefore the linear relationship between runoff and leachate amounts is not statistically significant.

Leachate dominates the hydrological response of soils ALL, LITH and FER and non-soils RD, NEW-WEA, HGF and COMB-WEA, showing leachate processes are just as important as runoff processes for several SFMs. High volumes of water movement on the surface and within a waste-rock dump will have risks associated with the transmission of contaminants and slumping (Hartman, 2002; Singh et al., 2002). In terms of erosion management on a mine-site it is important that erosion via both runoff and leachate is taken into account.

A comparison of the AD_{amc} runoff TSLs and leachate TSLs results shows soil SRE and non-soils PHY-WEA and HRS have significantly higher TSLs from runoff as compared with leachate. Conversely soil FER and non-soils RD, NEW-WEA and HGF were associated with significantly higher TSL in leachate as compared with runoff (Table 4.9).

Runoff is the dominant transport mechanism of soil SRE and non-soils PHY-WEA and HRS. Leachate is the dominant transport mechanism of soil FER and non-soil RD, NEW-WEA and HGF. Figure 4.15 illustrates that despite similarities in the hydrological response of SRE, PHY-WEA and HRS and also FER, RD, NEW-WEA and HGF, these results are in agreement with Curran et al. (2002), that hydrodynamic systems are different for non-soil and soil SFMs. Aggregate stability and subsequent availability of disaggregated material for entrainment and transport are key factors in determining whether surface sealing is sufficient in soils to generate sufficient runoff to cause erosion. Stable soil will maintain high infiltration rates during rainfall, causing high leachate formation.

For non-soils surface porosity and the availability of transportable material are key factors determining whether the surface seals and the resultant hydrological response is to generate leachate or runoff (Figure 4.15). Of the non-soils PHY-WEA is the exception, due to its mineralogy, which comprises aggregates^{NS} constituting 50.8% muscovite and 19.2% kaolinite clay (Table 4.3). Its high composition of muscovite, which has a low Moh's hardness of 2.5 (Roberts, 2004), implies PHY-WEA aggregates^{NS} are more susceptible to breakdown processes during rainfall. Therefore, non-soil PHY-WEA shows erosional behaviour similar to soil SFMs.

4.5.1.2 Field capacity antecedent moisture condition results

The Factorial ANOVA FC_{amc} runoff TSL and leachate TSL results show soil SRE and non-soil PHY-WEA generated significantly higher runoff TSL compared to leachate TSL. In comparison non-soils RD, HRS and HGF generated significantly higher TSLs by leachate as compared to runoff (Table 4.10). Different hydrological responses to rainfall shown by these SFMs highlights that simulated erosion assessments (as opposed to aggregate stability tests) are the only way a comprehensive assessment of a SFMs response to rainfall can be determined.

These results recognise that although the soils and non-soil SFMs are statistically different in their physical and chemical properties, some have the same hydrological response to rainfall. However, the fundamental processes that governs soil and non-soil leachate and runoff formation, as well as leachate and runoff TSL are, with the exception of PHY-WEA, different. A classification system that improves on using the narrow categories 'soils' and 'non-soils' is needed that recognises differences in the SFMs physical and chemical properties and response to rainfall, to strategically identify erosion control solutions that target runoff or leachate processes.

Table 4.10 Comparison of leachate and runoff volumes and TSLs at FC$_{amc}$

Slope Forming Material	Volume (ml)	TSL (g)
LITH leachate	4830_{c}	1.35_{bc}
LITH runoff	1027_{ab}	0.48_{ab}
ALL leachate	9900_{e}	0.75_{ab}
ALL runoff	120_{a}	1.07_{ab}
FER leachate	8933_{e}	0.86_{ab}
FER runoff	133_{a}	0.390_{a}
SRE leachate	3300_{c}	0.780_{ab}
SRE runoff	5000_{cd}	41.8_{f}
RD leachate	8367_{e}	3.79_{cd}
RD runoff	70_{a}	0.54_{ab}
PHY-WEA leachate	3067_{bc}	19.1_{ef}
PHY-WEA runoff	6238_{d}	166_{g}
HRS leachate	8700_{e}	5.37_{de}
HRS runoff	450_{a}	0.66_{ab}
HGF leachate	8683_{e}	7.37_{d}
HGF runoff	527_{a}	2.86_{ab}

Within the same column, values not followed by the same letter are significantly different ($p<0.05$), determined by Factorial ANOVA post-hoc Fisher LSD analysis (n=3).

Figures 4.16 and 4.17 show high standard error in the SFMs runoff and leachate volumes at both AD_{amc} and FC_{amc}. High variation is due to variability in SFM physical and chemical properties, which causes variations in aggregate breakdown, surface sealing and the amounts of runoff and leachate volumes produced in an otherwise controlled experimental environment. Differences in the surface area of rocks are thought to affect runoff and leachate generation, because rocks at the surface create an impermeable barrier restricting infiltration and promoting runoff (Poesen et al., 1994). The experimental design did not control the surface area of stones in the erosion tray because it was important to replicate the random sorting of SFMs as they would be stockpiled/dumped at a mine-site. Gerke et al. (1998) discuss how spoil properties are affected by the techniques used during mining and waste-rock dump formation which create different mixtures of spoil textures, including chunks of non-soil, rock or soil. As a consequence of high variability, a higher number of test replicates will be adopted in the experimental design of Phase II in order to improve the robustness of statistical analysis.

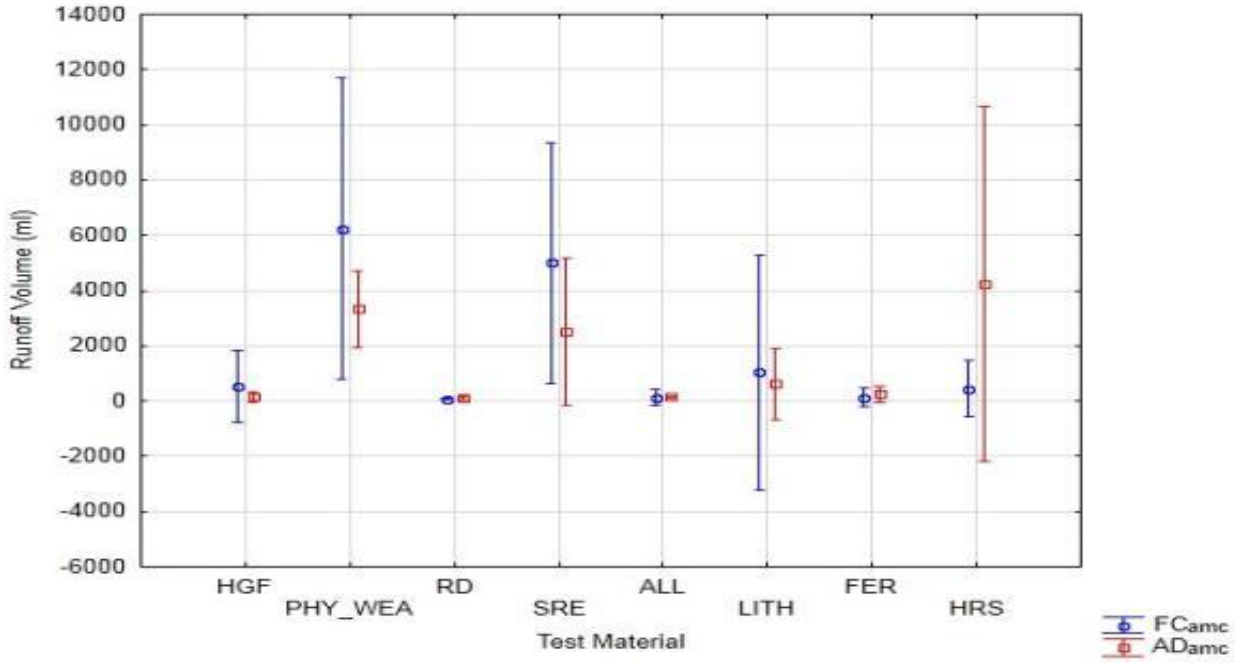

Figure 4.16 Comparison of SFM runoff volume (ml) at ADamc and FCamc
Note: For statistical differences between SFMs refer to Tables 4.9 and 4.10. Error bars denote ±1 Standard Error (n=3).

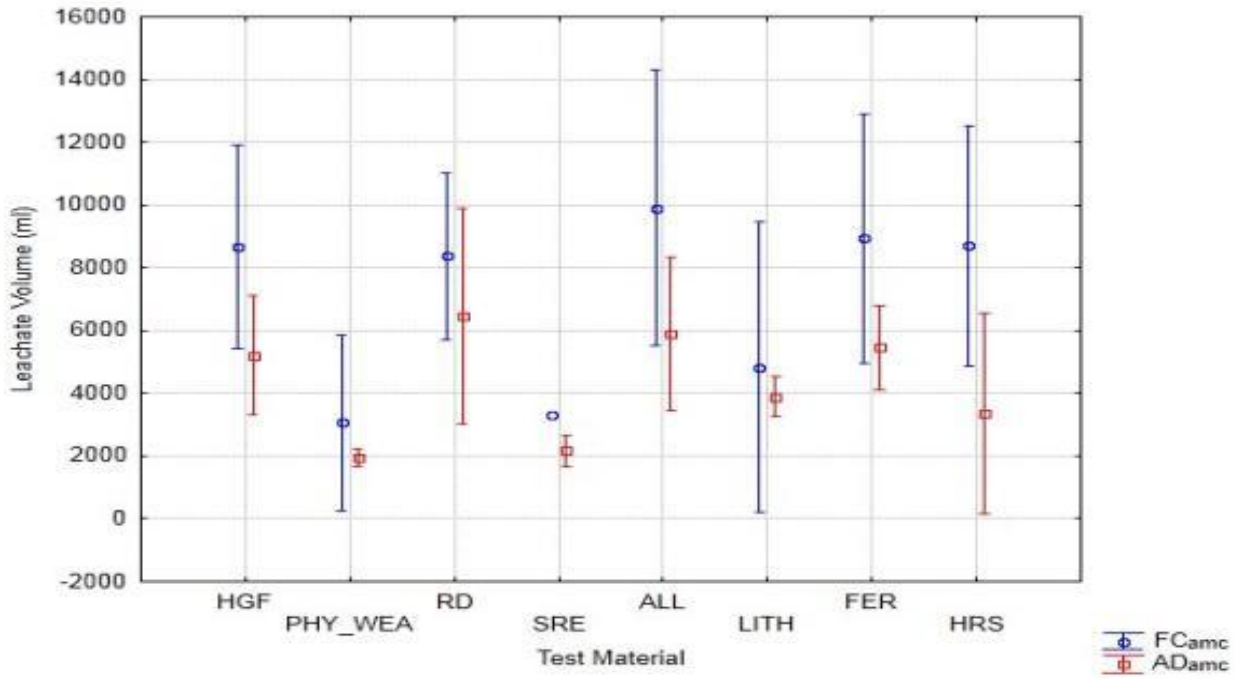

Figure 4.17. Comparison of SFM leachate volumes at ADamc and FCamc
Note: For statistical differences between SFMs refer to Tables 4.9 and 4.10. Error bars denote ±1 Standard Error (n=3).

4.5.2 Testing Hypothesis 3: The effects of changing antecedent moisture conditions on SFM erodibility and hydrological response

This study assessed SFM runoff, leachate and TSLs at two antecedent moisture conditions; namely, air-dry (AD_{amc}) and field capacity (FC_{amc}) to replicate field conditions in Guinea, which has a distinct dry and rainy season. It was hypothesised that changing antecedent moisture conditions will affect the hydrological response of the soil SFMs, as at field capacity increased moisture will affect soil strength and soil moisture holding capacity. Differences in SFM leachate volumes were expected as higher volumes of infiltrated water will be transferred to leachate at FC_{amc}. Due to differences in soil and non-soil physical and chemical properties it was not known whether antecedent moisture conditions would affect the non-soil SFMs in the same way as the soils.

Factorial ANOVA post-hoc Fisher LSD analysis ($p < 0.05$) was used to compare runoff rate (at 5-min intervals), runoff and leachate volumes, and associated TSLs at AD_{amc} and FC_{amc} (Tables 4.11 and 4.12). Of the soils results LITH showed significantly higher (425%) runoff rate at 0-5 mins FC_{amc} as compared with AD_{amc}. In contrast, ALL showed a significant increase in leachate volume (68%) at FC_{amc} as compared with AD_{amc}. FER showed an increased runoff TSL (1950%) and leachate volume (63%) between AD_{amc} and FC_{amc}. Soil SRE showed significantly higher runoff volume (198%) and runoff rates for the 5-30 min time intervals at FC_{amc} as compared with AD_{amc}.

Of the non-soil results PHY-WEA showed significantly higher runoff volume (187%) and leachate TSL (5026%) at FC_{amc} as compared with $AD_{amc.}$ During the 10-30min time intervals, PHY-WEA also had significantly higher runoff rates at $FC_{amc.}$ HGF showed significantly higher leachate volume (166%) and leachate TSL (968%) at FC_{amc} than $AD_{amc.}$ In contrast to all other SFMs, HRS was associated with significantly higher runoff volume (844%), runoff TSL (1848%) and runoff rates (0-30 mins) at AD_{amc} compared to FC_{amc}; but HRS had significantly higher leachate volumes (160%) and leachate TSL (272.5%) at FC_{amc} compared to $AD_{amc.}$

Table 4.11 Runoff volume, leachate volumes and associated TSLs at AD_{amc} and FC_{amc}

Slope Forming Material	Runoff Volume (ml)	Runoff TSL (g)	Leachate Volume (ml)	Leachate TSL (g)
LITH AD_{amc}	617_{a}	2.03_{b}	3884_{bcde}	0.80_{abc}
LITH FC_{amc}	1027_{a}	0.48_{b}	4830_{cdef}	1.35_{c}
ALL AD_{amc}	143_{a}	0.41_{b}	5889_{f}	0.90_{bc}
ALL FC_{amc}	120_{a}	1.07_{b}	9900_{h}	0.75_{abc}
FER AD_{amc}	267_{a}	0.02_{a}	5456_{ef}	0.94_{c}
FER FC_{amc}	133_{a}	0.39_{b}	8933_{h}	0.86_{abc}
SRE AD_{amc}	2520_{b}	10.2_{cd}	2168_{ab}	0.32_{a}
SRE FC_{amc}	5000_{d}	41.8_{cd}	3300_{abcd}	0.78_{abc}
RD AD_{amc}	123_{a}	0.56_{b}	6456_{fg}	4.09_{de}
RD FCa_{mc}	70_{a}	0.50_{b}	8367_{gh}	3.79_{de}
PHY-WEA AD_{amc}	3333_{c}	47.8_{de}	1945_{a}	0.38_{ab}
PHY-WEA FC_{amc}	6238_{e}	166_{e}	3067_{abc}	19.1_{f}
HRS AD_{amc}	4249_{d}	12.2_{c}	3346_{abcd}	1.97_{cd}
HRS FC_{amc}	450_{a}	0.66_{b}	8700_{h}	5.37_{e}
HGF AD_{amc}	140_{a}	0.44_{b}	5200_{def}	0.76_{abc}
HGF FC_{amc}	527_{a}	2.86_{b}	8683_{h}	7.37_{e}

Within the same column, values not followed by the same letter are significantly different at $p<0.05$ as determined by Factorial ANOVA post-hoc Fisher LSD analysis (n=3).

It was hypothesised that antecedent moisture conditions would affect the SFM erodibility and hydrological response to rainfall, and this was shown in the results of non-soils HRS, HGF and PHY-WEA and soils SRE, LITH and FER.

Soil SRE and non-soil PHY-WEA were the only SFMs associated with a significant increase in runoff volume and runoff rate between the AD_{amc} and $FC_{amc.}$ Both PHY-WEA and SRE contain 28.2% and 19.2% (w/w), respectively kaolinite clay (Table 4.4), which is a stable clay (White, 2006; Price, 2009); so swelling on wetting is not thought to be a key process affecting these materials. It is postulated that SRE and PHY-WEA have poorer drainage or else high moisture retention capacity, causing hydraulic conductivity to be slower than for the other SFMs (Nicolau, 2002). Antecedent moisture conditions would affect

PHY-WEA and SRE because at FC_{amc}, pore spaces become saturated quicker and this promotes saturation excess overland flow to occur at an earlier stage during the rain event than at $AD_{amc.}$ At $AD_{amc,}$ runoff is delayed as the dry material takes longer to wet up and reach saturation (Nicolau, 2002). Smith et al. (1995) suggests waste-rock SFMs containing a higher percentage of clay are more likely to experience dispersion on wetting. The results suggest both SRE and PHY-WEA were subject to reduced aggregate stability at FC_{amc}, so on wetting aggregates breakdown creates a supply of disaggregated material that promotes surface sealing processes (Kollet and Maxwell, 2006). Aggregate stability tests of SRE and PHY-WEA would be necessary to show with certainty how changing antecedent moisture conditions affect aggregate stability.

Table 4.12. Runoff rate (ml min^{-1}) at 5-min time intervals at AD_{amc} and FC_{amc}

Slope Forming Material	Runoff Rate (ml min^{-1})					
	0-5 mins	5-10 mins	10-15 mins	15-20 mins	20-25 mins	25-30 mins
LITH AD_{amc}	4.7_{a}	6.0_{a}	10.7_{ab}	16.7_{ab}	32.0_{ab}	53.3_{ab}
LITH FC_{amc}	20.0_{c}	20.7_{abc}	33.3_{ab}	28.0_{ab}	47.7_{ab}	55.7_{b}
ALL AD_{amc}	3.0_{a}	9.0_{a}	2.0_{a}	7.0_{a}	3.0_{a}	4.0_{a}
ALL FC_{amc}	1.3_{a}	3.3_{abc}	4.7_{ab}	4.3_{a}	3.0_{a}	7.3_{a}
FER AD_{amc}	ND	ND	ND	ND	ND	ND
FER FC_{amc}	ND	ND	ND	ND	ND	ND
SRE AD_{amc}	52.5_{b}	66.7_{abc}	84_{d}	90.2_{bc}	84.3_{be}	126_{bc}
SRE FC_{amc}	80.0_{b}	147_{d}	167_{c}	180_{de}	193_{cd}	233_{d}
RD AD_{amc}	ND	ND	ND	ND	ND	ND
RD FC_{amc}	ND	ND	ND	ND	ND	ND
PHY-WEA AD_{amc}	50.0_{b}	90_{bcd}	107_{e}	153_{cde}	140_{ce}	127_{bc}
PHY-WEA FC_{amc}	88.7_{b}	159_{d}	218_{f}	237_{ab}	245_{d}	301_{d}
HRS AD_{amc}	101.5_{b}	96.9_{cd}	212_{c}	143_{cd}	154_{cd}	207_{cd}
HRS FC_{amc}	7.7_{a}	9.7_{a}	14.0_{ab}	28.0_{e}	12.7_{ab}	18.0_{a}
HGF AD_{amc}	2.7_{a}	4.7_{a}	4.6_{ab}	8.0_{ab}	13.3_{ab}	26.7_{a}
HGF FC_{amc}	8.0_{a}	18.7_{ab}	19.3_{b}	16.7_{ab}	18.7_{ab}	24.0_{a}

Within the same column, values not followed by the same letter are significantly different at $p<0.05$ as determined by Factorial ANOVA post-hoc Fisher LSD analysis (n=3). Insufficient surface runoff (Non detectable ND) was generated from FER and RD for the determination of 5-min interval runoff rates.

Soil FER showed a significant increase in runoff TSL at FC_{amc}. As soils become wet their behaviour becomes more plastic, which causes a decline in soil strength, making aggregates^{S} more susceptible to slaking or dispersion by raindrop impact (Simmons, 1998). However FER only generated 0.39 g runoff TSL (SRE created 41.8g of runoff TSL at FC_{amc}), the lowest amount of all soils. So although changing moisture conditions causes higher runoff TSLs, FER is still significantly more stable than the other soils. Soils ALL (168%) and FER (151%) are associated with significant increases in leachate volume between AD_{amc} and FC_{amc}, which is an indication of good drainage, as high infiltration rates were sustained even at FC_{amc}.

Non-soils HRS and HGF are associated with significant increases in leachate volume between AD_{amc} and $FC_{amc.}$ HRS (10.1%) and HGF (16.3%) have a high content of aggregates^{NS} sized >19 mm (Table 4.4), which causes high surface porosity. HRS and HGF are largely comprised of primary particles of hematite (56.2% and 86.8%) respectively, and goethite (24.1% and 0.8%) respectively, which have low water retention (Price, 2009), so infiltrating water is freely drained, irrespective of antecedent moisture conditions.

Only non-soil HRS was associated with a significant decrease in runoff volume, runoff TSL and runoff rate between the AD_{amc} and FC_{amc}. This result is unexpected and is thought to be caused by hydrophobic properties. The mineralogical constitution of HRS compared with COMB-WEA, HGF and RD is similar (Table 4.4). HRS could therefore only be differentiated to the other non-soils by hydrophobic properties. Organic matter is associated with causing soil hydrophobicity (Piccolo and Mbagwu, 1999), but HRS has just 0.47% w/w organic carbon. It is deduced that as HRS is used for haul road surfacing, hydrophobic elements could have accumulated from inorganic sources, such as hydro-carbons deposited by vehicular exhausts or lubricant oils absorbed during rainfall (Oregon Resources Corporation, 2009). Haul roads in Oregon, USA, have shown hydrophobic properties caused by oils and vehicle fumes (Oregon Resources Corporation, 2009). At $AD_{amc,}$ dehydration causes the hydrophobic surface to become exposed, which repels water and deters infiltration; at FC_{amc} the material is wetted and the hydrophobic effects are reduced (Slay, 2008). These results have major implications for the management of runoff and erosion from haul roads at Simandou. It is recommended that HRS is kept wet to reduce the potential for high runoff volumes and runoff TSL caused during heavy rainfall.

4.5.3 Testing Hypotheses 4: The erodibility and hydrological responses of SFMs explained by their physical and chemical properties

Few studies have explored how non-soil and soil SFM properties affect differences in erodibility and hydrological response to rainfall (Vacher et al., 2004; Gilley et al., 1977; Riley, 1995). MRA is used to explore associations between independent runoff, leachate and erosion variables and the SFM properties given in Section 4.2 (Tables 4.1 to 4.4). It is expected that there will be significant differences in the characteristics which correlate with the soil and non-soil runoff, leachate and TSL results at AD_{amc} and $FC_{amc.}$ A better knowledge of these properties will better inform management decisions.

Principal Component Analysis (PCA) results revealed the soil and non-soil SFMs were distinct due to differences in their physical and chemical properties. Therefore the results are presented for the soil and non-soil SFMs at AD_{amc} and FC_{amc} separately. MRA prescribes that derived variables should be omitted, so CEC derived from exchangeable cation data was excluded. The medium-sand and 150-250 µm aggregate fractions were chosen at random to avoid bias, and removed from the PSD and DAD results to ensure that the related percentages did not sum 100%. To identify other highly correlated variables PCA was repeated using the remaining data. Only gibbsite and goethite were highly correlated for more than three principal components combinations, and as gibbsite had the higher reading, goethite was omitted.

Adjusted R^2 explains how well the MRA data fits the model; a value closer to 1 indicates a strong fit, taking into account the number of covariates. After consideration of how to best interpret the MRA using a data-set with a high number of properties it was decided adjusted R^2 would be accepted on a step-by step basis. Selecting the 'best' set of properties to include in the model was based on a critical judgement (Lark et al., 2007) of the step that gave the largest adjusted R^2 change, and subsequent steps gave only minor adjusted R^2 improvements. The MRA results were interpreted using the b* values, henceforth referred to as Beta (β).

The MRA results are presented in hierarchical order showing SFM properties that correlate most with the dependent variable in descending order, with positive or negative symbols inferring the direction of the correlation. All of the MRA outputs have an adjusted R^2 >0.9 which indicates strong associations between the SFM properties and the dependent variable results.

4.5.3.1. Soil runoff volume and runoff TSL at AD_{amc} and FC_{amc}

MRA sought to relate AD_{amc} runoff volumes to the physical and chemical properties of the four soil SFMs (Table 4.13). This revealed the following properties (in descending order) are significantly ($p > 0.05$) related to runoff volume generation; magnetic susceptibility (MS) (+β) > DAD 53-63 µm (-β) combined, account for 0.968 of the adjusted R^2 variation. MS is listed first in the running order of the model and accounts for the largest change in adjusted R^2 variability at 0.854, and so is inferred as the most important property in terms of soil runoff volume, and with a positive relationship increased MS relates to higher AD_{amc} runoff volumes.

MS, which is also shown to have a positive effect on FC_{amc} runoff TSL, is related to the concentration of iron bearing minerals (Dearing et al., 1999). SRE had the highest MS in the data set at 438.3 $m^3\ kg^{-1}$ and had the highest soil runoff volume and runoff TSL. The results infer that the iron chemistry is important in terms of aggregate^S stability. The literature suggests (Dearing et al., 1999) iron compounds have contrasting effects on soil erodibility, which is due to differences in the formation of the Fe (hydro)oxide, size of the Fe Oxide crystal, pH, ionic composition of the soil solution and the presence of organic molecules (Duiker et al., 2003). It is thought that iron compounds existing as discrete particles in the soil are having a dispersive rather than a flocculating effect on SRE, which is promoting the formation of smaller sized aggregates^S (Rhoton et al., 1998; Figueiredo et al, 1999). Aggregate^S size is an important factor that can alter soil hydraulic conductivity, and smaller aggregates have been linked to poor drainage in soils (Skidmore and Layton, 1992). Small aggregate^S size classes (<0.5 mm) are also associated with increased susceptibility to aggregate^S breakdown (Igwe and Nkemekosi, 2007). Studies in the Memphis catena, USA, found Fe oxide as the principal factor affecting aggregate^S stability when compared to organic carbon and clay, in a best fit model with water dispersible clay (Rhoton et al., 1998). Further research is required about the linkages between iron chemistry, aggregate^S size and erodibility, and as well MS as an indicator of soil iron chemistry.

Table 4.13. Soil runoff volume and runoff TSL MRA results

AD_{amc} Runoff Volume				FC_{amc} Runoff Volume			
Soils SFMs							
Significant SFM properties	Adjusted R^2	beta (β) coefficient	Standard Error	Significant SFM properties	Adjusted R^2	beta (β) coefficient	Standard Error
Magnetic Susceptibility	0.854	8.41	0.56	Coarse sand	0.767	353.3	38.2
DAD 53 - 63µm	0.968	-811.8	132.9	DAD 2.0 - 5.6mm	0.857	102.5	20.5
				DAD 5.6 - 19 mm	0.883	-84.8	25.9
				DAD 63 - 125 µm	0.903	-1162.5	150.04
				DAD125-150µm	0.988	2367.3	366.5
AD_{amc} Runoff TSL				**FC_{amc} Runoff TSL**			
Significant SFM properties	Adjusted R^2	beta (β) coefficient	Standard Error	Significant SFM properties	Adjusted R^2	beta (β) coefficient	Standard Error
Clay	0.842	-0.53	0.06	Coarse sand	0.724	0.30	0.11
DAD 53 - 63µm	0.934	-2.18	0.59	DAD 2.0 - 5.6mm	0.864	0.38	0.026
				DAD 0.5 - 1.0mm	0.926	0.96	0.10
				Maghemite	0.966	-0.77	0.11
				Exch-Na	0.976	-14.4	4.08
				Magnetic Susceptibility	0.989	0.0076	0.0027

Properties are significant predictors at $p<0.05$ as determined by Step-wise Multiple Linear Regression Analysis. The strength of correlated independent variables are listed in descending order, as calculated by the statistical model. Note: runoff volume is shaded in grey and runoff TSL in green for ease of reference.

MRA results revealed the following properties are significant in terms of FC_{amc} runoff volume generation ($p >0.05$) in the hierarchical order: Coarse sand (+β) > DAD 2.0-5.6 mm (+β) > DAD 5.6-19 mm (-β) > DAD 63-125 µm (-β) and DAD 125-150 µm (+β) (Table 4.13). These results infer that runoff generation is sensitive to aggregate^S size, as DAD 2.0-5.6 mm and 125-150 µm, with positive β coefficients, relate to increased surface runoff, and DAD 5.6-19 mm and 63-

125 µm with negative β coefficients relate to less surface runoff. Both the FC_{amc} runoff volume and runoff TSL results show coarse sand and DAD 2.0-5.6 mm at the top of the MRA output, contributing 0.857 and 0.864 of the observed adjusted R^2 variation respectively.

Studies of Mediterranean soils (Boix-Fayos et al., 2001) found a strong correlation between aggregates^S sized 2.0-5.0 mm, coarse sand (% w/w) and aggregate^S stability. Studies by Boix-Fayos et al. (2001) found large aggregates^S >2mm were associated with high amounts of water stable aggregates^S (WSA). This concurs with the 5.6-19 mm aggregate^S in these results. It is implied that medium sized aggregate^S 5.6-19 mm are most stable during rainfall, reducing runoff formation from surface sealing processes.

Both ALL and FER have double the amount of 5.6-19 mm aggregates^S at 25.6% and 20.8% than the other soils, and generated significantly low runoff TSLs and showed no change in runoff rates over time when compared to SRE and LITH. WSA assessments of acidic Nigerian soils, with a loamy to sandy clay texture, revealed significant variation (>42%) in the size fractions of WSA from soils from a similar geographic region. This study concluded that larger aggregates^S >0.5 mm were less erodible under high intensity tropical rainfall, because they were more resistant to slaking and sealing processes (Igwe and Nkemekosi, 2007). To discern whether aggregate^S size is a function of aggregate^S stability, further testing would be necessary.

MRA results for the four soil SFMs revealed the following properties are significantly related to AD_{amc} soil runoff TSL ($p > 0.05$); Clay (-β) > DAD 53-63 µm (-β), which combine to account for 0.934 of the adjusted R^2 variation in the data set (Table 4.13). Clay is of primary importance in terms of runoff TSL as it is listed first, and accounted for 0.842 of adjusted R^2; and a negative β coefficient implies increasing clay is associated with less runoff TSL.

Soils FER, LITH and ALL had significantly higher clay content compared to SRE, and were associated with significantly lower soil runoff TSL. The observed relationship between low soil TSL and clay content is expected as clay content has been shown to improve particle cohesion and aggregate^S stability, particularly in sandy soils, resulting in low erodibility (Landon, 1991; Rhoton et al., 1998).

DAD 53-63 µm is shown to have a negative effect on both runoff TSL and runoff volume at AD_{amc}. It may be that these small aggregates^S in a cohesive soil

matrix are more stable to disaggregation during rainfall, and hence high amounts will cause soils to have a more stable structure. Observations of tropical soils by El-Swaify and Dangler (1977; in Loch et al., 1998), found the amount of aggregates sized <0.25 mm correlated best with high erodibility. The findings in this study suggest the opposite to this, and instead, aggregates^{S} sized 53-63 µm are associated with being relatively stable, and the soil less erodible. However the results show the soils have between 0.23% and 1.84% 53-63 µm aggregates^{S}, and at such low amounts it is thought that this finding is based on an association in the aggregate^{S} size and runoff data, as opposed to a direct relationship.

The FC_{amc} MRA runoff TSL results indicate that coarse sand (+β) > DAD 2.0-5.6 mm (+β) > DAD 0.5-1 mm (+β) > maghemite (-β) > Exch-Na (-β) > MS (+β) combined account for 0.989 of the variability in adjusted R^2 (Table 4.13). Coarse sand listed first in the model, shows the highest change in adjusted R^2 at 0.724 and increasing amounts of coarse sand are associated with increasing runoff TSLs.

Coarse sand was the most important variable in both the FC_{amc} runoff volume and runoff TSL results. SRE generated significantly the highest soil runoff volume, and had significantly higher coarse sand amounts (18%) compared with the other soils. Aggregates^{S} comprising a high proportion of coarse sand tend to lack the cohesiveness associated with clay aggregates^{S} (White, 2006), and sands >0.02 mm tend not to be included in water stable aggregates^{S} (Loch and Rosewell, 1994), as coarse sand causes structural instabilities, making SRE more susceptible to disaggregation by raindrop impact than the other soils. Further aggregate stability testing of the soils would be necessary to assess the relationship with coarse sand.

4.5.3.2. Non-soil runoff volume and runoff TSL at AD_{amc} and FC_{amc}

MRA sought to relate AD_{amc} runoff volumes to the properties of the five non-soil SFMs. DAD 250-500 µm (+β) > DAD <53 µm (-β) > DAD 63-125 µm (+β) > pH (-β) > DAD 53-63 µm (+β) > coarse sand (+β) > MS (-β) (Table 4.14), combined accounted for 0.885 of the adjusted R^2 variation in AD_{amc} runoff volume. DAD 250-500 µm appeared first in the model and had the largest adjusted R^2 change at 0.392, inferring that as the proportion of aggregates sized 250-500 µm increases, runoff volume will increase.

Non-soil PHY-WEA had significantly higher runoff volume than all non-soils, and significantly high amounts of 250-500 µm aggregates[NS]. Studies by Kemper and Rosenau (1986) found surface aggregate[NS] size assemblage important in terms of runoff generation, and that small pores at the surface reduce infiltration. The MRA output also showed that the proportions of 250-500 µm, 53-63 µm and 63-125 µm aggregate[NS] have a positive effect on runoff volume. Higher amounts of small aggregates[NS] will lower surface porosity. These aggregates[NS] may also be more susceptible to entrainment by rain splash, and when re-deposited, block pores and cause a decline in infiltration leading to increased runoff.

Table 4.14. Non-soil runoff volume and runoff TSL MRA results

AD_{amc} Runoff Volume				**FC_{amc} Runoff Volume**			
Non-Soil SFMs							
Significant SFM properties	Adjusted R^2	beta (β) coefficient	Standard Error	Significant SFM properties	Adjusted R^2	beta (β) coefficient	Standard Error
DAD 250-500µm	0.392	874.4	162.3	Muscovite	0.866	90.9	15.5
DAD <53µm	0.402	-1439.8	200.7	Exch-Na	0.88	195867.8	71374.8
DAD 63-125µm	0.454	865.6	191.9				
pH	0.487	-20895.6	3407.7				
DAD 53-63µm	0.592	1337.3	311.9				
Coarse sand	0.746	355.9	83.3				
Magnetic Susceptibility	0.885	-131.8	43.01				
AD_{amc} Runoff TSL				**FC_{amc} Runoff TSL**			
Significant SFM properties	Adjusted R^2	beta (β) coefficient	Standard Error	Significant SFM properties	Adjusted R^2	beta (β) coefficient	Standard Error
Kaolinite	0.859	4.36	0.35	Muscovite	0.849	10.78	3.841
Exch-Mg	0.897	-78.3	13.2	Exch-Na	0.868	8142.9	1700.8
DAD 125-150µm	0.989	-1.98	0.41	DAD 250-500µm	0.897	11.8	4.15
Coarse sand	0.969	0.57	0.20	DAD <53µm	0.924	-10.6	3.58

Properties are significant predictors at $p<0.05$ as determined by Step-wise Multiple Linear Regression Analysis. The strength of correlated independent variables are listed in descending order, as calculated by the statistical model. Note: runoff volume is shaded in grey and runoff TSL in green for ease of reference.

MRA using the dependent FC_{amc} runoff volume data of non-soils revealed Muscovite (+β) > Exch-Na (+β) (Table 4.14), combined account for 0.880 of the adjusted R^2 variation. Muscovite has the largest adjusted R^2 change at 0.806 and appears first in the hierarchical model and is also listed in the FC_{amc} runoff TSL and leachate TSL results (Table 4.16). PHY-WEA was the only non-soil to have significant amounts of muscovite (50.8% w/w), and had the highest FC_{amc} runoff volume and runoff TSL. Key properties thought to affect the erodibility of the weathered Phyllite PHY-WEA is low cohesion among separate muscovite sheets, and also that it is associated with higher susceptibility to raindrop impact stresses because it has been exposed to weathering processes (Price, 1985; Butcher et al., 1992; Price, 2009). Muscovite is known to be a very soft mineral with a Mohs hardness of 2.5, and it readily splits into thin flexible sheets with perfect basal cleavage (Roberts, 2004). The flat sheet-like silicate shape of muscovite minerals (Price, 2009) is thought to be more conducive to plugging surface pores and also why PHY-WEA is subject to high runoff volumes.

Geological studies discuss the longer term breakdown of muscovite minerals by dispersion weathering processes (Essington, 2004; Vacher et al., 2004), with reference to non-disturbed (*in-situ*) materials (Price, 2009); but less is known about the effects of raindrop impact during a single rainfall event. Furthermore, less is known about susceptibility of weathered phyllites, particularly those excavated by mining processes, to rainfall erosion, either chemically or physically. There are many types of phyllites and a detailed assessment that compared mineralogy and erodibility would uncover the relationship between muscovite and erodibility under rainfall. Short term changes to muscovite based SFMs are more relevant to mine-site erosion control, which highlights the importance of future studies in this area.

MRA using the AD_{amc} Runoff TSL results revealed that kaolinite (+β) > Exch-Mg (-β) > DAD 125-150 µm (-β) > coarse sand (+β) combined to account for 0.969 of adjusted R^2 variation (Table 4.14). The MRA showed kaolinite appeared first in the hierarchical model, accounts for 0.859 of adjusted R^2 and is associated with increasing runoff TSL at AD_{amc}. Kaolinite is also shown to be an important factor in the FC_{amc} leachate TSL results (Table 4.16).

PHY-WEA generated significantly high runoff TSLs and has the highest kaolinite amount at 19.2% (w/w). Clay minerals are effective retaining positive cations, and so clay particles are often associated with greater stability (Ehansani and Sullivan, 2010). However, this will depend on the SFM's other

chemical properties (White, 2006). PHY-WEA has 50.8% (w/w) muscovite, which has been discussed as having low cohesive properties; further PHY-WEA has a low CEC at just 2.43 meq 100 g^{-1}. Smith et al. (1995) suggests mine spoil materials can be categorised by their level of cohesion, and more cohesive materials usually have a higher percentage of clay. These results infer that there are weak attractive forces between muscovite and kaolinite clays, which results in PHY-WEA being more susceptible to breakdown under rainfall.

The presence of kaolinite clay is thought to be an important factor in why PHY-WEA's high erodibility is distinct compared to the other non-soils. PHY-WEA's is thought to behave like a soil, and aggregates^{NS} of muscovite and kaolinite experience dispersion during rainfall, which leads to a supply of disaggregated materials and surface sealing processes. At FC_{amc} PHY-WEA has significantly higher leachate and runoff TSL, as compared with other non-soil SFMs inferring that increasing moisture is making it more susceptible to aggregate^{NS} breakdown.

MRA using the FC_{amc} non-soil runoff TSL results revealed muscovite (+β) > Exch-Na (+β) > DAD 250-500 µm (+β) > DAD <53 µm (-β) combined account for 0.924 of the adjusted R^2 variation (Table 4.14). DAD <53 µm has a negative association with both AD_{amc} runoff volume and FC_{amc} runoff TSL and positive association with AD_{amc} leachate volume. Aggregates^{NS} <53 µm are presumed to be primary particles because of their silt/clay size, and are significantly higher in non-soils RD and HGF at 5.28% and 10.3%, respectively, which were both associated with significantly lower runoff TSLs of 0.5 g and 2.86 g respectively. It is postulated that fine <53 µm material is readily entrained by surface runoff. However, in SFMs with high surface porosity, <53 µm sized material is disturbed by rainfall impact at the surface and transported by leachate through surface voids. Therefore the fine <53 µm sized aggregates adds to the leachate TSL and not the runoff TSL.

4.5.3.3. Soil leachate volume and leachate TSL at AD_{amc} and FC_{amc}

MRA revealed the following properties of the soil SFMs were significantly related to AD_{amc} leachate volume ($p>0.05$); organic carbon (+β) > DAD 5.6-19 mm (+β) > coarse sand (-β) > clay (+β) > bulk density (-β) (Table 4.15). The results infer that soil organic carbon content is important in terms of soil leachate volumes, as this variable accounts for 0.862 of the adjusted R^2

variability. With a positive β coefficient it is inferred that increasing organic carbon is associated with increasing leachate volume.

Evans (1980; in Morgan, 2006) suggests that soils with <2% organic carbon are more erodible than soils with >2% organic carbon. Studies by Boix-Fayos et al. (2001) found stable aggregates^S showed positive correlations with clay amounts when organic matter was >6%. Voroney et al. (1981; in Morgan, 2006) also report declining soil erodibility with increasing organic matter content (0-10%). SRE does not confer as it has the highest soil organic carbon at 10.35%; but significantly the lowest leachate volume. Different types of organic matter may cause differences in aggregate^S stability (Chenu et al., 2000; Morgan, 2006). Studies of French soils (Chenu et al., 2000) found organic matter created hydrophobic conditions that restricted infiltration. To determine more reliably the effects of organic carbon amounts on soil erodibility, further testing would be necessary.

The MRA results show that $FC_{amc,}$ leachate volume was significantly related with fine sand (+β) > Exch-Ca (-β) (see Table 4.15). Fine sand is of particular importance as it appears first in the model, accounts for 0.886 of adjusted R^2 variation and increasing amounts of fine sand are associated with increasing leachate volumes. Soils ALL and FER showed significantly higher leachate volumes at FC_{amc} compared with LITH and SRE, and contained significantly higher fine sand amounts at 13.6% and 11.6% (w/w) than the other soils. Un-expectantly coarse sand (2.0-0.63 mm) was associated with increasing soil runoff volumes and runoff TSLs, and was linked to reduced aggregate^S cohesion and stability (White, 2006). Fine sand sized particles (0.212–0.063 mm) may have a positive effect on aggregate^S cohesion and stability, resulting in higher infiltration during rainfall, as inferred by the high leachate volumes and low runoff TSLs recorded for ALL and FER.

Table 4.15. Soil leachate volume and leachate TSL MRA results

AD_{amc} Leachate Volume				FC_{amc} Leachate volume			
Soils SFMs							
Significant SFM properties	Adjusted R^2	beta (β) coefficient	Standard Error	Significant SFM properties	Adjusted R^2	beta (β) coefficient	Standard Error
Organic carbon	0.862	646.3	218.1	Fine sand	0.886	722.5	153.4
DAD 5.6-19mm	0.865	279.9	63.5	Exch-Ca	0.914	-458.	187.7
Coarse sand	0.870	-178.7	81.5				
Clay	0.884	355.6	68.2				
Bulk density	0.953	-21.2	4.90				
AD_{amc} Leachate TSL				FC_{amc} Leachate TSL			
Significant SFM properties	Adjusted R^2	beta (β) coefficient	Standard Error	Significant SFM properties	Adjusted R^2	beta (β) coefficient	Standard Error
DAD >37.5mm	0.580	-0.25	0.04	DAD 2.0 - 5.6mm	0.178	-0.12	0.02
Bulk density	0.616	0.01	0.00	Exch-Ca	0.554	-0.37	0.06
DAD 1-2mm	0.631	-0.30	0.05	Clay	0.699	-0.14	0.04
Exch-Ca	0.693	0.07	0.03	pH	0.728	4.38	1.33
Organic carbon	0.735	0.43	0.09	Bulk density	0.858	0.02	0.01
Magnetic Susceptibility	0.924	0.01	0.00				

Properties are significant predictors at $p<0.05$ as determined by Step-wise Multiple Linear Regression Analysis. The strength of correlated independent variables is listed in descending order, as calculated by the statistical model. Note: leachate volume is shaded in grey and leachate TSL in green for ease of reference.

MRA revealed that at AD_{amc} DAD >37.5 mm (-β) > bulk density (+β) > DAD 1-2 mm (-β) > Exch-Ca (+β) > organic carbon (+β) > MS (+β), were significantly correlated to soil leachate TSL and when combined, account for 0.924 of the adjusted R^2 variability (Table 4.15). The results infer DAD >37.5 mm is of primary importance, as this appears first in the model, and accounts for the

largest difference in the adjusted R^2 (0.580) and is associated with decreasing leachate TSLs.

SRE had significantly higher DAD >37.5 mm of all the soils (9.8%). The DAD methodology adopted in this study for both soil and non-soil SFMs does not discriminate between stones and large aggregates^S. For future studies, it is recommended that the two are categorised separately. Observations of SRE showed it had a high stone content. SRE also had a high proportion of large aggregates^S in the DAD results with 9.81% w/w >37.5 mm (Table 4.4). A high stone content can increase porosity and leachate occurrence (White, 2006). However, SRE generated significantly less leachate volume than the other soils. Poesen et al. (1994) surmises that the effect of rock fragments will depend on the scale of erosion processes which are taking place. This process/spatial scale interaction determines whether the stones are having an increasing or decreasing effect on infiltration and runoff. Joma et al. (2012) found that erosion and runoff rates were proportional to the soil area exposed to rainfall, where stones increased the area of impermeable surface. It is hypothesised that a large surface area of stones at and/or just below the surface restricts infiltration, reduces leachate occurrence and also minimises the availability of detachable material, thus causing differences in leachate TSL.

MRA results for FC_{amc} leachate TSL revealed; DAD 2.0-5.6 mm (-β) > Exch-Ca (-β) > clay (-β) > pH (+β) > bulk density (+β) (Table 4.15) combined account for 0.858 of the adjusted R^2 variation. Exch-Ca shows the largest step change in adjusted R^2 from 0.178 to 0.554 and is correlated with increasing FC_{amc} soil leachate TSL. Exch-Ca is a cementing agent (Morgan, 2006) and as such has a positive effect on aggregate^S stability (Donsova and Norton, 2002). Increasing Exch-Ca is associated with increasing soil leachate TSL at $AD_{amc,}$ but decreasing soil leachate TSL at FC_{amc}. It is thought that differences in moisture conditions change the relationship of Exch-Ca and aggregate^S stability.

At AD_{amc}, there is greater ionic potential because the polarising effects of the Ca cations on clay anions are concentrated on fewer water molecules, so the potential for the cation to disassociate is increased. As soil water increases at $FC_{amc,}$ organic matter and minerals in the soil disassociate, creating more competition for clay exchange sites (Phillips and Greenway, 1998; White, 2006). It is thought that as antecedent moisture content shifts from AD_{amc} to FC_{amc} there is a point that defines when maximum Ca ions are absorbed by the kaolinite clays, and Ca begins to contribute to aggregate^S stability (Phillips and

Greenway, 1998; White, 2006). The amount of water retained by clays depends on clay mineralogy, organic matter chemistry and pH (White, 2006).

Igwe et al. (1999; in Igwe and Nkemakosi, 2007) found that exchangeable Ca and Mg had no effect on the stability of tested Nigerian soils. Later studies showed that Ca^{2+} cations in the clay fraction correlated negatively with a clay flocculation index, indicating that increasing Ca^{2+} was making the soil more susceptible to dispersion (Igwe and Nkemakosi, 2007). These findings were supported by observations of similarly weathered soils from Brazil (Roth and Oaran, 1991; in Igwe and Nkemakosi, 2007). It would seem that the current understanding about Exch-Ca promoting aggregation may not apply to weathered tropical soils, and mineralogy and moisture conditions will affect this relationship (Igwe and Nkmakosi, 2007). Future research on changing soil moisture and its electrostatic relationship with soil exchangeable cations and aggregate^{S} stability would explore the mechanisms operating between these properties.

4.5.3.4. Non-soil leachate volume and leachate TSL at AD_{amc} and FC_{amc}

MRA revealed that at AD_{amc} the following properties were significantly related to leachate volume; DAD 2.0-5.6 mm (+β) > DAD <53 µm (+β) > pH (+β) > DAD 53-63 µm (-β) > Quartz (-β) > Exch-Ca (-β) > MS (+β) (Table 4.16). DAD 2.0-5. 6mm is of particular importance as this variable accounts for 0.607 of the variability in adjusted R^2, inferring that increasing amounts of aggregates^{NS} 2.0-5.6 mm is associated with increasing non-soil leachate volume.

DAD 2.0-5.6 mm aggregates^{NS} are considered important for leachate generation as their prevalence and arrangement will affect surface permeability. RD and COMB-WEA had significantly the highest amounts of DAD 2.0-5.6 mm aggregates at 19.9% and 17.7%, and significantly high AD_{amc} leachate volume. Hydrological behaviour will largely be controlled by the connectivity between coarser material fragments, and the amounts and mobility of smaller aggregates^{NS} and primary particles (Smith et al., 1995; Hawkins, 1998; Fala et al., 2003), which block pores. Increasing the amount of coarse materials as represented by the PSD and DAD results, can increase hydraulic conductivity up to the point when the coarse particles start to join and porosity is reduced (Smith et al., 1995).

Smaller DAD 53-63 µm aggregates[NS] have a negative association with leachate volume. It is thought that these smaller aggregates are more readily entrained by raindrop impact and surface water, plugging small voids at the surface. Erosion studies by Curran et al. (2002) on coal stock piles discussed how coal does not concur with Darcy's (1865; in Curran et al., 2002) soil infiltration flow properties where water is transmitted through pore spaces. This is because water in coal spoil moves preferentially through large pore spaces created by the large pieces of coal.

It is inferred that the 'exact' aggregate[NS] size class assemblage at the surface is not primarily important; but rather the ratio of smaller to larger aggregate[NS] that determines the hydrological response of the non-soils to rainfall. The heterogeneous nature of the non-soil SFMs has been discussed (Section 4.5.2). In further studies, an assessment of surface porosity change between rain events would facilitate a better understanding of which aggregate[NS] size-class combinations favour high and low porosity and hence control SFM hydrological response.

The FC_{amc} leachate volume MRA results (Table 4.16) revealed the following properties are significantly important; muscovite (-β) > DAD 5.6-19.0 mm (+β) > DAD 63-125 µm (-β) > pH (+β) > 37.5 mm (+β) > silt (+β). Muscovite was listed first in the running order of the model and has 0.849 of the variability in adjusted R^2. Muscovite was also found important in the FC_{amc} runoff volume and runoff TSL results. These results imply that increasing muscovite content is associated with increasing non-soil runoff volume and decreasing leachate volume at FC_{amc}.

Aggregate[NS] sizes including DAD 5.6-19 mm, DAD 63-125 µm and DAD >37.5 mm are also important properties in FC_{amc} leachate volume. These results mirror the findings of the AD_{amc} leachate volume results. Larger aggregate[NS] size classes 5.6-19 mm and >37.5 mm are shown to have a positive effect on leachate volume, as they allow for the free movement of comparably large volumes of rainfall between the larger inter-rock voids. Small aggregates[NS] sized 63-125 µm have a negative association with leachate volume, as they are more mobile during rainfall, plugging surface voids and deterring leachate formation.

Table 4.16. Non-soil leachate volume and leachate TSL MRA results

AD_{amc} leachate volume				FC_{amc} leachate volume			
Non-Soils SFM							
Significant SFM properties	Adjusted R^2	beta (β) coefficient	Standard Error	Significant SFM properties	Adjusted R^2	beta (β) coefficient	Standard Error
DAD 2.0-5.6mm	0.607	317.0	56.8	Muscovite	0.849	-1.64	0.60
DAD <53µm	0.672	599.9	77.6	DAD 5.6-19mm	0.680	3.16	0.42
pH	0.703	5184.7	873.4	DAD 63-125µm	0.889	-4.84	0.75
DAD 53-63µm	0.735	-1196.3	269.1	pH	0.934	48.61	8.35
Quartz	0.785	-330.5	134.3	DAD >37.5mm	0.938	0.77	0.22
Exch-Ca	0.843	-415.3	94.1	Silt	0.978	1.80	0.67
Magnetic susceptibility	0.927	64.1	20.1				
AD_{amc} leachate TSL				FC_{amc} leachate TSL			
Significant SFM properties	Adjusted R^2	beta (β) coefficient	Standard Error	Significant SFM properties	Adjusted R^2	beta (β) coefficient	Standard Error
Coarse sand	0.409	0.86	0.10	Silt	0.154	2.18	0.51
Quartz	0.494	-1.30	0.15	Exch-Na	0.271	-2287.3	557.8
pH	0.546	20.08	2.03	Kaolinite	0.503	-6.61	1.73
Rutile	0.609	-75.4	9.42	DAD 53-63µm	0.698	-0.86	0.12
Exch-Ca	0.624	0.86	0.14	Coarse sand	0.732	8.28	3.33
Organic Carbon	0.739	-18.4	2.55				
DAD 125-150µm	0.798	-0.54	0.09				
Clay	0.954	0.47	0.09				

Properties are significant predictors at $p<0.05$ as determined by Step-wise Multiple Linear Regression Analysis. The strength of correlated independent variables are listed in descending order, as calculated by the statistical model. Note: leachate volume is shaded in grey and leachate TSL in green for ease of reference.

The MRA indicated the following non-soil properties were significantly ($p>0.05$) related to AD_{amc} leachate TSL namely, coarse sand (+β) > Quartz (-β) > pH (+β)

> Rutile (-β) > Exch-Ca (+β) > organic carbon (-β) > DAD 125-150 µm (-β) > Clay (+β) (Table 4.16). Coarse sand appears first in the model, and accounts for the highest change in adjusted R^2 at 0.409. Coarse sand is also associated with increasing leachate TSL in the FC_{amc} non-soil leachate TSL results.

The coarse sand sized fraction was significantly high in all the non-soils, except PHY-WEA with amounts ranging from 16-37%; at-least double that of soils ALL, FER and LITH. The highest AD_{amc} leachate TSL was associated with non-soils RD, NEW-WEA and COMB-WEA. Leached sediment load could be sourced from low cohesive material such as primary particles of coarse sand within the profile (Smith et al., 1995), or entrained at the surface and transported through surface voids in highly porous RD, NEW-WEA and COMB-WEA (Imaehsoar et al., 2012).

Finally, at FC_{amc}, the non-soil MRA results infer that leachate TSL is associated with silt (+β) > Exch-Na (-β) > kaolinite (-β) > DAD 53-63 µm (-β) > coarse sand (+β) (Table 4.16). Silt is of particular importance as this property was listed first in the model where it is inferred that increasing the proportion of silt sized material results in increasing leachate TSL at FC_{amc}.

It is postulated that a high proportion of silt sized material >65% is readily entrained by both leachate and runoff and is causing high TSLs. PHY-WEA had significantly the highest content of silt sized particles and generated half the volume of leachate (3066ml) compared to runoff (6238ml) at FC_{amc}, but still generated the highest leachate TSLs at 19.1 g.

Preferential leaching pathways have been observed in mine waste materials having textures dominated by silt and fine sand (Tran, 2003; in McLemore et al., 2009). Mine waste materials high in silt (>70%) have been associated with tunnelling processes by liquefaction; because silt dominated SFMs have weak inter-particle bonds that are easily destroyed by flowing water (Vacher et al., 2004). Observations of PHY-WEA mid-rainfall showed the surface with shallow terrace formations 2-3 cm in elevation leaving a consolidated armoured surface. These features are thought to be caused by the immediate surface becoming compact and sealed, with continuing rainfall causing stress fractures at the surface, which eventually fault leading to the removal of large sections of the surface at a given time, as illustrated in Figure 4.18.

The PHY-WEA results have shown that differences between soils and non-soil SFMs are not straightforward. Saprolite soils are common to tropical regions and identified as being derived from *in situ* rock weathering where the original

rock, texture, fabric and structure is retained (Massey and Pang, 1988; in Gan and Fredlund, 1996). Graham et al. (2010) discusses the transition of hard rock to soil, and identifies the regolith stage as the transition between the two. PHY-WEA's has chemical and physical properties of a non-soil, but its hydrological behaviour is found to be comparable to soil SRE. PHY-WEA is also found to undergo aggregate breakdown processes, like a soil, because of its kaolinite clay and muscovite mineralogy. PHY-WEA is evidence that a comprehensive assessment of a SFM's response to rainfall, be it a soil or non-soil, is necessary in order to assess its erodibility risk during rainfall.

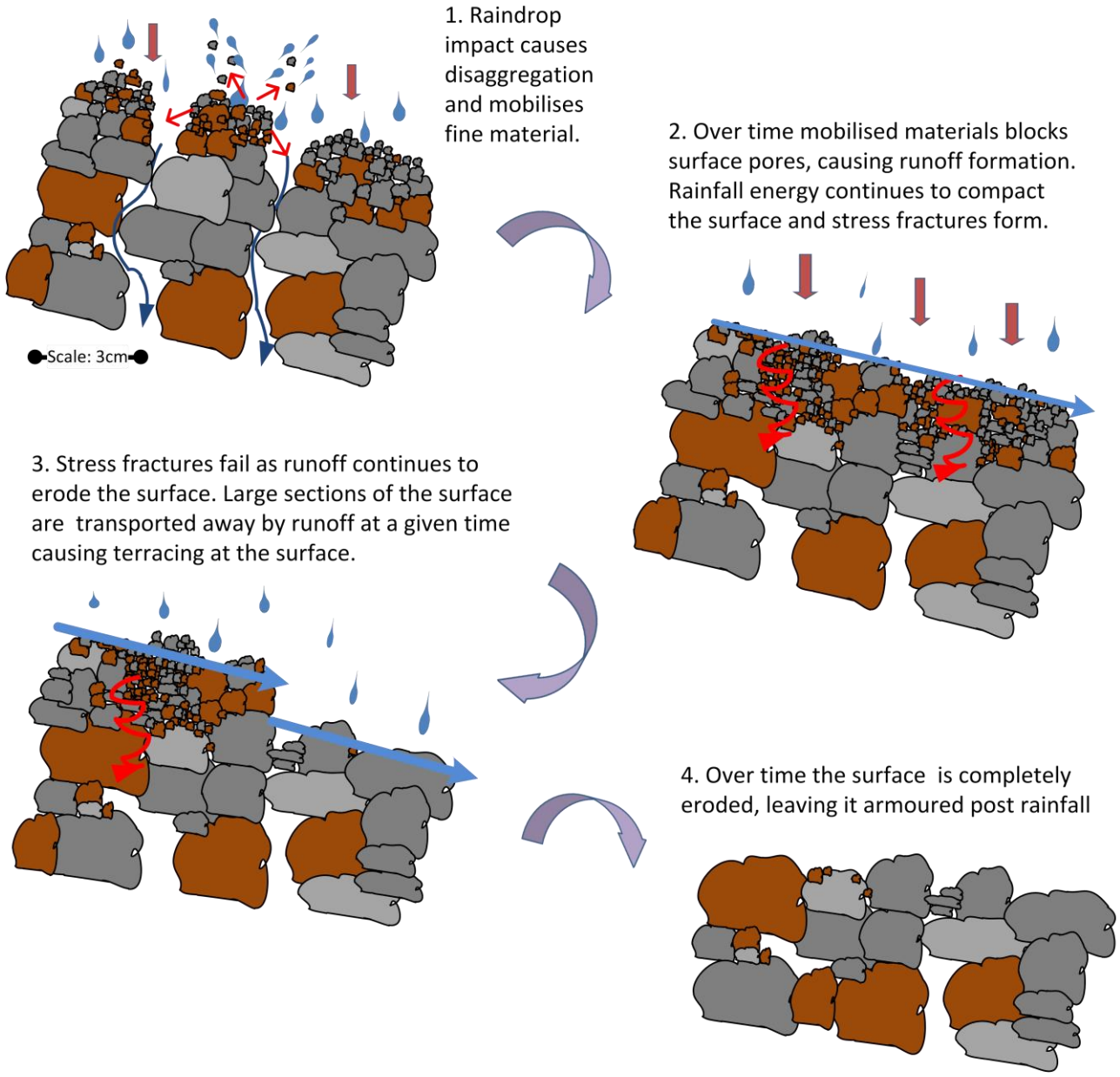

Figure 4.18. The hydraulic response of non-soil PHY-WEA to rainfall *(Source: Author, 2012).*

4.6 Conclusions to Phase I results

The Phase I results have shown that the soil and non-soil SFMs are primarily different in their physical and chemical properties. Soil SFMs were associated with significantly higher clay, CEC and organic carbon values, and significantly lower bulk density compared to the non-soil SFMs.

Changing antecedent moisture conditions had different effects on runoff, leachate and erosion for different SFMs. Runoff volume and runoff rates were significantly higher for SRE and PHY-WEA at field capacity antecedent moisture conditions as compared to air dry, and PHY-WEA also had significantly higher runoff TSLs. Leachate volumes were significantly higher for ALL, FER, HGF and HRS, and leachate TSLs were significantly higher for HGF, HRS and PHY-WEA under field capacity. These results highlight the additional risk of increased runoff, leachate and erosion in Guinea during the rainy season. In contrast, the haul road sample (HRS) was associated with significantly lower runoff and lower runoff TSL at field capacity compared to air-dry antecedent moisture conditions.

Despite commonalities in how soils and non-soils responded to rainfall, the processes that govern this response are, with the exception of PHY-WEA, primarily different for soils and non-soil SFMs. The ability of soils to generate leachate or runoff volume is affected by erodibility during rainfall, and the extent of surface sealing processes. The MRA soil results showed small 53-63 µm and larger 5.6-19 mm DAD^S promotes high drainage, but medium sized 2.0-5.6 mm $aggregates^S$ do not. MS, clay, organic carbon, coarse and fine sand were all important in the soil hydrological response to rainfall. SRE is 39 times more erodible by runoff than the next soil SFM at field capacity antecedent moisture conditions. MRA found these results were associated with SRE's significantly high coarse sand particle size fraction, high organic carbon content and iron chemistry implied by its significantly high magnetic susceptibility.

Non-soil runoff and leachate generation is affected by the ratio of small (53-63 µm, 63-125 µm and 250-500 µm) to large >37.5 mm aggregates/stones, which determines surface porosity and plugging of pores and surface sealing processes. The ultra-fine <53 µm aggregates are easily transported into large voids by any flow, so also reducing runoff formation. Further studies should distinguish between stones and aggregates, as this could be an important factor for porosity assessments.

Non-soil mineralogy is important in whether primary particles withstand the stresses of raindrop impact. The non-soils have a textural makeup consisting

mainly of hematite and goethite of different sized fractions. Highly erodible PHY-WEA has a PSD dominated by the silt size fraction, and distinctly different mineralogy when compared with the other non-soils. With higher clay content than the other non-soils, PHY-WEA has aggregates formed from muscovite minerals bound by clay, which makes aggregates susceptible to aggregate breakdown and surface sealing processes during rainfall in the same way as erodible soil behaves. PHY-WEA generated the highest runoff volume, runoff TSL and leachate TSLs recorded. PHY-WEA is 57 times more erodible than the next most erodible non-soil SFM by runoff, and 2.5 times by leachate at FC_{amc}. Maximum PHY-WEA runoff TSLs were recorded at FC_{amc} with 165 g of sediment equating to TSC of 26.2 g l^{-1}, which are well in excess of the mine water quality target of <0.05 g l^{-1} (Lucas Kitchen, Personal Communication, 26th November 2010). These results highlight the need to prioritise PHY-WEA for erosion control; and so PHY-WEA will be taken into Phase II of this study.

These results have shown DAD, mineralogy and MS, properties not commonly assessed in erosion studies, are important in determining SFM erodibility. More research is needed about how these variables affect rainfall erosion processes.

The Phase I results show that for some SFMs, leachate volumes and leachate TSLs were significantly higher than those associated with runoff. This highlights the importance to undertake a comprehensive assessment of SFM erodibility on a mine-site. A SFM classification system that recognises differences in the SFMs response to rainfall will improve water and sediment management in the mining sector, and help identify management solutions that target leachate and/or runoff processes. High variability in the SFM response to rainfall has made it necessary to investigate whether three test replicates is sufficient to detect statistical differences in the data, and this will be taken into account in the experimental design of Phase II.

Chapter 5. Phase II results and discussion: polymer-based treatments to control SFM runoff, leachate and erosion

5.1 Introduction

Polymer Based Treatments (PBTs) including polyacrylamides (PAMs) and polyvinylacrylic latex (PVALs) have been recognised as effective erosion control solutions, because they mitigate erosion at source (Zejun et al., 2002; Vacher et al., 2003; Martínez-Rodríguez et al., 2007; Lee, 2009). In addition, they can potentially provide 'temporary' erosion control during on-going operations where the mined landscape is continuously changing (Kennedy, 1990; Sojka et al., 2007). They are considered cost effective when compared to Class-A Type-1 erosion mats (Nwankwo, 2001; Sojka et al., 2007). As discussed in Chapter 3 (Section 3.3.1) three commercially available PBTs were selected for testing, namely Siltstop® APS 705 powder (PAM), Siltstop® APS 605 emulsion (PAM) and Soilfloc® DC90 liquid (PVAL). There is limited literature (Mahardhika et al., 2008) concerning the effectiveness of PBTs on mine SFMs, and specifically no research on the effectiveness of these products on the SFMs used in this study.

Four SFMs were selected in order to critically assess the efficacy of the selected PBTs in modifying the erodibility and hydrological response of the selected SFMs. The selected SFMs are:

- Haul Road Sample (HRS),
- Transitional Material (TRN; formerly known as HGF),
- Very Weak Weathered Phyllite (PHV; formerly known as PHY-WEA), and
- Lithosol (LITH).

During the course of this research, and as a result of continued exploration on site, Rio Tinto changed the nomenclature of PHY-WEA and HGF to PHV and TRN, respectively, based on a more detailed understanding of their physio-chemical characteristics (Lucas Kitchen, Personal Communication, 3rd December 2012). All four SFMs were imported in two separate batches for experimental Phase I and Phase II. One-way ANOVA post-hoc Fisher LSD analysis (Appendix G (Tables 1-4)) demonstrated that the SFMs used in Phase I and Phase II are from the same respective populations.

The SFMs are characterised in Table 5.1 and Table 5.2. PHV (formerly known as PHY-WEA) and HRS were chosen because they were the most erodible SFMs from Phase I (Chapter 4; Section 4.3 and 4.4) and were also associated

with high runoff volumes. TRN (formerly known as HGF) was chosen because it was associated with high leachate volume and leachate TSL in Phase I. A review of the literature demonstrates that there are more studies regarding the use of PBTs particularly PAMs on soil SFMs than on non-soil SFMs. Therefore, LITH was chosen to compare the erodibility and hydrological response of a soil SFM as opposed to the three selected non-soil SFMs.

It was important to represent field conditions as accurately as possible, and so the SFMs were air dried and thoroughly mixed (see methodology Section 3.3.2), so that they represented the inherent variability of the different materials when on-site, where they would have heterogeneous aggregate sizes.

Table 5.1. Physical and chemical characteristics of SFMs used in Phase II

Characterisation Parameter	Slope Forming Material			
	HRS	**LITH**	**PHV**	**TRN**
Type of SFM	Non-soil	Soil	Non-soil	Non-soil
pH	6.0_b	4.73_a	5.1_a	6.43_b
Coarse sand (% w/w)	26.0_a	11.3_c	4.0_b	25.7_a
Medium Sand (% w/w)	16.7_c	7.67_b	3.33_a	26.0_d
Fine Sand (% w/w)	16.0_b	6.67_a	5.0_a	35.3_c
Silt (% w/w)	25.3_b	28.7_c	70.3_d	9.3_a
Clay (% w/w)	16.0_a	45.7_c	17.3_a	3.67_b
Bulk Density (Mg m^3)	2.0_b	1.15_a	1.1_a	2.29_c
Electrical Conductivity (μS cm^{-1})	1380.0_b	1330.0_a	1810.0_c	1876.7_d
Exch-Ca (meq 100g)	1.8_a	15.1_c	1.8_a	0.10_b
Exch-K (meq 100g)	0.11_a	0.22_b	0.15_a	0.10_a
Exch-Mg (meq 100g)	0.05_b	0.27_c	0.01_a	0.01_a
Exch-Na (meq100g)	0.001_a	0.01_b	0.001_a	0.001_a
CEC (meq 100g)	2.53_a	17.7_c	1.83_a	0.001_b
Organic Carbon (% w/w)	0.60_a	3.9_c	0.57_a	0.1_b

For a given parameter values between columns, not followed by the same letter, are significantly different at $p<0.05$ as determined by One-Way ANOVA post-hoc Fisher LSD analysis (n=3).

Table 5.2. Mineralogy of SFMs used in Phase II

Mineralogy Composition of Test Materials (%w/w)											
SFM	Quartz	Plagioclase	K-Feldspar	Hematite	Goethite	Magnetite	Gibbsite	Muscovite	2:1 Clays	Kaolinite	Halloysite
HRS	1.5	0.2	0.5	52.0	33.1	0.8	9.8	0.0	1.9	0.3	0.0
LITH	21.2	0.9	1.5	18.9	27.3	2.2	6.2	0.0	10.1	7.5	4.3
PHV	7.7	0.2	0.0	14.9	4.8	0.2	5.2	36.9	2.5	27.6	0.0
TRN	0.7	0.0	0.0	67.9	24.3	4.8	2.3	0.0	0.0	0.0	0.0

Note only single mineralogical results was obtained for each SFM and so could not be statistically analysed for variance. The XRPD method used has been extensively validated (Omotoso et al., 2006) and mineralogical composition of the same SFM is very likely to give identical XRD patters (Stephen Hillier, *Personal Communication*, 31st January 2012).

PBT efficacy was assessed in terms of runoff volume (ml), runoff TSL (g), leachate volume (ml) and leachate TSL (g) under the design storm of 100 mm hr^{-1} for 30 min duration as adopted in Phase I. Polymer effectiveness was assessed using three different PBTs at two different application rates, with and without the addition of gypsum (as detailed in the methodology Table 3.6, Section 3.3.1). The fourteen treatment codes are listed in Table 5.3. The results for each of the four SFMs are discussed in turn starting with HRS, then LITH, PHV and subsequently TRN.

The following hypotheses were formulated to test the effectiveness of PBTs in terms of erodibility and hydrological response of the four different SFMs:

1. PBTs will have a significant effect on key indicators of the erodibility and hydrological response of selected SFMs, namely runoff volume, runoff total sediment load (TSL), leachate volume and leachate TSL.

2. There is a negative relationship between PBT application rate and rate of erosion.

3. For the selected SFMs, the addition of gypsum will enhance the efficacy of the PBTs.

4. For the selected SFMs, the greatest decline in surface roughness after rainfall will be associated with the untreated control.

Surface Roughness (SR) and 3D Surface Area (SA) describe the elevation variability of a topographic surface at a given scale (Grohmann et al., 2009). These parameters are directly linked to the severity of erosion processes (Bergsma and Farshad, 2007). As stated in Section 2.6, these parameters have been adopted here as a means of quantifying and understanding the effectiveness of PBTs at a sub-process level. SR and SA (m^3) data derived using NSPASS are used to better understand how the different PBTs work (or not) in controlling runoff, leachate and erosion on the different types of SFM.

Table 5.3. Treatments evaluated in experimental Phase II

Treatment Code	Polymer Product	PBT Type	Application Rate	Gypsum Addition
Control	No product	n/a	n/a	No
$Control_{GYP}$	No product	n/a	n/a	Yes
DC_L	Dc90	PVAL	Low	No
DC_L_{GYP}	Dc90	PVAL	Low	Yes
DC_H	Dc90	PVAL	High	No
DC_H_{GYP}	Dc90	PVAL	High	Yes
SS6_L	Siltstop 605 emulsion	Anionic PAM	Low	No
$SS6\_L_{GYP}$	Siltstop 605 emulsion	Anionic PAM	Low	Yes
SS6_H	Siltstop 605 emulsion	Anionic PAM	High	No
$SS6\_H_{GYP}$	Siltstop 605 emulsion	Anionic PAM	High	Yes
SS7_L	Siltstop 705 powder	Anionic PAM	Low	No
$SS7\_L_{GYP}$	Siltstop 705 powder	Anionic PAM	Low	Yes
SS7_H	Siltstop 705 powder	Anionic PAM	High	No
$SS7\_H_{GYP}$	Siltstop 705 powder	Anionic PAM	High	Yes

5.2 Effects of PBTs on the erodibility and hydrological response of HRS

One Way ANOVA post-hoc Fisher LSD (Table 5.4) demonstrates that none of the PBTs reduced mean runoff volume or runoff TSL significantly as compared with the untreated control. However, DC_L and DC_H generated significantly lower runoff volumes (32 ml and 54 ml, respectively) when compared to SS7_H (241 ml), $SS7\_H_{GYP}$ (278 ml) and SS6_H (342 ml). Figure 5.2 illustrates higher mean runoff TSL is associated with $Control_{GYP}$ (0.73 g), DC_H_{GYP} (0.32g) and SS6_H (0.50g) as compared with the untreated control (0.18 g).

$SS7\_H_{GYP}$ (538 ml) and SS6_H (606 ml) generated significantly less mean leachate volume as compared with the untreated Control (913 ml). DC_L and DC_H_{GYP} show comparatively lower variability in leachate volume than all other treatments (Figure 5.3 and Table 5.4).

SS7_L (0.37 g) and SS6_H (0.32 g) generated significantly less leachate TSL than the untreated Control (0.76 g). In contrast, four treatments (DC_L_{GYP}; DC_H_{GYP}; $SS6\_L_{GYP}$; and $SS6\_H_{GYP}$ g) had significantly higher leachate TSL

than the Control. Figure 5.4 shows SS7_L and SS7_H with comparatively lower variability in leachate TSL as compared with all other treatments.

Table 5.4. HRS: Effect of PBTs on runoff volume, runoff TSL, leachate volume and leachate TSL

HRS				
Treatment	**Runoff Volume (ml)**	**Runoff TSL (g)***	**Leachate Volume (ml)**	**Leachate TSL (g)**
Control	116_{ab}	0.18_{a}	913_{cde}	0.76_{bc}
$Control_{GYP}$	275_{d}	0.73_{c}	669_{abcd}	0.99_{cde}
SS7_L	188_{abcd}	0.13_{ab}	706_{abcd}	0.37_{a}
SS7_H	241_{cd}	0.39_{abc}	706_{abcd}	0.58_{ab}
$SS7\_L_{GYP}$	213_{bcd}	0.37_{abc}	700_{abcd}	0.90_{bcd}
$SS7\_H_{GYP}$	278_{d}	0.41_{abc}	538_{a}	0.75_{bcd}
DC_L	32_{a}	0.03_{a}	925_{cde}	0.59_{ab}
DC_H_	54_{ab}	0.09_{a}	1038_{e}	0.66_{abc}
DC_L_{GYP}	102_{ab}	0.20_{ab}	894_{bcde}	1.29_{ef}
DC_H_{GYP}	188_{abcd}	0.32_{bcd}	650_{abc}	1.04_{de}
SS6_L	86_{abc}	0.05_{a}	950_{de}	0.58_{abc}
SS6_H	342_{d}	0.50_{bc}	606_{ab}	0.32_{a}
$SS6\_L_{GYP}$	81_{abc}	0.06_{a}	856_{bcde}	1.44_{f}
$SS6\_H_{GYP}$	129_{ab}	0.19_{abc}	863_{bcde}	1.27_{ef}

Within the same column, values not followed by the same letter are significantly different at $p<0.05$ as determined by One-Way ANOVA post-hoc Fisher LSD analysis (n=4).* *Indicates data have been transformed by log^2 for statistical analysis.*

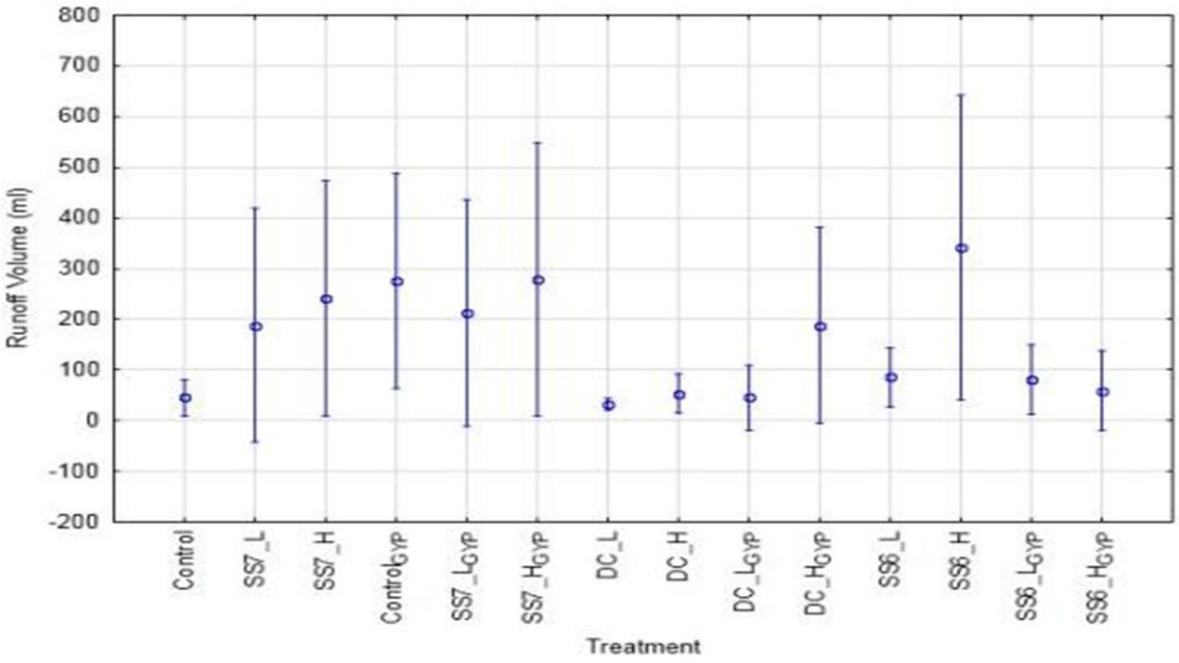

Figure 5.1. HRS: Effect of PBTs on runoff volume as compared to the untreated control

Note: For statistical differences between SFMs refer to Table 5.4. Error bars denote ±1 Standard Error (n=4).

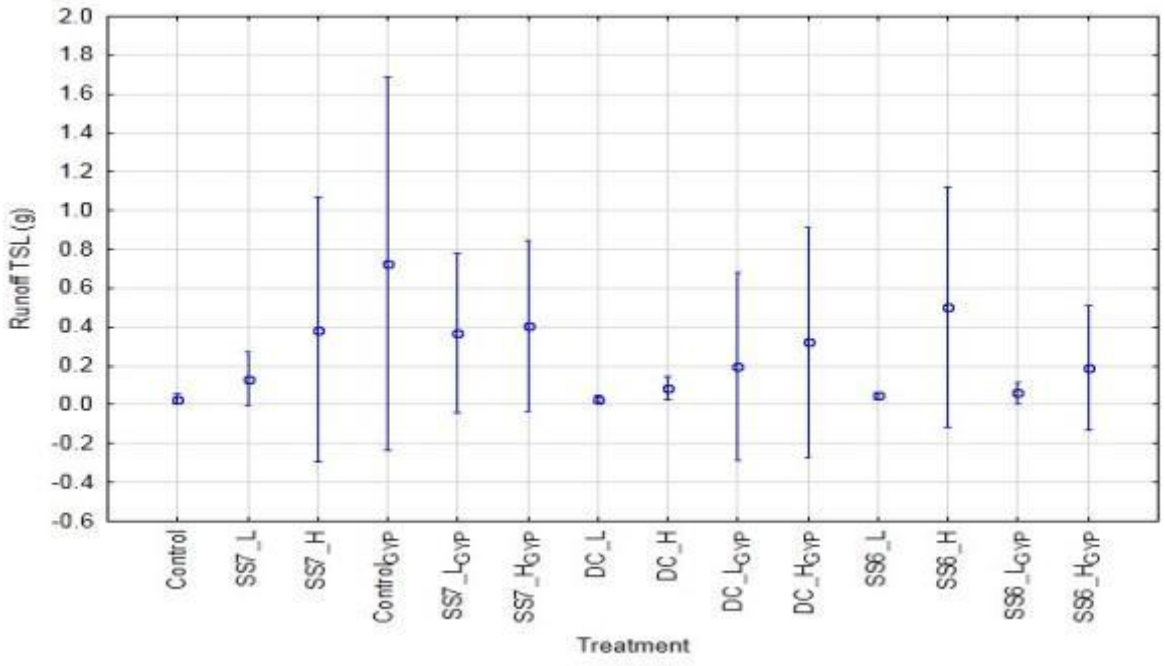

Figure 5.2. HRS: Effect of PBTs on runoff TSL as compared to the untreated control

Note: For statistical differences between SFMs refer to Table 5.4. Error bars denote ±1 Standard Error (n=4).

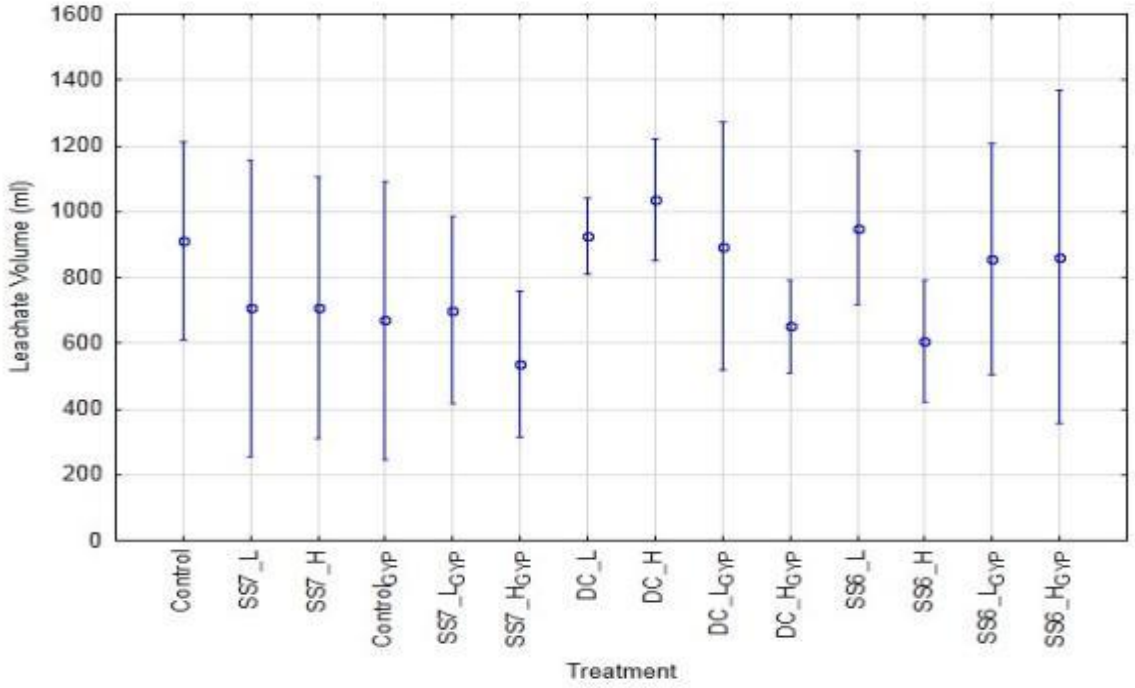

Figure 5.3. HRS: Effect of PBTs on leachate volume compared to the untreated control

Note: For statistical differences between SFMs refer to Table 5.4. Error bars denote ±1 Standard Error (n=4).

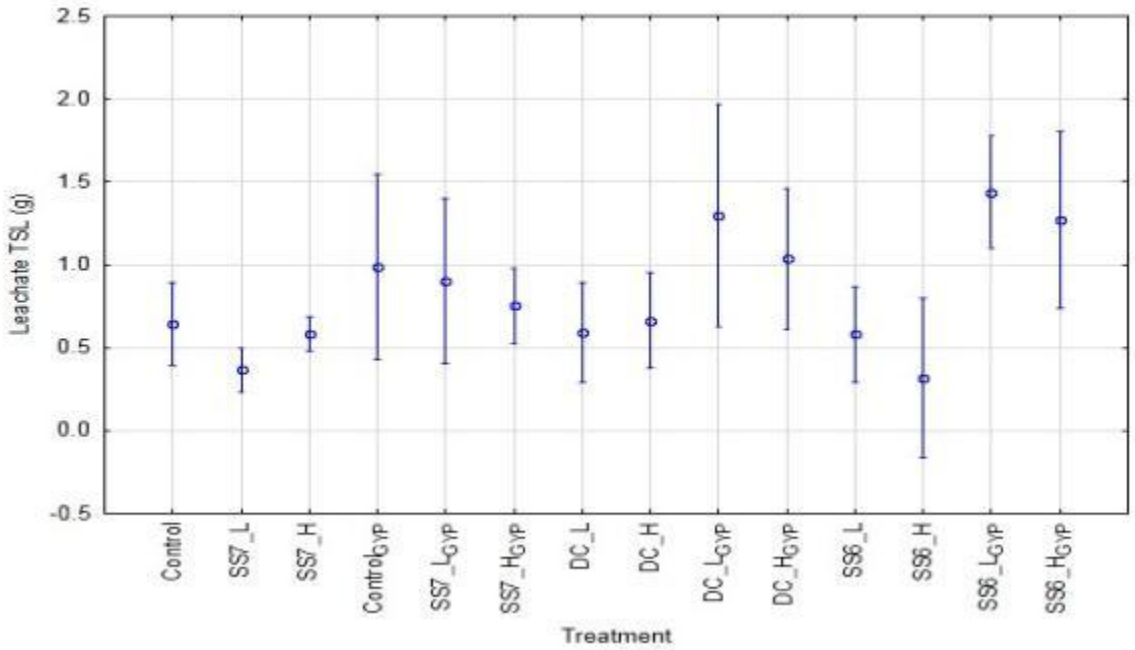

Figure 5.4. HRS: Effect of PBTs on leachate TSL compared to the untreated control

Note: For statistical differences between SFMs refer to Table 5.4. Error bars denote ±1 Standard Error (n=4).

Significantly low CEC (2.53 meq 100g) combined with low clay content (2.2% w/w) associated with HRS (Tables 5.1 and 5.2) would explain why few PBTs are effective controlling runoff and leachate volumes and associated TSLs (Vacher et al., 2003; Sojka et al., 2007). In other studies, application of anionic PAMs (A86, Aeotil, A311, X-135 and LT25) on mine soils were more effective in reducing erosion on soils with clay (representing kaolinite/smectite and ilite mineralogy) contents >50% (Vacher et al, 2003). This was explained by the shorter distances between the anionic PAMs and the charge site associated with clay minerals (Vacher et al., 2003), causing higher polymer adsorption than for soils with low clay contents (1-16%). Field testing on soils using an anionic PAM (Siltstop 634 emulsion PAM) and a hydroseed mix in Georgia, USA, found no significant difference in erosion control for the PAM plus hydroseed treatment as compared to the hydroseed alone (Markewitz and Glazer, 2009). The authors suggest that low CEC (1.29-3.20 meq 100g) associated with the test soil's clay content (4-14% w/w) inhibited bonding between the soil and the polymer. In the present study, the CEC of HRS was 2.53 meq 100g, which is in the range of that found in the Georgia study. This suggests that the low CEC associated with HRS is an important factor in why the PBTs were not effective in controlling runoff and leachate volumes and associated TSL.

SS6_H is the only PBT to increase runoff volume, runoff TSL, and yet reduce leachate volume and leachate TSL significantly when compared to the untreated control. This performance may still be useful in the mining industry, because reducing leachate volume and leachate TSL within and at the base of waste-rock dumps may for certain SFMs be more desirable than controlling surface runoff and erosion. Other approaches, such as check dams, hydro-seeding, vetiver planting or geotextiles, may then be employed by land managers to control surface runoff and erosion.

Figures 5.1 to 5.4 illustrate that for HRS, there is a high degree of variability in the runoff volume, runoff TSL, leachate volume and leachate TSL results for many treatments. High variability was observed in the Phase I HRS runoff and leachate results (Section 4.5.1.2), and is attributed to the heterogeneous nature of the physical and chemical properties of HRS replicates. It is postulated that spatial variations in the distribution of the clay fraction (<0.002 mm) at the surface of HRS will cause variations in charge sites for polymer absorption via cation bridging. Furthermore, variations in the surface distribution of rock sized aggregates^{NS} will cause geometric irregularities at the surface (Khansbasi and Abdalla, 2006), and cause differences in the effective surface area for polymer adsorption (as detailed in Section 2.5.2).

HRS is dominated by hematite (52% w/w) and goethite (33% w/w). No known studies report directly about the mechanisms of polymer adsorption on hematite and goethite. The adsorption properties of hematite and goethite were observed by Giménez et al. (2007), where arsenic adsorption occurs through weak van der Waal forces or hydrogen bonding, resulting in a weak net surface charge depending on pH. The physical and chemical properties of the HRS test sample used in Phase II were found to be statically comparable to the HRS sample used in Phase I (Appendix G). HRS was found to have 30% (w/w) aggregates sized 5.6 mm to >37.5 mm (Table 4.4 Section 4.2.9). A high distribution of coarse sized hematite and goethite aggregates^{NS} at the surface may result in high polymer adsorption, but the net surface charge is too weak to promote cationic bridging with clay minerals. Further testing would be necessary to better understand the adsorption properties of the polymers evaluated in this study, on the hematite and goethite minerals found in HRS. This spatial variability in the surface area of hematite, goethite and kaolinite at the surface of HRS will affect polymer adsorption; subtle variations in surface properties are amplified using small (0.2 m x 0.11 m) erosion trays. The spatial variability in surface porosity and mineralogy will decrease as scale increases.

Figures 5.1 to 5.4 illustrate DC_L, DC_H, SS6_L and SS6_L$_{GYP}$ produced low variability in the runoff volume, runoff TSL, leachate volume and leachate TSL results. This suggests that the efficacy of SS6 anionic PAM and DC90 PVAL treatments (in terms of reducing the erodibility and the hydrological response of HRS) is more consistent than others. Although the DC_L and DC_H runoff volume and runoff TSL results are not significantly different to the untreated control, Table 5.4 shows that runoff volumes are 3 to 4 times less, and runoff TSLs are 2 to 6 times less than the untreated control. Furthermore, the DC_L and DC_H runoff volume and runoff TSL results are significantly lower than the SS7_H, SS7_H$_{GYP}$ and SS6_H treatments. Coupled with the low within-treatment variability, the DC_L and DC_H PBTs have potential to successfully reduce runoff volumes and runoff TSLs from HRS.

5.2.1 Effects of application rate on PBT efficiency

A comparison of the high and low PBT application rates using One-way ANOVA post-hoc Fisher LSD analysis shows that of all the results only higher application rate SS6_H generated significantly higher runoff volume and runoff TSL, and as well significantly lower leachate volume than SS6_L (Table 5.4).

The results indicate that the different viscosities of low application rate SS6_L and high application rate SS6_H may in part be causing differences in runoff

and leachate volumes. PAMs SS6_H and SS6_L are associated with viscosities of 13.74 and 10.61 m.Pa.S, respectively (Table 3.6 Section 3.3.3). Anionic PAMs applied at application rates higher than those recommended by the manufacturer will be associated with higher viscosities (no amount defined) (Green and Stott, 2001), and may be difficult to dissolve in water, which would cause uneven distribution of the polymer across the surface (Nwankwo, 2001). Consequently, a portion of the soil surface may be left unprotected. However, poor spatial coverage was not observed during the application of the SS6 PBTs in this study.

Other studies have observed that if the PAM application solution is too concentrated, high viscosity can restrict infiltration, thereby generating more runoff (Green et al., 2001; Vacher et al., 2003; Soupir et al., 2004; in Sojka et al., 2007). The benefits of using anionic PAM in terms of erosion and runoff reduction are shown not to be straightforward (Lee, 2009), and the results for PBT SS6 (without gypsum) show 14.03 l ha^{-1} is approximately the optimum application rate when erosion control is maximised.

Optimum PBT application rate will depend on a range of factors, including the type of polymer, slope gradient and SFM characteristics (Lentz, 2003: in Sojka et al., 2007). The high viscosity SS6_H treatment may seal pores that would otherwise drain freely, so enhancing runoff generation and causing significantly lower leachate volumes compared to the control (Soupir, 2004; Sojka et al., 2007).

5.2.2 Effects of gypsum on PBT efficiency

The one-way ANOVA post-hoc Fisher LSD analysis in Table 5.4 shows that $Control_{GYP}$ generated significantly higher runoff volume and runoff TSL compared to the untreated control. In contrast $SS6\_H_{GYP}$ was associated with significantly lower runoff volume than non-gypsum SS6_H. The gypsum treatment DC_H_{GYP} had significantly higher runoff TSLs compared to DC_H. Significant differences between gypsum and non-gypsum treatments were most prevalent in the leachate TSL results; and gypsum treatments $SS7\_L_{GYP}$, DC_L_{GYP}, DC_H_{GYP}, $SS6\_L_{GYP}$ and $SS6\_H_{GYP}$ generated significantly higher leachate TSLs as compared to their respective non-gypsum treatments, as illustrated in Figure 5.4.

These results are surprising as Mahardhika et al. (2008) reported successful reduction in runoff TSLs using anionic PAM with gypsum amendments on waste-rock materials from a mine-site in Australia. However, the properties of

the waste-rock were not reported, so the results cannot be compared to findings in this study. It is thought that the poor efficacy of the PBT-gypsum treatments in this study in terms of runoff TSL, may in part be due to the low clay mineral content (2.2% w/w Table 5.2) associated with HRS, resulting in a sub-optimal availability of charge sites for the polymer to form 'cation-bridge' bonds (Lee, 2009). Therefore, an excess of charged Ca^{2+} cations through gypsum addition is redundant if there are insufficient receptor sites for absorption.

5.2.3 Surface roughness change associated with the PBTs

An assessment of surface roughness (SR) and surface area (SA) of selected PBT treatments on HRS was carried out using NSPASS. The treatments selected and justification for their selection is listed in Table 5.5.

Table 5.5. Non-soil HRS: treatments selected for NSPASS assessment

HRS Treatment	Reasons For Selection
Control	To compare PBT effects on surface roughness and surface area, with the untreated control.
$Control_{GYP}$	Associated with the highest runoff TSL.
DC_H	Associated with low runoff volume and runoff TSL.
DC_H_{GYP}	Associated with higher runoff volume than DC_H where no gypsum was added.
SS6_H	Associated with significantly higher runoff volume, runoff TSL and lower leachate volume than the control.
$SS6\_H_{GYP}$	Associated with significantly lower runoff volumes and higher leachate TSL than SS6_H where no gypsum was added.
SS6_L	A low application rate PBT associated with significantly lower runoff volumes and runoff TSL than the same treatment at a higher application rate (i.e. SS6_H).

It was hypothesised that after rainfall, there would be a reduction in SR and SA (T0 – T1) for all treatments. The net change in SR and SA was expected to reflect differences in the efficacy of PBTs. The largest change in SA and SR was expected from the untreated control, followed by the gypsum only treatments, polymer without gypsum and finally polymer with gypsum. The latter was expected to show the least surface change, because the PBT would

stabilise the surface and gypsum would improve polymer efficiency, as illustrated in Figure 5.5.

The hypothesis was not supported by the experimental results and the greatest change in SR and SA was shown by SS6_L (PBT without gypsum) and the least change in SR and SA was shown by the Control plus gypsum treatment ($Control_{GYP}$). This implies that SS6_L had experienced the greatest re-distribution of material by raindrop impact and surface runoff, and that the surface of $Control_{GYP}$ was most stable during rainfall. Also, treatments led to an increase in SA ($Control_{GYP}$ and $SS6\_H_{GYP}$) and SR ($SS6\_H_{GYP}$), not a decrease as was expected (Table 5.6).

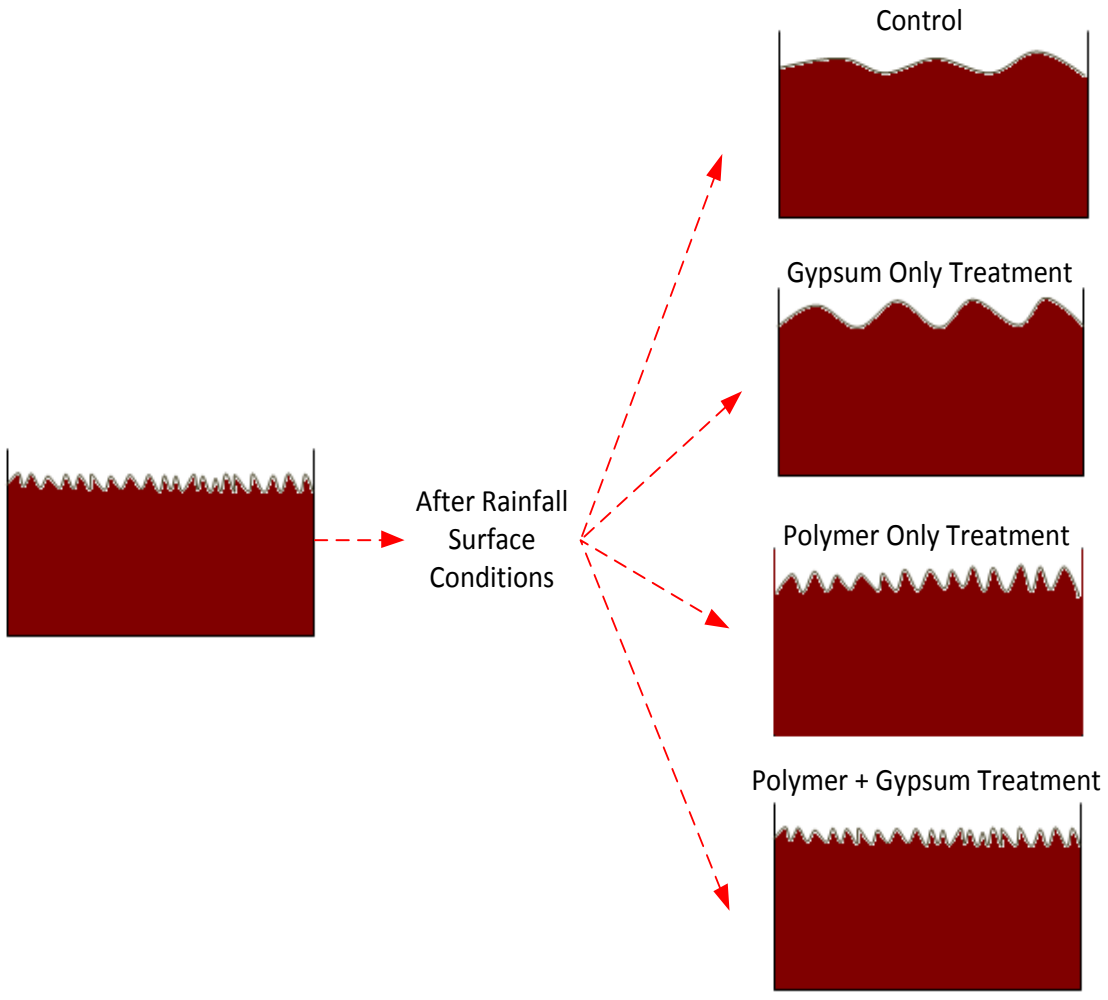

Figure 5.5 Conceptual diagram illustrating the predicted response of surface roughness to rainfall using the different treatments
(Source: Author, 2012)

Table 5.6. HRS: Surface Roughness (SR) and 3D Surface Area (SA) variables for selected treatments

	BEFORE RAINFALL (T0)		AFTER RAINFALL (T1)		SR AND SA DIFFERENCE (T0 – T1)				RUNOFF TSL	
PBT	Mean SR	Mean SA (m^3)	Mean SR	Mean SA (m^3)	SR Change	SR Change Ranking	SA Change (m^3)	SA Change Ranking	Runoff TSL (g)	Runoff TSL Ranking
Control	2.42	0.27	1.71	0.19	-0.71	**3**	-0.08	**3**	0.18	**5**
$Control_{GYP}$	1.66	0.18	1.64	0.18	-0.02	**7**	0.00	**7**	0.73	**1**
DC_H_{GYP}	2.13	0.24	2.03	0.23	-0.10	**6**	-0.01	**6**	0.32	**3**
DC_H	3.44	0.32	3.05	0.29	-0.39	**5**	-0.03	**4**	0.09	**6**
$SS6\_H_{GYP}$	3.17	0.34	3.82	0.35	0.66	**4**	0.02	**5**	0.19	**4**
SS6_H	3.81	0.40	2.35	0.25	-1.47	**2**	-0.15	**2**	0.50	**2**
SS6_L	6.33	0.64	1.97	0.22	-4.36	**1**	-0.43	**1**	0.05	**7**

SR, SA and Runoff TSL values are ranked, 1 being the highest value in the data set and 7 being the lowest. Note the ranked values do not reflect statistical differences in the data-set.

It was also hypothesised that the highest change in SR and SA would correspond with the highest runoff TSL values, as erosion (indicated by runoff TSL) led to a decrease in SR post rainfall. To test this hypothesis, runoff TSL, SR change and SA change for each treatment are ranked in descending order (1 assigned to the highest value and 7 to the lowest) in Table 5.6. SS6_H was the only treatment where the rankings of SR change, SA change and runoff TSL are the same. A direct relationship between SR change and runoff TSL, or SA change and runoff TSL was not observed for the other PBTs, and suggests that more complex non-linear micro-erosional processes are operating during rainfall. As discussed in Chapter 4, leachate TSL from HRS can originate from infiltration of particles detached and entrained at the surface, as well as those detached from the SFM matrix by subsurface flow. Therefore, the loss of material from the surface may not necessarily be reflected in the runoff TSL results alone. Some of this material may leave the plot via subsurface flow (leachate). It was beyond the scope of this thesis to determine the relative proportions of leachate TSL derived from surface detachment and subsequent infiltration, and that detached from within the SFM. Consequently, it is not possible to accurately relate the HRS runoff TSL results to SR and SA change.

In addition, the poorly observed relationship between runoff TSL and SR and SA change may, in part, be due to subtle differences in the surface starting

conditions. Differences in the shape, orientation and percentage cover of rock fragments (>2 mm) located on or immediately below the HRS surface (that become exposed during the rainfall event), may cause changes in SR and SA that are associated with the newly exposed surfaces, rather than decreasing roughness. It follows that these new surfaces may not be related to runoff TSL results. Furthermore, a post rainfall armoured surface, may generate a rougher SR value than starting conditions. This may in part explain why some PBTs are associated with increases in SR and SA.

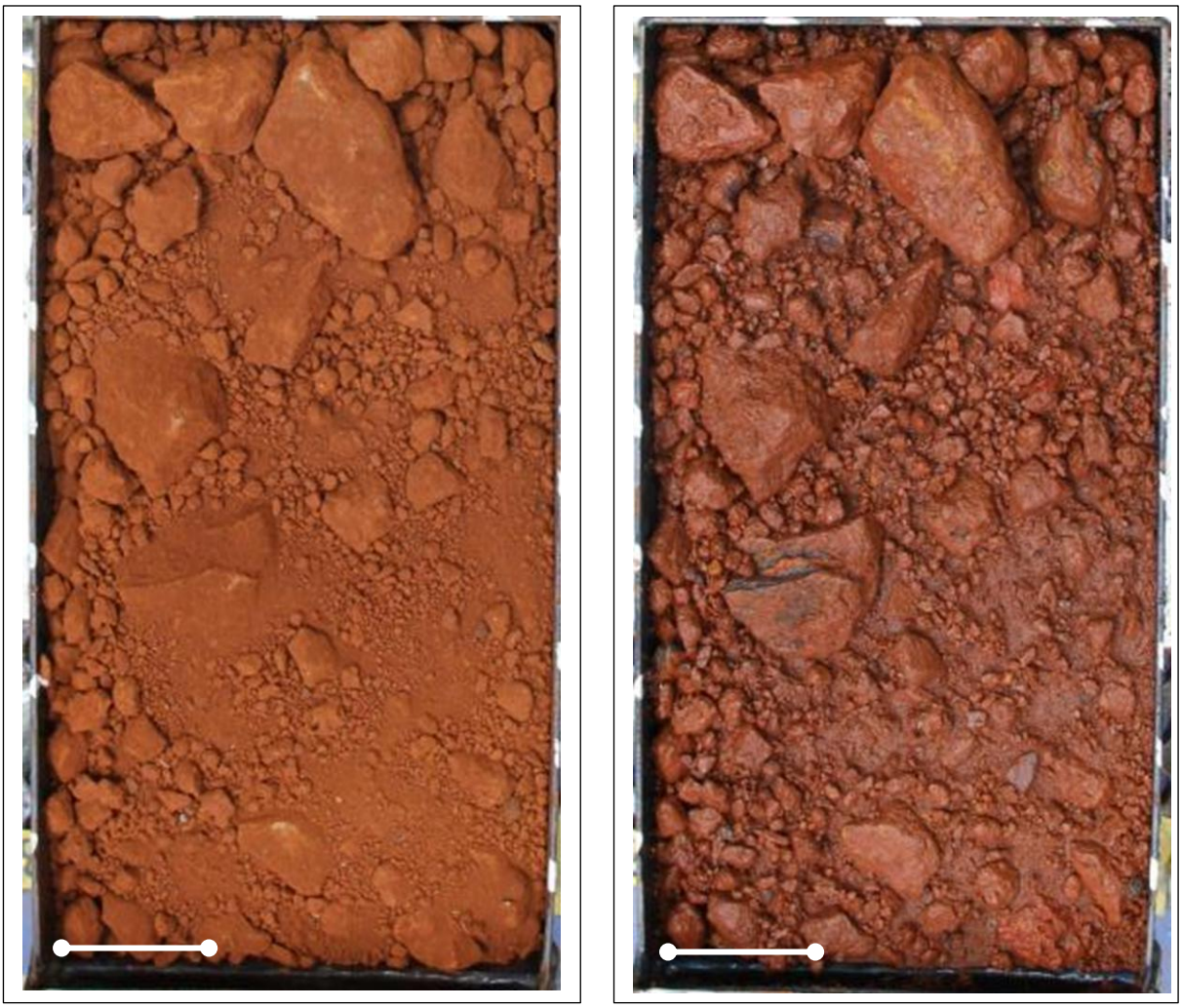

Figure 5.6. HRS Control treatment photographed before (left) and after (right) rainfall *(scale 2 cm = 3 cm)*

Subtle differences in the starting conditions of HRS replicates are magnified because NSPASS detects changes in SA and SR with an accuracy of between 2-3 mm, over a surface area of just 0.112 m^2. Therefore, changes at the surface, particularly the exposure of relatively smooth and large rocks may

reflect a disproportional change in SR and SA in relation to the amount of sediment that has been transported in runoff. It is unrealistic to exactly replicate the surface characteristics of HRS in each erosion tray, because of its inherent heterogeneous physical characteristics, as illustrated in Figure 5.6. Further testing is necessary to determine whether variability in SR and SA, caused by larger rocks, is less pronounced and so causes fewer anomalous results, when assessed at a larger spatial scale.

5.3. Effect of PBTs on the erodibility and hydrological response of LITH

One-way ANOVA post-hoc Fisher LSD analysis in Table 5.7 shows SS7_H (60 ml), DC_H_{GYP} (47 ml), SS6_L (75 ml), DC_H (41 ml) and SS6_H_{GYP} (103 ml) generated significantly lower runoff volumes compared with the control. DC_H_{GYP} is the only treatment with significantly less runoff TSL than the control (0.35 g).

DC_L (938 ml) and SS6_H (916 ml) were the only treatments to generate leachate volumes significantly higher than the control (713 ml). Significantly higher leachate TSL than the control (0.44 g) was associated with $Control_{GYP}$ (0.85 g), SS7_L_{GYP} (0.85 g), DC_L_{GYP} (1.31 g), DC_H_{GYP} (1.0 g), SS6_L_{GYP} (0.96 g) and SS6_H_{GYP} (1.27 g).

DC_H_{GYP} generated significantly lower runoff volume, runoff TSL, but significantly higher leachate TSL than the control. The effects of anionic PAM on erosion are reported extensively in the literature (Aase et al., 1998; Mahardlika et al., 2008; Sojka et al., 2007; Zejun et al., 2002; Vacher et al., 2003; Green and Stott, 2001); but less is known about the adsorption properties of latex based vinyl acrylic solutions (PVALs), such as DC90. It is believed the success of DC_H_{GYP} at reducing runoff volume and runoff TSL from LITH is fundamentally related to its latex addition.

The adsorption of anionic charged PAMs onto soils can happen by means of cation bridging, covalent bonding, hydrogen bonding or by van der Waal electrostatic forces (Simmons, 1998; Lu et al., 2002; Kanungo, 2005), as opposed to non-ionic PVALs that are absorbed primarily by just hydrogen or by van der Waal electrostatic forces bonding mechanisms (Kanungo, 2005). Therefore, theoretically there are more bonding opportunities for anionic PAMs (Kanungo, 2005). However, PVAL DC90 after dehydration forms a permeable

film at the surface that changes the mechanical properties of particles it is adhered to, and acts like glue, by adhering particles in place and preventing detachment and entrainment from raindrop impact and the shear forces of runoff (Khansbasi and Abdalla, 2006). It is thought that this film is also protecting the underlying aggregates from the full extent of kinetic energy associated with impacting raindrops, and thus is protecting the surface from aggregate breakdown. A continuous latex film forms from coalescence of individual latex particles, which are usually repelled in water, but when water evaporates after the treatments has dried, these forces are overcome and latex particles are connected by inter-particle friction (Khansbasi and Abdalla, 2006). The stabilising properties of a latex based PVAL (NeoCARTM Acrylic 820) was recognised by means of mechanical testing in Khansbasi and Abdalla (2006), and was successful stabilising unconsolidated desert sand samples (Khansbasi and Abdalla, 2006). Therefore, it is the stabilising properties of latex based DC_H_{GYP} and DC_H that makes these PBTs successful in reducing runoff and TSLs from soil LITH.

Table 5.7 LITH: Effect of PBT on runoff volume, runoff TSL, leachate volume and leachate TSL

LITH				
Treatment	**Runoff Volume (ml)***	**Runoff TSL (g)**	**Leachate Volume (ml)***	**Leachate TSL (g)**
Control	166_{de}	0.35_{bcd}	713_{ab}	0.44_{a}
$Control_{GYP}$	197_{de}	0.40_{d}	575_{a}	0.85_{bcd}
SS7_L	117_{acde}	0.07_{abc}	725_{abc}	0.58_{abc}
SS7_H	60_{abc}	0.15_{bcd}	788_{bcd}	0.69_{abcd}
SS7_L_{GYP}	160_{cde}	0.19_{bcd}	819_{bcd}	0.85_{bcd}
SS7_H_{GYP}	191_{e}	0.19_{d}	581_{a}	0.64_{abcd}
DC_L	72_{abcd}	0.14_{bcd}	938_{d}	0.56_{abc}
DC_H_	41_{a}	0.05_{ab}	831_{bcd}	0.52_{ab}
DC_L_{GYP}	113_{bcde}	0.22_{cd}	900_{bcd}	1.31_{e}
DC_H_{GYP}	47_{ab}	0.09_{a}	750_{abcd}	1.00_{de}
SS6_L	75_{abc}	0.12_{bcd}	831_{bcd}	0.70_{abcd}
SS6_H	88_{abcde}	0.16_{bcd}	916_{cd}	0.79_{abcd}
SS6_L_{GYP}	110_{abcde}	0.26_{cd}	850_{bcd}	0.96_{bcd}
SS6_H_{GYP}	103_{abc}	0.10_{bcd}	788_{bcd}	1.27_{e}

Within the same column, values not followed by the same letter are significantly different at $p<0.05$ as determined by One-Way ANOVA post-hoc Fisher LSD analysis (n=4).* *Indicates data have been transformed by log for statistical analysis.*

5.3.1 Effects of application rate on PBT efficiency

A comparison of the higher and lower PBT application rates in Table 5.7 shows DC_H_{GYP} is associated with significantly lower runoff TSL than lower application rate DC_L_{GYP}.

Higher application SS7_H_{GYP} is associated with significantly lower leachate volumes compared to lower application rate SS7_L_{GYP}. Significantly higher leachate TSLs are associated with higher application rate SS6_$H_{GYP,}$ as compared with lower application rate SS6_L_{GYP}.

With the exception of the PVAL DC_H_{GYP} treatment, increasing application rate did not cause significant reductions in in the overall erodibility and hydrological response of LITH. A study that assessed the longevity of anionic PAMs to control erosion on Costa Rican soils tested three application rates including 20 kg ha^{-1}, 80 kg ha^{-1} and 120 kg ha^{-1} (Martínez-Rodríguez et al., 2007). The study showed that after the first rainfall event, there were no significant differences between the two higher application rate treatments (80 kg ha^{-1} and 120 kg ha^{-1}), which may at first lead decision makers to favour the 80 kg ha^{-1} application rate treatment, as it seems there are marginal benefits by using the higher application rate 120 kg ha^{-1}. However, further testing revealed that the higher application rate 120 kg ha^{-1} treatment sustained the least erosion losses after being exposed to five natural rainfall events over a 60 day period (Martínez-Rodríguez et al., 2007). These findings show firstly that the two highest application rates used in the Costa Rica study were higher than the application rates used for the anionic PAMs in this study. Therefore it may be that further experimentation using the same PBTs at even higher application rates would cause significant differences in the application rate results. The Costa Rican study also shows that product longevity is important and it is essential to understand PBT response to rainfall over a longer time period, or after a higher number of successive rainfall events; which is an experimental design recommended for future studies in this subject area.

5.3.2 Effects of gypsum on PBT efficiency

A comparison of the gypsum and non-gypsum treatments in Table 5.7 shows the gypsum treatment SS7_H_{GYP} had significantly higher runoff volume than non-gypsum treatment SS7_H. Gypsum treatment SS7_H_{GYP} had significantly less leachate volume than SS7_H. The gypsum treatments SS6_H_{GYP}, DC_H_{GYP}, DC_L_{GYP} and $Control_{GYP}$ were associated with significantly higher

leachate TSL than their respective non-gypsum treatments, SS6_H, DC_H, DC_L and Control.

It is surprising that few anionic PAM treatments with gypsum were successful on soil LITH considering the literature base that reports improved infiltration rates and lower erosion rates using gypsum with PAMs on soils (Aase, et al., 1998; Vacher et al., 2003; Sojka et al., 2007; Mahardhika et al., 2008; Akbarzadeh et al., 2009; Lee, 2009; Kumar and Saha, 2011). It is possible that differences in the SFMs, experimental procedure, gypsum application method or rainfall conditions explain why the outcomes of this study are different to PAM with gypsum studies reported in the literature.

It is postulated that anionic PAMs may not be as successful reducing TSLs on tropical soils compared to those studies that have tested PAMs on temperate soils (Aase, et al., 1998; Akbarzadeh et al., 2009; Lee, 2009; Kumar and Saha, 2011). Differences in soil clay mineralogy and lower CEC associated with many tropical soils compared to temperate soils (Landon, 1991) may explain why the PAMs are not as successful reducing erosion on soil LITH, but further testing is necessary to vindicate this. A fundamental difference in the experimental procedure reported in both Vacher et al. (2003) and Mahardhika et al. (2008) is that the SFMs used were screened for gravel materials >50 mm. Removing larger gravels and rocks, particularly using mine waste and ore SFMs that contain high amounts of coarse rocks and stones, will fundamentally change the SFM's texture, and so this approach does not replicate the material as it would exist in the field. Results in this study have shown that the SFMs tested contain coarse fragments of rock, which has caused differences in polymer adsorption and whether the treatment was successful reducing runoff, leachate and erosion; and as such, experimental procedures that alter the original texture of the material could be misleading.

Vacher et al. (2003) used the same 5000 kg ha^{-1} gypsum application rate and simulated rainfall event to this study at 100 mm hr^{-1} for 30 minutes on a 9° slope. The Anionic PAMs (A86, Aerotil, A311, X-125 and LT25) were also applied by hand, but a layer of mulch was applied to the surface of selected treatments. In addition to the PAM, the use of mulch would have provided additional protection from raindrop impacts and this is why the Gypsum-PAM plus mulch treatments were associated with the most significant reductions in sediment loss. Kumar and Saha (2011) tested an anionic PAM and gypsum to manage erosion, applying half the amount of gypsum used in this study at 2500 kg ha^{-1}, but the simulated rainfall event had a lower intensity and shorter

duration at 50 mm hr^{-1} for 10 min. Therefore, rainfall erosivity would be considerably less assuming a similar rainfall drop-size distribution.

Mahardhika et al. (2008) used a more intense simulated rainfall event (120 mm hr^{-1}), with double the amount of gypsum (10,000 kg ha^{-1}), which was applied by hand and, like this study, mixed with the upper 2-3 cm of surface material. Some studies have also reported that gypsum is best applied directly on the surface and not mixed with the top soil (Wallace and Wallace, 1986; in Morgan, 2006). Conversely erosion amounts were less in Lake Baringo, Kenya, when the gypsum was raked into the top 20 mm of soil (Fox and Bryan, 1992; in Morgan, 2006). These observations highlight the different options for applying gypsum to soils, and also that there are no standard guidelines on how to apply gypsum to non-soil SFMs. It is possible gypsum treatments would have been more successful if the gypsum was not mixed into the surface, but simply scattered on top. This is because mixing may reduce the amount of gypsum exposed to the polymer treatment and hence the amount available for bridging the polymer with the SFM. It may be that further testing using different application techniques or higher gypsum application rates improves PBT efficiency. However, these initial results suggest that this is not going to cause discernible differences in the runoff, leachate or erosion results, as in some cases, the gypsum treatments were associated with higher runoff volumes as compared with the control. It would not be practical or financially viable to increase gypsum application rates considerably more, without there being significant reductions in the erosion and runoff results, as this will only increase management costs with minimal benefit.

5.3.3. LITH: surface roughness changes associated with the PBTs

An assessment of surface roughness (SR) and surface area (SA) of selected LITH PBT treatments was carried out using NSPASS. The treatments selected and justification for their selection is listed in Table 5.8.

It was hypothesised that after rainfall, there would be a reduction in SR and SA (T0 – T1) for all treatments. For the LITH NSPASS results (Table 5.9) the control was associated with the highest ranked SR (-3.43) and SA (-0.28 m^3) changes. Subsequently, $Control_{GYP}$ was ranked second in the SR (1.80) and SA (0.16m^3) results and SS7_H ranked third in the SA (-1.11) and SR (-0.10) results. The polymer with gypsum treatments including $SS6\_L_{GYP,}$ $DC\_L_{GYP,}$ DC_H_{GYP} and $SS7\_H_{GYP,}$ were associated with the lowest SR (0.8 to -0.06) and SA (0.07 to -0.02 m^3) changes. These results indicate that for the soil LITH, all

the treated surfaces maintain surface micro-relief better during rainfall than the untreated control, and erosion control efficiency is maximised using the polymer plus gypsum treatments.

Table 5.8. Soil LITH: treatments selected for NSPASS assessment

LITH Treatment	Reasons For Selection
Control	To compare PBT effects on surface roughness and surface area, with the untreated control.
$Control_{GYP}$	Associated with significantly higher leachate TSL than the control.
SS7_H	Associated with significantly lower runoff volumes than the control.
$SS7\_H_{GYP}$	Associated with significantly higher runoff volumes than non-gypsum SS7_H.
DC_L_{GYP}	Associated with significantly higher runoff TSL than higher application rate $DC\_H_{GYP.}$
DC_H_{GYP}	Associated with significantly lower runoff volumes and runoff TSL than the control, and higher leachate TSL than the control.
$SS6\_L_{GYP}$	Associated with significantly higher leachate TSL than the control.

Table 5.9. LITH: Surface Roughness (SR) and 3D Surface Area (SA) variables for selected treatments

	BEFORE RAINFALL (T0)		AFTER RAINFALL (T1)		SR AND SA DIFFERENCE (T1 - T0)				Runoff TSL Generated	
PBT	Mean SR	Mean SA (m^3)	Mean SR	Mean SA (m^3)	SR Change	SR Change Rank	SA Change (m^3)	SA Rank	Runoff TSL (g)	Runoff TSL Rank
$SS7\_H_{GYP}$	3.07	0.31	3.00	0.33	-0.06	**7**	0.02	**7**	0.19	**5**
DC_L_{GYP}	1.81	0.20	1.47	0.16	-0.34	**6**	-0.04	**6**	0.22	**4**
DC_H_{GYP}	2.14	0.24	1.46	0.16	-0.68	**5**	-0.07	**5**	0.09	**7**
Control	6.10	0.56	2.67	0.28	-3.43	**1**	-0.28	**1**	0.35	**2**
$Control_{GYP}$	2.34	0.25	4.15	0.41	1.80	**2**	0.16	**2**	0.4	**1**
$SS6\_L_{GYP}$	1.51	0.17	2.31	0.24	0.80	**4**	0.07	**4**	0.26	**3**
SS7_H	3.11	0.32	2.00	0.22	-1.11	**3**	-0.10	**3**	0.15	**6**

SR, SA and Runoff TSL values are ranked, 1 being the highest value in the data set and 7 being the lowest. Note the ranked values do not reflect statistical differences in the data-set.

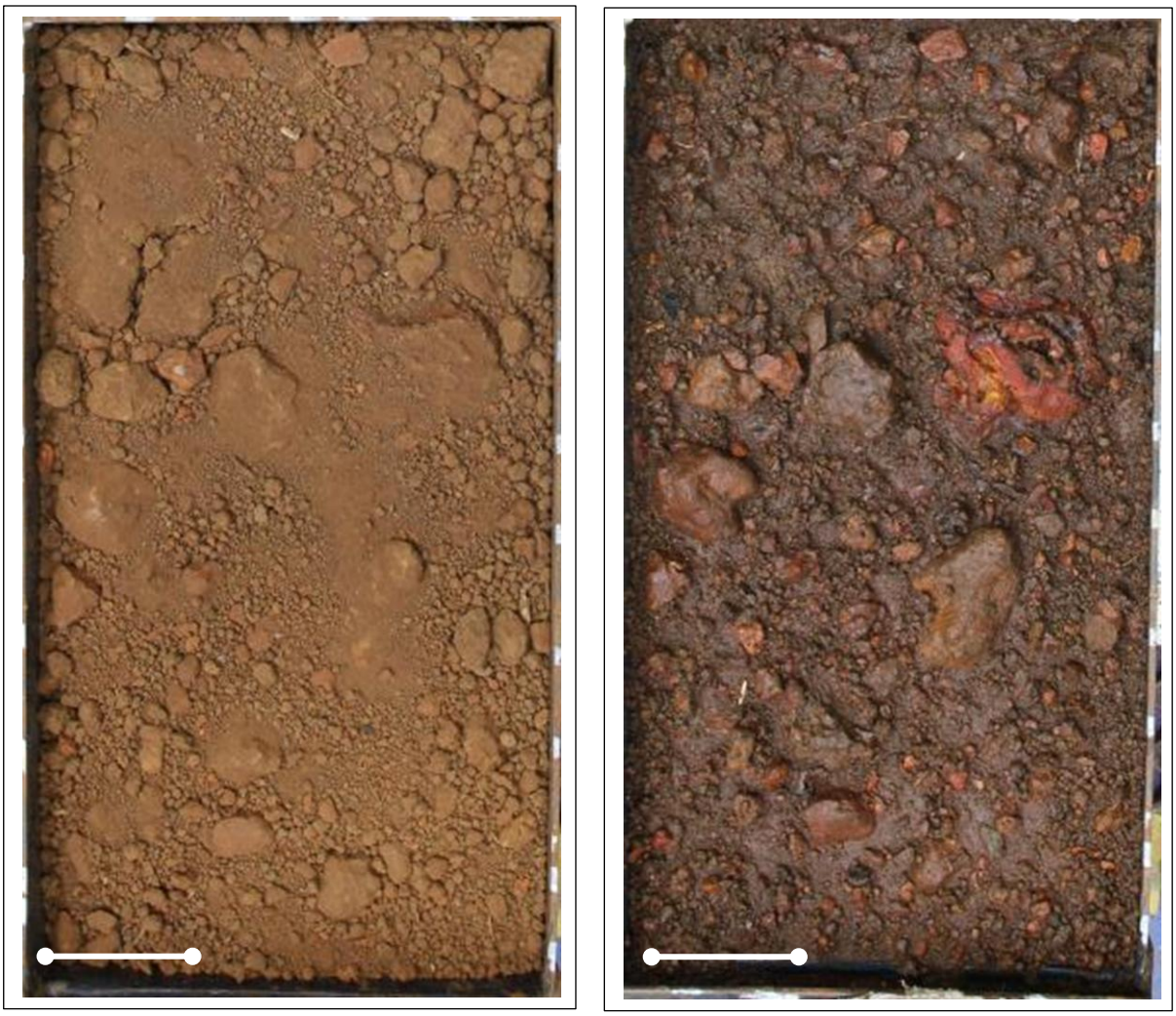

Figure 5.7. LITH Control treatment photographed before (left) and after (right) rainfall *(scale 2 cm = 3 cm)*

The ranking assigned to the LITH runoff TSL results show no correlation with the rankings assigned to either SR or SA change. Most treatments are associated with a decline in SR and SA, and the control shows the biggest decline. Figure 5.7 shows the control surface post-rainfall is associated with less finer material and is notably armoured and sealed. However, not all treatments are associated with a decline in SR and SA, as $Control_{GYP}$ and $SS6\_L_{GYP}$ are associated with an increase in SR and SA change post-rainfall. Kinnell (2005) suggests erosion process models do not convey temporal changes in surface (micro) topography very well, as surface changes are not linear and often very complex. Poesen et al. (1994) also recognises that differences in the surface area that stones and rocks occupy, either immediately at the surface or below the surface, can lead to varying effects on erosion rates,

because as the starting surface is eroded down during rainfall a new surface is uncovered (Poesen et al., 1994). Rock fragments are defined as minerals >2.0 mm in size (Poesen et al., 1994), and the LITH DAD results (Table 4.4 Section 4.2.9) shows LITH has 20.3% (w/w) aggregates >2.0 mm. Therefore, differences in the size and distribution of rock fragments, irrespective of the type of PBT used, would explain why SR and SA changes in LITH do not correspond with the amount of runoff TSL recorded. It is inferred that when the erosion process has become more advanced and surface armouring has commenced, then continuing SA and SR changes caused by rainfall impact and runoff are less predictable over time.

5.4 Effects of PBTs on the erodibility and hydrological response of PHV

One-way ANOVA post-hoc Fisher LSD analysis shows that the application of selected PBTs had no significant effects on runoff volume (Table 5.10). SS7_H (6.22g), SS7_H_{GYP} (6.21g), DC_H (4.53g) and DC_H_{GYP} (3.38g) were associated with runoff TSLs significantly lower than the control and all other treatments, which ranged between 17.27–9.60 g (Table 5.10 and Figure 5.8).

DC_H and DC_H_{GYP} are associated with leachate volumes significantly higher than the untreated control, as well as being significantly higher than Control$_{GYP}$, SS7_H, SS7_H_{GYP}, DC_L_{GYP} and SS6_L_{GYP}. DC_H_{GYP} is also associated with leachate TSLs (1.85 g) significantly higher than the control (0.26 g), and also significantly higher than all other leachate TSL results, which range between 0.14 g and 1.5 g.

Soil LITH showed in the previous Section 5.3 that only DC_H_{GYP} was successful at significantly reducing runoff TSL. In contrast, the results for non-soil PHV demonstrate that four PBTs, including two PAM treatments (SS7_H and SS7_H_{GYP}) and two PVAL treatments (DC_H and DC_H_{GYP}), reduced runoff TSLs as compared to the untreated control. SFM properties that are associated with high anionic PAM adsorption include high CEC as CEC represents the exchange sites for polymer anions to form ionic bridges with; and increasing clay, as clay provides a surface area for polymer adsorption (Schamp et al., 1975; in Vacher et al., 2003; Bratby, 2006). However, differences in the CEC and clay content of LITH and PHV do not explain differences in the respective runoff TSL results of these two SFMs. PHV has 30% w/w clay mineral content (2:1 clays and kaolinite combined) and a CEC of 1.83 meq 100g as compared

with soil LITH, which has a lower clay content than PHV at 21% w/w, but at 17.7 meq 100g the CEC of LITH is significantly higher (Table 5.1 and Table 5.2).

Table 5.10. PHV: Effect of PBTs on runoff volume, runoff TSL, leachate volume and leachate TSL

PHV				
Treatment	**Runoff Volume (ml)**	**Runoff TSL (g)**	**Leachate Volume (ml)***	**Leachate TSL (g)***
Control	766_{a}	13.5_{def}	22_{ab}	0.26_{a}
$Control_{GYP}$	706_{a}	12.3_{cdef}	22_{ab}	0.17_{a}
SS7_L	569_{a}	17.1_{ef}	24_{abc}	0.33_{a}
SS7_H	716_{a}	6.22_{abc}	40_{ab}	0.46_{a}
$SS7\_L_{GYP}$	703_{a}	15.5_{def}	375_{bcd}	0.52_{a}
$SS7\_H_{GYP}$	797_{a}	6.21_{abc}	11_{a}	0.17_{a}
DC_L	647_{a}	9.66_{abcd}	128_{bcd}	1.50_{a}
DC_H	591_{a}	4.53_{ab}	219_{cd}	0.62_{a}
DC_L_{GYP}	810_{a}	10.5_{bcde}	8_{a}	0.14_{a}
DC_H_{GYP}	582_{a}	3.38_{a}	225_{d}	1.85_{b}
SS6_L	756_{a}	18.07_{f}	56_{abcd}	0.50_{a}
SS6_H	669_{a}	14.7_{def}	38_{abcd}	0.51_{a}
$SS6\_L_{GYP}$	716_{a}	17.3_{ef}	12_{ab}	0.14_{a}
$SS6\_H_{GYP}$	772_{a}	12.2_{cdef}	19_{abc}	0.33_{a}

Within the same column, values not followed by the same letter are significantly different at $p<0.05$ as determined by One-Way ANOVA post-hoc Fisher LSD analysis (n=4).* *Indicates data have been transformed by log (leachate volume) and square root (leachate TSL) for statistical analysis*

A key difference in the properties of LITH and PHV is PHV's high proportion of silt sized material at 70.3% (w/w), which is more than double that of LITH (28.7% w/w). PHV is dominated by muscovite, which at 37% (w/w) is more than a third of PHV's mineralogical composition. Igwe et al. (1997) found that the silt fraction in Nigerian soils were just as important as the clay fraction in terms soil base properties. However, the CEC results show PHV has low base properties in part as muscovite is associated with low CEC (Essington, 2004). This is due to the inaccessibility of muscovite's K^{+} cations caused by the 2:1 atomic structure of muscovite, where silicate sheets are bonded by layers of potassium ions (Essington, 2004). Lu et al. (2002) suggest that silt as well as clay layers

constitute active sites for anionic PAM sorption. PHV has a combined muscovite and clay mineral fraction of 67% (w/w). Therefore, it is inferred that the mineralogy of the non-clay fraction is as important for providing a specific surface area for polymer adsorption; particularly for non-ionic PVAL treatments, which are less sensitive to the presence of cations compared to surface area, in terms of absorption (Khansbasi and Abdalla, 2006).

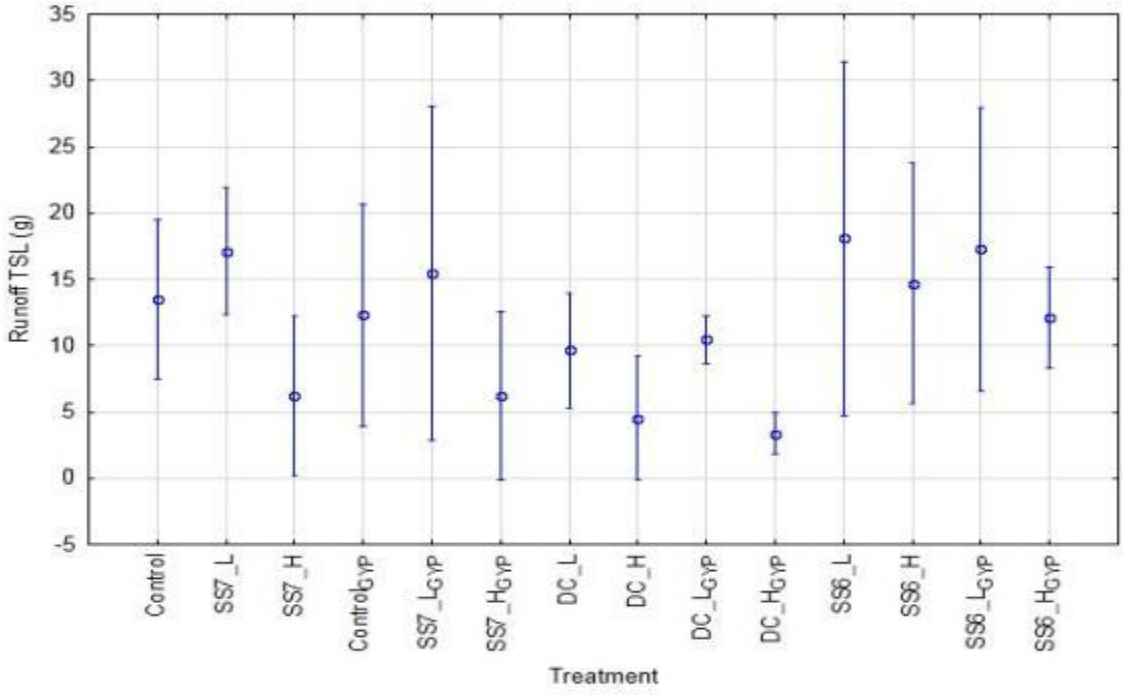

Figure 5.8. PHV: Effect of PBTs on runoff TSL compared with the untreated control

Note: For statistical differences between SFMs refer to Tables 5.10. Error bars denote ±1 Standard Error (n=4).

DC_H$_{GYP}$ and DC_H generated significantly lower runoff TSLs than the untreated control. The same treatments are also associated with significantly higher leachate volumes, and DC_H$_{GYP}$ is also associated with higher leachate TSLs than the control, inferring that these PBTs were successful at maintaining infiltration at the surface. SS7_H and SS7_H$_{GYP}$ were also associated with significantly less runoff TSL than the control, but the associated leachate volumes and leachate TSL were not significantly different from the control. Due to having a higher charge density than non-ionic PVALs, the PAMs would potentially cause higher rates of flocculation. PHV has a clay mineral content of 30% (w/w) and so SS7_H and SS7_H$_{GYP}$ would have promoted the aggregation of clay minerals and perhaps unconsolidated primary particles of muscovite. Consequently, larger aggregates would require more energy to be transported by runoff (Yonts, 2008). It is conceived, therefore, that the PAM treatments will

deter sediment from being transported away from the plot, but the PAM does not prevent the redistribution of sediment being entrained and deposited close to source. However, the PVAL treatments would stick particles in place and so inter-plot redistribution is less prevalent and the potential for surface sealing is reduced as compared with the PAM treatments. By preventing aggregate[NS] breakdown and aggregate[NS] movement, high infiltration rates are sustained during rainfall and this explains why PVALs DC_H_{GYP} and DC_H have significantly higher leachate volumes and leachate TSLs as compared to PAMs SS7_H, SS7_H_{GYP} and the untreated control.

5.4.1 Effects of application rate on PBT efficiency

The results in Table 5.10 show that high application rate treatments DC_H_{GYP}, SS7_H and SS7_H_{GYP} have significantly lower runoff TSLs compared to the respective lower application rate treatment. Higher application rate SS7_H_{GYP} has significantly lower leachate volume than lower application rate SS7_L_{GYP}. In contrast, higher application rate DC_H_{GYP} is associated with 28 times more leachate volume and more than 4 times higher leachate TSL than lower application rate treatment DC_L_{GYP}.

It is inferred that at higher application rates, the DC90 and SS7 treatments are more effective at reducing runoff TSL because there are more polymer molecules available for polymer surface and inter-polymer adsorption. However, the behaviour of the PVAL and PAM PBTs is shown to be different. The SS7 anionic PAM treatments cause lower runoff TSLs, by increasing the negative charge sites available to bridge with cations and kaolinite minerals (and perhaps primary particles, such as muscovite). The flocculation process increases the distribution of larger sized aggregates, which are able to withstand entrainment and transportation by surface runoff. Higher application rate PVAL DC90 treatments have a higher concentration of latex molecules that increases the latex cohesion and strength of the latex film that coats the surface (Steven Iwinski, Personal Communication, 24th August 2011), and so the surface becomes more stable during rainfall, resulting in significantly lower runoff TSLs. Likewise, increasing DC90 application rates and maintaining the structure of PHV at the surface also causes significantly higher leachate volumes and leachate TSLs than the control. Therefore, land managers may be inclined to consider whether it is more favourable to use DC_H_{GYP} or DC_H to attain very low runoff TSLs (up to four times lower than the control), and plan for significantly higher leachate volumes and leachate TSLs than the control (which may have implications for sub-surface piping and associated erosion); or to use

SS7_H or SS7_H_{GYP} and obtain runoff TSLs approximately half that associated with the control (not as low as could be achieved using DC90), but maintain leachate volume and leachate TSLs comparable to the control.

5.4.2 Effects of Gypsum on PBT efficiency

For PHV, the gypsum and non-gypsum treatments in Table 5.10 show that there are no significant differences between the gypsum and non-gypsum runoff volume or runoff TSL results, and only a few differences in the leachate results. Only gypsum treatment DC_L_{GYP} is associated with significantly less leachate volume than non-gypsum treatment DC_L. Significantly higher leachate TSL is associated with gypsum treatment DC_H_{GYP} than non-gypsum DC_H.

It was hypothesised that gypsum would improve PBT efficiency. However, the PHV results do not agree with this hypothesis. It is thought that sufficient exchangeable cations are present in the SFMs used in this study, and there are no efficiency gains in terms of cation bridging from having additional cations in the form of gypsum amendments. Alternatively, the application technique adopted in this study of mixing the gypsum at the immediate surface, as discussed with reference to LITH in Section 5.3.2, may be causing only a proportion of the gypsum to make contact with the polymer when it is sprayed at the surface. Changing application techniques or the amount of gypsum used may reveal an improved outcome on the PHV results; but taking into account these results showed few significant differences it is not thought likely.

5.4.3 Surface roughness change associated with the PBTs

An assessment of surface roughness (SR) and surface area (SA) of selected PBT treatments on PHV (Figure 5.9) was carried out using NSPASS, and a justification for the treatments selected is listed in Table 5.11.

It was hypothesised that after rainfall, the net change in SR and SA (T0 –T1) would reflect differences in PBT efficacy. Table 5.12 shows that the PHV Control is associated with the highest decline in SR at -3.39 and the polymer with gypsum treatments DC_L_{GYP} and SS7_H_{GYP} are associated with the lowest change in SR at -1.36 and 0.01, respectively. The post rainfall SA change results in part reflect the SR results, where the polymer with gypsum treatment SS7_H_{GYP} is associated with no change in SA at 0.00 m^3. However, the control is not ranked as showing the highest change in SA with a post rainfall SA

change of 0.10 m^3 (ranked 5 out of 6). It is reasoned that discrepancies between the SR and SA ranking may be the outcome of subtle differences in the starting conditions of the treatments.

Table 5.11. Non-soil PHV: treatments selected for NSPASS assessment

PHV Treatment	Reasons For Selection
Control	To compare PBT effects on surface roughness and surface area, with the untreated control.
SS6_L	Associated with the highest recorded mean runoff TSL.
SS7_H_{GYP}	Associated with significantly lower runoff TSL than the control.
DC_H_{GYP}	Associated with significantly low runoff TSL and high leachate volume and leachate TSL compared to the control.
DC_L_{GYP}	Associated with significantly higher runoff TSL, lower leachate volume and leachate TSL than higher application rate DC_H_{GYP}.
DC_H	Associated with significantly low runoff TSL and significantly higher leachate volumes than the control.

Table 5.12. PHV: Surface Roughness (SR) and 3D Surface Area (SA) variables for selected treatments

	BEFORE RAINFALL (T0)		AFTER RAINFALL (T1)		SR AND SA DIFFERENCE (T0 – T1)				Runoff TSL Generated	
PBT	Mean SR	Mean SA (m^3)	Mean SR	Mean SA (m^3)	SR Change	SR Change Rank	SA Change (m^3)	SA Rank	Runoff TSL (g)	Runoff TSL Rank
DC_L_{GYP}	2.54	0.24	1.19	0.13	-1.36	**5**	-0.11	**4**	10.48	**3**
SS7_H_{GY}	1.26	0.14	1.27	0.14	0.01	**6**	0.00	**6**	6.21	**4**
SS6_L	3.88	0.36	2.05	0.20	-1.84	**2**	-0.16	**2**	18.07	**1**
DC_H_{GYP}	3.14	0.36	1.33	0.15	-1.81	**3**	-0.21	**1**	3.38	**6**
DC_H	2.83	0.29	1.32	0.15	-1.51	**4**	-0.15	**3**	4.53	**5**
Control	4.52	0.22	1.13	0.13	-3.39	**1**	-0.10	**5**	13.51	**2**

SR, SA and Runoff TSL values are ranked, 1 being the highest value in the data set and 6 being the lowest. Note the ranked values do not reflect statistical differences in the data-set

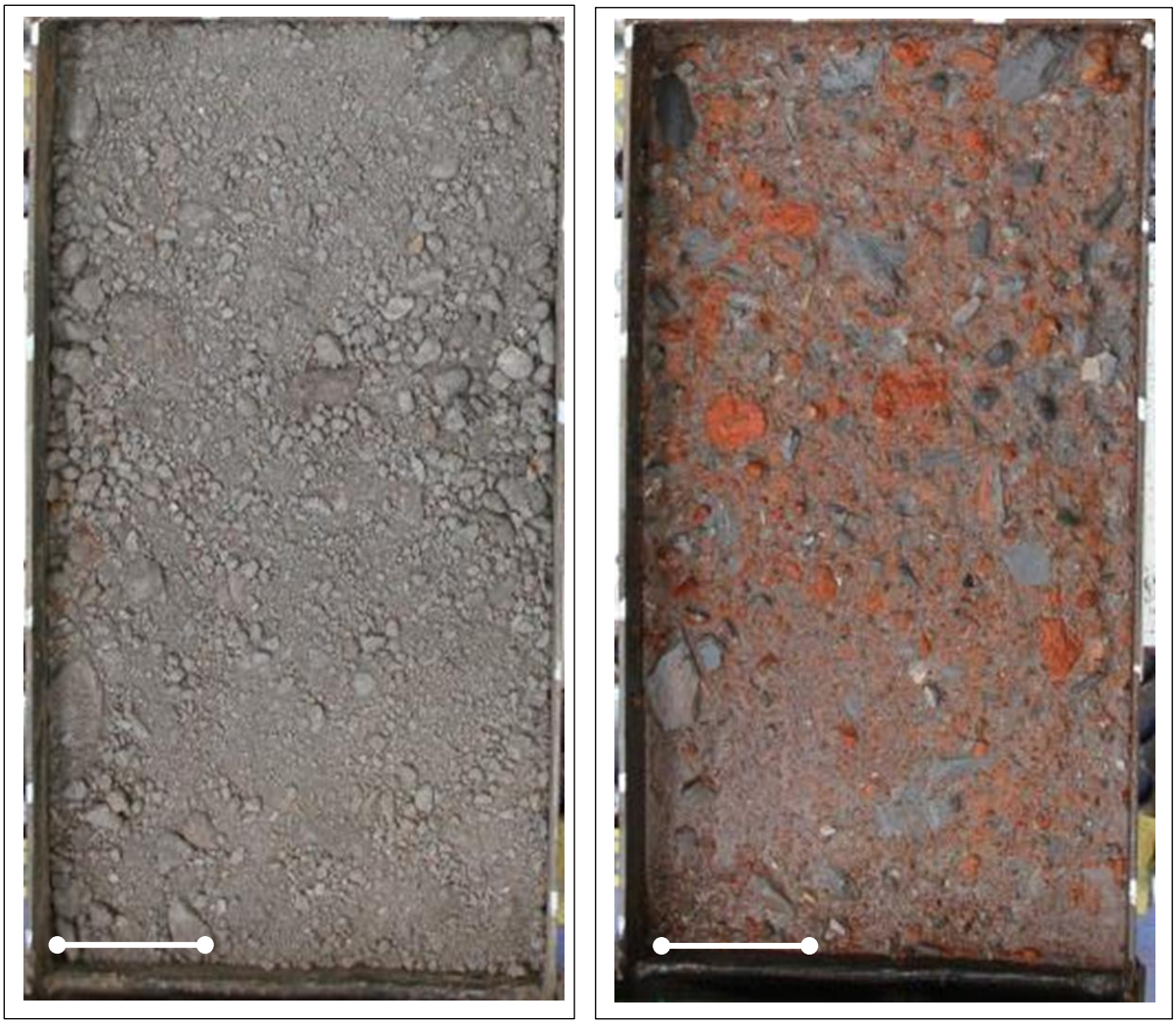

Figure 5.9. PHV Control treatment photographed before (left) and after (right) rainfall *(scale 2 cm = 3 cm)*

It was expected that the greatest changes in SR and SA would correspond with the highest runoff TSL. However, like LITH and HRS, this was not found for any treatments. It is reasoned that differences in how the PAM and PVAL treatments interact with the surface will cause non-linear SA and SR change during rainfall. PVAL treatments DC_H and DC_H_{GYP} were associated with significantly less runoff TSL than the control, because the polymer was successful in preventing detachment by raindrop impact and runoff. This then reduced the movement of material from its source, which is reflected by a moderate decline in SR (-1.51 and -1.81), which is not as high as the SR change shown by the untreated control (-3.39). PAM treatment SS7_$_{GYP}$ was also associated with significantly less runoff TSL than the control and has a negligible change in SR at 0.01. It is inferred that this is because SS7 treatments prevent erosion by flocculation and so promoting aggregation^{NS}, but this does not deter aggregated materials being entrained and re-deposited

locally within the erosion tray. Furthermore, the PAM SS7 does not provide a barrier to raindrop impacts or raindrop compaction (Vacher et al., 2003). The inter-plot movement of sediment would leave some parts of the plot rougher than starting conditions and some areas smoother, causing the net change in SR to be negligible.

5.5 Effects of PBTs on the erodibility and hydrological response of TRN

One-way ANOVA post-hoc Fisher LSD analysis shows no significant difference in the TRN runoff volumes or runoff TSLs results (Table 5.13). SS7_L_{GYP} generated significantly less leachate volume (913 ml) than the untreated control (1006 ml). Significantly higher leachate TSLs were generated by $Control_{GYP}$ (2.16g), SS7_L_{GYP} (2.11 g), SS7_H_{GYP} (1.76 g), DC_L_{GYP} (1.92 g), DC_H_{GYP} (1.76 g) and SS6_L_{GYP} (2.05 g) than the Control (0.60 g).

Table 5.13. TRN: Effect of PBTs on runoff volume, runoff TSL, leachate volume and leachate TSL

TRN				
Treatment	**Runoff Volume (ml)**	**Runoff TSL (g)**	**Leachate Volume (ml)***	**Leachate TSL (g)**
Control	44_{a}	0.11_{a}	1006_{bcd}	0.60_{a}
$Control_{GYP}$	41_{a}	0.04_{a}	1025_{cd}	2.16_{b}
SS7_L	44_{a}	0.06_{a}	1094_{d}	0.64_{a}
SS7_H	50_{a}	0.08_{a}	963_{bcd}	0.60_{a}
SS7_L_{GYP}	47_{a}	0.03_{a}	913_{a}	2.11_{b}
SS7_H_{GYP}	82_{a}	0.11_{a}	900_{abc}	1.76_{b}
DC_L	44_{a}	0.10_{a}	1206_{cd}	0.71_{a}
DC_H_	35_{a}	0.08_{a}	963_{ab}	0.67_{a}
DC_L_{GYP}	35_{a}	0.05_{a}	931_{abcd}	1.92_{b}
DC_H_{GYP}	41_{a}	0.05_{a}	1044_{cd}	1.76_{b}
SS6_L	32_{a}	0.06_{a}	919_{abc}	0.50_{a}
SS6_H	46_{a}	0.12_{a}	944_{bcd}	0.66_{a}
SS6_L_{GYP}	38_{a}	0.13_{a}	956_{abcd}	2.05_{b}
SS6_H_{GYP}	32_{a}	0.07_{a}	1031_{cd}	1.89_{a}

Within the same column, values not followed by the same letter are significantly different at $p<0.05$ as determined by One-Way ANOVA post-hoc Fisher LSD analysis (n=4). * *Indicates data have been transformed by log_{10} for statistical analysis.*

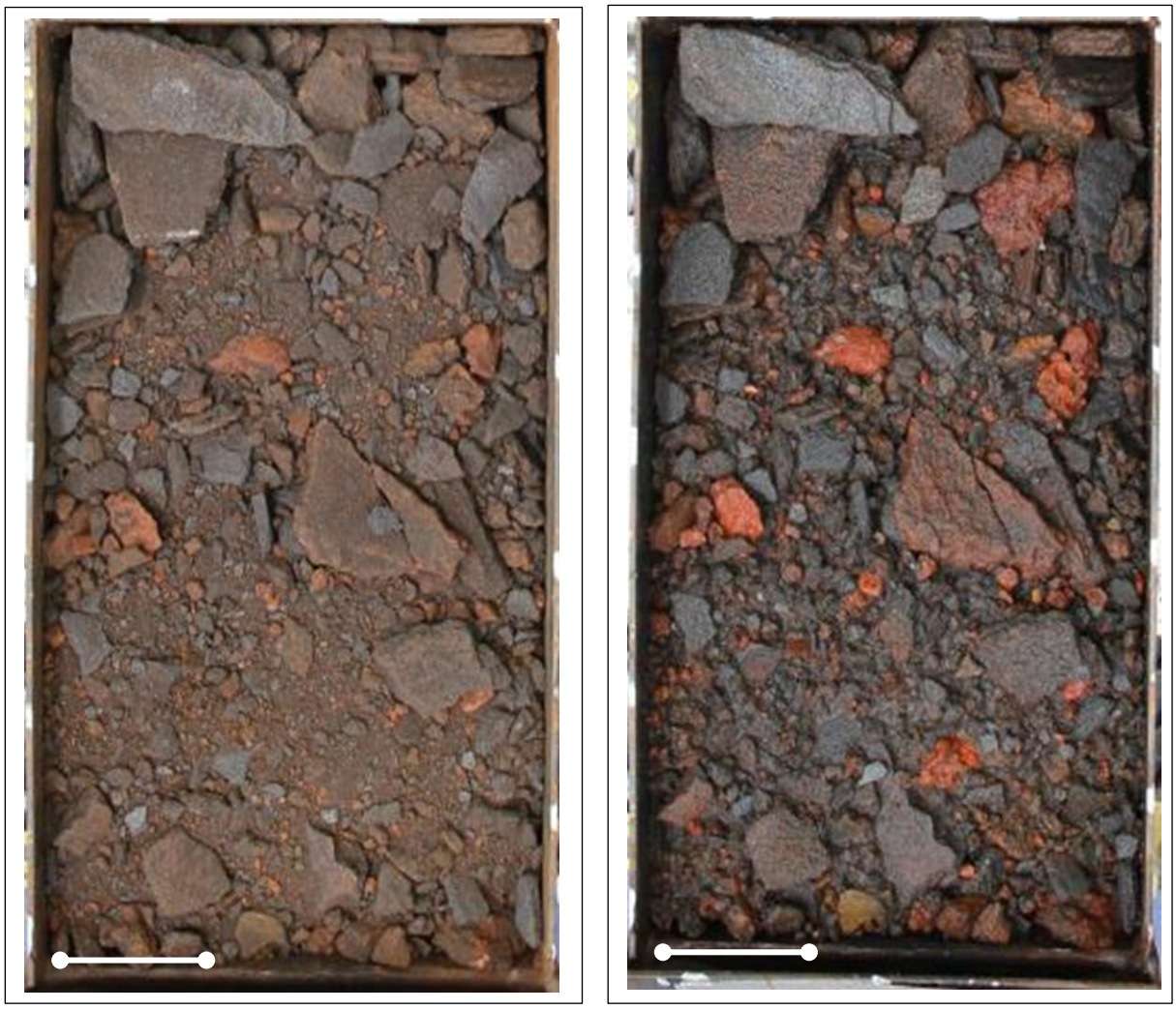

Figure 5.10 TRN Control treatment photographed before (left) and after (right) rainfall *(scale 2 cm = 3 cm)*

TRN shows PBTs do not alter the amounts of runoff volume or runoff TSL generated during rainfall. TRN has a significantly low CEC at 0.001 meq 100g, so it has low inherent cations needed for cation bridging with the anionic PAM treatments. TRN is comprised of <0.001% clay and 86.8% hematite, and is associated with having a high content (43% w/w) of large sized aggregates^{NS} (>5.6 mm, Table 4.4 Section 4.2.9). Larger aggregates^{NS} of hematite and goethite are thought to be associated with a weaker net surface charge than clay minerals (Giménez et al., 2007); which means that the anionic PAM treatments would be associated with low flocculation rates and this would result in no differences in the SS6 and SS7 PAM runoff volume or runoff TSL results. It is thought that having high amounts of coarse aggregates^{NS} at the surface (see Figure 5.10) in an unconsolidated SFM like TRN creates a more irregular surface and increases proximity between finer sediment distributed at the

surface. This would reduce connectivity between absorbed PVAL, preventing latex molecules coalescing and forming a film, which explains why runoff volumes and TSLs are similar to the control in the DC90 PBT results.

5.5. 1 Effects of application rate on PBT efficiency

Comparing the higher and lower PBT application rates in Table 5.13 shows that other than DC_H (963 ml), which has significantly lower leachate volume than DC_L (1206 ml); and SS6_H_{GYP} (1.89 g), which has significantly lower leachate TSL than SS6_L_{GYP} (2.05 g), application rate has no significant effect on the TRN results.

PBTs show no effect on TRN's runoff volumes and runoff TSLs because TRN is inherently associated with low runoff volumes and low runoff TSLs. Therefore any differences in runoff volume or runoff TSL directly related to the PBT would be less detectable, taking into account high variability within the data-set as illustrated in Figure 5.11. The hydrological response of TRN is to generate leachate and so TRN is associated with low runoff volumes <50 ml, but comparatively higher leachate volumes between 900 ml and 1094 ml. Land managers may be more interested in reducing leachate formation from TRN, and as such it would be necessary to tailor the PBT to enhance runoff formation and reduce leachate volumes. Higher PAM application rates with higher viscosities could be used to change leachate-runoff ratios, as has been discussed with reference to HRS. This could potentially reduce surface porosity. Further testing would be necessary to assess if this is possible.

5.5.2 Effects of gypsum on PBT efficiency

Comparing the gypsum and non-gypsum PBTs in Table 5.13 shows gypsum has no significant effect on runoff volume or runoff TSL. Gypsum treatment SS7_L_{GYP} is associated with significantly less leachate volume than without gypsum SS7_L. In contrast gypsum treatment DC_H_{GYP} is associated with significantly higher leachate volume than DC_H. Significantly higher leachate TSLs are associated with $Control_{GYP}$, SS7_L_{GYP}, SS7_H_{GYP}, DC_L_{GYP}, DC_H_{GYP} and SS6_L_{GYP} than the respective non-gypsum treatments, as illustrated in Figure 5.12.

Increased leachate TSL associated with the gypsum treatments was seen also in the results of HRS (DC_L_{GYP}, DC_H_{GYP}, SS6_L_{GYP} and SS6_H_{GYP}), LITH

(Control$_{GYP}$, DC_L$_{GYP}$, DC_H$_{GYP}$, SS6_H$_{GYP}$) and PHV (DC_H$_{GYP}$). With the exception of DC_H$_{GYP}$ (TRN) significantly higher leachate TSLs does not correspond with significantly higher leachate volumes. It is uncertain why gypsum causes significantly higher leachate TSLs; as much as 360% in the case of TRN. Such trends are not reported in the literature. It is expected that mixing gypsum with the upper (2-3 cm) surface disturbs the arrangement of aggregates^{NS} and in doing so is aerating the surface. The aerated surface has increased permeability over the non-gypsum treatment, and as such has more potential routes for infiltrated water to percolate, which in turn increases the possible surface area that sediment can become entrained by leached water. It is also possible that some gypsum granules are entrained by leachate, so supplementing the leachate sediment load, or else the gypsum is having dispersive effect on SFMs during rainfall. Further analysis of the characteristics of the leachate load is needed to test this. These findings are important for future studies that may consider the use of gypsum as an amendment to improve the efficiency of PBTs on a mine-site. In this context, sediment movement occurs both at the surface and within the waste-rock dump or stock pile, so any potential benefits found by using gypsum to control surface runoff and erosion, may be offset by the effect it has on increasing leachate TSL.

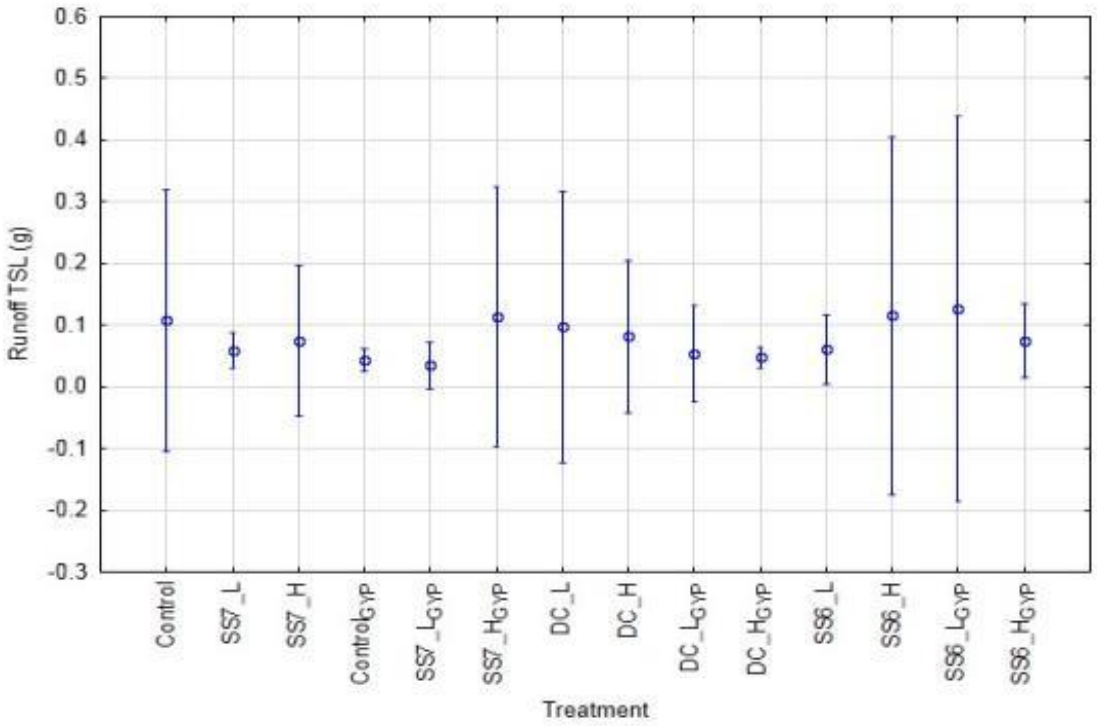

Figure 5.11. TRN: effect of gypsum treatments on runoff TSLs as compared with the non-gypsum treatments

Note: For mean results and statistical differences between SFMs refer to Table 5.13. Error bars denote ±1 Standard Error (n=4).

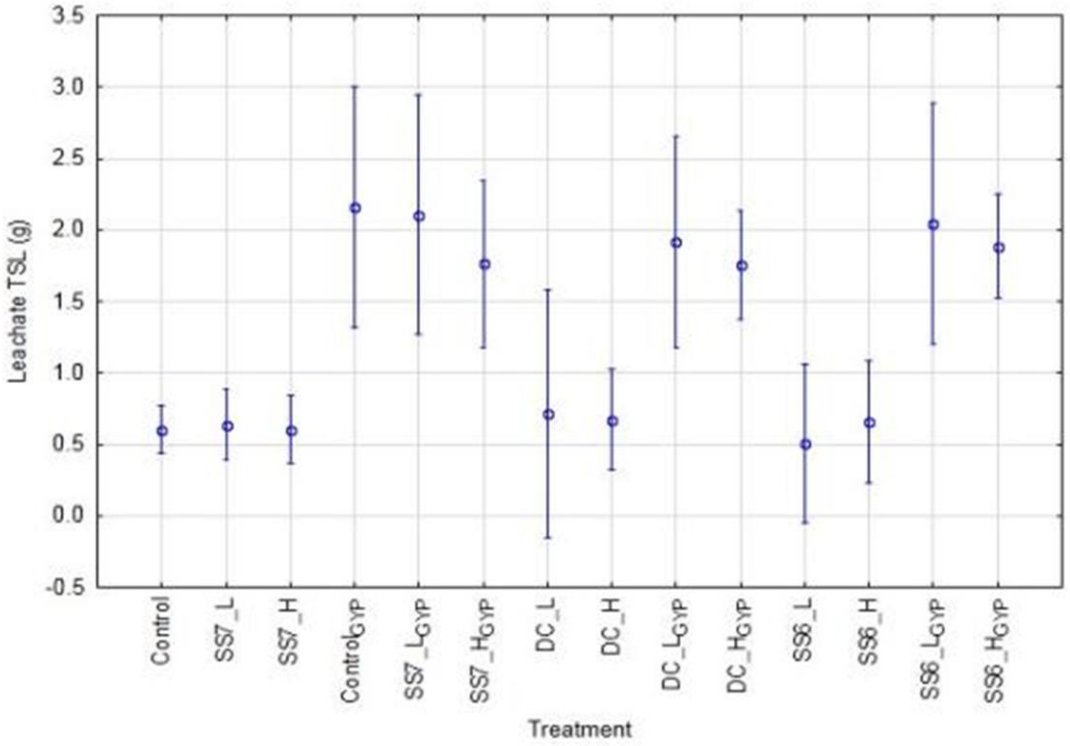

Figure 5.12. TRN: effect of gypsum treatments on leachate TSLs as compared with the non-gypsum treatments
Note: For mean results and statistical differences between SFMs refer to Table 5.13. Error bars denote ±1 Standard Error (n=4).

5.5.3 Surface roughness change associated with the PBTs

The treatments selected for NSPASS testing are listed in Table 5.14. The results in Table 5.15 shows that the polymer with gypsum treatments DC_H_{GYP} and SS7_L_{GYP} did show the least change in SA and SR, ranked 6th and 7th, respectively, but the control was not associated with highest ranked change in SR and SA. Most NSPASS treatments were associated with a decline in SA and SR, but DC_H_{GYP} and SS7_L_{GYP} were associated with increases. As with other SFMs tested, it is deduced that the relocation and/or uncovering of coarser materials can lead to both positive and negative change in SR and SA. Figure 5.10 shows the control post rainfall with the finer materials removed and the underlying surface armoured. Surface armouring has been associated with creating both a smoother and rougher surface depending on the distribution, shape and surface area of rocks in particular.

Table 5.14. Non-soil TRN: treatments selected for NSPASS assessment

TRN treatment	Reasons For Selection
Control	To compare PBT effects on surface roughness and surface area, with the untreated control.
SS7_L_{GYP}	Associated with significantly lower leachate volume and higher leachate TSL than the without gypsum SS7_L.
SS7_L	Associated with significantly higher leachate volume and lower leachate TSL than with gypsum SS7_$L_{GYP.}$
SS7_H	Associated with significantly lower leachate TSL than with gypsum SS7_H_{GYP}.
SS7_H_{GYP}	Associated with significantly higher leachate TSL than without gypsum SS7_H.
DC_H_{GYP}	Associated with significantly higher leachate volume and leachate TSL than non-gypsum DC_H.
DC_H	Associated with significantly lower leachate volume and leachate TSL than with gypsum DC_H_{GYP}.

Table 5.15. TRN: Surface Roughness (SR) and 3D Surface Area (SA) Variables associated with select treatments

	BEFORE RAINFALL (T0)		AFTER RAINFALL (T1)		SR AND SA DIFFERENCE (T1 - T0)				Runoff TSL Generated	
PBT	Mean SR	Mean SA (m^3)	Mean SR	Mean SA (m^3)	SR Change	SR Change Rank	SA Change (m^3)	Surface Area Rank	Runoff TSL (g)	Runoff TSL Rank
SS7_L_{GYP}	1.28	0.14	1.37	0.15	0.09	**7**	0.01	**7**	0.03	**7**
SS7_L	1.55	0.18	1.37	0.15	-0.18	**5**	-0.03	**5**	0.06	**5**
SS7_H	2.07	0.20	1.44	0.16	-0.62	**4**	-0.04	**4**	0.08	**4**
SS7_H_{GYP}	2.76	0.28	1.22	0.14	-1.55	**2**	-0.15	**1**	0.10	**2**
DC_H_{GYP}	1.22	0.14	1.32	0.15	0.11	**6**	0.01	**6**	0.05	**6**
DC_H	2.92	0.28	1.31	0.15	-1.61	**1**	-0.13	**2**	0.09	**3**
Control	2.33	0.22	1.39	0.16	-0.94	**3**	-0.07	**3**	0.11	**1**

SR, SA and Runoff TSL values are ranked, 1 being the highest value in the data set and 7 being the lowest. Note the ranked values do not reflect statistical differences in the data-set.

The TRN runoff TSL ranking correlates with the SA and SR ranking of SS7_L_{GYP}, SS7_L, SS7_H and DC_H_{GYP}. It is reasoned low runoff TSLs <0.13g may be causing some inconsistencies (control, DC_H and SS7_H_{GYP}) in the correlation between SA and SR change and runoff TSLs. These findings give some indication that SR and SA assessments can be used to deduce inferences about TRN erosion rates. Further experimental testing using more test replicates would be necessary to determine the strength of this correlation.

5.6 Conclusions to Phase II Results

PBTs can be cost effective, applied to large sites and will control erosion at source. Few papers have tested PBTs, specifically PVALs, on mine-site soil and non-soil SFMs. Initial results presented here show select PAM and PVAL treatments can significantly reduce runoff, leachate and erosion from a range of SFMs, including TRN, HRS, LITH and PHV. The results highlight the importance of identifying the appropriate SFM treatment, as some PAMs and PVAL treatments were found to significantly increase runoff, leachate and erosion from the tested SFMs. Future research is necessary to identify the longevity of the PVALs, in terms of the length of time and number of rainfall events the treatment is able to sustain erosion control.

PAM treatments were found to be sensitive to differences in CEC and mineralogy distribution in terms of polymer adsorption and cation bridging. The latex based formulation of the PVAL creates a glue-like film at the surface, which stabilises the surface, irrespective of the SFM CEC. The PHV results show PAM treatments caused moderate reductions in runoff TSLs; however the PVALs caused considerably lower runoff TSLs, and also significantly higher leachate volumes and TSLs than the untreated control. For PHV, environmental managers will need to identify the PBT that generates runoff to leachate TSL ratios that is appropriate for the site.

Increasing the application rate of select PBTs lowered leachate volumes, runoff TSLs and leachate TSLs. Increasing application rate did not reduce runoff volumes or runoff TSLs from HRS or TRN. Increased PVAL application rates increases latex molecules at the surface and the strength of the film to hold the surface in place and stop sediment detachment by rainfall impact and runoff. Higher PAM application rates have more polymer molecules available for absorption, but this is redundant if there are insufficient sites for adsorption. It is postulated that DC90 (without gypsum) will after further testing with a higher

number of treatment replications, reveal significant reductions in runoff TSLs from HRS.

Higher application rate PAMs have higher viscosities, which has been linked to lower leachate volumes than the control. Reducing leachate amounts may be beneficial for SFMs like TRN, which were inherently associated with low runoff volume and TSLs, but very high leachate volumes. Further testing is necessary to see if this is achievable. These results highlight the importance of understanding the hydrological response of different SFMs for effective management.

Two PAM and two PVAL treatments were successful in reducing runoff TSLs from highly erodible non-soil PHV, but only one treatment was successful in reducing runoff TSLs from soil LITH. SFM mineralogy and associated mineral adsorption properties determine the effectiveness of the PBT. The silt as well as the clay fraction is important for providing a surface area for polymer adsorption. Net surface charge will affect polymer efficacy, and minerals with large surface areas may have a weaker net surface charge after adsorption.

Overall, there was a poor response using gypsum to improve polymer efficiency. Most SFMs have low clay amounts and so excess Ca^{2+} supplied by the gypsum was redundant, as there were insufficient charges sites for the Ca^{2+} to bridge with. The non-ionic PVALs are not absorbed by cation bridging and so showed few significant differences in the gypsum results. There are no standard guidelines for applying gypsum. It is thought mixing the gypsum at the surface may have reduced gypsum efficiency, and also led to significant increases in SFM leachate TSL amounts.

Different research approaches in terms of polymer application method, rainfall design, type of PBT and type of SFM may lead to different research outcomes. This study has tested tropical SFMs using PBTs under an extreme tropical rainfall event, whereas other studies have used rainfall events with lower kinetic energies. Some studies have screened SFMs prior to testing, but this is not recommended using mine-site SFMs, as it is in part their high stone content that dictates their response to rainfall, and so changing these properties will produce misleading results.

Differences in mineral distribution and surface porosity cause high variability when SFMs are assessed at a small scale (0.2 x 0.11 m). Laboratory experiments are confined to replicating field scale erosion processes, such as interrill and rill erosion, and so future testing is necessary to assess the SFMs at field-scale. At this scale, other erosion processes, such as gullying and tunnelling, can be generated.

Non-soils TRN, HRS and PHV did not conform to the hypothesis that the untreated control would show the biggest change in SR and SA and the polymer plus gypsum treatment the least, according to the NSPASS methodology. PVALs and PAMs have different effects on SR and SA; where PVALs maintain surface micro-topography with a latex film, the PAMs are susceptible to raindrop impact, entrainment and re-deposition of entrained sediment within the erosion plot. Therefore, declining SR and SA during rainfall cannot be used to indicate polymer efficacy on the non-soil SFMs.

There was no direct relationship between SR and SA, and runoff TSL for HRS, LITH and PHV, because eroded sediment could have been transported away from the surface by either infiltration or surface runoff. Also, once erosion had initiated, SA and SR change became non-linear and less predictable. The onset of armouring uncovered a new surface and also exposed large stones or rocks, which may cause SA and SR to be either rougher or smoother than the pre-rainfall surface conditions.

NSPASS is a novel methodology that can detect surface change at an accuracy of 2-3 mm. This approach has revealed differences in surface micro-topography undetectable by the naked eye. ArcGIS has a range of surface analysis tools, so there are opportunities to further refine and develop this methodology beyond the functionality demonstrated in this study. Future studies should consider more replications of the results, confining analysis to fewer treatments, and simulating larger spatial scales to reduce anomalous results.

Chapter 6. Main conclusions and future research

High erosion losses and runoff volumes can disrupt mining operations, making roads impassable and causing detrimental impacts on the local environment. Managing this can become expensive (Brotons et al., 2010; Schwab et al, 1981). Steep slopes coupled with erodible SFMs in high intensity rainfall environments, like central Guinea, present a significant erosion risk. Polymer Based Treatments (PBTs), including polyacrylamides (PAMs) and polyvinylacrylic latex (PVALs), are effective erosion control solutions because they mitigate erosion at source (Zejun et al., 2002; Vacher et al., 2003; Martínez-Rodríguez et al., 2007; Lee, 2009). Our understanding of the erodibility and hydrological response of mine-site SFMs including waste-rock, ore and soils is limited. There is no research about PVALs to control runoff, leachate and erosion from mine-site SFMs.

The mining sector is a global industry and the results of this study highlight the necessity to understand SFM erodibility and hydrological response, in order to identify best practise sediment and water management solutions. The purpose of this chapter is to test the Phase I and Phase II hypotheses, which are listed in Section 1.3.

6.1 Phase I Key Findings

1. Soil and non-soil SFMs are significantly different in a number of their physical and chemical properties. Principal Component Analysis (PCA) demonstrated that the soil and non-soil SFMs should be analysed as statistically different populations. Soil SFMs were associated with significantly higher clay, CEC and organic carbon values, and significantly lower bulk density, when compared to the non-soil SFMs. Mineralogy was also different, with non-soils containing higher amounts of hematite and goethite, and the soils containing higher amounts of kaolinite and quartz.

2. Most soil and non-soil SFMs generated leachate volumes and associated TSLs significantly higher than runoff volumes and associated TSLs; HRS, SRE and PHY-WEA are the only exceptions.

3. Of all SFMs, the weathered phyllite (PHY-WEA) is significantly the most erodible by both runoff and leachate. PHY-WEA generated 57 times more erosion by runoff than the next most erodible non-soil SFM, and 2.5 times more erosion by leachate than the next most erodible non-soil SFM at field

capacity antecedent moisture conditions. Multiple regression analysis (MRA) demonstrated that this is largely due to PHY-WEA having a significantly high proportion of fine (250–500 µm and 125-150 µm) DAD size fractions, low CEC and an absence of cementing cations (Ca, Mg and K), mineralogy dominated by muscovite and a significantly high amount of readily transported silt sized particles.

4. Soil rejuvenated by erosion (SRE) generated significantly more erosion by runoff than the other soil SFMs, and is 39 times more erodible than the next soil SFM at field capacity antecedent moisture conditions. MRA found that these results were associated with SRE's significantly high coarse sand particle size fraction, high organic carbon content and significantly high magnetic susceptibility.

5. Changing antecedent moisture conditions had different effects on runoff, leachate and erosion by rainfall. Runoff volume and TSLs were significantly higher for SRE and PHY-WEA, and leachate volumes and leachate TSLs were significantly higher for HGF and HRS under field capacity as compared to air dry antecedent moisture conditions. In contrast and unexpectedly, HRS was associated with significantly lower runoff volumes and runoff TSLs at field capacity, when compared to air-dry antecedent moisture conditions.

6. MRA identified that characteristics, including magnetic susceptibility, mineralogy and dry aggregate distribution, which are not commonly assessed in erosion studies, are strongly correlated with SFM erodibility and hydrological response to rainfall.

6.2 Phase II Key Findings

1. Several PAM and PVAL treatments significantly reduced SFM runoff, leachate and erosion compared to the untreated control.

    - Higher application rate SS7, DC90 (with and without gypsum), and lower and higher application rates SS6 (with gypsum) were successful in reducing runoff volumes from LITH.
    - High application rate DC90 (with gypsum) was successful in reducing runoff TSLs from LITH.
    - Higher application rates SS7 (with and without gypsum) and higher application rates DC90 (with and without gypsum) were successful in reducing runoff TSLs from PHV.

- Higher application rate SS7 (with gypsum) and higher application rate SS6 were successful in reducing leachate volumes from HRS.
- Lower application rate SS7 (with gypsum) was successful in reducing leachate volumes from TRN.
- Lower application rate SS7 and higher application rate SS6 were successful in reducing leachate TSLs from HRS.

2. Several PAMs and PVAL treatments significantly increased runoff, leachate and erosion from the tested SFMs compared to the untreated control.

    - Higher application rate SS6 caused higher runoff volumes from HRS.
    - Gypsum alone, SS7 with gypsum and higher application rate SS6 caused higher runoff TSLs from HRS.
    - Higher application rate SS6, lower application rate DC90 (LITH) and higher application rates DC90, with and without gypsum (PHV), caused higher leachate volumes from LITH and PHV.
    - Several PAM and PVAL treatments (not listed for brevity) caused significantly higher leachate TSLs in all four SFMs tested.

3. Increasing the application rate of select PBTs significantly lowered leachate volumes, runoff TSLs and leachate TSLs. Increasing application rate did not reduce runoff volumes or runoff TSLs from HRS or TRN. Increased PVAL application rates increases latex molecules at the surface and the strength of the film to hold the surface in place and stop sediment detachment by rainfall impact and runoff. Increasing PAM application rate increases the amount of polymer molecules for absorption, but this is redundant if there are insufficient sites for adsorption.

4. Gypsum addition had no significant effect on polymer efficacy in terms of controlling runoff, leachate and erosion. Most SFMs tested have low clay amounts, so excess Ca^{2+} is redundant without sufficient charge sites for bridging with anionic PAMs.

5. Declining surface roughness during rainfall cannot be used to indicate polymer efficacy on the non-soil SFMs. Once erosion is in its more advanced stages, surface area and surface roughness changes become non-linear and less predictable. However, NSPASS has shown the prospects of being able to digitally and accurately evaluate changes in surface micro-relief in order to understand micro scale erosion processes, which can be developed for future erosion studies.

6.3 Contributions to new knowledge

1. This research has added to our understanding of the erodibility and hydrological response of soil and non-soil SFMs, specifically iron ore, waste-rock and Guinean soils.

2. This is the first study to evaluate critically the efficacy of PVALs as an erosion control solution for iron ore mine-site SFMs.

3. NSPASS is a novel method that integrates digital image capture and GIS used to record and detect surface micro-relief changes not visible to the naked eye with an accuracy of 2-3mm.

6.4 Recommendations

1. Future research is needed to identify optimum PAM and PVAL application rates for specific SFMs, based on SFM properties e.g. surface porosity, surface charge and mineralogy.

2. Further research is required to test the durability of the PAM and PVAL treatments tested in terms of length of time and number of rainfall events over which they are able to sustain their erosion control performance.

3. PBTs that were found to be successful in the laboratory should be considered for testing in the field to determine whether runoff, leachate and erosion control efficiency is maintained under local climatic conditions and at field scale.

4. The experimental design of this study had to take into account the costs and logistics of storing and importing high quantities of SFMs from Guinea to the UK, and so the number of treatment replications in the experimental design was the minimum as determined by Principal Component Analysis. Future studies using these types of SFMs should increase the number of treatment replications to further improve the robustness of statistical analysis

5. Future studies should develop the use of NSPASS in terms of its functionality monitoring changes in surface micro-relief, and improve its CE90 and LE90 accuracy from testing different cameras, camera lens and apparatus set-up.

6. Future erodibility studies using weathered phyllites from sites located in different parts of the world would help to understand more about which of

this type of SFMs characteristics is causing it to generate significantly high runoff and leachate total sediment loads during rainfall.

7. This study has shown the importance of a comprehensive assessment of SFM erodibility on a mine-site in order to identify best management practices to target leachate and/or runoff processes. Continued development of a classification system that recognises differences in the SFMs response to rainfall and the SFM physical and chemical characteristics will improve water and sediment management in the mining sector.

8. PVAL PBTs are recommended for non-soil mine-site SFMs with low CEC or clay content, as these PBTs are not dependent on cation bridging for polymer adsorption.

9. Anionic PAM PBTs have shown that increasing the application rate increases polymer viscosity, and future testing is recommended to assess whether this functionality could be useful for controlling high leachate volumes generated from mine-site SFMs that have a hydrological response to generate leachate.

6.5 Limitations of this research

This research has demonstrated the importance of controlled experimental conditions to compare and understand the hydrological response of SFMs, and to design water and sediment control strategies that will be appropriate throughout the 'life of a mine'. However, laboratory experiments using 0.125 m^2 erosion trays with a tray depth of 0.07 m, as used in this study, will not fully replicate field scale erosion processes, such as rilling, gullying, through-flow or tunnelling. It is also not possible to replicate actual field conditions such as construction methods used, site erosion history and traffic maintenance with plot scale studies of mined landscapes (Riley, 1995). Field based assessments were not within the scope of this project. A continuation of this research is necessary at the plot / field scale to further test the PAM and PVAL treatments that caused reductions in runoff, leachate and erosion. Furthermore, the inter-storm variability of kinetic energy (Obi and Salako, 1995) highlights that it is not possible to exactly simulate natural rainfall kinetic energy in the laboratory, and therefore it is important that PBTs are tested under natural rainfall at the mine-site's location. Finally if this research was carried out again it would be recommended that the dry aggregate distribution results distinguish between stones, soil aggregates and non-soil aggregates, as this could be an important factor in SFM hydrological behaviour.

Reference List

Aase, K. J. Bjorneberg, D. L. Sojka, R. E. (1998) *Sprinkler Irrigation Runoff and Erosion Control with Polyacrylamide – Laboratory Tests.* Soil Science Society of American Journal 62 (6). 1681-1687

Abiven, S. Menasseri, S. Chenu, C. (2009) *The Effects of Organic Inputs Over Time on Soil Aggregate Stability – A Literature Analysis.* Soil Biology and Biochemistry 41. 1-12

Addison, K. Atkinson, K. Smithson, P (2002). *Fundamentals of the Physical Environment. 3rd Edition.* Routledge, London

Ajayi. G (1982) *Statistical Property of Tropical Rainfall Intensity Measured in Nigeria for Microwave and Millimetre Wave Application.* Annals of Telecommunications 37 (11-12). 477-483

Akbarzadeh, A. Taghizadeh Mehrjardi, R. Refahi, H. G. Rouhipour, H. Gorji, M. (2009) *Using Soil Binders to Control Runoff and Soil Loss in Steep Slopes Under Simulated Rainfall.* International Agrophysics 23. 99-109

Amézketa, E. (1999) *Soil Aggregate Stability: A Review*. Journal of Sustainable Agriculture 142. 83-151

Asensio, E. Nicolau, J. M. (2000) *Rainfall Erosion on Opencast Coal Mine Lands: Ecological Perspective***.** Land Reconstruction and Management 1. 51-73, in, Haigh, M. J. (2000) *Reclaimed Land: Erosion Control, Soils and Ecology.* Balkema Publishers, Brookfield, USA. 51-74

Assouline, S. (2009) *Drop-Size Distribution and Kinetic Energy Rates in Variable Intensity Rainfall.* Water Resources Research 45. 1-7

Barthès. B. Roose, E. (2002) Aggregate Stability as an Indicator of Soil Susceptibility to Runoff and Erosion; Validation at Several Levels. CATENA 47. 133-149

Bergsma, E. Farshad, A. (2007) *Monitoring Erosion Using Microtopographic Features.* In: Chapter 14, Monitoring and Evaluation of Soil Conservation and Watershed Development Projects. De Graaff, J. Cameron, J. Sombantpanit, S. Pieri, C. Woodhill, J. 239-256. Science Publishers, Enfield, USA

Bhardwaj, A. K. McLauhlin, R. A (2007) *Understanding Interactions between Clay Mineralogy and Polyacrylamide for Turbidity and Flocculation Control in Discharged Waters from Construction Sites.* Poster. NC State Department of Soil Science. North Carolina, USA

Boix-Fayos, C. Calvo-Cases, A. Imeson, A.C. Soriano-Soto, M. D. (2001) *Influence of soil properties on the aggregation of some Mediterranean soils and the use of aggregate size and stability as land degradation indicators.* Catena 44. 47-67

Brade-Birks, S.G. (1959) *Good Soil.* The English University Press, London

Bratby, J. (2006) *Coagulation and Flocculation in Water and Wastewater Treatment.* IWA Publishing, London

Brotons, J. M. Romero Díaz, A, Alonso Surría, F. Belmonte Serrato, F. (2010) *Wind Erosion on Mining Waste in Southeastern Spain*. Land Degradation and Development 21. 196-209

Bryan, R. B. (2000) *Soil Erodibility and Processes of Water Erosion on Hillslopes.* Geomorphology 32 (3-4). 385-415

Buol, S. W. Southard, R. J. Graham, R. C. McDaniel, P. A. (2003) *Soil Genesis and Classification Fifth Edition.* Blackwell Publishing Professional, Iowa, US

Butcher, S. S. Charlson, R. J. Orians, G. H. Wolfe, G. V. (1992) *Global Biogeochemical Cycles.* Academic Press, London

Carter, R. (1993) *Soil Sampling and Methods of Analysis.* CRC Press, Florida

Chandler, J. (1999) *Technical Communication. Effective Application of Automated Digital Photogrammetry for Geomorphological Research.* Earth Surface Processes and Landforms 24. 51-63

Chenu, C. Le Bissonanais, Y. Arruuays, D. (2000) *Organic Matter Influence on Clay Wettability and Soil Aggregate Stability.* Soil Science Society of America Journal 64. 1479-1486

Clark , J. P. (2010) *Treatment of Mine Site Runoff Containing Suspended Solids Using Materialation Ponds – Optimising Flocculent Addition to Ensure Discharge Compliance.* Wolkersdorfer and Freund. eds,. International Mine Water Association. Sydney, Nova Scotia 5-9th September 2010. 217-22

Creamer Media (2009) *The Global Iron-Ore Market 2009 Report*. Creamer Media Ltd, Johannesburg. www.miningweekly.com/attachment.php?aa_id=25018 (accessed 18/09/2010)

Curran, K. J. Droppo, I. G. Irvine, K. N. (2002) *Hydrology of Stockpiled Industrial Coal Exposed to Rainfall.* Hydrological Processes 16. 2781-2790

Day, P.R. (1965) *Particle Fractionation and Particle Size Analysis.* In Methods of Soil Analysis, chapter 43. American Agronomy Society. Wisconsin, USA. 545-567.

Dearing, J. Chapter 4. *Magnetic Susceptibility*. In; Environmental Magnetism A Practical Guide. (1999) Edited Walden, J. Oldfield, F. Smith, J. Quaternary Research Association, London

Dontsova, K. M. Norton, L. D. (2002) *Clay Dispersion, Infiltration and Erosion as Influenced by Exchangeable Ca and Mg.* Soil Science 167. 184-193

Duiker, S. W. Rhoton, F.E. Torrent, J. Smeck, N. E. Lal, R. (2003) *Iron Hydro(oxides) Crystallinity Effects on Soil Aggregation.* Soil Science Society of American Journal 67. 606-611

Earley, D. Kidd, D. A. Shelley, T. Walder, I. Saluas, E. A. (2003) *Slope Stability of Leached Copper Stockpiles.* Tailings and Mine Waste. Swets and Zeitlinger B. V. Lisse, The Netherlands. 121-131

Ehansani, R. Sullivan, M (2010) *Soil Electrical Conductivity (EC) Sensors Factsheet.* Ohio State University, Ohio, USA

Essington, M. E. (2004) *Soil and Water Chemistry: An Integrated Approach.* CRC Press, Florida, USA

Evans, K. G. Loch, R. J. Aspinall, T. O. Bell, C. C. (1997) *Laboratory rainfall simulator studies of selected open-cut coal mine overburden spoils from Central Queensland.* Australian Journal of Soil Research 35 (1). 15-29

Fala, O. Aubertin, M. Molson, J. Bussiére, Wilson, G. W. Chapuis, R. Martin, V. (2003) *Numerical Modelling of Unsaturated Flow in Uniform and Heterogeneous Waste Rock Piles.* 6th International Conference Acid Rock Drainage. Cairns, Queensland, Australia. 12th-18th July, 2003

Figueiredo, M. do A. Augustin, C. H. R. R. Fabris, J. D. (1999) *Mineralogy, size, morphology and porosity of aggregates and their relationship with soil susceptibility to water erosion.* Hyperfine Interactions 122. 174-184

Fox, N. I. (2004) *Technical Note: The Representation of Rainfall Drop-Size Distribution and Kinetic Energy.* Hydrology and Earth System Sciences 8(5). 1001-1007.

Gan, J. K. M. Fredlund, D. G. (1996) *Shear Strength Characteristics of Two Saprolithic Soils.* Canadian Geothchnical Journal 33. 595-609

Gatto. L. W, Halvorson, J. J, McCool. D. K. (2003) *Over Winter Changes to Near Surface Bulk Density, penetration to Resistance and Infiltration Rate in Compact Soils.* Journal of Terramechanics 40. 1-24

Gerke, H. H. Molson, J. W. Frind, W. O. (1998) *Modelling the effect of chemical heterogeneity on acidification and solute leaching in overburden mine spoils.* Journal of Hydrology 209. 166-188

Gessesse, G. G, Fuchs, H. Mansberger, R. Klik, A. Rieke-Zapp, D. H. (2010) *Assessment of Erosion, Deposition and Rill Development on Irregular Soil Surfaces Using Close Range Digital Photogrammetry*. The Photogrammetric Record 25 (131). 299-318

Gilley, J. E. Gee, G. W. Bauer, A. (1977) *Runoff and Erosion Characteristics of Surface Mined Sites in Western North Dakota***.** Transactions of the ASAE 20(4). 697-700

Giménez, J. Martínez, de Pablo, J. Rovira, M. Duro, L (2007) *Arsenic Sorption onto Natural Hematite, Magnetite, and Goethite.* Journal of Hazardous Materials 141(3). 575-80.

Graham, R. C. Rossi, A. M. Hibbert, K. R. (2010) *Rock to Regolith Conversion: Producing Hospitable Substrate for Terrestrial Ecosystems.* The Geological Society of America 20 (2). 4-9

Green, V.S., Stott, D. E. (2001) *Polyacrylamide: Use, effectiveness, and cost of a soil erosion control amendment.* In: Stott, D. R. Mohtar, R. and Steinhardt, G. (eds.). The Global Farm – Selected papers from the 10th International Soil Conservation Organization Meeting. USDA-ARS National Soil Erosion Research Laboratory, May 24-29, 1999, Purdue University, West Lafayette, Indiana, USA.

Grohmann, C. H. Smith, M. J. Riccomini, C. (2009). *Surface Roughness of Topography: A Multi-Scale Analysis of Landform Elements in Midland Valley, Scotland.* Proceedings of Geomorphometry Conference. 2009. Zurich, Switzerland. 31st August – 2nd September. 2009.

Haigh, M. J. Sv. Gentcheva-Kostadinova (2000) *Ecological Erosion Control on Coal Spoil Banks: An Evaluation.* Ecological Engineering 18. 371-377

Hancock, G. R.Crater, D. Fityus, G. Chandler, J. Wells, T. (2008**)** *The Measurement and Modelling of Rill Erosion at Angle Repose Slopes in Mine Spoil.* Earth Surface Processes and Landforms 33. 1006-1020

Hartman, H. L. Mutmamsky, J. M. (2002) *Introductionary Mining Engineering: 2nd Edition*. John Wiley & Sons Inc. New Jersey.

Hawkins, J. W. (1998) *Chapter 3: Hydrological Characteristics of Surface Mine Spoil.* In: Coal Mine Drainage Prediction and Pollution Prevention in Pennsylvania. Pennsylvania Department of Environmental Protection. Pennsylvania, USA.

Hendrickx, J. M. H. Bruce, J. Harrison, J. Van Dam, R. L. Borchers, B. Norman, D. I. Dedzoe, C.D. Antwi, B. O. Asiamah, R. D. Rodgers, C. Vlek, P. Friesen, J. (2005) *Magnetic Soil Properties in Ghana.* Detection and Remediation Technologies for Mines and Mine like Targets 5794. 165-176

Hillier, S (2012) The James Hutton Institute, *Personal Communication*, 31/01/2012

Hudson, N. (1989) *Soil Conservation* (*reprint*). B.T Batsford Ltd, London

Hustrulid, W. A. McCartes, M.K. Van Zyk, D. J. A. (2000) *Slope Stability in Surface Mining.* Society for Mining, Metallurgy and Exploration Inc. Colorado, USA

Igwe, C. A., Nkemekosi, J. T (2007) *Nutrient Element Contents and Cation Exchange Capacity In Fine Fractions of Southeastern Nigerian Soils In Relation To Their Stability.* Communications in Soil Science and Plant Analysis 38. 1221-1242

Imahshoar, F. Tabataba, M. R. M. Hassanzadeh, J. Rostamipoor, M. (2012) *Experimental Study of Subsurface Erosion in River Banks.* World Academy of Science Engineering and Technology 61. 791-795

International Finance Corporation (IFC) (2006). *IFC Project's Summary of the Simandou Iron-ore Project.* www.ifc.org/ifcext/spiwebsite1.nsf/projects/5676B9E7496BE13E852576BA000E2833 (accessed 17/09/2010)

Iwinski, S. (2011) Applied Polymer Systems, Inc. *Personal Communication*. 24/08/2011

Jenness, J. S. (2004) *Calculating Landscape Surface Area from Digital Elevation Models.* Wildlife Society Bulletin 32 (3). 829-839

Jester, W. Klik, A. (2005) *Soil Surface Roughness Measurement – Methods, Applicability, and Surface Representation.* Catena 64. 154-192

Joma, S. Barry, D. A. Broveli, A. Heng, B. C. P. Sander, G. C. Parlange, J. Y, Rose, C. W. (2012). *Rainsplash Soil Erosion Estimation in the Presence of Rock Fragments.* Catena 92. 38-48

Kamphorst, E. C. Jetten,V. Guérif, J. Pitakänen, B. V. Iversen, J. T. Douglas, T. Paz, A (2000) *Predicting Depression Storage from Surface Roughness.* American Journal of Soil Science 64. 1749-1758

Kanungo, S. B (2005) *Effect of some commercial flocculating agents on settling and filtration rates of low grade, fragile manganese ores of Andhra Pradesh.* Indian Journal of Chemical Technology 12. 550-559

Karimor, A. Qadir, M. Noble, A. Vyshpolsky, F. Anzelm, K. (2009) *Development of Magnesium-Dominant Soils under Irrigated Agriculture in Southern Kazakhstan.* Pedosphere 19 (3). 331-343

Kemper, W.D. and Rosenau, R.C. (1986) *Aggregate Stability and Size Distribution.* Methods of Soil Analysis, Part 1. In; Physical and Mineralogical Methods (2nd Edition). Agronomy Monograph, No. 9. 425-442

Kennedy, B. A (1990) *Surface Mining. 2nd Edition.* Port City Press, Maryland, USA

Khansbasi, A. L. Abdalla (2006) *Evaluation of Three Water Borne Polymers as Stabilizers for Sandy Soils.* Geotechnical and Geological Engineering 24. 1603-1625

Kinnell, P. I. A. (2005) *Raindrop-Impact-Induced Erosion Processes and Prediction: A Review.* Hydrological Processes 19. 2815-2844

Kissell, F. N. (2003) *Handbook for Dust Control in Mining.* US Department for Health and Human Services IC9465, Pittsburgh, USA

Kitchen, L (2010) Rio Tinto *Personal Communication*. 26/11/2010

Kitchen, L (2012) Rio Tinto *Personal Communication*. 03/12/2012

Kollet, S. J. Maxwell, R.M (2006) *Integrated surface–groundwater flow modelling: A free-surface overland flow boundary condition in a parallel groundwater flow model.* Advances in Water Resources 29. 945-958

Kumar, A. Saha, A. (2011) *Effect of Polyacrylamide and Gypsum on Surface Runoff, Material Yield and Nutrient Losses on Steep Slopes.* Agricultural Water Management 98. 999-1004

Lal, R. (1988) *Erodibility and Erosivity.* Soil Erosion Research Methods. Soil and Water Conservation Society, Ankeny, Iowa, USA. 141 – 162

Lal, R. (1988i) *Soil Erosion by Wind and Water: Problems and Prospects.* Soil Erosion Research Methods. Soil and Water Conservation Society, Ankeny, Iowa, USA. 1–9

Lal, R. (1998) *Drop-Size Distribution and Energy Load of Rainstorms at Ibadan, Western Nigeria.* Soil and Tillage Research 48. 103-114.

Landon, J. R. (1991) *Booker Tropical Soil Manual*. John Wiley and Sons, New York, USA

Lane, S. N. Chandler, J. H. (1998) *Assessment of DEM quality for Characterising Surface Roughness Using Close Range Digital Photogrammetry.* Photgrammetric Record 16 (92). 271-291

Lark, R. M. Bishop, T. F. A. Webster, R. (2007). *Using Expert Knowledge with Control of False Discovery Rate to Select Regressors for Prediction of Soil Properties.* Geoderma 138. 65-78

Lascelles, B. Parsons, T. Favis-Mortlock, D. Boardman, J. (2002) *Automated Digital Photogrammetry: A valuable Tool for Small Scale Geomorphological Research for the Non-Photogrammetrist.* Transactions in GIS 6(1). 5-15

Le Bissonnais, Y. Renaux, B. Delouche, H. (1995) *Interactions between soil properties and moisture content in crust formation, runoff and interrill erosion from tilled loess soils*. Catena 25. 33-46

Lee, S. S. (2009) *Polyacrylamide for Erosion and Runoff Control on Soils of Differing Characteristics.* Thesis Submitted in Part Fulfilment of the Requirements for the Degree of Doctor of Philosophy. University of Missouri, USA

Loch, R. J. Rosewell, C. J. (1992) *Laboratory Methods for Measurements of Soil Erodibilities (K Factors) for the Universal Soil Loss Equation.* Australian Journal of Soil Research 30. 233-248

Loch. R. J. (1994) *A Method For Measuring Aggregate Water Stability for Dryland Soils with Relevance to Surface Seal Development.* Australian Journal of Soil Research 32. 687-700

Loch, R. J. Foley, J. L. (1994) *Measurement of Aggregate Breakdown Under Rain – Comparison with Tests of Water Aggregate Stability and Rain Relationships with Field Measurements and Infiltration.* Australian Journal of Soil Research 32 (4). 701-720

Loch. R. J. Slater, B. K. Devoil, C. (1998) *Soil Erodibility (Km) Values for Some Australian Soils.* Australian Journal of Soil Research 36. 1045-1055.

Lu, J. H. Wu, L. Letey, J. (2002) *Effects of Soil and Water Properties on Anionic Polyacrylamide Sorption.* Soil Science Society of American Journal 66. 578-584

Luk. S (1985) *Effect of Antecedent Soil Moisture Content on Rainwater Erosion.* Catena 12. 129-139

MAFF (Ministry of Agriculture, Fisheries and Food) (1973) *The Analysis of Agricultural Materials.* Technical Bulletin 27, HMSO, London.

MAFF Ministry of Agriculture Fisheries and Food. (1986) *Reference Book RB427: Analysis of agricultural materials.* HSMO, London.

Mahardhika, H. Ghadiri, H, Yu, B (2008) *Effects of Polyacrylamide on Soil Erosion and Material Transport.* 14th International Soil Conference. 19-23rd May 2008. 1-4. Atmospheric Environment Research Centre Environmental Futures Centre. Budapest, Hungry.

Maher, B. A. (1998) *Magnetic Properties of Modern Soils and Quaternary Loessic Paleosols: Palaeoclimatic Implications.* Palaeogeography, Palaeoclimatology, Palaeoecology 137 (1-2). 25-54

Markewitz, D. Glazer, R. L (2009) *Use of Polyacrylamide (PAM) for Controlling Soil Erosion on Steep Slopes in the Piedmont of Georgia.* Georgia Water Resources Conference 27-29th April 2009, University Georgia, USA

Martínez-Rodríguez, G.A. Vázquez, M. A. Guzmán, J. L. Ramos-Santana, R. Santana, O. (2007) *Use of Polyacrylamide as an Erosion Control Strategy in a Highly Eroded Soil of Puerto Rico.* The Journal of Agriculture of the University of Puerto Rico 91(3-4). 87-100

McIntyre, D. S. (1958) *Soil Splash and the Formation of Surface Crusts by Raindrop Impact.* Soil Science 85. 261-266

McLemore, V. T. Fakhimi, A. Van Zyl, D. Ayakwah, G. F. Anim, K. Boakye, K. Ennin, F. Felli, P. Fredlund, D. Luiza, A.F. Nunoo, G. Tachie-Menson, S. Viterbo, V. S. (2009) *Questa Rock Pile Weathering Stability Project. Literature Review of Other Rock Piles: Characterization, Weathering, and Stability*. New Mexico Bureau of Geology and Mineral Resources Open-file Report OF-517 Molycorp Task B4.2.5

Merel A. P., Farres P. J. (1998). *The Monitoring of Soil Surface Development Using Analytical Photogrammetry.* Photogrammetric Record, 16(92) 331–345.

Mining Watch (2002) *Introduction: Mining's Problem with Waste.* Mining Watch STD Toolkit Publications. www.miningwatch.ca/en/submarine-tailings-disposal-toolkit (accessed 16/09/2010)

Mohamed, A. M. Elbasit, A. Anyoji, H. Yasuda, H. Yamamoto, S. (2009) *Potential of Low Cost Close-Range Photogrammetry System in Soil Microtopography Quantification.* Hydrological Processes 23. 1408-1417

Moore, H. M. Fox, H. R. Elliott, S. (2003) *Land Reclamation: extending the boundaries*. Swets and Zeittlinger. The Netherlands.

Morgan, R. P. C (2006) *Soil Erosion and Conservation. 3rd Edition.* Blackwell Science Ltd, Oxford.

Moritani, S. Yamamoto, T. Andry, H. Inoue, M. Kaneuchi, T. (2010) *Using Digital Photogrammetry to Monitor Soil Erosion under Conditions of Simulated Rainfall and Wind.* Australian Journal of Soil Research 48. 36-42

Movahedan, M. Abbasi N. Keramati, M. (2012) *Wind Erosion Control of Soils Using Polymeric Materials.* Eurasian Journal of Soil Science. 81-86

Mutchler, C. K. Carter, C. E. (1983) *Soil Erodibility Variations during the year.* Transactions of the ASABE 26(4). 1102-1104 Geochimica et Cosmochimica Acta 65 (7). 1047-1057

Nicolau, J. M. (2002) *Runoff generation and routing on artificial slopes in a Mediterranean–continental environment: the Teruel coalfield, Spain.* Hydrological Processes 16 (3). 631-647

Nimmo, J. R. Perkins, K. S. (2002) *Aggregate Stability and Size Distribution*. In Dane, D. H. Topp, G. C. Methods in Soil Analysis Part 4, Physical Methods. Soil Science Society of America. Wisconsin, USA. 317-328

Nouwakpo, S. Huang, C. Frankenberger, J. Bethel, J. (2010) *A Simplified Close Range Photogrammetry Method for Soil Erosion Assessment.* 2nd Joint Federal Interagency Conference, Las Vegas, USA. 27th June – 1st July 2010

Nwankwo, K, N. (2001) *Polyacrylamide as a Soil Stabiliser for Erosion Control:* Report W1-06-98*.* Wisconsin Department of Transportation, USA. 1-13 http://trid.trb.org/view.aspx?id=673430 (accessed 01/08/2011)

Obi, M. E. Salako, F. K. (1995) *Rainfall Parameters Influencing Erosivity in Southeastern Nigeria.* Catena 24. 275-287

Omotoso, O. McCarty, D. K. Hillier, S. Kleeberg, R. (2006) *Some Successful Approaches to Quantitative Mineral Analysis as Revealed by the 3rd Reynolds Cup Contest.* Clay and Minerals 54 (6). 748-760.

Oregon Resources Corporation (2009) *Storm water Assessment for West Beaver Hill Road and Haul Road.* Oregon Resources Company Heavy Minerals Sand Project. www.deq.state.or.us/wq/wqpermit/docs/ORC/06-0073HaulroadStormwater01162009.pdf (accessed 08/09/2010)

Phillips, R. Greenway, M. (1998) *Changes In Water-Soluble and Exchangeable Ions, Cation Exchange Capacity, and Phosphorus$_{max}$ In Soils Under Alternating Waterlogged and Drying Conditions.* Communications in Soil Science and Plant Analysis 29 (1-2). 51-65

Piccolo, A. Mbagwu, J. S. C. (1999) *Soil Organic Matter Hydrophobic Components and Aggregate Stability.* Soil Science Society 63. 1801-1810

Poesen, J. W. Torri, D, Bunte, K. (1994) *Effects of Rock Fragments on Soil Erosion by Water at Different Spatial Scales: a review.* Catena 23. 141-166

Price, W. A. (1985) *Reclamation of Waste Rock Dumps Slopes at Kitsault Mine Site.* Proceedings of the 9th Annual British Colombia Mine Reclamation Symposium IN Karmloops BC. The Technical and Research Committee on Reclamation. Kamloops British Colombia. May 8-10th 1985

Price, D. G. (2009) *Engineering Geology Principles and Practice.* Springer, Berlin, Germany

Rejman, J. Turski, R. Paluszek, J. (1998) *Spatial and Temporal Variations in Erodibility and Loess Soil.* Soil and Tillage Research 46. 61-68

Rhoton, F. E. Romkens, M. J. M. Lindbo, D. L. (1998) *Iron Oxides – Erodibility Interactions for Soils of the Memphis Catena.* Soil Science Society of America Journal 62 (6). 1693-1703.

Rieke-Zapp D, Nearing MA. (2005). *Digital close range photogrammetry for measurement of soil erosion.* The Photogrammetric Record 20 (109): 69–87.

Rieke-Zapp, D. H., Wegmann, H., Santel, F. and Nearing, M. A. (2001) *Digital photogrammetry for measuring soil surface roughness.* Proceedings of the American Society of Photogrammetry & Remote Sensing 2001 Conference: Gateway to the New Millennium, St Louis, Missouri, USA. 8 pages.

Riley, S. J. (1995) *Aspects of the Differences in the Erodibility of the Waste Rock Dump and Natural Surfaces, Ranger Uranium Mine, Northern Territory, Australia.* Applied Geography 15(4). 309-323

Rio Tinto Website (2010) *Rio Tinto Project Information Summary Download Sheet.* RT_Simandou_Info_Sheet_EN_Mar_2010[1]. www.riotintosimandou.com/ENG/index.asp (accessed 17/09/2010)

Roberts, J. L (2004) *A Photographic Guide to Minerals, Rocks and Fossils.* New Holland Publishers, London

Rose, G. (2011) *Basic Photogrammetry in Remote View.* Imstrat Cooperation, Canada, USA. imstrat.on.ca/FCKeditor/editor/.../PhotogrammetryIntro-7.pdf (accessed 02/12/2011)

Rybàr, J.Stremberk, J. Wagner, P. (2002) *Landslides: Proceedings of the First European Conference on Landslides Prague, Czech Republic June 24-26, 2002.* Swets and Zeitlanger Publishers, The Netherlands

Schwab, G. O. Frevert, R. K. Edminster, T. W. Barnes, K. E (1981) *Soil and Water Conservation Engineering. Third Edition.* John Wiley & Sons, Canada

Selkirk, J. M. Riley, S. J. (1996) *Erodibility of Road Batters under Simulated Rainfall.* Hydrological Sciences Journal 41. 363-376

Shi, Z. H. Cai, C. F. Ding, S.W. Wang, T. W. Chow, T. L. (2004) *Soil Conservation Planning at the Small Watershed Level Using RUSLE with GIS: a case study in the Three Gorge area of China.* Catena 55. 33-48

Siegrist. S. Schaub, D. Pfiffner, L. Mäder, P. (1998) *Does Organic Agriculture Reduce Soil Erodibility? The Results of a Long Term Field Study of Loess in Switzerland.* Agriculture, Ecosystems and Environment 69 (3). 253-264

Simmons, R. (1998) *The effects of Polyacrylamide Based Soil Conditioners on Structural Sealing at a Sub-process Level.* Thesis Submitted in Part Fulfilment of the Requirements for the Degree of Doctor of Philosophy. University of Canterbury, Kent, UK.

Singer, M. J. Munns, D. N. (1999) *Soils an Introduction: 4th Edition***.** Prentice-Hall Inc, New Jersey.

Singh, A. N. Raghubanshi, A. S. Singh, J. S. (2002) *Plantations as a Tool for Mine Spoil Restoration.* Current Science 82 (12). 1436-1441

Singh, M. J. Khera, K. L. (2008) *Soil Erodibility Indices on Different Land Uses in Lower Shiwaliks.* Tropical Ecology 49 (2). 113-119.

Skidmore, E. L. Layton, E. L. (1992) *Dry Soil Aggregate Stability as Influenced by Selected Soil Properties.* Soil Science Society of America Journal 56. 557-561

Slay. M. (2008) *Identification and Cause of Hydrophobic Soil in Hawkers Bay.* Final Report. FITT Project 07FT187. www.beeflambnz.com/Documents/Farm/Identification%20and%20cause%20of%20hydrophobic%20soil%20in%20Hawke's%20Bay.pdf (accessed 12/11/2011)

Smith, L. Lopez, D. L. Beckie, R. Morin, K. Dawson, R. Price, W. (1995) *Hydrogeology of Waste Rock Drainage.* Final Report to Department of Natural Resources Canada. 1-111

Smith, K. A. Mullins, C. E. (2006) *Soil Environmental Analysis. Physical Methods. Second Edition Revised and Expanded*. Marcel Dekker Inc, New York, USA

So, H. B, Yatapanage, K. Horn, C. P. (2002) *Mine Erosion: An Integrated Erosion and Landscape Design Package for Monitoring and Modelling Erosion from Steep Hillslopes on Minespoils.* 12th ISCO Conference, 2002 Beijing. 36-41

Sojka, R.E., Surapaneni, A. (2001)*. Potential use of Polyacrylamide (PAM) in Australian agriculture to improve off- and on-site environmental impacts and infiltration management.* http://eprints.nwisrl.ars.usda.gov/1247/1/1140.pdf (accessed 13/04/2011)

Sojka, R, E. Bjornberg, D. L. Entry, J. A. Lentz R. D. (2007) *Polyacrylamide in Agriculture and Environmental Land Management.* Advances in Agronomy 92. 75-162

Soupir, M. L. (2004) *Effectiveness of Polyacrylamide (PAM) in Improving Runoff Water Quality from Construction Sites.* Journal of the American Water Resources (JAWRA) 40 (1). 53-66

Tindall, J. A Kunkel, J. R (1999) *Unsaturated Zone Hydrology for Scientists and Engineers.* Prentice- Hall Inc, New Jersey.

Vacher, C. A. Loch, R. J. Raine, S. R. (2003) Effects of Polyacrylamide Additions on Infiltration and Erosion of Disturbed Lands. Australian Journal of Soil Research 41. 1509-1520

Vacher, C. A. Raine, S. R. Loch, R. J. (2004) *Strategies to Reduce Tunnelling on Dispersive mine Spoil Materials.* ISCO 2004 - 13th International Soil Conservation Organisation Conference – Brisbane, July 2004 Conserving Soil and Water for Society: Sharing Solutions. Paper 139. 1-6

Vidal Vàzquez, E. Garcia Moreno, R. Miranda, J. G. V. Diaz, M. C. Saà Requejo, A. Paz Ferreiro, J. P. Tarquis, A. M (2008) *Assessing Soil Surface Roughness Decay During Simulated Rainfall by Multifractal Analysis.* Nonlinear Processes in Geophysics 15. 457-468.

Walkley, A. Black, I.A. (1934) *An examination of the Jar method for determining soil organic matter, and a proposed modification of the chromic acid titration method.* Soil Science 34. 29-38.

Weston, D.P. Lentz, R. D. Cahn, M. D. Ogle, R. S. Robert, A. K. Lydy, M. J. (2009) *Toxicity of Anionic Polyacrylamide Formulations when used for Erosion Control in Agriculture*. Journal of Environmental Quality 38. 238-247

White, R. E. (2006) *Principles and Practices of Soil Science. The Soil as a Natural Resource 4th Edition.* Blackwell Publishing, Oxford, UK

Wild. A. (1995) *Soils and the Environment: An Introduction.* University of Cambridge, Cambridge

Williams, D. J (2001) *Prediction of Erosion from Steep Mine Waste Slope.* Environmental Management and Health 12 (1). 35-50

Wolf, P. R. Dewitt, B. A (2000) *Elements of Photogrammetry with Applications of GIS, Third Edition.* McGraw-Hill Companies Inc, New York USA

Wong, W. N. L. Greene, R.S.B. Dalal, R. C. Murphy, B. W. (2009) *Soil Carbon Dynamics in Saline and Sodic Soils: A review.* Soil Use and Management 26 (1). 2-11

Wood, P. J. Armitage, P. D (1997) *Biological Effects of Fine Material in the Lotic Environment.* Environmental Management 21 (2). 203-217

Xu, L. F. Liu, M. L. (1999) *Impacts of Rare-Earth Mining on the Environment and the Effects of Ecological Recovery Measures on the Soils.* Remediation and Management of Degraded Lands. CRC Press LLC, Florida USA. 103-110

Yonts, C. D (2008) *Using Polyacrylamide to Reduce Soil Erosion. Water Resources Management Water Quality.* University of Nebraska, Nebraska Lincoln.

Young, R. A. Mutchler, C. K. (1977) *Erodibility of Some Minnesota Soils.* Journal of Soil and Water Conservation 32 (3). 180-182

Zejun, T., Tingwu, L., Qingwen, Z., Jun, J. (2002) *The Sealing Process and Crust Formation at Soil Surface Under the Impacts of Raindrops and Polyacrylamide*. 12th ISCO Conference (Ministry of Water Resources) May 26th - 31st 2002. Beijing, China. 456-462

Appendix A. Experimental Phase I rainfall simulator calibration

To simulate the design rainfall intensity of 100 mm hr $^{-1}$, 200 plastic cups as shown in Figure A.1 were used to measure spatial rainfall intensities across the erosion rig (using the below equation).

$$\text{Rainfall Intensity (mm hr}^{-1}) = \frac{\text{Amount of Rainfall (ml)}}{\text{Surface area of cup (cm}^2)} \times \frac{60}{\text{Time (min)}} \times \frac{10}{1}$$

Figure A.1 The erosion rig with 200 plastic cups to calibrate rainfall intensity

There are few published papers on rainfall erosivity characteristics in Guinea-Africa, but there is rainfall characterisation information from Nigeria, which has comparable rainfall seasonality to Guinea. Rainfall data from Samaru in northern Nigeria gave median drop sizes (D_{50}) ranging between 2.34 mm to 4.86 mm (Lal, 1998). Aina et al. (1977; in Lal, 1998) observed drop sizes ranging from 1.9 mm to 4.5 mm in Ibadan, Nigeria. In Salako, eastern Nigeria rainfall D_{50} was found to be 2.3 mm (Lal, 1995; in Lal, 1998), and more recent studies in Ibadan found D_{50} to range between 2.35 mm and 2.5 mm (Lal, 1998).

Target rainfall for the erosion trays was to therefore have a kinetic energy of (KE) 35 to 50 J m² with a drop size range between 2-4 mm (Hudson, 1989; Morgan, 2006). A 10% tolerance range was decided acceptable, because small scale (<1 m²) spatial and temporal rainfall intensity variation is normal in any storm event and should be expected (Assouline, 2009). Few rainfall simulator nozzles are designed to produce large rain drops >2.0 mm, so a range of simulator nozzles, pressure and boom arm height scenarios were tested; firstly using the entire rig, and then positioning the erosion trays at different locations within the top two thirds of the rig, where desired rainfall intensity and drop sizes were found to be most prevalent. The spatial variability in rainfall intensity at the surface of the rig was illustrated graphically after each calibration attempt using Microsoft Excel. Target rainfall intensity with a maximum 10% variance is shown in red and green in Figure A.2. This is where the erosion trays were then positioned.

Rainfall KE was measured using the *Flour pellet method,* as detailed in Simmons (1998). The Flour Pellet method uses household flour to create rain drop casts (shown in Figure A.3). KE is calculated using data about the number and size of rain drops (Simmons, 1998). Nine sieves (0.71 mm, 1.1 mm, 1.4 mm, 1.7 mm, 2.2 mm, 3.6 mm, 3.35 mm, 4.0 mm, 5.6 mm) were used to measure raindrop size KE (J m^2 s^{-1}). The Cumulative Drop Class Method equation (Simmons, 1998) below was used to determine the respective velocity and KE for each raindrop within the different size ranges (Simmons, 1998; White, 2006).

KE (J m²) = 0.5 (mass (terminal velocity²)

(White, 2006)

Cumulative Storm KE (J m^2 s^{-1}) = $\sum$ (KE of individual drop per size class) x drop size-class frequency

(Simmons, 1998)

It was finally concluded that three erosion trays could be placed on the rig at a given time and achieve the desired storm intensity and KE conditions. The maximum raindrop size was 2.9 mm and D_{50} across the target area was between 1.30 mm and 1.34 mm (Table A.1). Mean (n=3) rainfall intensity in the three tray positions was ±10% 100 mm hr^{-1} (Table A.2) with a mean (n=3) KE of 43.2 J m² (Table A.1). It was crucial rainfall erosivity was kept constant, both spatially and temporally, and so the erosion rig position was maintained using foot breaks and the erosion rig's location was drawn onto the ground. The erosion trays positions were also drawn onto the erosion rig.

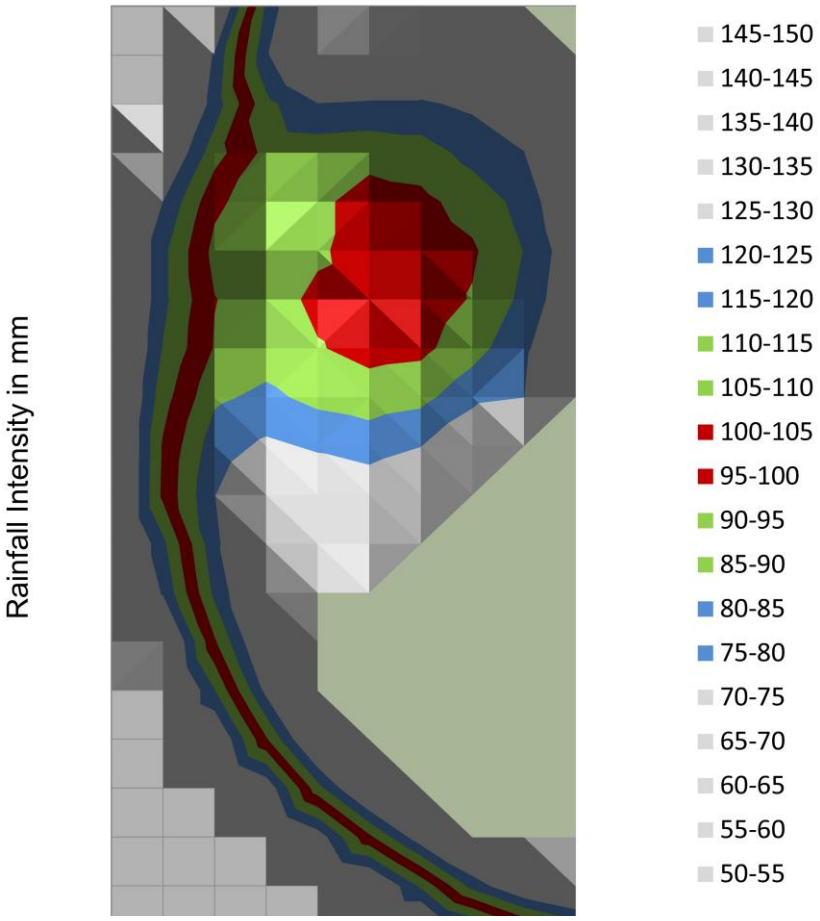

Figure A.2 Final rainfall intensity (mm hr^{-1}) at the erosion rig's surface (Calibration number 4 of 4)

Figure A.3 Different sized flour casts of simulated rainfall made during the rainfall calibration process

Table A.1 Rainfall kinetic energy (KE) and D_{50} measured in the final experimental set-up

Location of Flour Pellet Test	KE Rep 1 (J m²)	D_{50} Rep 1 (mm)	KE Rep 2 (J m²)	D_{50} Rep 2 (mm)	KE Rep 3 (J m²)	D_{50} Rep 3 (mm)
Top Left of Rig	52.4	1.33	47.8	1.38	45.1	1.34
Mid-Bottom Left of Rig	31.1	1.42	31.6	1.23	13.1	1.23
Mid-Bottom Right of Rig	49.2	1.04	57.6	1.38	34.1	1.32
Top Right of Rig	45.7	1.42	56.3	1.38	71.0	1.36
Mean KE and mean D_{50} (n=4)	*44.6*	*1.30*	*48.3*	*1.34*	*40.8*	*1.31*
Mean (n=3) storm KE (J m^2)	**43.2**					
Mean (n=3) D_{50} (mm)	**1.32**					

Table A.2 Rainfall intensity at the surface of the three erosion tray positions used in the final experimental set-up

	Rainfall Intensity Erosion Tray 1 (mm hr^{-1})	Rainfall Intensity Erosion Tray 2 (mm hr^{-1})	Rainfall Intensity Erosion Tray 3 (mm hr^{-1})
Calibration Rep 1	110.7	102.8	103.8
Calibration Rep 2	115.6	108.6	104.4
Calibration Rep 3	106.5	105.9	106.7
Mean (n=3)	**109.9**	**105.8**	**105.0**

Appendix B. Phase I experimental schedule

Test No:	Tray Position	Material Code	Treatment	Test No:	Tray Position	Material Code	Treatment
1	Tray 1	PHY-WEA-1	AD_{amc}	11	Tray 1	HGF-6	FC_{amc}
	Tray 2	RD-1			Tray 2	HRS-5	
	Tray 3	PHY-WEA-3			Tray 3	LITH-6	
2	Tray 1	SRE-2	AD_{amc}	12	Tray 1	FER-4	FC_{amc}
	Tray 2	ALL-3			Tray 2	HRS-4	
	Tray 3	RD-3			Tray 3	HGF-4	
3	Tray 1	SRE-3	AD_{amc}	13	Tray 1	ALL-6	FC_{amc}
	Tray 2	PHY-WEA-2			Tray 2	RD-5	
	Tray 3	HGF-3			Tray 3	LITH-5	
4	Tray 1	HGF-1	AD_{amc}	14	Tray 1	HGF-5	FC_{amc}
	Tray 2	HRS-2			Tray 2	PHY-WEA-5	
	Tray 3	HGF-2			Tray 3	ALL-4	
5	Tray 1	FER-1	AD_{amc}	15	Tray 1	HRS-6	FC_{amc}
	Tray 2	FER-3			Tray 2	SRE-4	
	Tray 3	FER-2			Tray 3	RD-4	
6	Tray 1	SRE-1	AD_{amc}	16	Tray 1	PHY-WEA-4	FC_{amc}
	Tray 2	LITH-3			Tray 2	ALL-5	
	Tray 3	LITH-1			Tray 3	RD-6	
7	Tray 1	LITH-2	AD_{amc}	17	Tray 1	PHY-WEA-6	FC_{amc}
	Tray 2	HRS-1			Tray 2	FER-6	
	Tray 3	RD-2			Tray 3	FER-5	
8	Tray 1	HRS-3	AD_{amc}	18	Tray 1	SRE-5	FC_{amc}
	Tray 2	ALL-1			Tray 2	LITH-4	
	Tray 3	ALL-2			Tray 3	SRE-6	
9	Tray 1	NEW WEA-1	AD_{amc}				
	Tray 2	NEW WEA-2					
	Tray 3	NEW WEA-3					
10	Tray 1	COMB WEA-1	AD_{amc}				
	Tray 2	COMB WEA-2					
	Tray 3	COMB WEA-3					

Appendix C. Designing the spatial calibration target frame used in the NSDP image acquisition system

The spatial calibration target frame was originally designed to position eight 0.2 m x 0.11 m erosion trays. The frame was made with perforated steel which was pre-drilled, so the X and Y co-ordinates could be determined very accurately based on the number of drill holes from the 0 origin (located in the top right corner of the rectangular frame). 57 different sized 8 mm bolts were fitted to the steel sheet. The X and Y location of the 57 bolts were precisely measured to create a co-ordinate system with ±0.01 mm accuracy and would later form the Ground Control Points (GCPs) for digitising the images. The Z axis of the 57 bolts was measured manually (+/- 0.01 mm) with vernier calipers.

It was important to have (approximately) >60% overlap in the view finder of both cameras to perform image triangulation (Wolf and Derwitt, 2000). Similar Triangles theory explains how maximum depth of field, controlled by the distance between the two cameras, improves the ability of the cameras to focus on the target and so depict maximum detail (Wolf and Derwitt, 2000). The maximum distance the cameras could be positioned apart (B_{max}) was estimated using the Similar Triangles 'focal length to camera array ratio expression' (Wolf and Derwitt, 2000) as illustrated in Figure C.1.

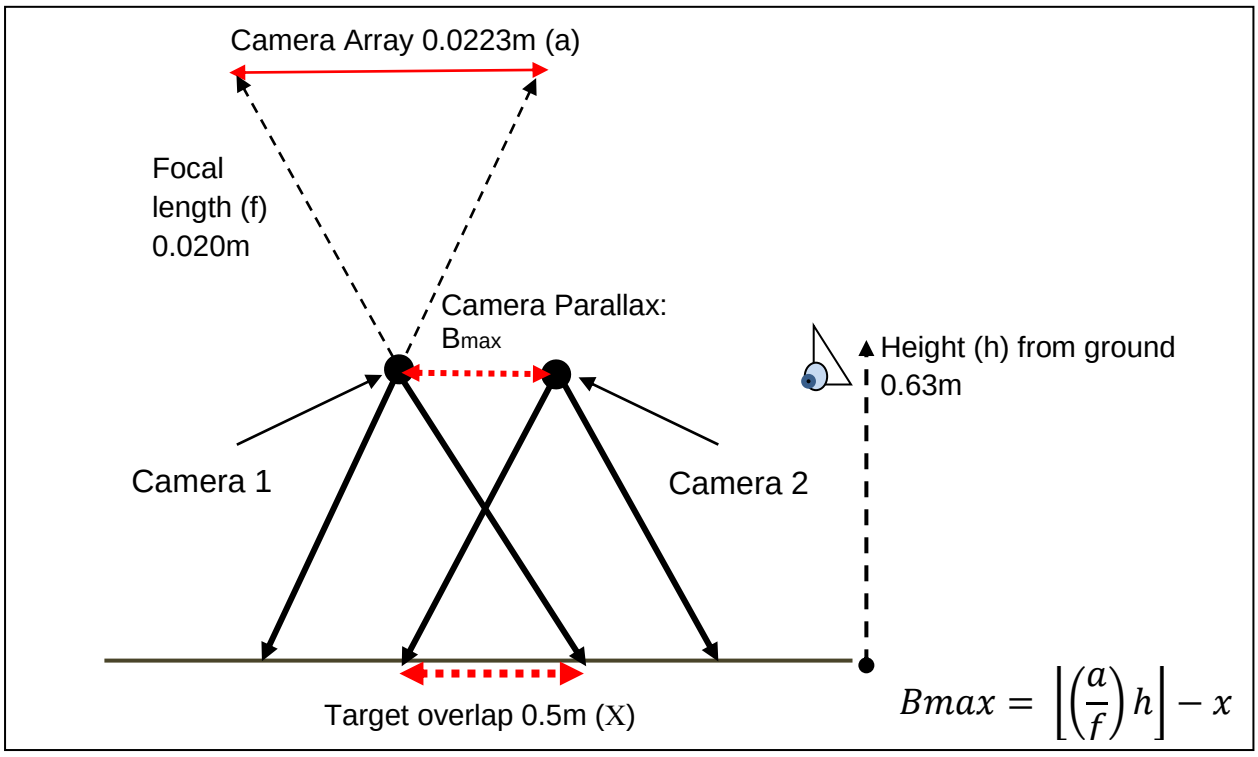

Figure C.1. 'Similar Triangles' expression used to determine the maximum theoretical distance the cameras could be positioned

B_{max} increases with camera height, and a spreadsheet was created using different camera heights and B_{max} values, to identify the camera height and B_{max} combinations that would generate stereo images with approximately 0.5 m² target area overlap (X); ensuring the cameras height (h) were practical for the user. It was found that B_{max} 56 cm and camera height 1.5 m was the minimum values that could retain 0.5 m ² target area overlap. However, it was not possible to focus the images and run the dual image triangulation using this set-up, so it was decided to use a smaller section of the target board. The apparatus set-up was modified, and the cameras were set at 0.63 m height and the B_{max} 13 cm to account for a smaller target area overlap of approximately 0.2 m². Using this new set-up meant only one erosion tray could be positioned on the frame at a given time instead of eight. Post image accuracy analysis was found to be satisfactory using this new set-up with an accuracy of 2-3 mm.

Appendix D. Assessment of stereo image spatial accuracy

Geo-referenced stereo-image error was measured using the LE90 (Linear Error of 90%) and CE90 (Circular Error of 90%), which are commonly used for quoting and validating geodetic images, DEMs and topographic contours' accuracy (Wolf and Dewitt, 2000); and are explained below (Rose, 2011).

- A **LE90** value represents the linear vertical distance that 90% of control points and their respective twin matching counterparts acquired in an independent geodetic validation survey should be found from each other.

- A **CE90** value is the minimum diameter of the horizontal circle that can be centred on all photo-identifiable control points, and also contains 90% of their respective twin counterparts acquired in an independent geodetic validation survey.

Accuracy is defined in Wolf and Dewitt (2000, p495) "as the degree of conformity of the true value…. but since the true value is never known, accuracy is only ever estimated, and often using an independent standard", which in this case was having well distributed 'check-points' in the model.

8 to 15 ground control points (GCPs) with about half of them converted to check-points (per image) is recommended for sufficient accuracy to deter error that may be present in the co-ordinate system (Wolf and Dewitt, 2000). And so image accuracy was assessed using the CE90 and LE90 of the block-file, which was geo-referenced with 11 GCPs, of which 6 GCPs were converted to check-points.

The CE90 and LE90 for digitised stereo images was recorded and ranged between 0.84 mm and 2.49 mm, which was considered satisfactory, based on the limitations of using this method with the equipment and time at hand (Wolf and Dewitt, 2000).

Appendix E. Photographs of AD_{amc} SFMs taken before and after design rainfall event (scale 1 cm = 7 cm)

PHY-WEA-2 before rainfall

PHY-WEA-2 after rainfall

SRE-3 before rainfall

SRE-3 after rainfall

HRS-1 before rainfall

HRS-1 after rainfall

COMB-WEA-2 before rainfall

COMB-WEA-2 after rainfall

HGF-1 before rainfall

HGF-1 after rainfall

LITH-2 before rainfall

LITH-2 after rainfall

NEW-WEA-3 before rainfall

NEW-WEA-3 after rainfall

ALL-3 before rainfall

ALL-3 after rainfall

RD-1 before rainfall

RD-1 after rainfall

FER-1 before rainfall

FER-1 after rainfall

Appendix F. Photographs of FC_{amc} SFMs taken before and after design rainfall event (Scale 1 cm = 7 cm)

PHY-WEA-5 before rainfall

PHY-WEA-5 after rainfall

SRE-5 before rainfall

SRE-5 after rainfall

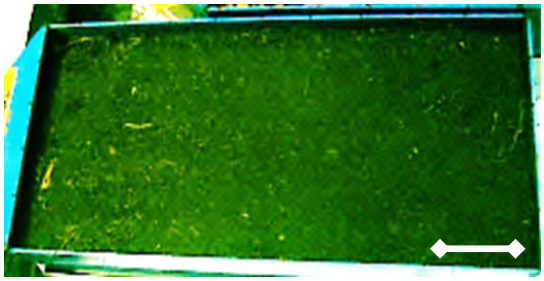

LITH-5 before rainfall

LITH-5 after rainfall

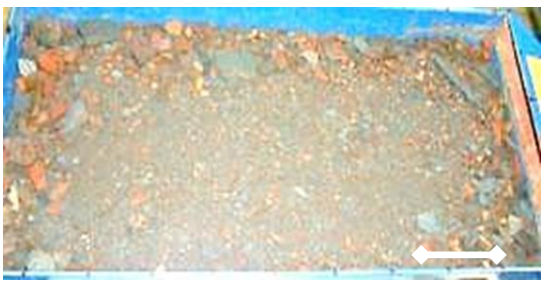

HGF-6 before rainfall

HGF-6 after rainfall

HRS-5 before rainfall

HRS-5 after rainfall

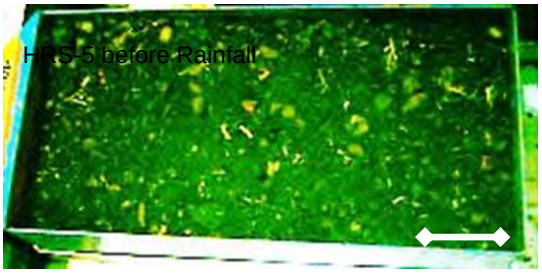

FER-5 before rainfall

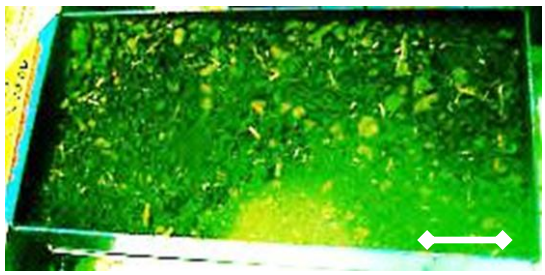

FER-5 after rainfall

ALL-6 before rainfall

ALL-6 after rainfall

RD-5 before rainfall

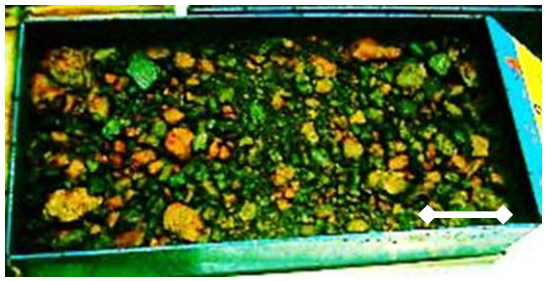

RD-5 after rainfall

Appendix G. Comparison of the physical and chemical characteristics of the SFMs used in both Phase I and Phase II (Tables G.1 to G.4)

Table G.1 PHY-WEA Phase I and PHV Phase II

SFM	Bulk Density Mg m³	pH	EC µS cm^{-1}	Coarse Sand % w/w	Medium Sand % w/w	Fine Sand % w/w	Silt % w/w	Clay % w/w	Exch-Ca meq 100g	Exch-K meq 100g	Exch-Mg meq 100g	Exch-Na meq 100g	CEC meq 100g	Org-C % w/w
PHY-WEA	1029_a	5.63_b	1680_a	6.33_a	4.67_b	7.67_b	65.7_a	15.7_a	1.17_a	0.05_a	0.11_b	0.03_b	2.43_a	0.23_a
PHV	1100_a	5.10_a	1810_a	4.00_a	3.33_a	5.00a	70.3_a	17.3_b	1.80_a	0.15_b	0.01_a	0.001_a	1.84_a	0.57_b

Within the same column, values not followed by the same letter are significantly different at $p<0.05$ as determined by One-Way ANOVA post-hoc Fisher LSD analysis (n=3).

Table G.2 HRS Phase I and HRS Phase II

SFM	Bulk Density Mg m³	pH	EC µS cm^{-1}	Coarse Sand % w/w	Medium Sand % w/w	Fine Sand % w/w	Silt % w/w	Clay % w/w	Exch-Ca meq 100g	Exch-K meq 100g	Exch-Mg meq 100g	Exch-Na meq 100g	CEC meq 100g	Org-C % w/w
HRS I	1760.7_a	6.07_a	1480.0_a	27.0_a	27.7_b	20.3_b	14.3_a	10.7_a	3.87_b	0.02_a	0.08_b	0.02_a	5.23_b	0.47_a
HRS II	2003.3_b	6.0_a	1380.0_a	26.0_a	16.7_a	16.0_a	25.3_b	16.0_b	1.80_a	0.11_b	0.05_a	0.001_a	2.53_a	0.60_a

Within the same column, values not followed by the same letter are significantly different at $p<0.05$ as determined by One-Way ANOVA post-hoc Fisher LSD analysis (n=3).

Table G.3 LITH Phase I and LITH Phase II

SFM	Bulk Density Mg m³	pH	EC μS cm^{-1}	Coarse Sand % w/w	Medium Sand % w/w	Fine Sand % w/w	Silt % w/w	Clay % w/w	Exch-Ca meq 100g	Exch-K meq 100g	Exch-Mg meq 100g	Exch-Na meq 100g	CEC meq 100g	Org-C % w/w
LITH I	811.0$_a$	5.10$_b$	1454.7$_b$	8.0$_a$	6.33$_a$	5.0$_a$	50.0$_b$	30.7$_a$	6.53$_a$	0.29$_b$	0.38$_b$	0.04$_b$	24.2$_a$	6.5$_b$
LITH II	1151.7$_b$	4.73$_a$	1330.0$_a$	11.3$_a$	7.67$_b$	6.67$_a$	28.7$_a$	45.7$_b$	15.1$_b$	0.22$_a$	0.27$_a$	0.01$_a$	17.7$_a$	3.9$_a$

Within the same column, values not followed by the same letter are significantly different at $p<0.05$ as determined by One-Way ANOVA post-hoc Fisher LSD analysis (n=3).

Table G.4 HGF Phase I and TRN Phase II

SFM	Bulk Density Mg m³	pH	EC μS cm^{-1}	Coarse Sand % w/w	Medium Sand % w/w	Fine Sand % w/w	Silt % w/w	Clay % w/w	Exch-Ca meq 100g	Exch-K meq 100	Exch-Mg meq 100g	Exch-Na meq 100g	CEC meq 100g	Org-C % w/w
HGF	2604.0$_b$	5.43$_a$	1830.0$_a$	17.7$_a$	20.7$_a$	40.0$_a$	18.3$_b$	3.33$_a$	0.77$_b$	0.01$_a$	0.03$_b$	0.03$_a$	1.93$_b$	0.001$_a$
TRN	2286.7$_a$	6.43$_b$	1876.7$_b$	25.7$_b$	26.0$_a$	35.3$_a$	9.33$_a$	3.67$_a$	0.10$_a$	0.1$_b$	0.01$_a$	0.001$_a$	0.01$_a$	0.10$_a$

Within the same column, values not followed by the same letter are significantly different at $p<0.05$ as determined by One-Way ANOVA post-hoc Fisher LSD analysis (n=3).

Glossary of Terms

Accuracy
An estimation of the degree of conformity of the true value.

Antecedent Moisture Conditions
The moisture content of a material prior to a rainfall event.

Antiferromagnetic Minerals
Minerals associated with lower magnetic susceptibility.

Ariel Triangulation
Used to transform 2D images into 3D images using a set of x, y and z co-ordinates.

Cation Exchange Capacity
Overall base cation concentration.

Check Points
Independent points in a model to evaluate image accuracy.

CE90
Is a value of the minimum diameter of the horizontal circle that can be centred on all photo-identifiable GCPs and also contain 90% of their respective twin counterparts acquired in an independent geodetic validation survey.

Close Range Digital Photogrammetry
Uses a pair of cameras at low height (<300 m) above the surface to produce a pair of stereo images with at least 60% overlap.

Covalent bond
Chemical bonds formed by the sharing of electrons between atoms.

Digital Elevation Model
Is a 3D representation of the earth's surface.

Dispersion
When a soil aggregate breaks up into separate particles.

Erodibility
The resistance of a material to detachment and transport by wind or rainfall.

Erosivity
The ability of wind or water to cause erosion.

Ferromagnetic
Magnetic minerals that dominate the magnetic signature.

Field Capacity
The amount of water retained in saturated soils that have been allowed to drain for at least one day.

Focal Length
Distance between the centre of a lens and its focus.

Geographic Information System (GIS)
An integrated computer-based tool that facilitates the input, processing, display and output of spatially referenced data.

Hydraulic Conductivity
A measure of the ease that water flows through a soil at a given gradient.

Hydrophilic
Having an affinity for water and readily absorbed or dissolved in water.

Hydrophobic
Repelling, tending not to combine with or incapable of dissolving in water.

Infiltration excess overland flow
Happens when rainfall intensities exceed soil infiltration rate.

Kinetic Energy
The energy available for compactive and dispersive processes that may result in aggregate breakdown.

LE90
A value that represents the linear vertical distance that 90% of control points and their respective twin matching counterparts acquired in an independent geodetic validation survey should be found from each other.

Leachate
Any liquid and dissolved solids that has passed through the surface of the soil.

Magnetic Sustainability
The measure of the ‘magnetizability’ of a material.

Minerals
Any of the non-organic soil constituents, including Al, Si and O.

Moh's Scale of Mineral Hardness

Measures the resistance of a mineral to scratching on a ten point scale: 1) Talc; 2) Gypsum; 3) Calcite 4) Fluorspar; 5) Apatite; 6) Orthoclase; 7) Quartz; 8) Topaz; 9) Corundum; 10) Diamond.

Muscovite

A form of Mica mineral with a 2:1 structure made of aluminium octahedral sheets between two silicon tetrahedral sheets.

NSPASS

A near-surface digital photogrammetry and integrated GIS technique that can be used to assess surface micro-relief.

Photogrammetry

Is a technique that determines the geometric properties of objects or surfaces from photographic images.

Phyllosilicates

Minerals that have crystal layers with varying silicon to aluminium ratios.

Polymer adsorption

The process of attachment of a polymer to the surface of a clay or silt mineral.

Polymer Based Treatment

Are soil conditioners that are long chain, soluble, synthetic copolymers with different functional group monomers, including acrylamide (PAMs) and acrylic latex functional groups (PVALs).

Polymerization

The process of joining at least two molecules together.

Porosity

The volume of pores divided by the sample volume.

Saturation Excess Overland Flow

Happens when soil moisture storage meets capacity and no longer can infiltrate water.

Slaking

A process of aggregate breakdown caused by pressure gradient changes when water uptake causes air to expand.

Slope Forming Material

Unconsolidated waste-rock, soil and geological material from a mine-site.

Sodic

A material high in exchangeable sodium.

Splash Erosion

The detachment of soil particles by water jets caused by impacting raindrops.

Subsurface Return Flow

Happens when through-flow exfiltrates at a different point in the slope profile.

Surface Area

The total area of a surface or a solid figure.

Surface Micro Relief Processes

Erosion processes operating at a micro scale <1 m^2.

Surface Roughness

The elevation variability of a topographic surface at a given scale.

Van Der Waal Forces

Polar attractions between charged molecules.

Weathering

Biological, chemical and physical breakdown of rock minerals caused by air and water.